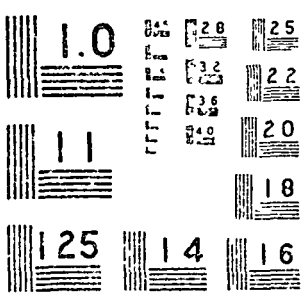

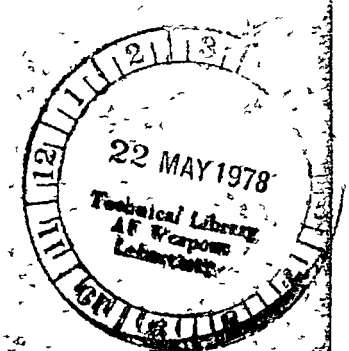

R-7585

THERMODYNAMIC IMPROVEMENTS IN LIQUID HYDROGEN TURBOPUMPS

Contract No. NAS8-20324

Second Interim Report
September 1968

Prepared For

National Aeronautics and Space Administration
Propulsion and Vehicle Engineering Division
George C. Marshall Space Flight Center
Huntsville, Alabama

Prepared By

Advanced Systems and Turbomachinery Departments
Engineering
Rocketdyne
A Division of North American Rockwell Corporation
Canoga Park, California

G. S. Wong
Principal Engineer
Supervisor, Advanced Turbomachinery

W. R. Wagner
Supervisor, Heat Transfer

Approved:

S. F. Iacobellis
Manager
Advanced Systems

PRECEDING PAGE BLANK NOT FILMED

FOREWORD

Rocketdyne, a division of North American Rockwell Corporation, has prepared this interim report which documents the work performed in fulfillment of the program, "Thermodynamic Improvements in Liquid Hydrogen Turbopumps," during the period from 17 August 1967 to 16 August 1968. This program is sponsored by the National Aeronautics and Space Administration under Contract No. NAS8-20324. The work was performed by the Advanced Turbomachinery Unit of the Turbomachinery Department and by the Heat Transfer Unit of the Advanced Systems Department. The program was administered by Mr. F. Suddreth of NASA Headquarters and by Messrs. T. W. Winstead, J. Vaniman, L. Gross, and H. F. Beduerftig of Propulsion and Vehicle Engineering, NASA Marshall Space Flight Center. Mr. H. F. Beduerftig, as Technical Project Manager, provided overall technical direction for the study.

ABSTRACT

This report describes the continued effort in the evaluation of thermal conditioning problems in liquid hydrogen turbopumps to enhance mixed-phase operation and to minimize the system constraints on engine starts and restarts. Both analysis and evaluation of experimental data are presented on the chilldown of turbopumps and rocket engine systems. The effects of two-phase hydrogen flow on turbopump performance and engine transient are also described.

CONTENTS

ILLUSTRATIONS

TABLES

ACKNOWLEDGMENT

This acknowledges the contributions made by F. M. Vahedi of the Heat Transfer Unit, in the chilldown analysis of turbopump and engine systems, by W. R. Bissell and R. K. Hoshide of the Advanced Turbomachinery Unit, for analysis of two-phase flow in hydrogen turbopump and by J. R Leonard of the Engine Analysis Unit of Advanced Systems, for the analysis of engine start transients.

INTRODUCTION

The requirements of minimum chilldown, warm and rapid starts, reduced pressurization or NPSH, engine flexibility and simplification are being emphasized for oxygen-hydrogen rocket engines. Both engine and components have been investigated to enhance mixed-phase performance. The liquid hydrogen pump results obtained from the previous program (Ref. 1) covering (1) thermal design, (2) materials, (3) preconditioning requirements, and (4) chilldown characteristics was utilized to relate the thermal conditioning problems and to minimize system constraints on engine start and restarts. Maximum use was made of pump, turbopump, and engine data from the various Mark 15, Mark 25, and Mark 29 programs and also from other experimental advanced engine programs. Heat soakback and chilldown data were also obtained from complementary experimental programs conducted at Rocketdyne. Heat transfer experimental data were also utilized from associated research study programs to support the thermal design analyses.

The Second Interim Report has been organized to present the technical results of the study in a manner most easily followed, i.e., by starting with the effect of two-phase flow on the turbopump operation and concluding with the effect of two-phase flow on engine start. To correlate with the objectives of the study program, index tabs are provided to indicate the results developed in each of the four tasks described below.

TASK I PUMP THERMAL DESIGN CRITERIA

The pump thermal design criteria, including two-phase flow analysis and design techniques, characteristics of pump start and throttling operation, a computer thermal analysis of the critical areas within the LH_2 turbopump, and a detailed evaluation of the heat transfer characteristics of the Mark 15 and Mark 29 LH_2 pumps, were investigated. Various approaches to predict the pump performance when encountering two-phase flow were conducted.

TASK II: ENGINE SYSTEM ANALYSIS AND OPTIMIZATION CRITERIA

In this task, a prototype engine system (J-2) as an integrated package considering the matching of the components within the engine system, factors affecting engine startup, detailed computer thermal analysis of the pump, line, and thrust chamber components were investigated The analysis of the engine system chilldown including an evaluation of the engine system component parts (e.g., feed lines, valves, thrust chamber) were conducted.

TASK III MIXED-PHASE FLOW INVESTIGATION

To evaluate the mixed-phase flow heat transfer coefficients and critical velocity characteristics of hydrogen, an experimental investigation of two-phase flow phenomena was defined The test plan and instrumentation requirements were submitted to the J-2 program office for a joint and complementary effort, however, because of a reduced overall effort of the J-2 program, this experimental investigation was not initiated.

TASK IV COMPARATIVE EVALUATION OF
INTERRELATED ENGINE SYSTEMS

Evaluation of integrated engine systems was conducted by studying and analyzing the J-2 and J-2S engine system test data. Experimentally defined variables including turbopump thermal conditioning and heat soakback, turbopump equilibrium temperature, and methods of propellant supply were studied to provide maximum engine system flexibility with mixed-phase starts and reduced system constraints and critical operating parameters.

SUMMARY

The evaluation study of the thermal conditioning problems in liquid hydrogen turbopumps to enhance mixed-phase operation and to minimize the system constraints on engine starts and restarts was continued. The program consisted of the following four interrelated tasks. Pump Thermal Design Criteria, Engine System Analysis and Optimization Criteria, Mixed-Phase Flow Investigation, and a Comparative Evaluation of Integrated Engine Systems. To complement this program, maximum use was made of (1) pump, turbopump, and engine data obtained from oxygen-hydrogen programs (such as the J-2X, J-2S, and nuclear research), and (2) heat transfer data including chilldown and heat soakback from various associated research study programs. Also, a wide range of literature was surveyed to provide additional support for the analyses and studies conducted under this program.

To make comprehension of this information easier, the format was reorganized such that supporting analyses precede the analyses being supported. Therefore, the major sections of this report are (1) Pumping Capability, in which the conditions of possible pump operation are defined without regard to the required preconditioning, (2) Chilldown Requirements, in which the methods of preconditioning and the preconditioning requirements for various turbopumps are evaluated, and (3) Engine Start Transients, in which various types of warm engine start transients are evaluated These sections are summarized as follows

PUMPING CAPABILITY

During a rocket engine start with little or no prechill, a two-phase (vapor-liquid) mixture enters the pump, and the pump flow passage surfaces are warmer than the propellant being pumped. The required amount of inlet line and pump prechill is dictated by the ability of the pump to tolerate both inlet vapor and a temperature differential between the flow passage surfaces and the propellant. Consequently, in analyzing these problems, the maximum amount of vapor that can be pumped was related to the pump

characteristic and to the pump operating point, and the regions of satisfactory pump operation were related to the surface-to-propellant temperature differential and to the pump operating point. In both analyses, experimental test data were used to develop performance prediction systems. Pump performance predictions were then made and were used to evaluate various pump geometries and various pump operating points.

CHILLDOWN REQUIREMENTS

In evaluating various chilldown procedures, an analysis of the Mark 29 pump was conducted in which the effects of chilldown flowrates of 0, 1.44, and 3 percent of total flowrate were determined. Mark 15-LH_2 pump chilldown test data, which were obtained from the J-2X program, were analyzed in detail to determine the chilldown characteristics. The results indicate that a quick pump chilldown is possible. For the test with the shortest chilldown time, the outlet hydrogen bulk temperature dropped to -415 F within 36 seconds. The chilldown characteristics of the J-2S engine system were analyzed to determine the chilldown characteristics of an engine system. The results indicate that a warm engine system can be chilled within 45 seconds by 35 to 40 pounds of hydrogen. The influences of other engine system components on turbopump chilldown were evaluated. In addition, a heat soakback analysis was conducted to determine the amount of time required for a turbopump to reach equilibrium temperature after shutdown.

ENGINE START ANALYSIS

To determine the two-phase pumping requirements and/or to determine when the pump can be started, the chilldown characteristics of the J-2S engine inlet lines were determined during a warm engine start. The pump inlet vapor fraction and the pump inlet flow temperature were predicted for two different types of flow transients. For each case, the pump inlet quality reached 2 percent within 60 seconds. Since this is approaching the quality at which pump operation is possible, a hydrogen turbopump

start should be possible in less than 2 minutes after propellant flow begins. In addition, a computer model for predicting engine start transients was developed. Using a simplified two-phase pump performance prediction system, the effects of pump two-phase flow and cooling tube heat transfer on engine start transients were evaluated. For both cases, the start times were increased and additional control sequencing was required. However, engine operation at a reduced level with mixed-phase propellants was possible.

PUMPING CAPABILITY

TWO-PHASE FLOW IN INLET LINE, COLD PUMP

During an engine start with a warm inlet line, vapor can be generated by two processes (1) heat transfer from the warm inlet line can vaporize some of the LH_2 before it reaches the pump, and (2) cavitation on low-pressure regions of the pump flow passages can vaporize some of the LH_2 within the pump. In this analysis, the amount of vapor generated by cavitation was assumed to be negligible as long as the pump was operating near its design liquid flow coefficient. Mark 15 LH_2 and Mark 25 pump two-phase test results verify this assumption as long as the liquid flow coefficient is not too high.

Preliminary Theoretical Analyses

Before any two-phase test data were obtained, various theoretical analyses of two-phase flow phenomena were conducted to obtain an understanding of two-phase flow problems and to assist in analyzing the anticipated test results. The two types of flow processes that theoretically form the boundaries of the real flow situation and the acoustic velocities for these two types of flow processes were investigated. These investigations were then used in developing an ideal pump performance prediction system for each flow process. In addition, a shock wave study was conducted to determine whether shock waves occur and, if so, to determine their possible effects on pump performance.

Flow Processes. The two types of flow processes that theoretically form the boundaries of a real homogeneous flow process are equilibrium and constant quality. The difference between the two is in the assumption of the vaporization and condensation rates. In the equilibrium case, these rates are assumed to be high enough to maintain equilibrium between the vapor and the liquid phases. Consequently, the vapor temperature is always equal to the liquid temperature, both phases are always at saturation, and the quality (vapor fraction by weight) varies with pressure

changes. An isentropic, equilibrium compression is illustrated by line 1-2 of Fig. 1.

For a constant quality flow process, the condensation and vaporization rates are assumed to be so low that no phase change takes place. Consequently, the quality remains constant throughout such a flow process, the temperatures of the two phases become different as the pressure varies from the initial state and, as shown in Fig. 1, an isentropic compression will subcool the liquid (line 3-4) and superheat the vapor (line 5-6). An excellent treatment of the constant quality flow process is presented in Ref. 2.

In a third type of process, the two phases flow separately, maintain thermal equilibrium, and choke when the vapor phase chokes. This is called the separated phase, thermal equilibrium model and was not treated here because the Reynolds number of hydrogen flow was felt to be high enough to maintain high turbulence and, consequently, homogeneity. This should be particularly true within the pump flow passages.

Various two-phase choking mass flowrate experimental test results are summarized and compared with each other and with theoretical predictions in Ref. 3 and 4. In general, the constant quality and the equilibrium flow processes bracket most of the test results for qualities below 10 percent. At higher qualities, the separated phase model appears to be more applicable. Since the qualities of interest in hydrogen pumping seldom exceed 3 percent (45 percent vapor by volume at 30 psia), the proper flow process for this study is, again, probably not separated phase.

In Ref. 3, a two-phase water study indicates that at low qualities, the bubble growth rate is insufficient to maintain equilibrium and, at qualities below 1 percent, is so low that a constant quality flow process is probably approached. This is of interest because, in 30-psia hydrogen, 1 percent quality equals 21 percent vapor by volume.

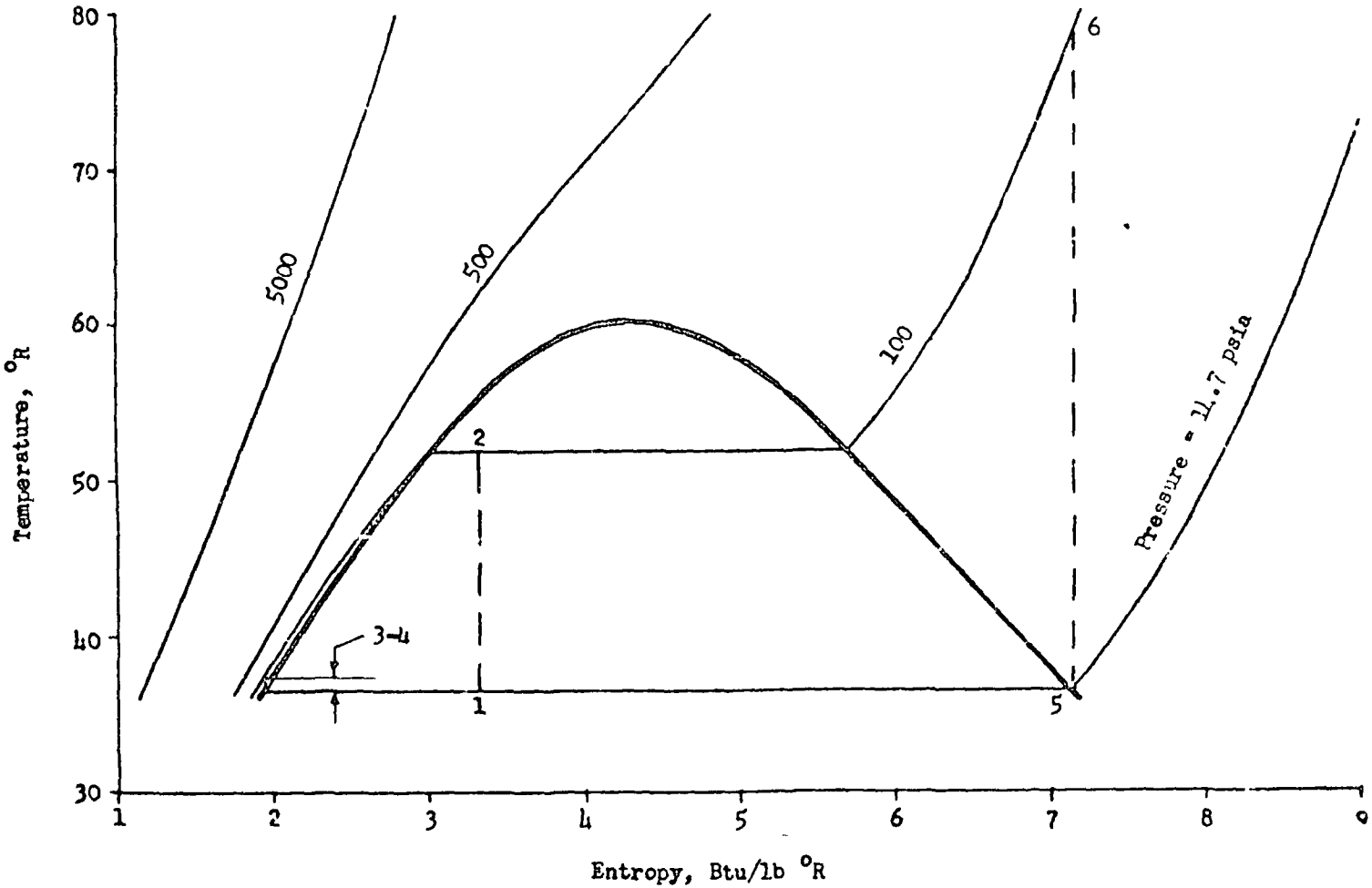

Figure 1 Temperature--Entropy Chart for Hydrogen

H B. Karplus (Armour Research Foundation, Illinois Institute of Technology) measured the propagation velocity of a finite amplitude pressure wave through a two-phase boiling water mixture His test results, which were reported in Ref 5, cover the vapor volume fraction range from 0 to 50 percent Although not noted in Ref 5, his results agree extremely well with the acoustic velocity prediction for a constant quality flow process

Some choking mass flowrate experimental test results in two-phase hydrogen were presented and compared with various two-phase flow process models in Ref. 6 . The final portion of the flow path was a 17.78-inch-long tube with a constant ID of 0.844 inch (L/D = 21) At discharge pressures below 3 atmospheres, the test mass flowrates are greater than the equilibrium model, less than the separated phase, vapor choking model, and agree quite well with the metastable model in which the flow follows an equilibrium flow process until choking occurs and then accelerates at constant quality until constant quality choking occurs.

It may be concluded from these studies that low-quality, two-phase hydrogen will approach equilibrium when passing at subsonic velocities through a long, constant-diameter duct. An example of such a case is the duct that carries hydrogen to the J-2 engine fuel pump (Mark 15 LH_2 pump). However, two-phase hydrogen will probably approach a constant quality flow process when passing through any sudden area contraction because it will not have enough time to reach equilibrium. An example of this case is the area contraction at the Mark 15 LH_2 pump inlet in which the pump inlet area is 81 percent of the duct area.

When passing through the pump, the flow velocities are so high and the area changes are so sudden that two-phase hydrogen will probably follow a constant quality flow process until the pressure becomes high enough to force a relatively gradual condensation. In other words, the condensation rates within a hydrogen pump should be much less than required to maintain equilibrium. Under such a flow process, the pump pressure rise

should be somewhat greater than that predicted by a constant quality flow process, but should have the same general trend.

As will be shown in the two-phase test data analysis section of this report, the use of these three flow models (i.e., equilibrium flow in the inlet duct, constant quality flow through the area contraction at the pump inlet, and gradual condensation within the pump) produces good agreement with the Mark 15 LH_2 and Mark 25 pump two-phase hydrogen test results. In addition, none of the other combinations of flow processes considered show satisfactory agreement.

Acoustic Velocities. In two-phase flow, the acoustic velocity is generally much lower than the value for either the pure liquid or the pure vapor phases. In addition, the type of flow process strongly effects the acoustic velocity at vapor volume fractions below 50 percent. Therefore, the two-phase flow Mach numbers in the inlet line are high, and, depending upon the type of flow process, choking can occur. Consequently, to avoid inlet line choking and the corresponding flow limitation, it is important to know both the type of flow process and the corresponding acoustic velocity.

The equilibrium and the constant quality flow processes have the two extremes in acoustic velocity for low-quality, two-phase flow. In equilibrium flow, a given pressure drop will cause vaporization as well as an expansion of the existing vapor. This will cause a relatively large drop in density because the vapor-to-liquid density ratio is very small (approximately 0.04 in 30-psia hydrogen). Therefore, referring to the general expression for acoustic velocity (Eq. 1), the acoustic velocity is relatively low because the partial derivative is small.

$$c = \sqrt{g\,(\partial P/\partial \rho)_s} \qquad (1)$$

In constant quality flow, however, no vaporization occurs and any density change is due to expansion of the existing vapor. As a result, the partial

derivative in Eq. 1 is larger than for equilibrium flow and, consequently, the acoustic velocity is much higher.

Equation 2 is the general expression for the acoustic velocity in two-phase flow

$$c = \frac{1 + x\left(\frac{\rho L}{\rho V} - 1\right)}{\sqrt{\frac{x}{c_v^2}\left(\frac{\rho L}{\rho V}\right)^2 - \frac{\rho L}{g}\left(\frac{\rho L}{\rho V} - 1\right)\left(\frac{\partial v}{\partial P}\right)_s}} \qquad (2)$$

with an incompressible liquid phase. Note that the partial derivative in the denominator is zero for constant quality flow and, for equilibrium flow, is both finite and negative, thereby increasing the denominator and decreasing the acoustic velocity. This illustrates more graphically the effect of flow process.

By correlating the hydrogen properties from Ref 7 linearly, substituting the correlations into Eq 2, and converting quality to vapor volume fraction, the expressions for acoustic velocity in both equilibrium and constant quality flow processes were obtained (Eq. 3 and 4, respectively).

$$c_{LQ} = \frac{901}{\sqrt{\left[R - \alpha\,(R-1)\right]\left\{\alpha + \frac{\left(1 - \frac{1}{R}\right)\left[2.21\,R\,(1-\alpha) - 3.18\,\alpha\right]}{(11.23 - 0.1659\,T)^2}\right\}}} \qquad (3)$$

$$c_{C\lambda} = \frac{901}{\sqrt{\alpha\left[R - \alpha\,(R-1)\right]\left(1 - \frac{14.2}{T}\right)}} \qquad (4)$$

where

$$R = \rho L/\rho V = 770/P \qquad (5)$$

Figure 2 , which was generated from these equations, illustrates the effects of flow process, vapor volume fraction, and saturation pressure on two-phase acoustic velocity. For constant quality flow, the acoustic velocity approaches the single-phase values at vapor volume fractions of 0 and 100 percent and reaches a minimum at approximately 50 percent vapor volume fraction. For equilibrium flow, the acoustic velocity reaches a minimum at 0 vapor fraction, thereby creating a discontinuity between the pure liquid and the two-phase values at that vapor fraction. Both the equilibrium and the constant quality values increase with increasing static pressure.

The minimum equilibrium value is approximately 25 percent of the minimum constant quality value and, at 15 psia, is approaching the flow velocity through a hydrogen pump inlet duct. Since the flow process in the duct is probably close to equilibrium, this indicates that choking is a definite possibility in extremely low pump inlet pressure applications. Therefore, an inlet duct acoustic velocity check should be made when designing such a system. Choking in the pump inlet annulus should not be a problem because two-phase hydrogen appears to follow a constant quality flow process in a sudden contraction and, as shown in Fig. 2 , the acoustic velocity in a constant quality flow process is much higher.

Theoretical Performance Maps. Before any two-phase hydrogen pump test data were obtained, two pump performance map prediction systems were developed, one for a constant quality flow process through the pump and the other for an equilibrium flow process. For both cases, homogeneous, isentropic flow was assumed throughout the pump. In addition, because of the exceedingly sharp leading edges on the inducer, shock wave effects were assumed to be negligible and, consequently, a supersonic flow entering the inducer was assumed to be accelerated by the expanding area. As a result, the two-phase pumping limit was predicted to be a relative Mach number of one at the inducer leading edge rms diameter.

The flow equations for these two-phase pump performance prediction systems are shown in Tables 1 and 2 , and the corresponding computer program flow

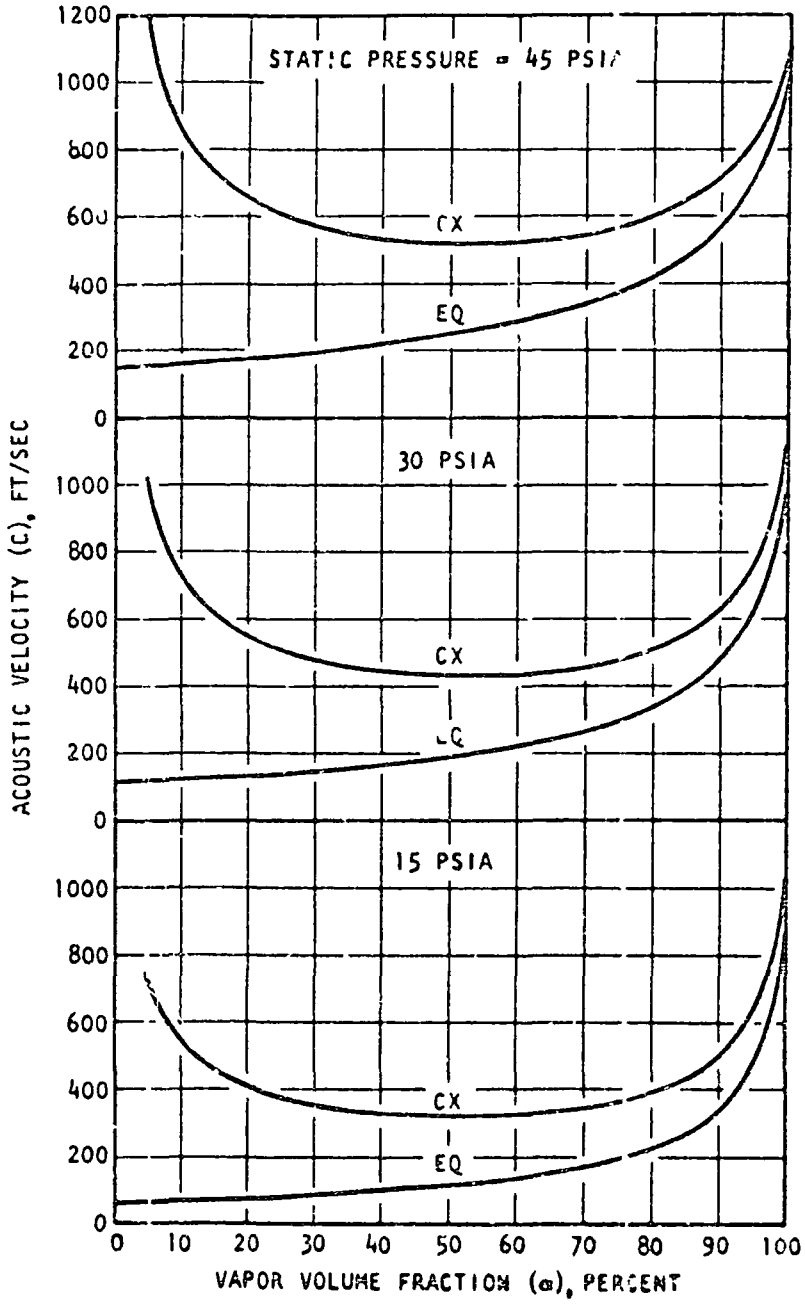

Figure 2 Two-Phase Hydrogen Acoustic Velocities

TABLE 1

EQUATIONS FOR EQUILIBRIUM TWO-PHASE HYDROGEN FLOW ANALYSIS

Description	Equations
Area Ratio	$\frac{A_2}{A_1} = \frac{\rho_1 h_1}{\rho_2 h_2}$
Density Ratio	$\frac{\rho_1}{\rho_2} = \frac{1 + \lambda_2\left(\frac{770}{P_2} - 1\right)}{1 + \lambda_1\left(\frac{770}{P_1} - 1\right)}$
Discharge Pressure	$P_2 = 14.7 e^{0.347 I_2^2 - 0.00276 I_2^2 - 0.27}$
Discharge Quality	$\lambda_2 = \frac{0.0269 (H_1 - H_2) + \lambda_1 (11.5 - 0.139 I_1)}{11.5 - 0.139 I_2}$
Relative Velocity Ratio	$\frac{h_2}{h_1} = \sqrt{\frac{(\lambda_2 v_{fg}^2 + v_f^2 - \lambda_2 v_f^2 - v_1) \rho_{11}}{\rho_{12} - \frac{\rho_1^2}{\rho_2}}}$
Exit Pipe Check	$A_2 = A_1 \left[0.0269 (H_2 - H_2^2) + \lambda_2 (H_2 - H_1) (11.5 + \lambda_2 I_2 - \lambda_1 I_1)\right.$ $\left. - 0.139 (\lambda_2 I_2 - \lambda_1 I_1^2) + 0.139 (\lambda_2 P_2 - \lambda_1 P_1)\right] \frac{1}{(\lambda_2 - \lambda_1)}$

Equations for CONSTANT QUALITY TWO-PHASE HYDROGEN

Description	Equations
Area Ratio	$\frac{A_2}{A_1} = \frac{\rho_1 V_1}{\rho_2 V_2}$
Density Ratio	$\frac{\rho_1}{\rho_2} = \frac{1 - \frac{\rho_1}{\rho_{v1}} \frac{x_1}{1 - x_1}\left(\frac{P_1}{P_2}\right)^{1/\gamma}}{1 + \frac{\rho_1}{\rho_{v1}} \frac{x_1}{1 - x_1}}$
Discharge Pressure	$P_2 = P_1 \left(\frac{P_2}{P_1}\right)$
Discharge Quality	$x_2 = x_1$
Relative Velocity Ratio	$\frac{w_2}{w_1} = \sqrt{\frac{(\theta_2 d_{1T})^2 - \phi_{1T}^2 - 2gJ(h_2 - h_1)/U_{1T}^2}{\phi_{1T}^2 + \frac{1 - x_1^2}{x_1}}}$
Enthalpy Change	$h_2 - h_1 = (1 - x_1)\left(\frac{144 P_1}{\rho_1}\right)\left(\frac{P_2}{P_1} - 1\right) + x_1 C_s T_1 \left[\left(\frac{P_2}{P_1}\right)^{\frac{\gamma-1}{\gamma}} - 1\right]$
Vapor Density	$\rho_{v1} = \frac{144 P_1}{RT_1}$
Gas Constant	$R = 770$
Vapor Specific Heat (Isentropic Process)	$C_s = 2.4$
Vapor Specific Heat Ratio	$\gamma = \frac{1}{1 - \frac{1}{C_s J}} = 1.087$

charts are shown in Fig. 3 and 4. Figures 5 and 6 are the equilibrium total pressure performance maps for a centrifugal pump with inlet qualities of 0.1 and 1.0 percent (4 and 34 percent vapor volume fraction), respectively, and Fig 7 and 8 are corresponding constant quality total pressure performance maps For comparison, the pure liquid performance map is shown in Fig 9

After observing the Mark 15 LH_2 and the Mark 25 pump two-phase test data, it may be concluded that the subacoustic velocity portions of the two performance map prediction systems would have bracketed the test data if on- and off-design pump efficiency effects had been included. However, the points of sudden performance deterioration that were predicted by the two programs did not correlate with the test results At the high test rotational speeds, the equilibrium program predicts performance deterioration with a saturated liquid (0 percent vapor) at the pump inlet whereas the test results indicated deterioration in the 25 to 40 percent vapor volume fraction range. The constant quality program predicted limiting vapor volume fractions in the 10- to 25-percent vapor volume fraction range at a limiting inlet relative Mach number of 1.0 and in the 20- to 50-percent range at a relative Mach number of 1.2 However, although the ranges were similar, the individual Mark 25 pump two-phase tests did not correlate with the constant quality relative Mach number theory. This lack of correlation is shown in the two-phase test data analysis section of this report

It may be concluded that some flow phenomena such as shock waves or flow stratification must occur within hydrogen pumps in such a way that the average relative flow velocities are kept below the acoustic velocity.

Shock Waves. The effects of two types of shock wave patterns on the performance of a flat-plate inducer were analyzed For one wave pattern a normal shock was assumed to occur before the flow was turned and, for the other, the normal shock was assumed to occur after turning. An

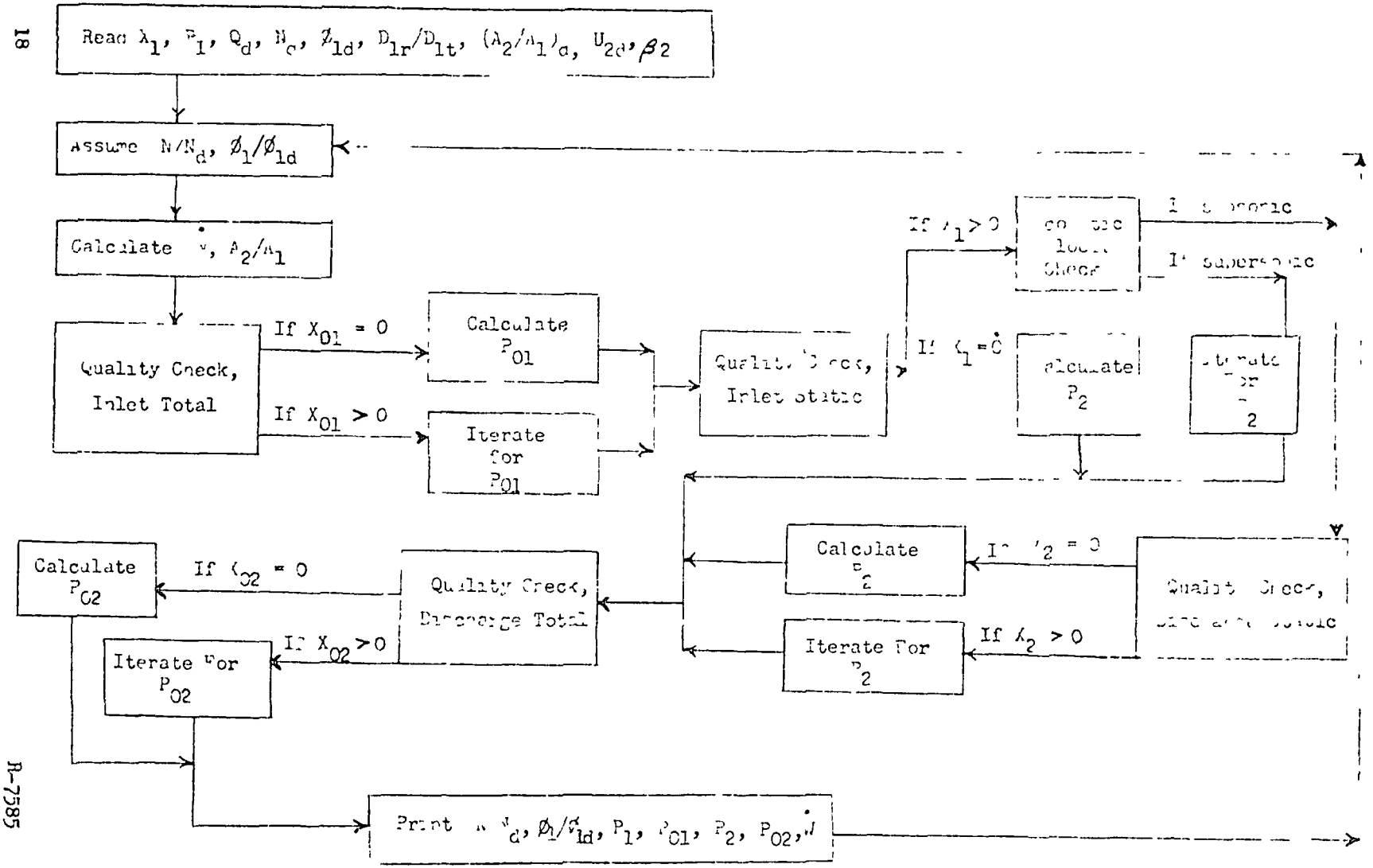

Figure 3 Flow Chart for Equilibrium Flow Process Pump Performance Prediction Program

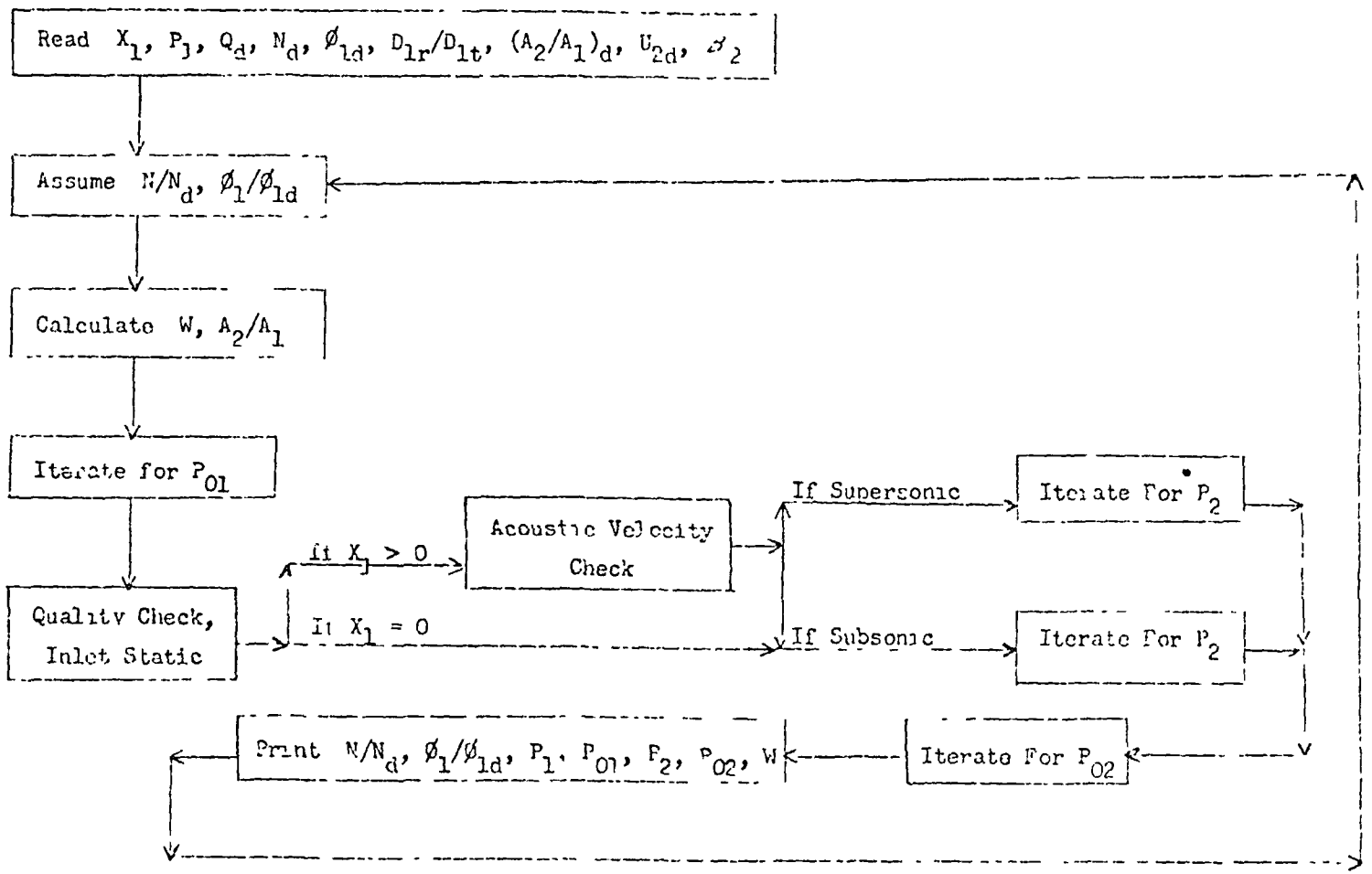

Figure 4. Flow Chart for Constant Quality Flow Process Pump Performance Prediction Program

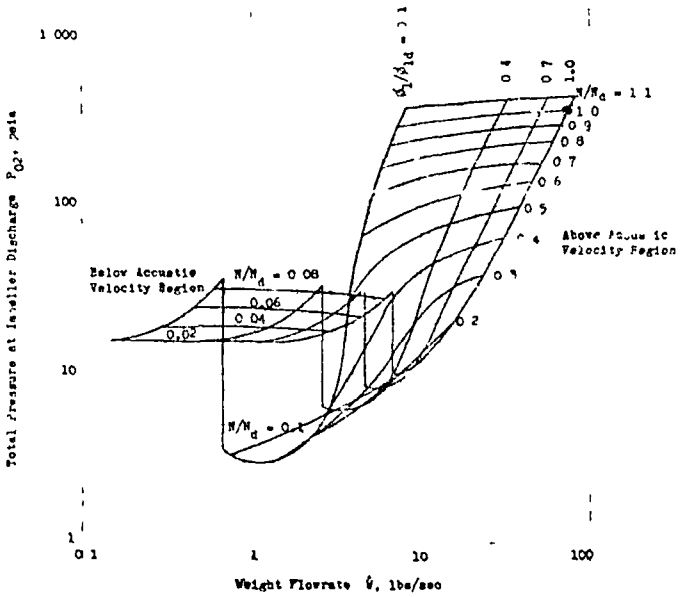

Figure 5. Hydrogen Pump Total Pressure Performance Map for an Equilibrium Flow Process With an Inlet Quality (χ_1) of 0.1 percent

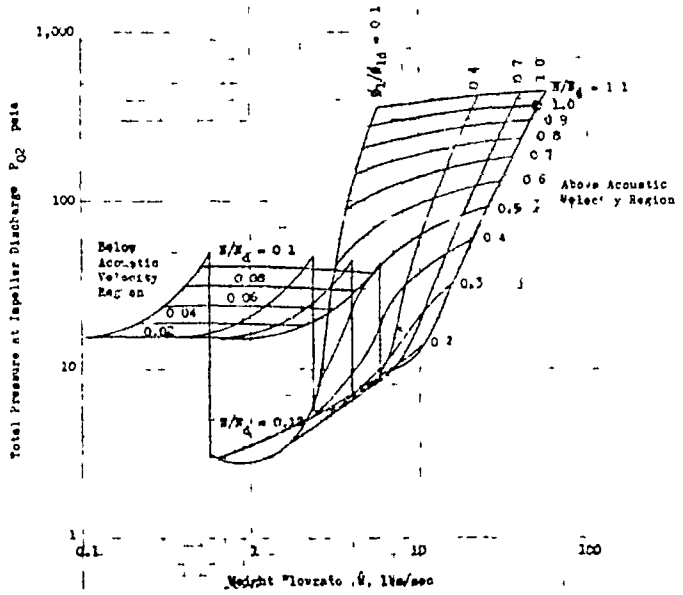

Figure 6. Hydrogen Pump Total Pressure Performance Map for an Equilibrium Flow Process With an Inlet Quality (χ_1) of 1.0 Percent

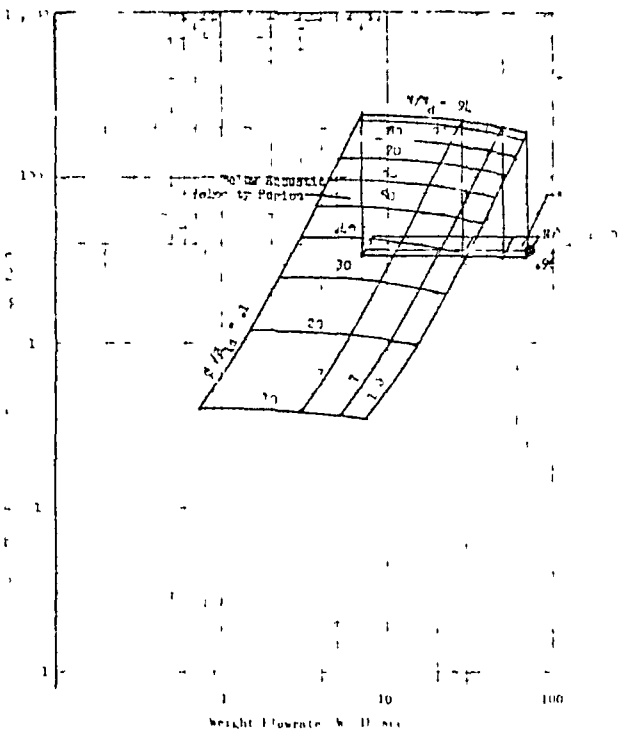

Figure 7. Hydrogen Pump Total Pressure Performance Map for a Constant Quality Flow Process With an Inlet Quality (X_1) of 0.1 Percent

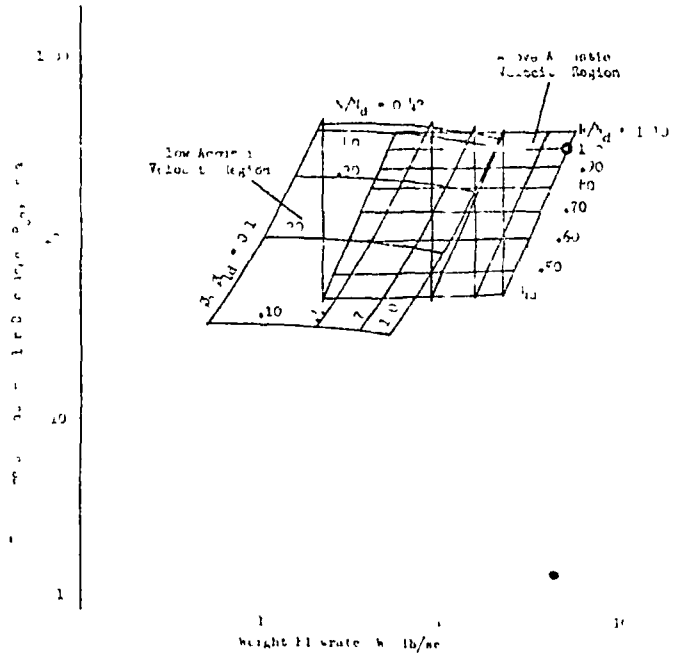

Figure 8. Hydrogen Pump Total Pressure Performance Map for a Constant Quality Flow Process With an Inlet Quality (X_1) of 1 Percent

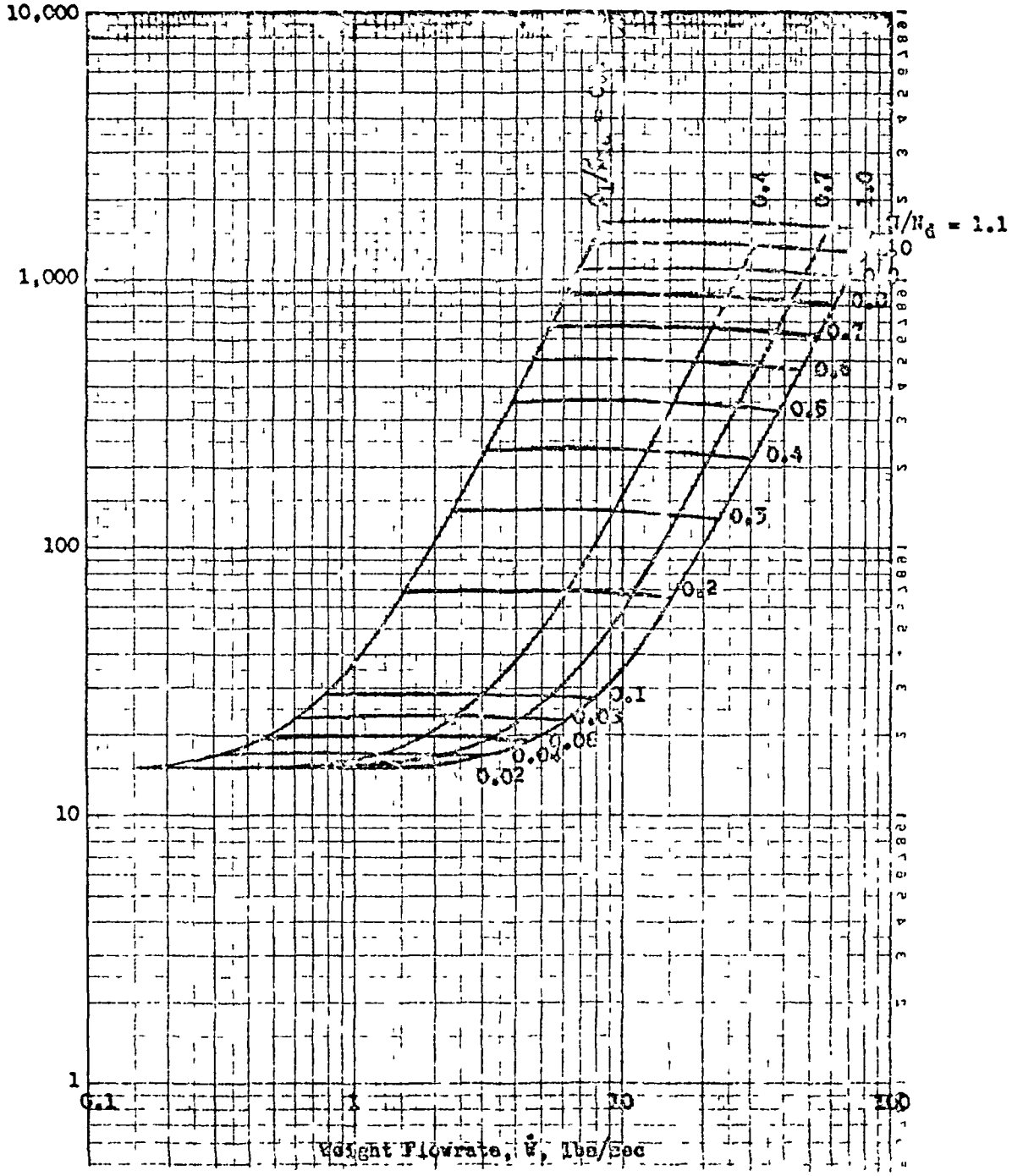

Figure 9. Hydrogen Pump Static Pressure Performance Map for an Equilibrium Flow Process With an Inlet Quality (X_1) of 0 0 Percent

equilibrium flow process was assumed for both cases As a result, the flow downstream of the shock was a pure liquid because, referring to Fig 2 , the equilibrium acoustic velocities at lower than freestream vapor fractions are less than the freestream acoustic velocity and, consequently, the only way to achieve subsonic flow is to shock down to a pure liquid which has an exceedingly high acoustic velocity

For the initial wave pattern (normal shock before turning), the pressure rise dropped gradually with increasing vapor fraction to 85 percent of the liquid value at a vapor volume fraction of 50 percent. For the other wave pattern (normal shock after turning), the pressure rise dropped to 80 percent of the liquid value at the first trace of vapor and then increased slightly to 82 percent as the vapor volume fraction was increased to 20 percent Because flat-plate inducer pressure rise normally represents only 5 to 10 percent of the pump overall pressure rise, these values of pressure loss would cause a drop in pump discharge pressure of only 1 to 2 percent Since shocks in which the downstream flow is a liquid should have the most severe losses and since the overall pump performance deterioration was very slight and very gradual, the abrupt deteriorations observed during the two-phase pump testing were probably not due to shock wave losses at the pump inlet.

Pump inlet shock waves should actually improve pump performance by preventing a supersonic expansion downstream of the inlet and by increasing the flow density which, in turn, increases the pumping capability of the downstream portions of the rotor. Reference 8 indicates that both normal and oblique shock waves do exist in two-phase flow and that they follow theoretical relationships over a wide range of Mach numbers and vapor volume fractions. The flow process treated in Ref. 8 was constant quality because the two phases were formed by injecting gaseous nitrogen into water. The constant quality theoretical approach may also apply to low-quality, single-component, two-phase flows such as two-phase hydrogen because other flow process observations previously discussed (Ref. 3 through 5 , as well as the Mark 15 LH_2 and Mark 25 pump two-phase test

data analyses) indicate that, in low quality flow, the vaporization and condensation rates are too low to permit much phase change during sudden transitions.

Test Data Analysis

To determine which analytical model predicts two-phase pump performance, the available two-phase hydrogen pump test data were analyzed. The three sources of this data were the Mark 15 LH_2 pump heated hydrogen testing that was conducted by Rocketdyne at the Santa Susana Field Laboratory under the J-2X program, the Mark 25 pump testing that was conducted by Nuclear Rocket Development Station, Nevada, under the University of California (Contract No. CTZ 39600-4), and the inducer testing that was conducted by NASA, Lewis Research Center (Ref. 9).

Mark 15-LH_2 Pump. The equipment used to measure pump inlet quality for the Mark 15 LH_2 pump heated hydrogen two-phase testing is shown schematically in Fig. 10. During the two-phase testing a pure liquid was maintained upstream of the 8-inch screen (station 7). The liquid state conditions at station 7 were obtained by measuring the static pressure and temperature. A pressure drop across the screen converted the pure liquid upstream to a two-phase mixture downstream. The static pressure in the two-phase region was measured close to the pump inlet (stations 1 and 3). A distance of 7 feet between the screen and the downstream pressure measurements was used to allow the two-phase hydrogen to reach equilibrium after passing through the screen.

The static pressure and temperature measurements were used to determine the enthalpy of the liquid upstream of the screen (station 7). Assuming that no energy was removed between station 7 and station 1, the total enthalpy at station 1 must equal the total enthalpy at station 7. Consequently, referring to a hydrogen T-S diagram, the intersection of the pump inlet static pressure (measured at station 1) and the constant enthalpy line yields the two-phase fluid state conditions at the pump

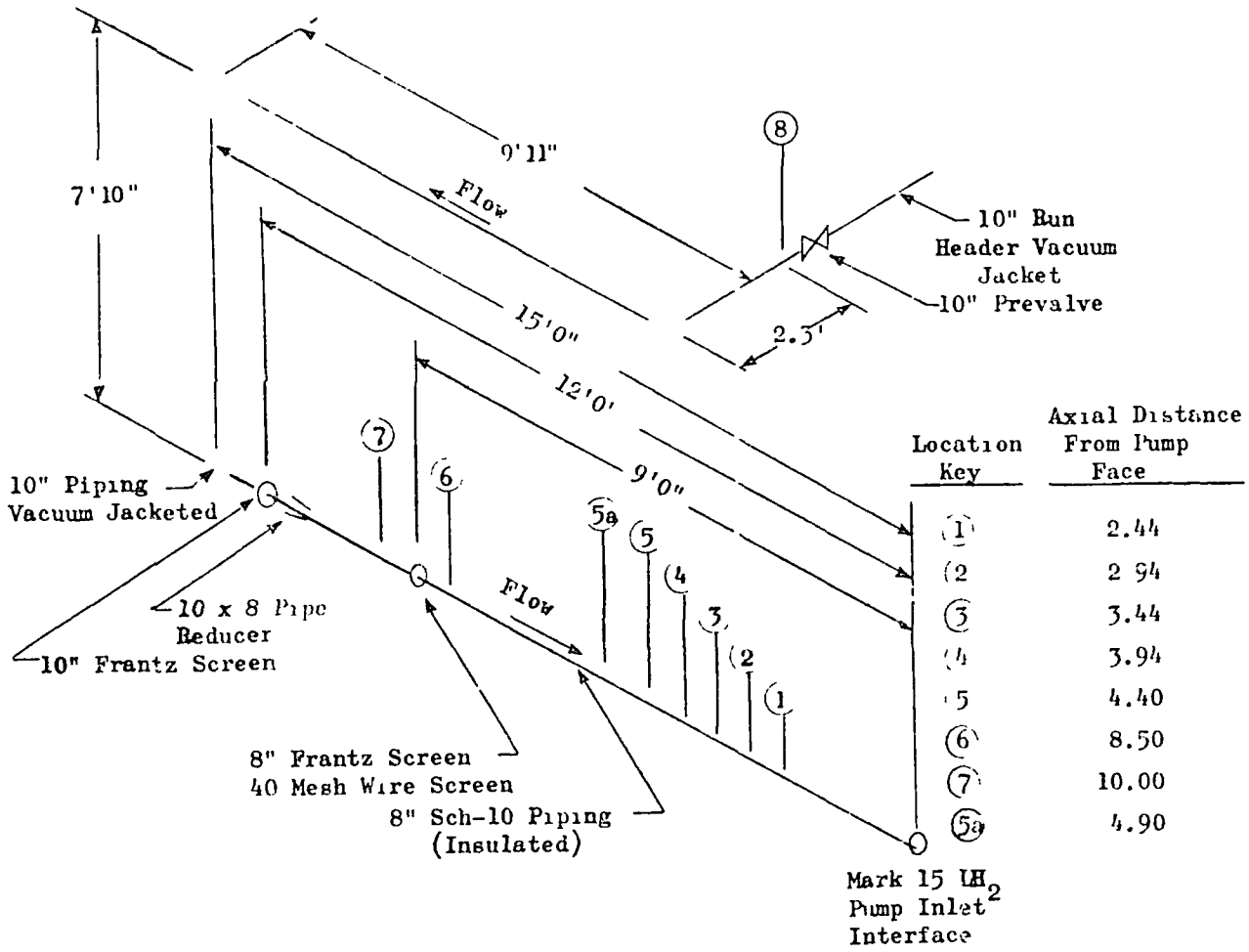

Location Key	Axial Distance From Pump Face
1	2.44
2	2 94
3	3.44
4	3.94
5	4.40
6	8.50
7	10.00
5a	4.90

Parameter	Location	Range	Transducer Type/Spec.
Inlet Static Pressure 1	1	100 psig	NA5-27247-1
2	3	100	
3	4	50	
4	5	50	
5	7	100	
6	8	100	
7	8	100	
8	2	100	
Inlet Total Pressure	6 7	100	
Inlet Screen Delta Pressure	4	10 psid	NA5-27279-1
Inlet Temperature 1	7	-403 to -440 F	Rosemount Model 134AH-22
2	7		Rosemount Model 134AH-22
3	7		Rosemount Model 134FK-22
4	8		Rosemount Model 134FK-22
5	5a		Rosemount Model 134FK-22

Figure 10. CTL-5, Cell 3b, LH_2 Inlet Duct Instrumentation Schematic

inlet and, therefore, yields both the quality and the vapor volume fraction at the pump inlet.

From the energy equation, the flow process between stations 7 and 1 is constant total enthalpy. However, to avoid extensive iteration, a constant static enthalpy flow process was used in reducing the data. Figures 11 and 12 indicate that this is a reasonable approximation because, for an extreme test condition of a static pressure drop of 6 psi, an upstream static pressure of 15 psia (9 psia at the pump inlet), and an upstream velocity of 50 ft/sec, the error in quality is 11 percent and the error in vapor volume fraction is less than 3 percent. At the more typical test point of a static pressure drop of 5 psi, an upstream static pressure of 30 psia (25 psia at the pump inlet), and an upstream velocity of 50 ft/sec, the error in quality is only 4 percent and the error in vapor volume fraction is less than 2 percent. Figures 11 and 12 also indicate that over the vapor fraction range of interest, the static pressure drop is large enough to be measured accurately.

From the above comments, it may be concluded that this approach will give accurate results if (1) the inlet pipe has enough insulation to maintain a constant enthalpy process, (2) the inlet pipe is long enough to permit the two-phase hydrogen to reach equilibrium, and (3) the instrumentation is accurate enough to locate the fluid state conditions on a T-S diagram.

The Mark 15 LH_2 pump test results for discharge volume flowrates of 8200 and 8600 gpm are presented in Fig. 13 and 14, respectively. As indicated, the total pressure rise fraction gradually decreased with increasing line vapor volume fraction until a total pressure rise fraction between 90 and 95 percent was reached. It then dropped suddenly, thereby indicating some sort of hydrodynamic limit. Increasing the pump inlet temperature increased the vapor volume fraction at which this hydrodynamic limit occurred. For a given inlet temperature, the vapor fraction at the hydrodynamic limit (Fig. 13 and 14) can be approximated by the vapor

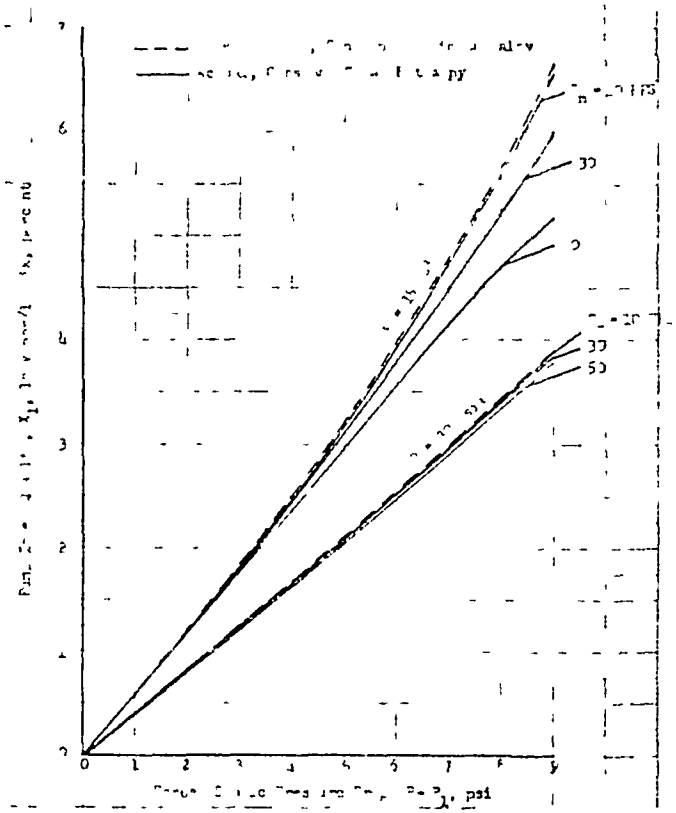

Figure 11. Effect of Constant Static Enthalpy Assumption on Quality

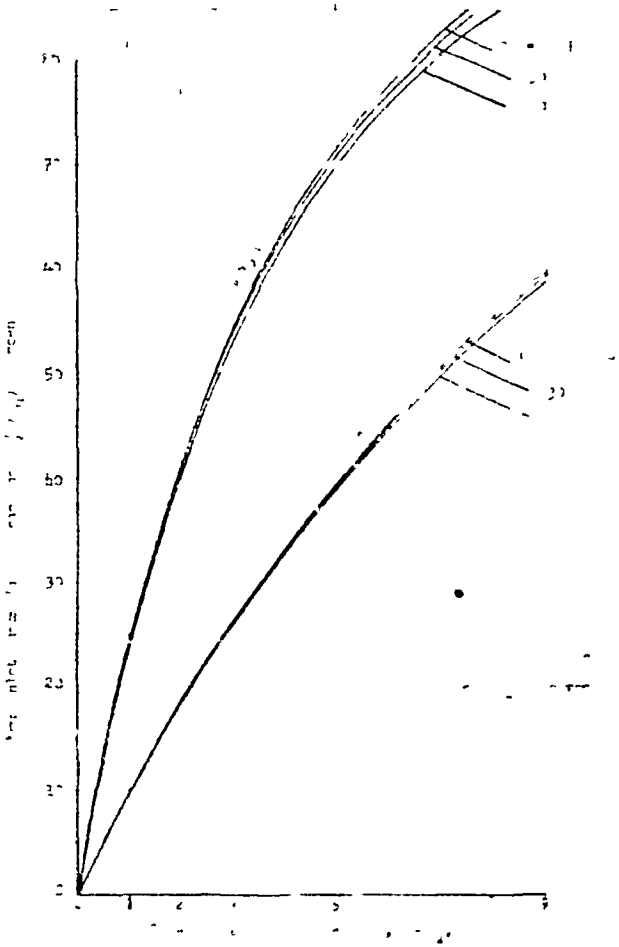

Figure 12. Effect of Constant Static Enthalpy Assumption on Vapor Volume Fraction

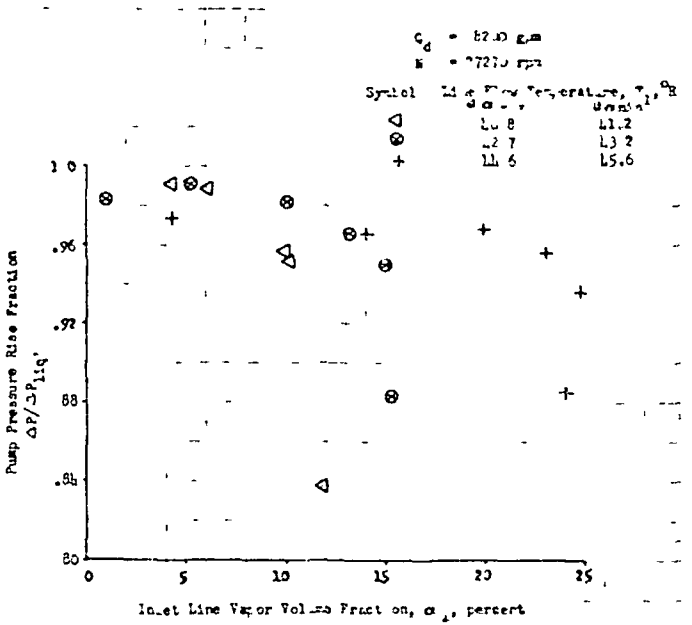

Figure 13. Mark 15-F Pump Two-Phase Test Data at 8200-gpm Discharge Flowrate

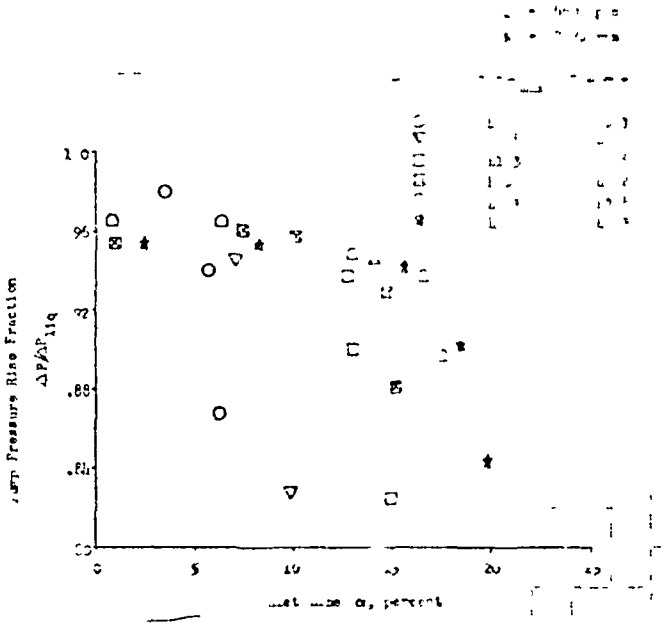

Figure 14. Mark 15-F Pump Two-Phase Test Data at 8600-gpm Discharge Flowrate

were at a total pressure rise fraction of 90 percent (i.e., 10 percent pressure drop). These 10 percent pressure drop data points indicate the inlet line conditions at which the hydrodynamic limit occurred and are shown as a function of inlet line hydrogen temperature in Fig. 15.

Analysis of these test data have been complicated by two factors: (1) the area contraction of 15 percent between the inlet line and the inducer inlet annulus, and (2) the bearing flow that recirculates back into the inducer inlet. Therefore, the inducer inlet conditions at the 10 percent total pressure drop test points (Fig. 15) were calculated over a range of recirculated flowrates by assuming both constant quality and equilibrium flow processes through the inlet contraction. The recirculated flow was assumed to be a pure saturated vapor at the pump inlet because the pump discharge flow, after throttling to the pump inlet pressure, is in excess of 80 percent quality. Since the bearing coolant flowrate has been estimated to be 0.50 lb/sec, the recirculated flowrate was assumed to range between 0 and 1.0 lb/sec.

Using these assumptions, the most probable correlating parameters for two-phase pumping were calculated. The parameters for the constant quality flow process through the contraction are shown in Fig. 16 through 18, and for the equilibrium flow process, in Fig. 19 through 21. For the constant quality flow process, Fig. 16 indicates that a constant quality relative Mach number of between 1.1 and 1.3 is a good correlating parameter if the recirculated flow is 0.25 lb/sec, Fig. 17 indicates that the inlet line is not choked, and Fig. 18 indicates that an inlet vapor fraction of between 30 and 35 percent is a good correlating parameter if the recirculated flow is 1.0 lb/sec. For the equilibrium flow process through the contraction, Fig. 19 indicates that the constant quality relative Mach number is not a good correlating parameter because it varies too much, Fig. 20 indicates that the pumping limit is not due to choking in the inlet annulus because choking is indicated at only one data point, and Fig. 21 indicates that a pump inlet vapor volume fraction of between 25 and 30 percent is a possible correlating parameter if the recirculated flow is not too great.

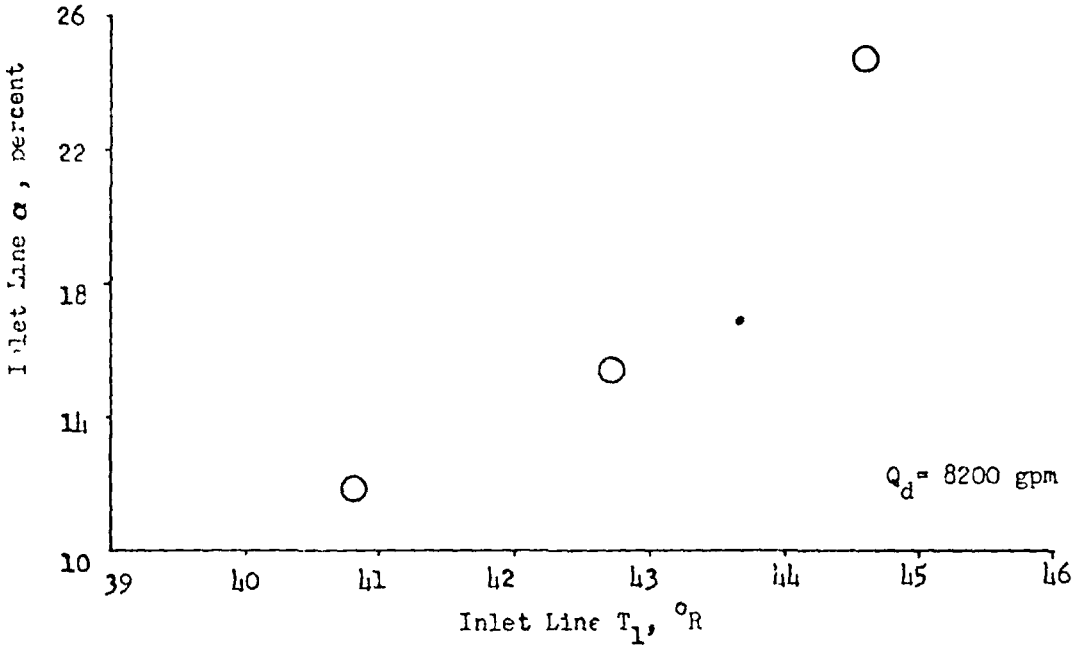

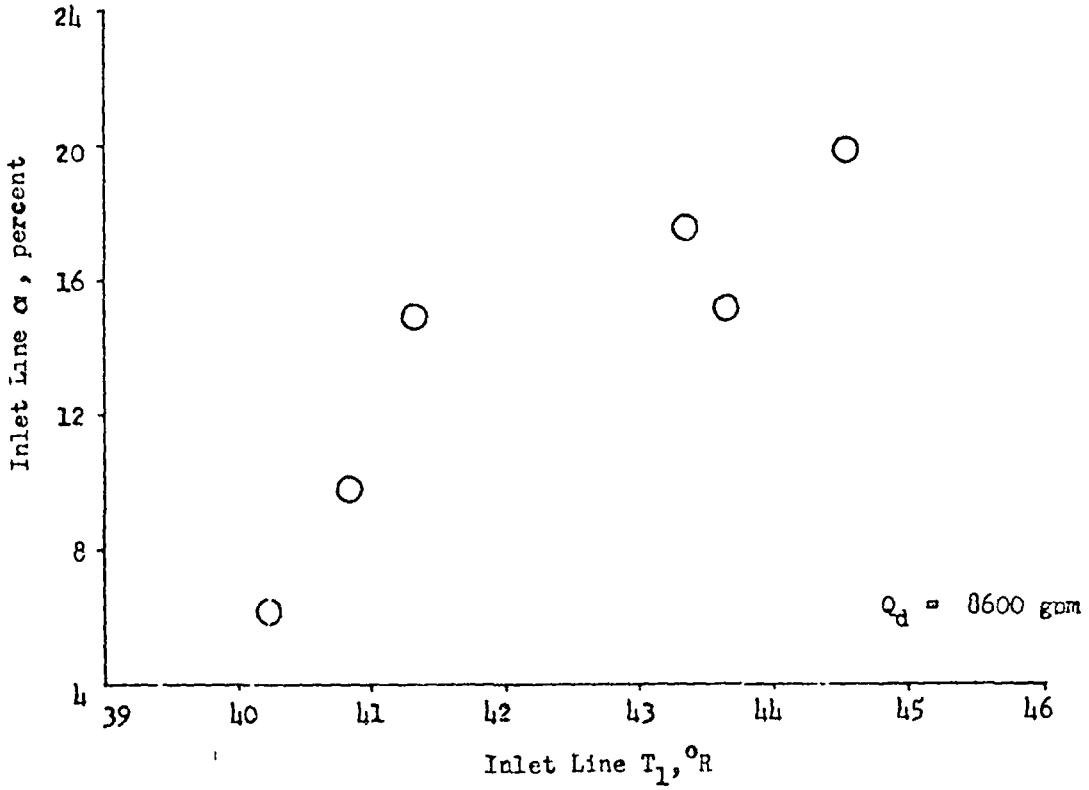

Figure 15 Mark 15-F Pump Two-Phase Test Data at a Pressure Rise of 90 Percent of the Liquid Value

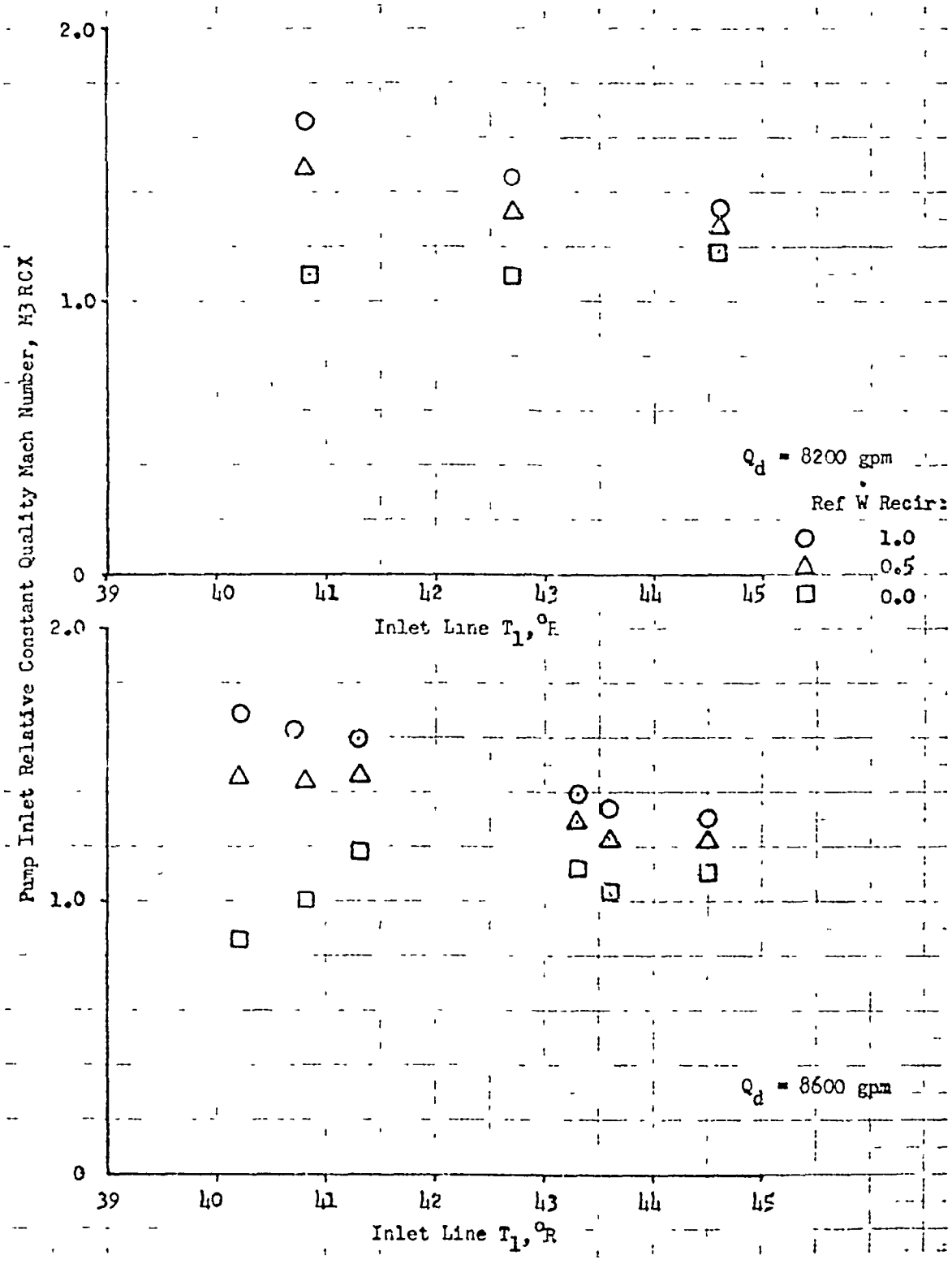

Figure 16 Mark 15-F Pump Inlet Relative Constant Quality Mach Numbers for a Constant Quality Flow Process Through the Inlet Contraction

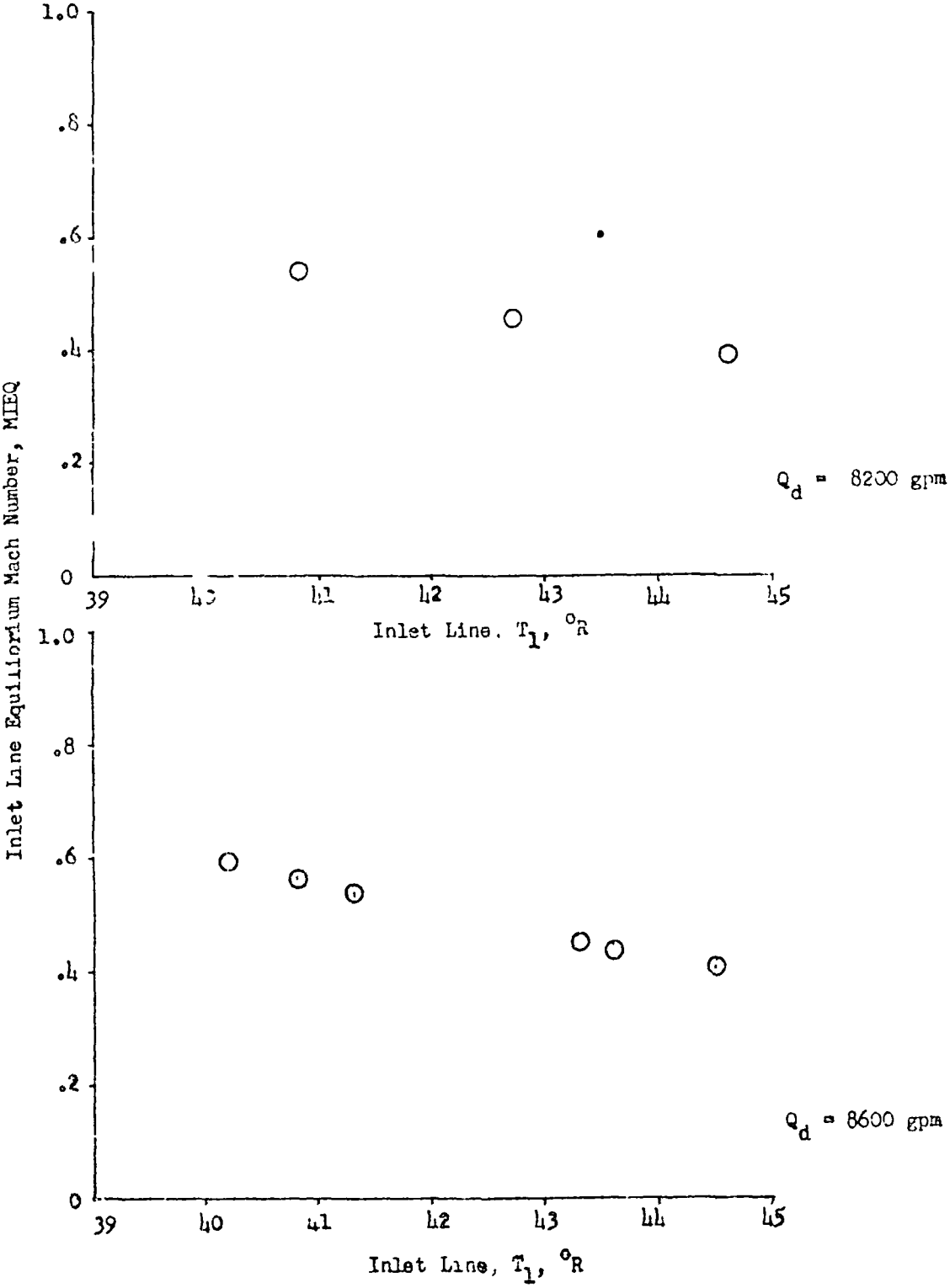

Figure 17 Mark 15-F Pump Inlet Line Equilibrium Mach Numbers

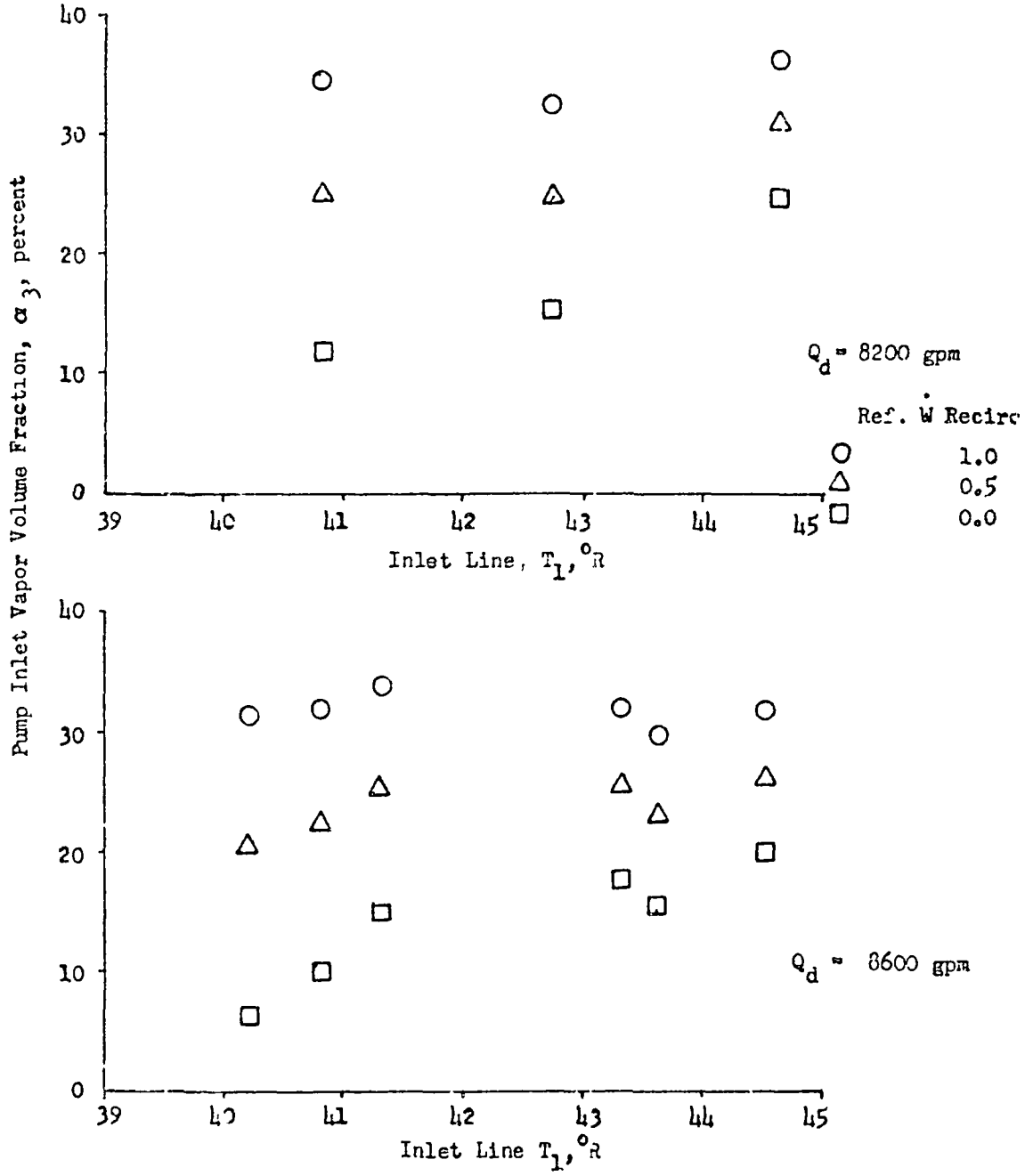

Figure 18 Mark 15-F Pump Inlet Vapor Volume Fraction for a Constant Quality Flow Process Through the Inlet Contraction

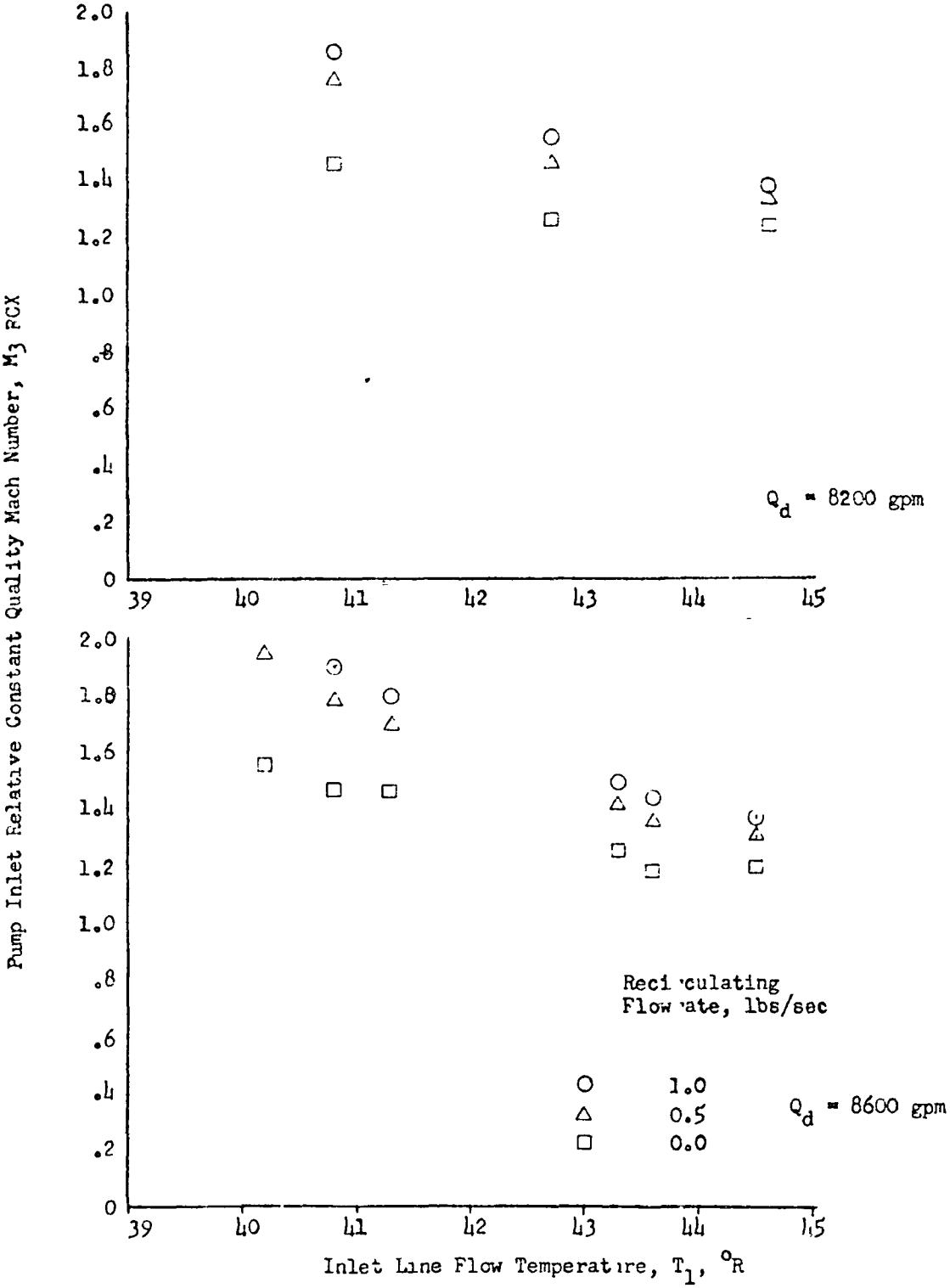

Figure 19 Mark 15-F Pump Inlet Relative Constant Quality Mach Numbers for an Equilibrium Flow Process Through the Inlet Contraction

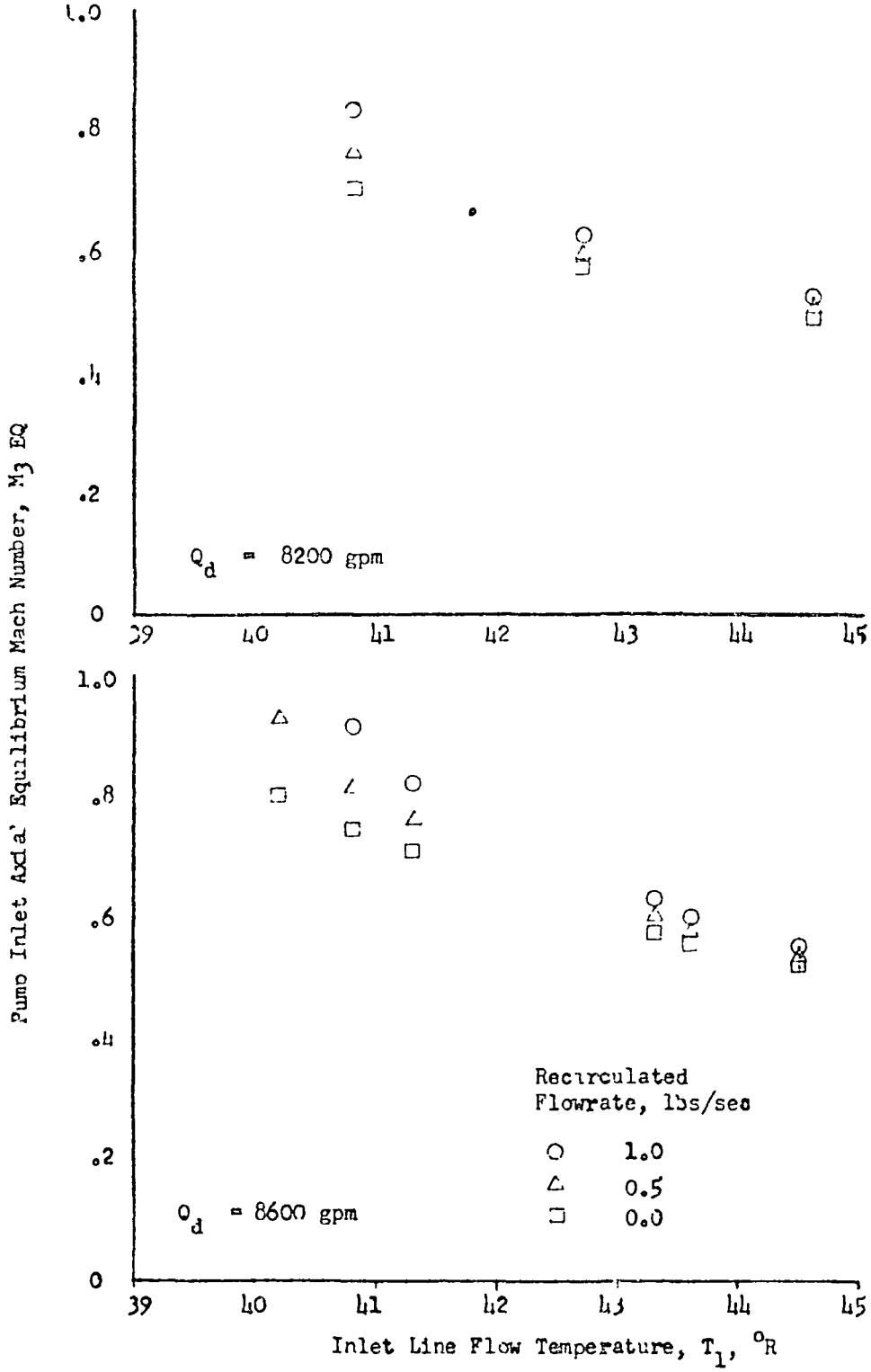

Figure 20 Mark 15-F Pump Inlet Axial Equilibrium Mach Number for an Equilibrium Flow Process Through the Inlet Contraction

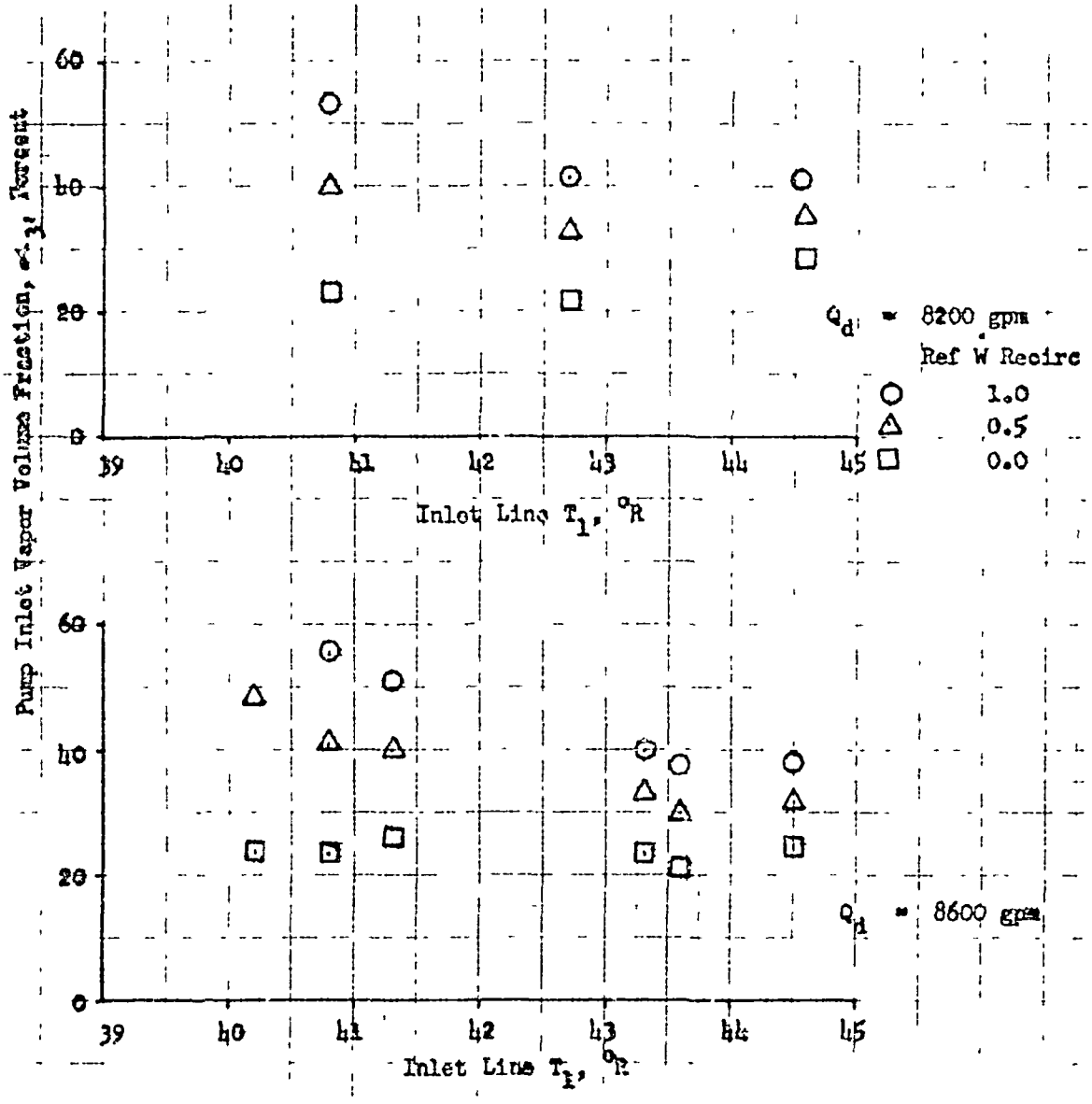

Figure 21 Pump Inlet Vapor Volume Fractions for an Equilibrium Flow Process Through the Inlet Contraction

Of the three remaining possible correlating parameters, the relative Mach number limit for the constant quality contraction flow process (Fig. 16) was tentatively eliminated by noting from the shock wave analyses that shock waves occur in two-phase flow and, as noted before, a shock wave could be more of a benefit than a detriment. In addition, the vapor volume fraction limit for the equilibrium contraction flow process (Fig 21) was eliminated because, from the flow process analyses, a constant quality flow process is probable in a sudden contraction Therefore, the pump inlet vapor volume fraction for a constent quality contraction flow process (Fig 18) is the most probable correlating parameter and 1 lb/sec is the most probable recirculation flowrate

The mechanism by which the vapor volume fraction limits the pumping capability can be understood by calculating the Mark 15 LH_2 pump inlet flow coefficients (Eq. 6) at

$$\phi_{max} \approx \frac{\phi_{liq}}{1-\alpha_{max}} = \frac{0.2291\, Q_{liq}}{N\,(1-\alpha_{max})} \qquad (6)$$

the limiting vapor fractions (Fig. 18) and plotting the results on the ϕ-ψ curve for the Mark 15 LH_2 pump (Fig. 22). These limiting values are tabulated below. Figure 22 indicates that these values of ϕ_{max} are almost identical to the flow coefficient at which the pump overall head coefficient goes to zero (ψ 103) Under these circumstances, the inducer stage is unable to do any work and, therefore, the second stage has nearly the same inlet conditions as the inducer stage. These conditions proceed through the pump with the net effect of zero pressure rise.

Q, gpm	N, rpm	Recirc W, lb/sec	α_{max}	ϕ_{max}
8200	27270	1.0	0.34	0.1043
8600	27270	1.0	0.31	0.1047

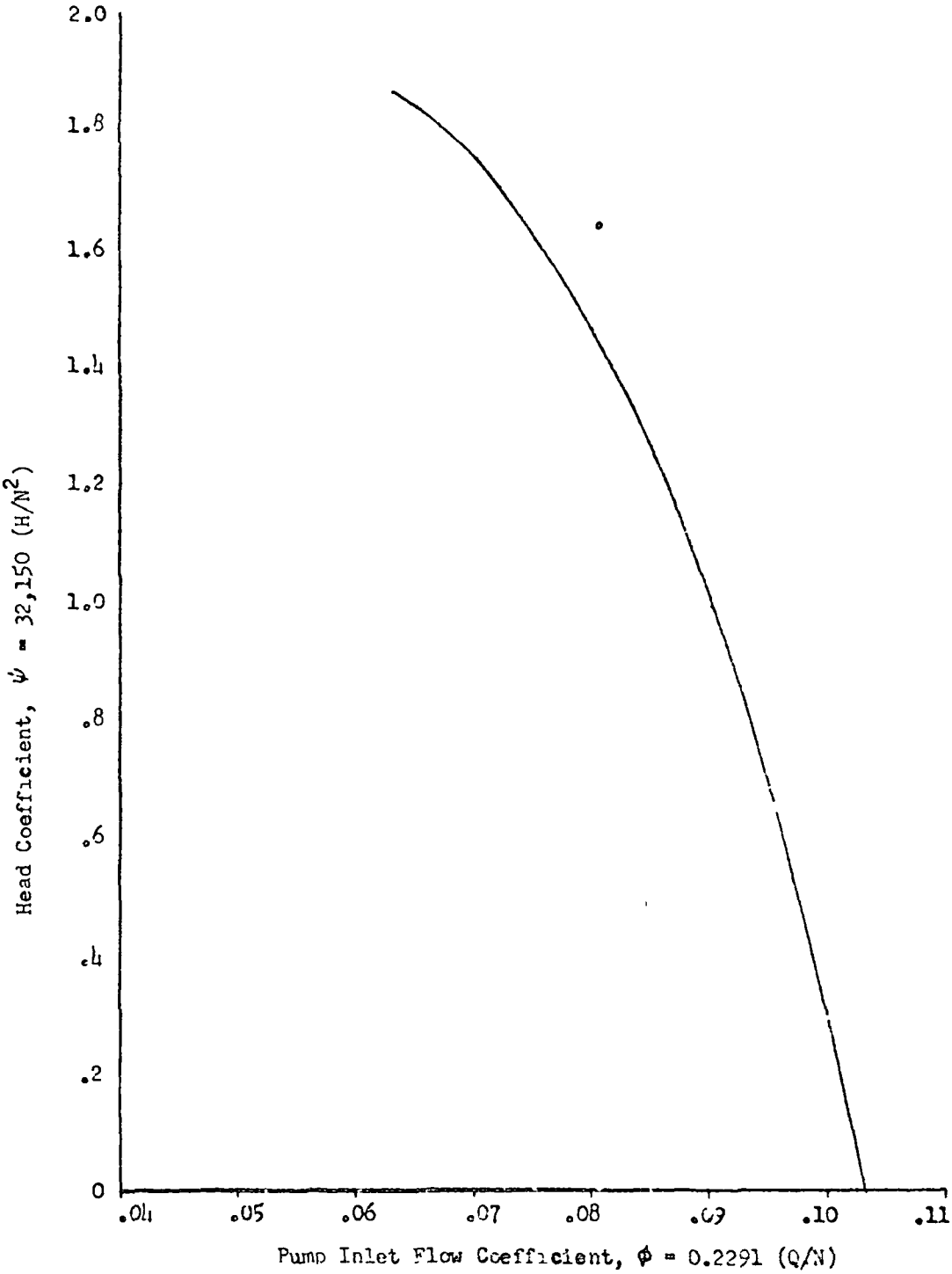

Figure 22 Mark 15 LH_2 Pump Performance Curve

The predicted pressure rise characteristics for the Mark 15 HH_2 pump are compared with test values (corrected for constant quality contraction and recirculation $\dot{W}$ = 1.0 lb/sec) at 45 degrees R inlet temperature in Fig. 23. This prediction system utilizes a stage-to-stage calculation to account for flow density variation and assumes a constant quality flow process. The predicted pressure rises are somewhat less than the test values because a certain amount of vapor condensation probably occurred as the flow passed through the test pump. However, similar to the test results, the predicted curves drop abruptly as vapor fractions of 0.54 and 0.51 (8,200 and 8600 gpm, respectively) are approached. This abrupt drop is due to the fact that a slight pressure rise in the inducer stage will permit successively greater pressure rises in the succeeding stages, thereby minimizing the pressure loss until the inducer stage is completely unloaded.

The limited amount of 20,000 rpm test data taken during the Mark 15 HH_2 pump heated hydrogen testing indicated no pumping capability during two-phase operation. Since this appeared to disagree with the 27,270 rpm test results, the lower speed data were investigated. As shown in Fig. 24a, the 20,000-rpm data is at a high inducer inlet flow coefficient (high Q/N value) and does not indicate pumping capability at low values of NPSH. However, at the same high flow coefficient, the 27,270 rpm data (Fig. 24b) indicated the same lack of pumping capability at low NPSH. Therefore, it may be concluded that the 20,000-rpm data are consistent with the 27,270-rpm data and that the poor suction performance is due to off-design operation.

Further investigation indicated that cavitation on the stator that follows the inducer is the cause of the poor suction performance at high flow coefficients. This is illustrated by the test data shown in Fig. 25. The inducer head rise exceeds 90 percent of the noncavitating value over the complete range in test NPSH whereas the head rise across both the inducer and the stator drops off severely at low NPSH. Therefore, at high flow coefficients, it may be concluded that inducer stator cavitation impairs

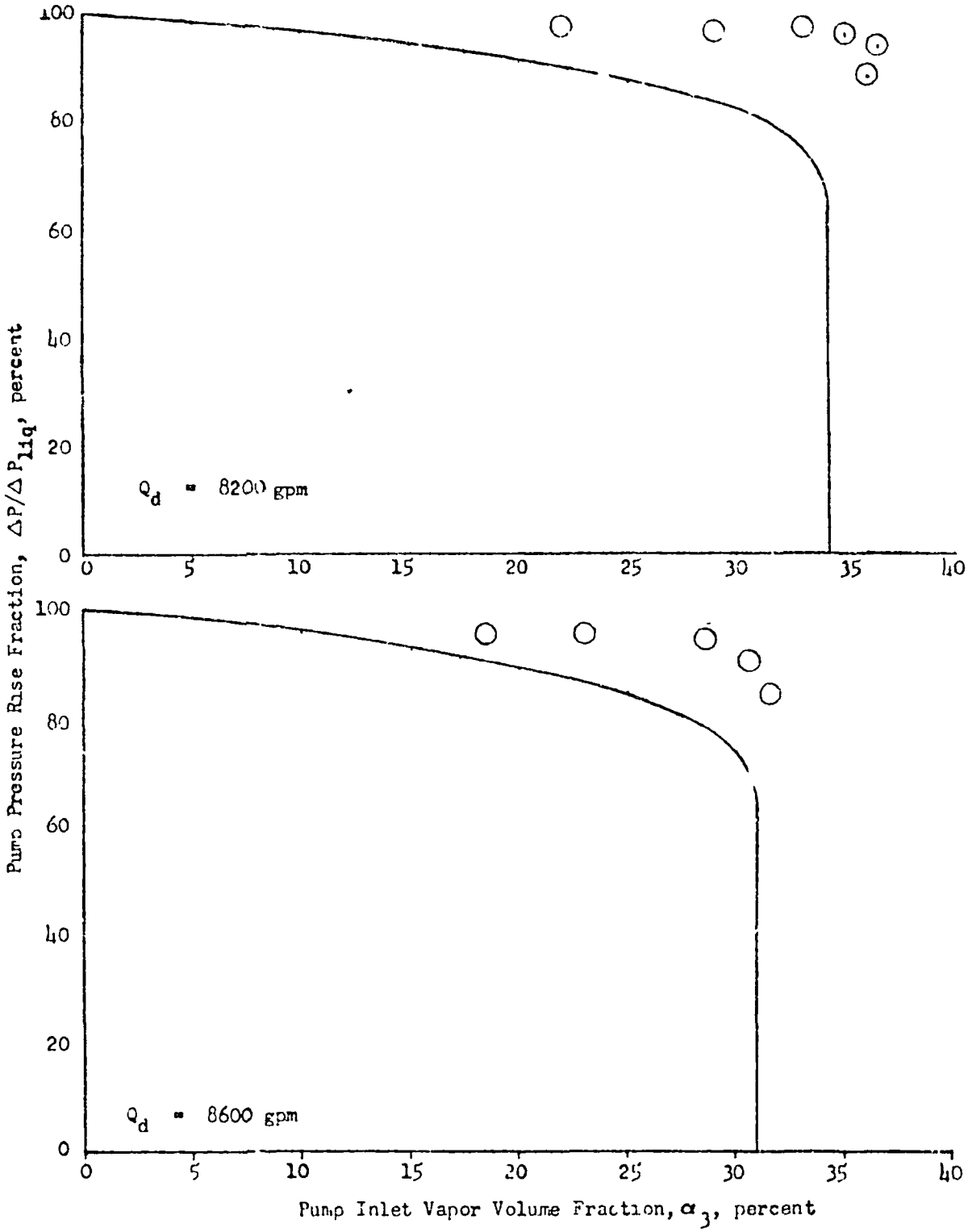

Figure 23 Comparison of Theoretical Prediction with Test at an Inlet Flow Temperature of 45 R, a Constant Quality Flow Process Through the Inlet Contraction, and a Recirculated Flowrate of 1 lb/sec

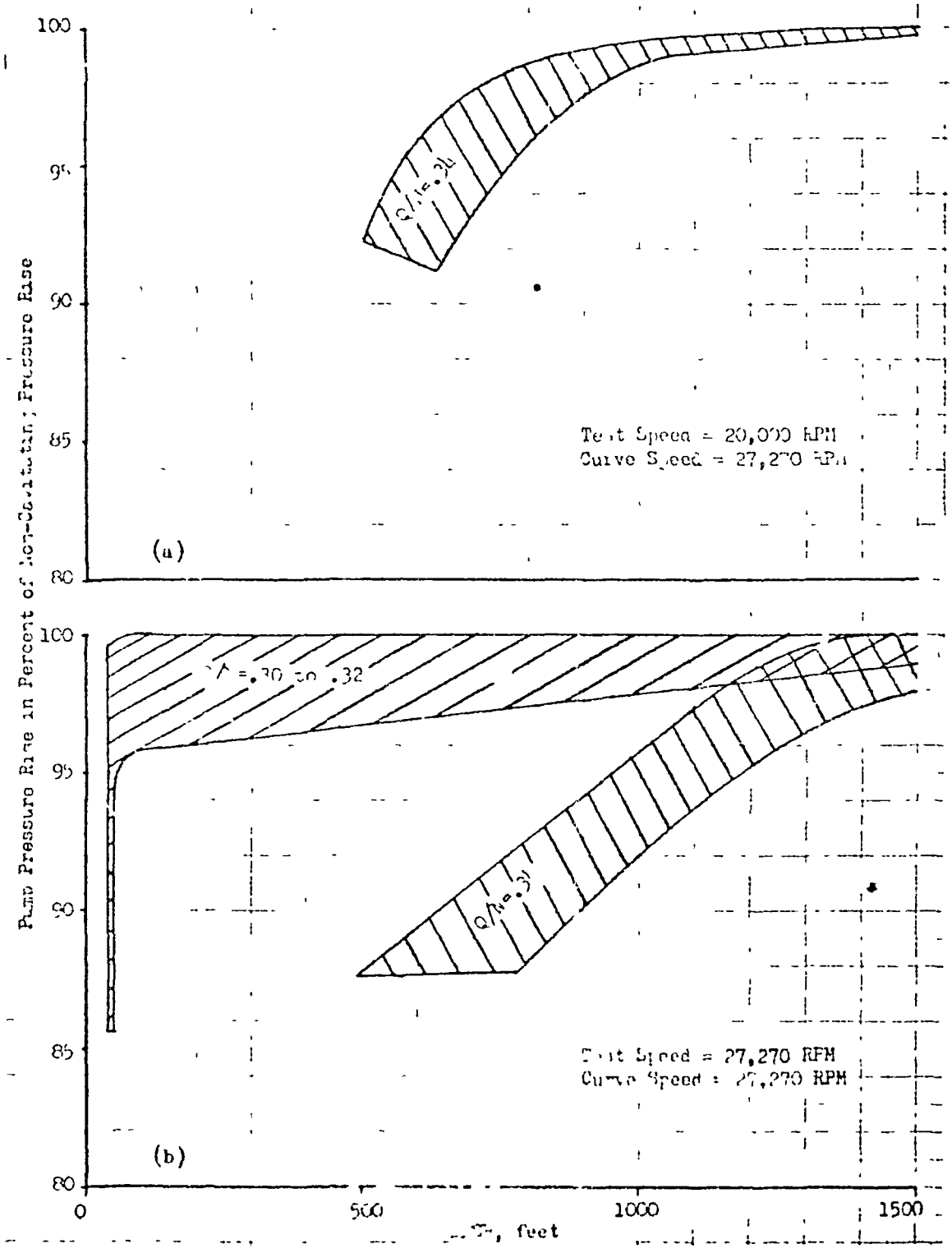

Figure 24 Mark 15-F Heated Hydrogen Test Data Range

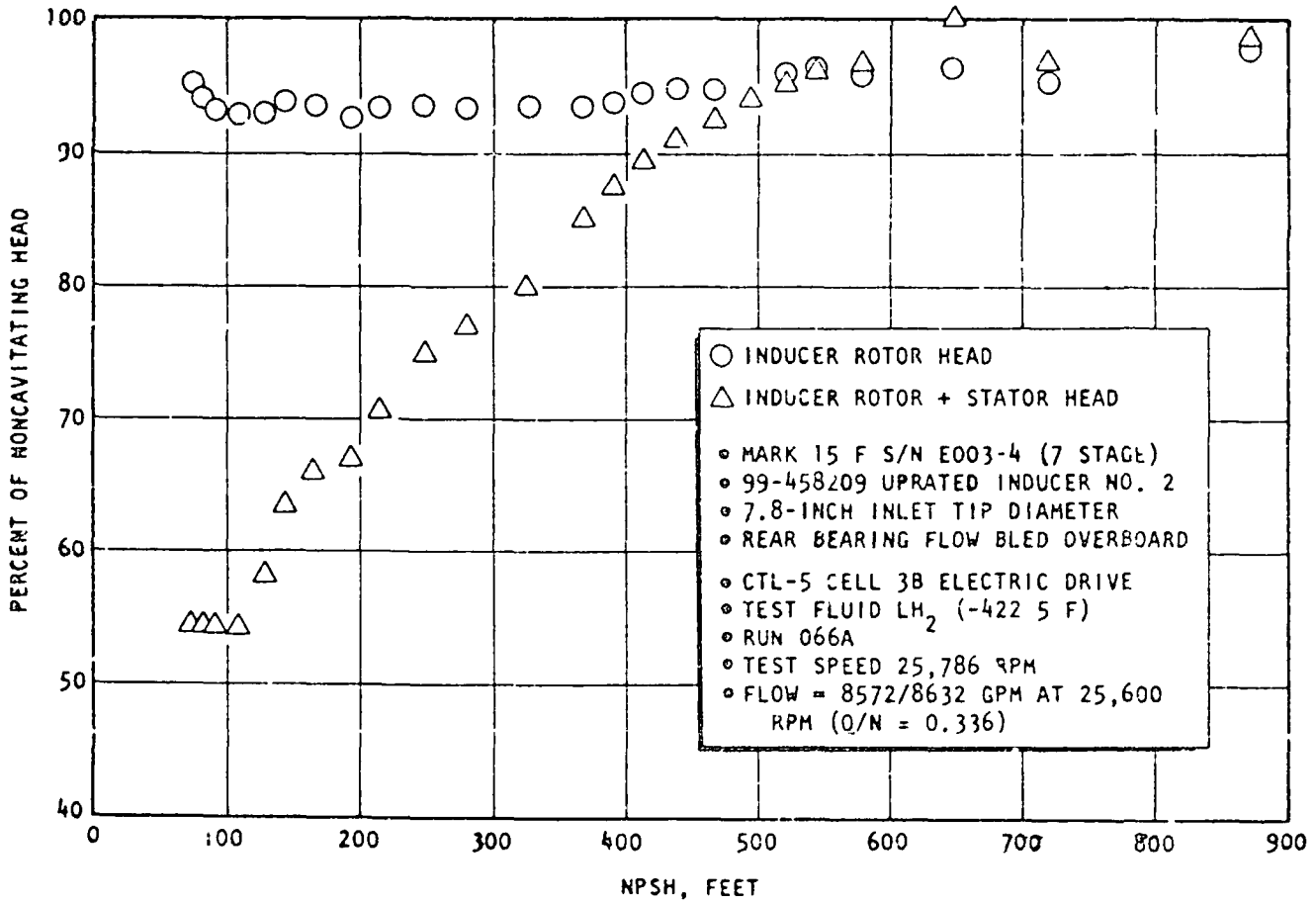

Figure 25 Mark-15 LH_2 Pump Inducer Guide Vane Cavitation Characteristics

the Mark 15 LH_2 pump suction performance and that the inducer alone performs satisfactorily.

This stator cavitation limitation applies only when the liquid flow coefficient is too high If the liquid flow coefficient is below the limiting value for the stator but the two-phase flow coefficient is above, no head loss will occur, as shown by the data Apparently the inducer compresses the two-phase flow enough to provid an acceptably low flow coefficient at the stator leading edge

Assuming a constent quality flow process through the inlet contraction, a pump inlet annulus area of 81 percent of the inlet line area, and a two-phase pump inlet flow coefficient limit of 0.103, the maximum inlet line vapor volume fraction was predicted as a function of liquid flow coefficient fraction for various values of inlet line static pressure and recirculation flowrate (Fig 26). As shown, the vapor pumping capacity decreases with inlet pressure if vapor is recirculated through the pump. At the pump design flowrate with 1 lb/sec recirculated flow, the maximum allowable inlet line vapor volume fraction is 18 percent at a line pressure of 45 psia, 9 percent at 30 psia, and 0 at 15 psia The reason for this variation is that the recirculated weight flowrate is a constant and, therefore, occupies a larger volume at lower pressures If the recirculation were eliminated, this compressibility effect on two-phase pumping capacity should not exist and the design point vapor fraction capacity should increase to nearly 29 percent

Also shown in Fig. 26 is the stator cavitation limitation at a liquid flow coefficient of 103 percent of design Either restaggering or recontouring this stator could alleviate this limitation At the low end of the test flow range, no indication of secondary limitations was evident. Therefore, the predicted curves were tentatively extended to pump stall.

Mark 25 Pump In August of this year, two-phase hydrogen testing of the Mark 25 axial pump was conducted in Nevada for the Los Alamos Scientific

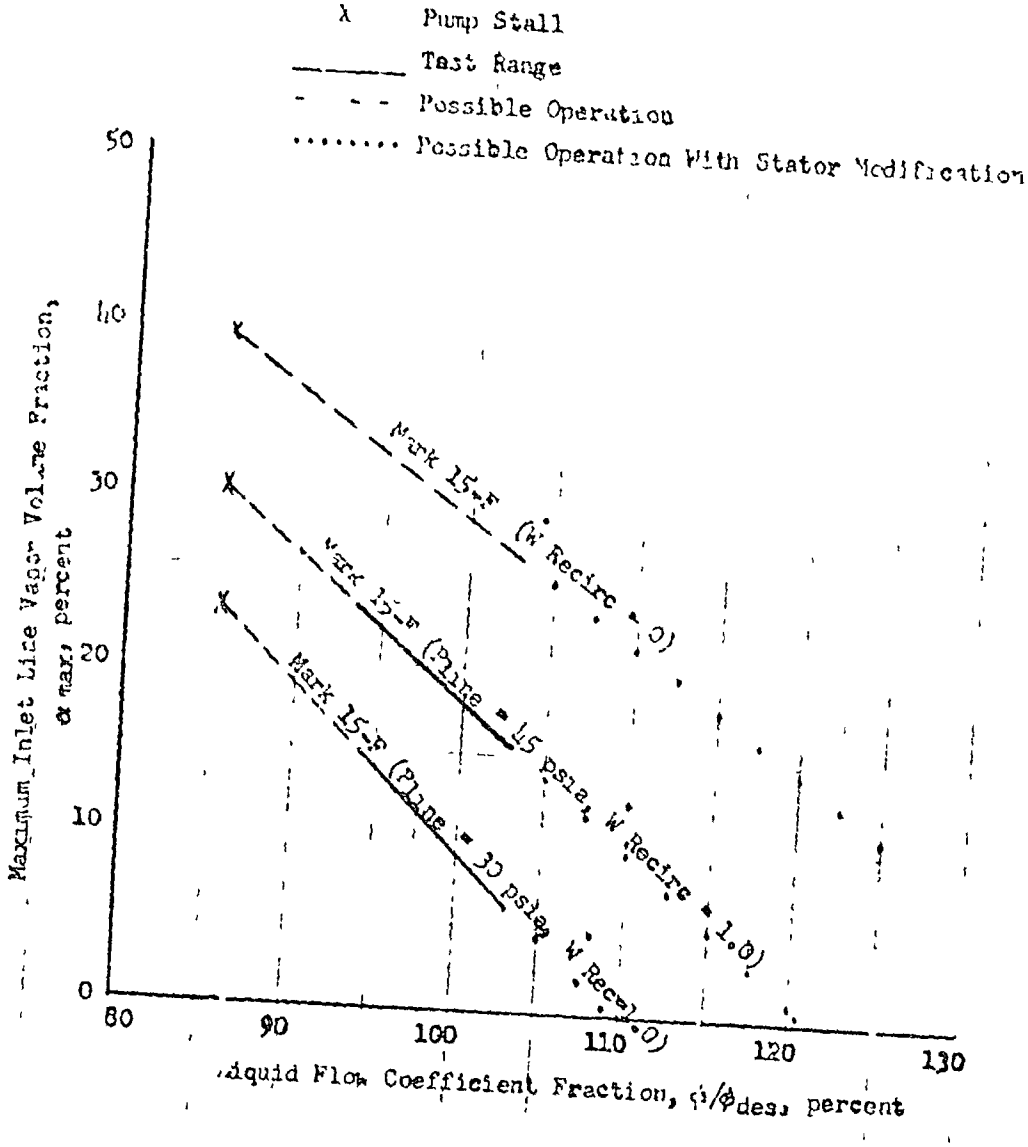

Figure 20 Estimated Vapor Volume Fraction Capabilities for Mark 15 HR_2 Pumps

laboratory. Again, the screen pressure drop, constant static enthalpy method of measuring vapor fraction was utilized. The major difference between this test and the Mark 15 LH_2 testing was the elimination of the recirculated flow. The hot recirculated piston flowrate, which is normally recirculated back into the Mark 25 pump inlet, was diverted to another line and, therefore, could not affect the pump two-phase performance.

Since the test data are still being reduced, the analysis has not been completed and no final conclusions have been drawn. However, an analysis of preliminary test results indicates that the hydrodynamic limitation might have been a two phase flow coefficient of 133 percent of the design flow coefficient and that the flow process through the inlet contraction was, as concluded from the Mark 15 LH_2 pump testing, constant quality. Other hydrodynamic limitation flow models investigated were (1) choking at the pump inlet with equilibrium flow in the contraction, (2) a two-phase flow coefficient of 133 percent of design with equilibrium flow in the contraction, and (3) a constant quality Mach number relative to the inducer leading edge rms diameter of 1.2 with constant quality flow in the contraction. None of the latter three models correlated with the preliminary data satisfactorily.

Since the two-phase flow coefficient limitation of 133 percent of design appears to be less than the flow coefficient at which the Mark 25 pump head coefficient goes to zero, the Mark 25 two-phase pumping limitation may be some other hydrodynamic limitation such as cavitation. An alternative conclusion could be that since 133 per cent is close to the Mark 15 LH_2 pump value of 143 percent, the fact that the Mark 15 value coincided with the zero head coefficient value could have been coincidental. A more complete analysis of the Mark 25 two-phase test data will be conducted as soon as the data reduction is completed. This analysis will be reported as it progresses.

Lewis Research Center Inducer. Inducer tests in two-phase hydrogen have been conducted by NASA at Lewis Research Center (Ref. 9). For these

tests, a constant area inlet duct was installed upstream of the inducer, thereby avoiding the inlet contraction complications of the Mark 15 LH_2 and Mark 25 pump tests. Also, none of the discharge flow was recirculated.

In one series of tests, the vapor was generated by heating the inlet duct, and the vapor fraction was determined by conducting a heat balance using the heat added by the heater and the measured hydrogen temperature differential between the tank and the pump inlet. The test results indicate that the maximum vapor volume fraction decreased with the heating rate or, in other words, the two-phase flow coefficient at the hydrodynamic limit was a function of the hydrogen inlet conditions. At present, this appears to disagree with the Mark 15 LH_2 and Mark 25 pump test results in which the limiting two-phase flow coefficients appeared to remain constant. Possible explanations for this apparent discrepancy are (1) since the Rocketdyne test pumps had stages downstream of the inducer, the hydrodynamic limitations for the inducer alone might have been cancelled out, (2) the heating method used to generate vapor in the inducer tests might not have evenly distributed the vapor, and (3) since the inducer test data at design flow coefficient and zero heating rate indicates an NPSH (at 10 percent head loss) that is lower than the inlet velocity head, some vapor other than that generated by heating could have existed in the inlet duct.

In a second series of tests, the heater was not used and the vapor was generated by expanding the flow from the tank to a pressure in the inlet duct that was below the tank vapor pressure. The resulting vapor fraction measurements show good agreement with equilibrium theory and, therefore, provide support for the assumption that two-phase hydrogen flow will approach equilibrium if given sufficient time in a constant area duct. Since the inducer hub was extended the length of the duct, the duct was actually an annulus. The length was 30 inches and the outside diameter was the same as the inducer, 5 inches.

Of the four data points discussed in Ref. 9 for the second series of tests, three had vapor volume fractions of 11 percent or less and one

had a fraction of 25 percent. The 25-percent vapor fraction data point is the only one in which any head loss was observed (3 percent). Since the corresponding two-phase flow coefficient was close to the design flow coefficient, this amount of head loss would not have been observed in the Mark 15 LH_2 and the Mark 25 pumps. This is logical because the downstream stages of the Rocketdyne pumps add enough head to make the inducer head loss appear small on an overall basis.

These four data points are compared with the predictions of the linearized equilibrium flow process computer program in Fig. 27. As shown, the constant quality Mach number relative to the inducer leading edge rms diameter exceeded 1.0 for the 25 vapor fraction data point. Therefore, some acoustic velocity phenomena could have caused a portion of the head loss in this low head coefficient test.

Two-Phase Experimental Investigation

The experimental investigation of two-phase flow phenomena in hydrogen was defined and the test plan and instrumentation requirements were submitted to the J-2 program for a joint and complementary effort. However, because of a reduced overall effort of the J-2 program, the experimental investigation was not initiated.

This experimental program was divided into three parts: investigation of adiabatic two-phase critical flow, investigation of two-phase critical flow with heat addition, and modeling of engine systems for chilldown. The proposed basic test apparatus for the initial part consists of an LH_2-GH_2 heat exchanger and mixer, an approach section, a converging-diverging nozzle, and a back-pressure control valve, as shown schematically on Fig. 28. An existing vacuum chamber can insulate the apparatus. Vertical mounting of the mixer and test sections prevents liquid-vapor stratification. The gaseous hydrogen is prechilled with LN_2, allowed to reach thermal equilibrium with the liquid in the mixer heat-exchanger coil, and then injected through the Rigimesh-faced injector to produce

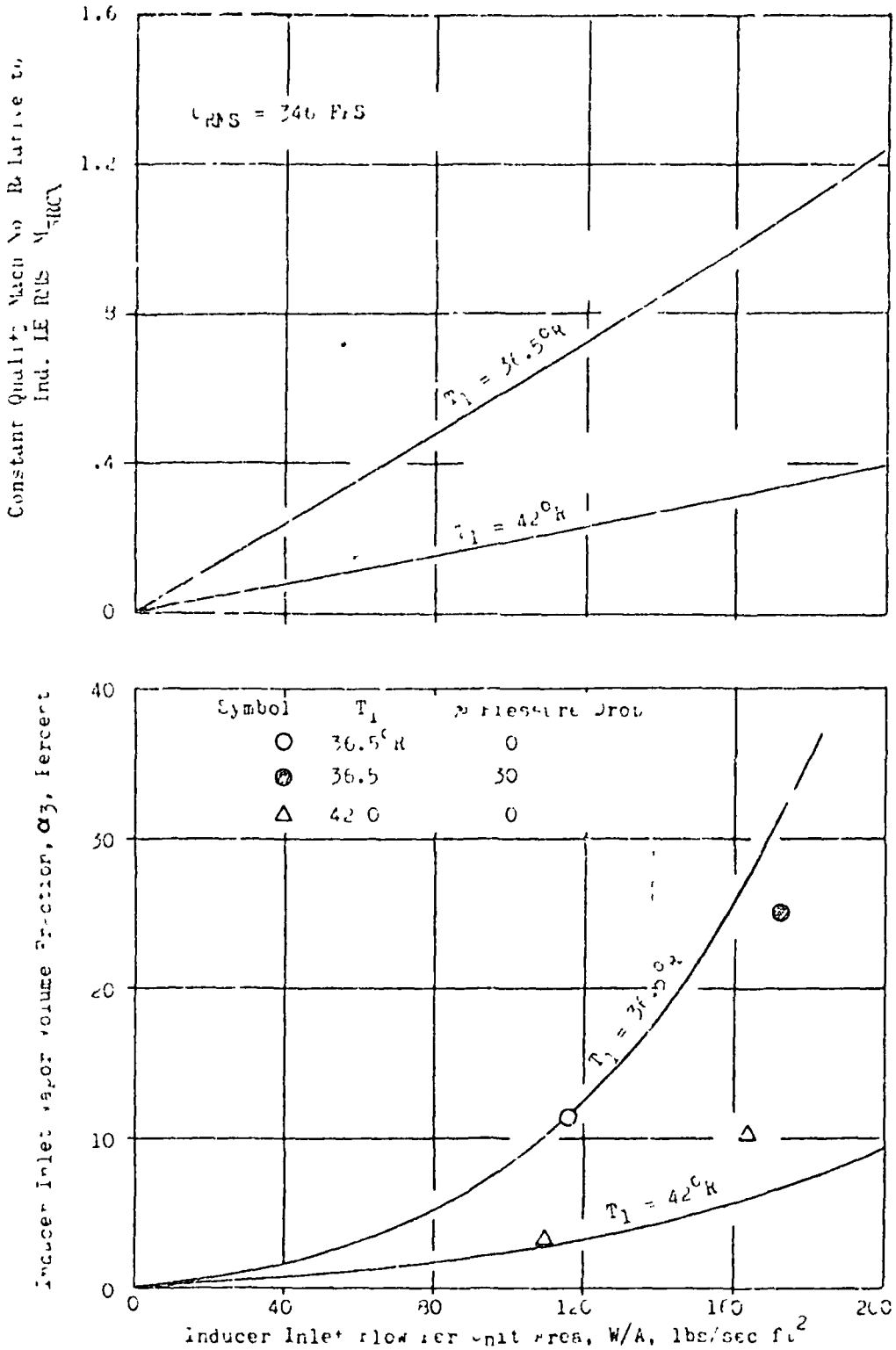

Figure 27 Analysis of NASA Inducer Two-Phase Test Data

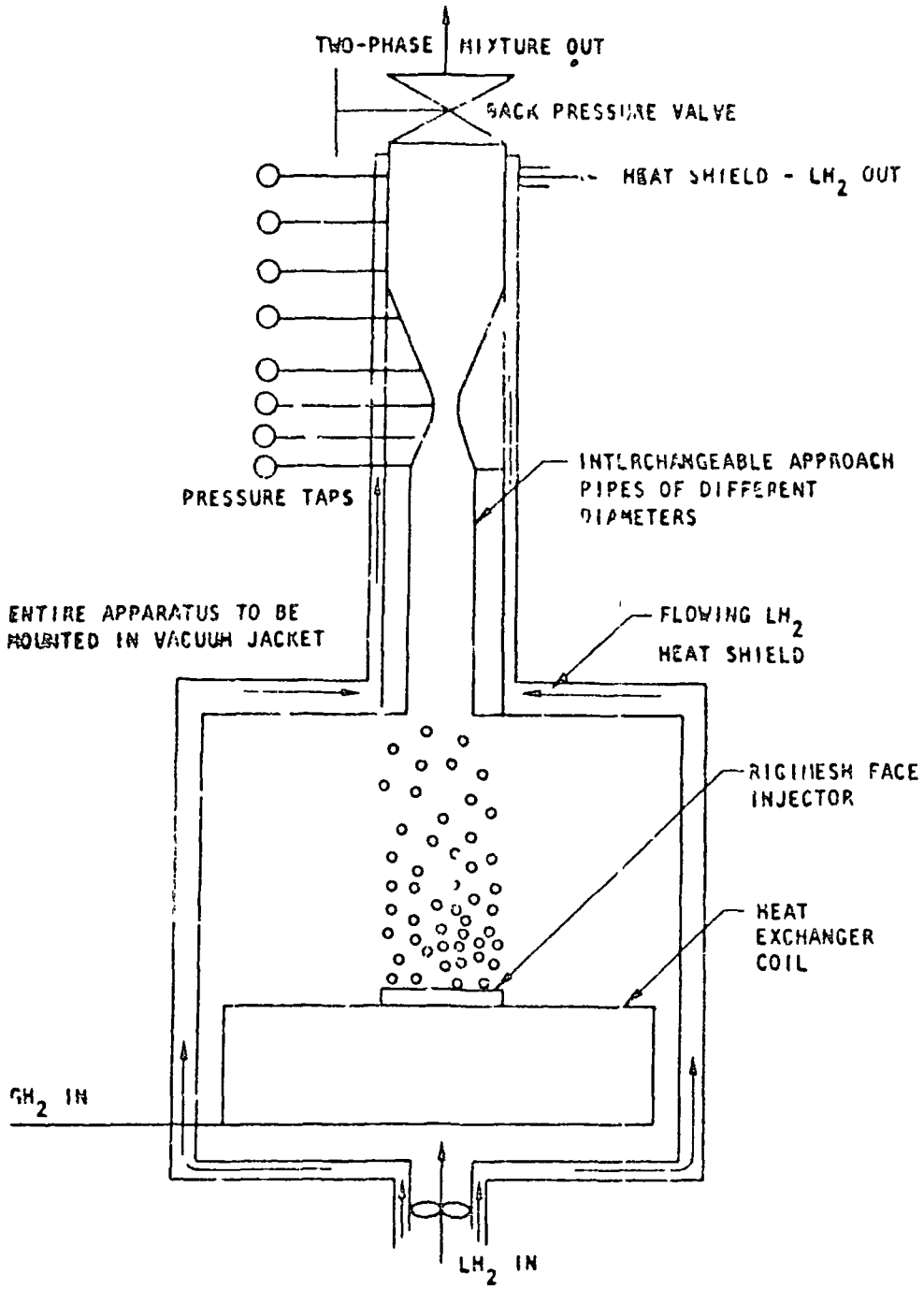

Figure 28 Schematic of the Proposed Test Apparatus for Mixed-Phase Flow Investigation

uniform bubble size. This method of producing two-phase hydrogen offers the greatest flexibility in varying the vapor fraction. The inlet vapor fraction can be calculated by using a heat balance and the measured flowrates for the liquid and the vapor. The static pressure distribution along the nozzle and, consequently, the flow process can be determined from the multiple static pressure taps. The apparatus for the heat addition and modeling parts of the test program can be obtained by modifying the basic test apparatus for the initial part.

Recommendations

Pump Geometry. For the Mark 15 LH_2 pump, the two-phase pumping capability can be improved significantly by eliminating the rear bearing coolant flow into the inducer inlet. For operation at the design liquid flow coefficient, the predicted improvement in maximum allowable inlet line vapor volume fraction is from values of 0, 9, and 18 percent at line pressures of 15, 30, and 45 psia, respectively, to 29 percent at all line pressures (fig. 26). As indicated, elimination of this recirculated flow is particularly important for operation at low inlet pressures. The test results indicated no vapor pumping capability with the recirculation if the inlet line flow temperature was below 39.5 R (23 psia).

To obtain Mark 15 LH_2 two-phase pumping capability at liquid flow coefficients greater than 103 percent of design, the stator blades that follow the inducer should be restaggered and/or recontoured. Such modifications should extend the two-phase pumping range by reducing the amount of cavitation at high flow coefficients.

The vapor pumping capacities of other pumps could not be predicted because the reduction and analysis of the Mark 25 pump test data were not completed. As indicated by the Mark 15 LH_2 data analysis, the two-phase pumping limit occurs when the two-phase flow coefficient equals the value at which the pump overall head coefficient goes to zero, a centrifugal pump should have a much larger vapor pumping capacity. The maximum flow coefficient

for a centrifugal pump can exceed 200 percent of design as compared to the Mark 15 LH_2 value of 140 percent. Without flow recirculation and for operation at design liquid flow coefficient, these values produce vapor volume fraction capacities of 50 percent for some centrifugal pumps as compared to 29 percent for the Mark 15 LH_2 pump. However, if the preliminary analysis of the Mark 25 preliminary test data applies, the two-phase pumping limit is a two-phase flow coefficient of 135 to 140 percent of design and, therefore, the type of pump characteristic would have no effect on vapor pumping capacity unless the pump head coefficient went to zero at less than 135 to 140 percent.

Tank Zero NPSH. Although not directly related to the pump preconditioning and restart problems, the possibility of zero tank NPSH (saturated hydrogen in the tank) operation is indicated by the two-phase pumping capability studies and is discussed here because of its possible importance in rocket vehicle design. The hydrogen tanks for hydrogen-fueled rocket vehicles are exceedingly large and, therefore, should be operated at low pressure to minimize the tank weight. If no tank pressurization is required above the saturation pressure, the pressure is minimized and simplification of tank pressurization equipment may be possible. However, the expansion from a saturated liquid in the tank to a velocity of 50 to 60 ft/sec in the pump inlet line produces vapor in the flow at the pump inlet. If this amount of vapor can be pumped without significantly affecting the pump pressure rise, zero tank NPSH operation is possible and, therefore, reductions in tank weight and system complexity may be possible.

To relate the tank conditions to the pump inlet line conditions, the linearized equilibrium flow process computer program was used to generate Fig. 29 through 31. An equilibrium flow process was assumed because the long, constant area inlet line should provide sufficient time for the flow to approach equilibrium (Ref. 6 and, for line velocities less than Mach 1, Ref. 9). Since line friction and heat transfer were neglected (isentropic flow process), the inlet line vapor fractions of Fig. 29 through 31 are the minimum values obtainable. Assuming no hydrogen vapor

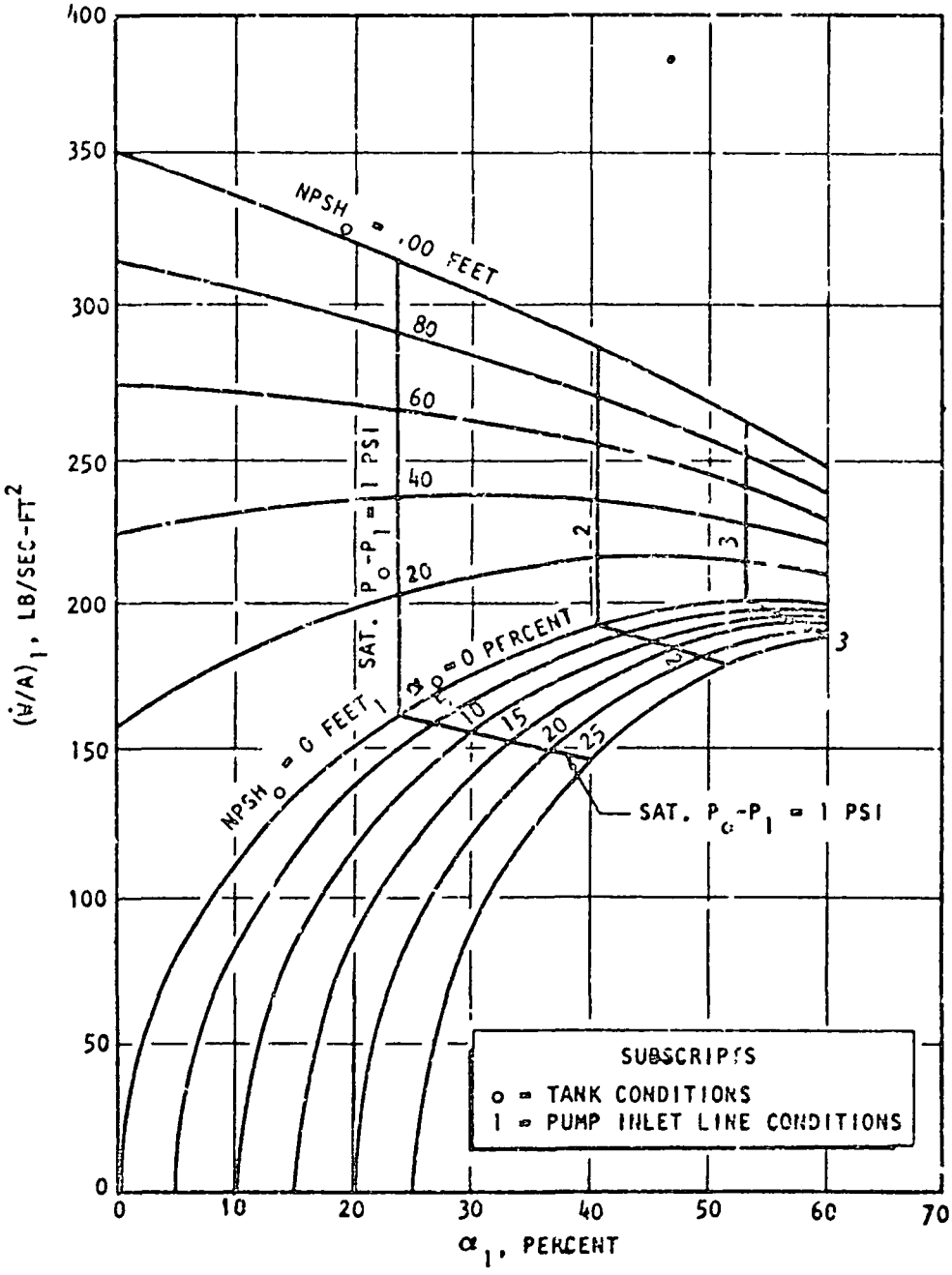

Figure 29 Pump Inlet Line Conditions for an Isentropic, Equilibrium Expansion from the Tank (Tank Saturation Pressure (P_o) = 15 Psia)

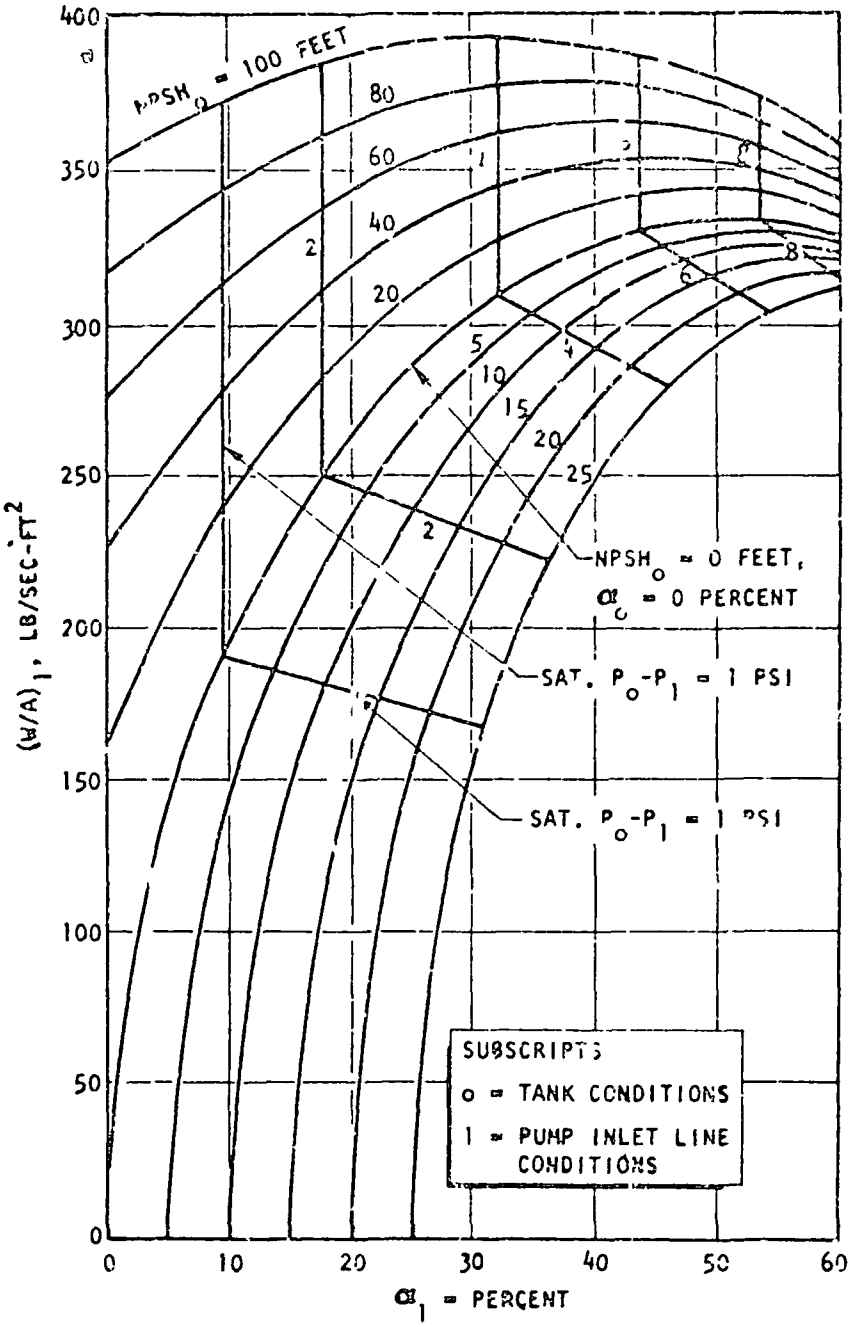

Figure 50 Pump Inlet Line Conditions for an Isentropic, Equilibrium Expansion from the Tank (Tank Saturation Pressure (P_o) = 30 Psia)

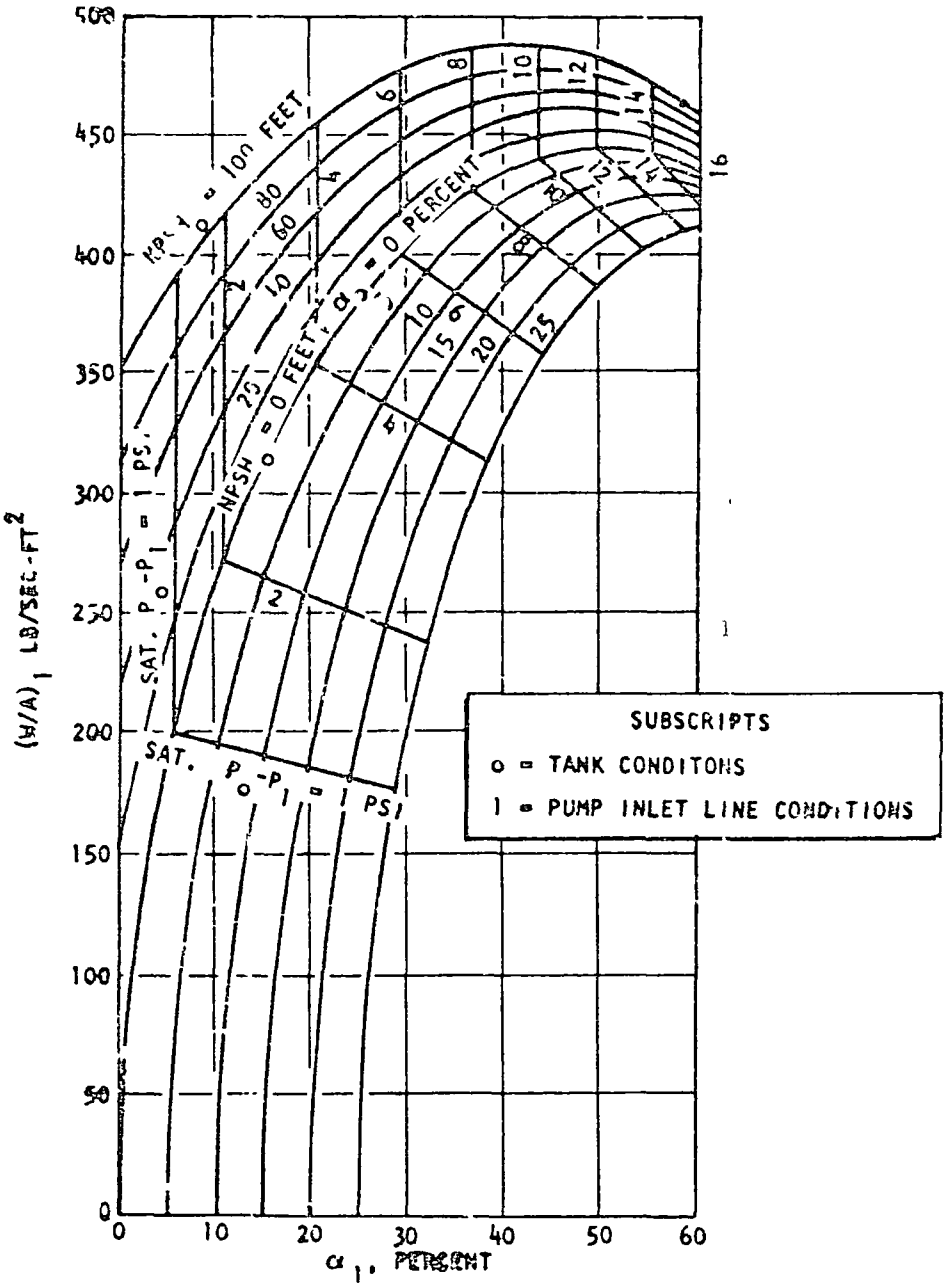

Figure 31 Pump Inlet Line Conditions for an Isentropic, Equilibrium Expansion From the Tank (Tank Saturation Pressure (P_o) = 45 Psia)

recirculation, the inlet line vapor volume fractions should approximate the pump inlet vapor volume fractions because a constant quality flow process is probable through a sudden contraction, and the volume fraction change for such a process through relatively small area contractions is small

The tank saturation pressures for Fig 29 through 31 are 15 30 and 45 psia, respectively. Each curved line represents an isentropic expansion from a given tank condition Indicated tank conditions range from 100 feet of NPSH to 25 percent vapor volume fraction.

For an inlet line flow per unit area of 250 lb/sec-ft^2 (an approximate value for the J-2 with an 8-inch inlet line), operation at a tank saturation pressure of 15 psia would require 50 feet of tank NPSH regardless of the vapor pumping capacity of the pump (Fig. 29). For a 30-psia tank saturation pressure, no tank NPSH would be required if the vapor pumping capacity were 17.5 percent by volume (Fig 30) and, for 45 psia, no NPSH would be required at a vapor pumping capacity of 9 percent (Fig 31) If the inlet line diameter were increased to 9 inches (198 lb/sec-ft^2), no tank NPSH would be required if the vapor volume fraction pumping capacities were 48, 10, 5 5 percent at tank saturation pressures of 15, 30, and 45 psia, respectively With a 10-inch inlet (160 lb/sec-ft^2), vapor volume fraction pumping capacities of only 23, 6 5, and 3 5, respectively, are required Therefore, referring to the values just quoted and to Fig 26, the existing Mark 15 LH_2 pump with its estimated 1 lb/sec recirculation flowrate would require a 9 5-inch-diameter inlet line to operate with saturated, 30-psia hydrogen in the tank The existing inlet line would be satisfactory for operation with saturated 45-psia hydrogen, and operation with 15-psia saturated hydrogen would be impossible By eliminating the recirculation flowrate (Fig 26), no inlet line modification would be required for 30-psia operation and, at 15 psia, a 9 5-inch-diameter line would be required

WARM PUMP, LIQUID FLOW IN INLET LINE

To determine the chilldown requirements for a liquid hydrogen pump, the pump inlet conditions under which pumping is possible must be known and, therefore, were predicted. Because no rotating pump test data that relate pumping capability to pump warmth were available, these predictions were largely analytical. The initial phase of this study was a correlation of the tube cooldown test data obtained from the Rocketdyne Research Division laboratories. The heat transfer coefficient correlations were then combined with pump relationships and the operating regions of pumping capability were predicted.

Analysis of Tube Cooldown Test Data

The analytical heat transfer study of the J-2 engine system during the start transient requires among other parameters a knowledgeable insight into the modes of the heat transfer taking place in the chilldown period. The difference in the component wall temperature and the bulk temperature of the hydrogen is continually changing from the start of the chilldown until a later time when steady-state flow is eventually established. Therefore, it is anticipated that film boiling, transition boiling, nucleate boiling, and finally forced convection heat transfer modes will be present during the transient chilldown time. Results from both uncoated and coated data obtained from Rocketdyne's Research Division were utilized to analyze the J-2 engine system chilldown characteristics.

Uncoated Tubes. The J-2 engine system as prepared for the thermal analyses (TVP 51) program is shown in Fig. 32. It was desirable to use, as much as possible, the results of the experimental tube cooldown data collected by the Research Division in these studies.

Before a discussion of the cooldown test data is presented, a brief description of the heat transfer under various modes is given. A typical pool boiling curve is presented in many heat transfer books (e.g., Ref. 10).

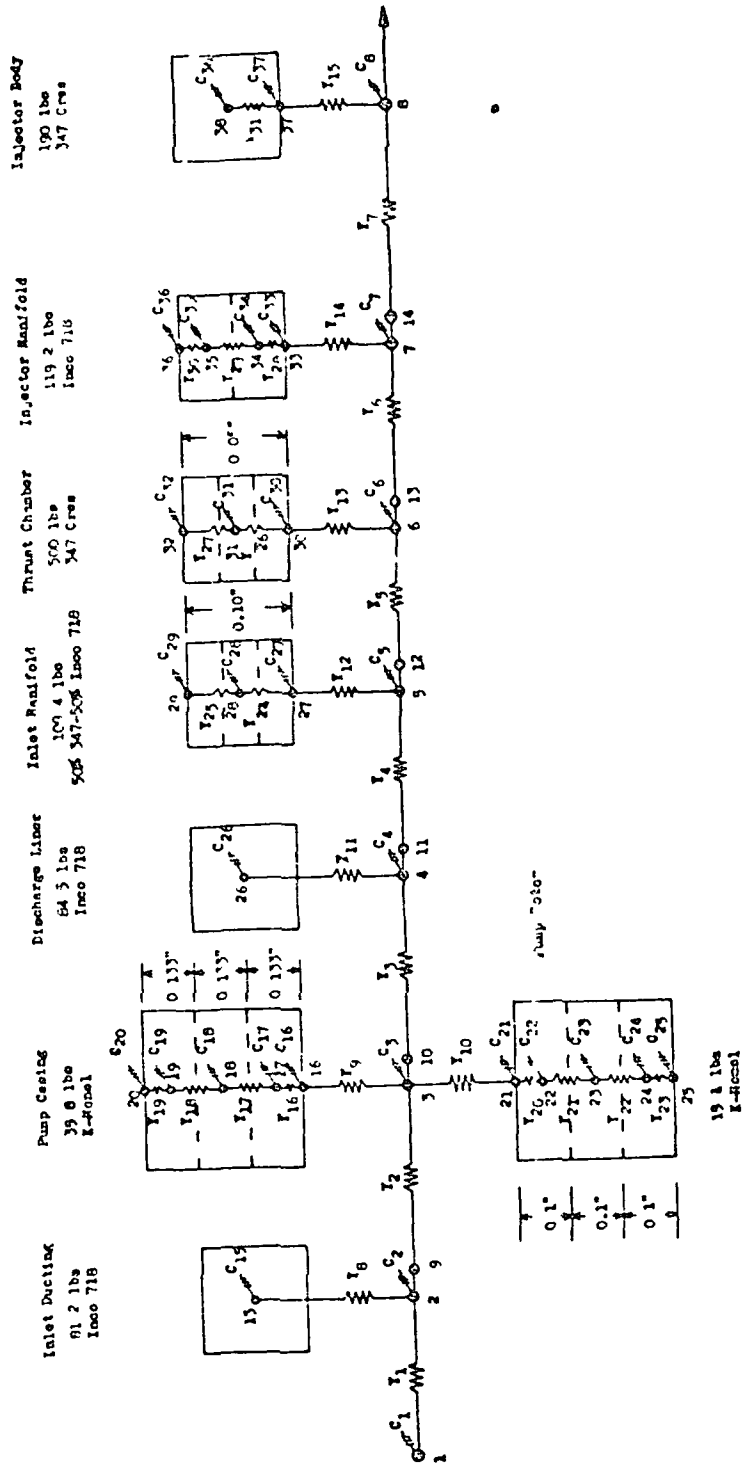

Figure 32. Simplified J-2 Engine System Component Breakdown for Chilldown Study

The boiling curve, which is a plot of heat flux versus ΔT on log-log paper, is normally divided into various regimes, as shown in Fig. 33. In normal experimental procedures carried out with heated wires or heated surfaces, the heat flux build up and the ΔT increase are very gradual, and the curve of Fig. 33 starts in Region I and ends in Region VI. In an unheated tube test, in contrast, the ΔT is highest at the start of the test and gradually decreases with time, the curve of Fig. 33 starts in Region VI and ends in Region I. Therefore, nearly all modes of heat transfer are present during a tube cooldown.

At the start of the test, when ΔT is large about 100 to 400 R, forced convection film boiling is predominant. This region is known to extend to a ΔT of approximately 40 R, as shown in Fig. 34 (taken from Ref. 11). At lower values of $T_W - T_B$ down to about 10 R, a transition region (unstable) film boiling normally takes place at a wall-to-bulk temperature difference of about 40 R. The region of nucleate boiling exists for $T_W - T_B$ under 10 R. The peak nucleate boiling for hydrogen occurs somewhere in the range of $T_W - T_B$ of about 4 to 10 R, depending on the test apparatus (Ref. 11).

The experimental tube cooldown data received from the Research Division were already reduced and tabulated (time, T_s, T_2, Q/A, and H). However, tube backside temperatures, hydrogen bulk temperatures, and pressures existed as raw data. When a plot of temperature versus time is available, such as sketched below,

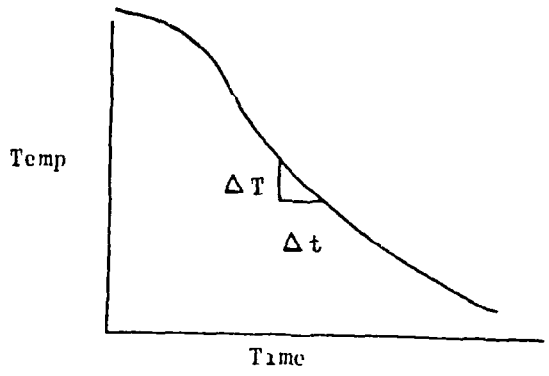

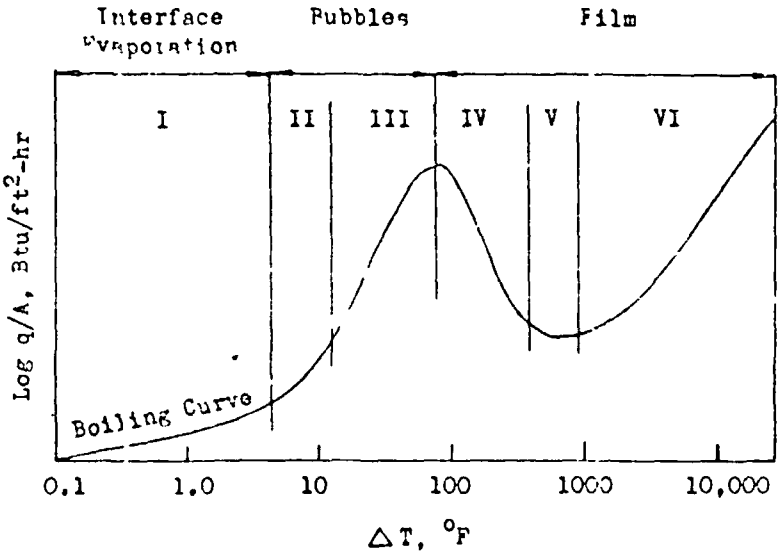

Figure 33 Typical Pool Boiling Curve

Regimes:

I - Pure convection, heat transferred by superheated liquid rising to the liquid-vapor interface where evaporization takes place.

II - Nucleate boiling bubbles condense in superheated liquid etc. as in Case I.

III - Nucleate boiling bubbles rise to interface.

IV - Partial nucleate boiling and unstable nucleate film.

V - Stable film boiling.

VI - Radiation coming into play.

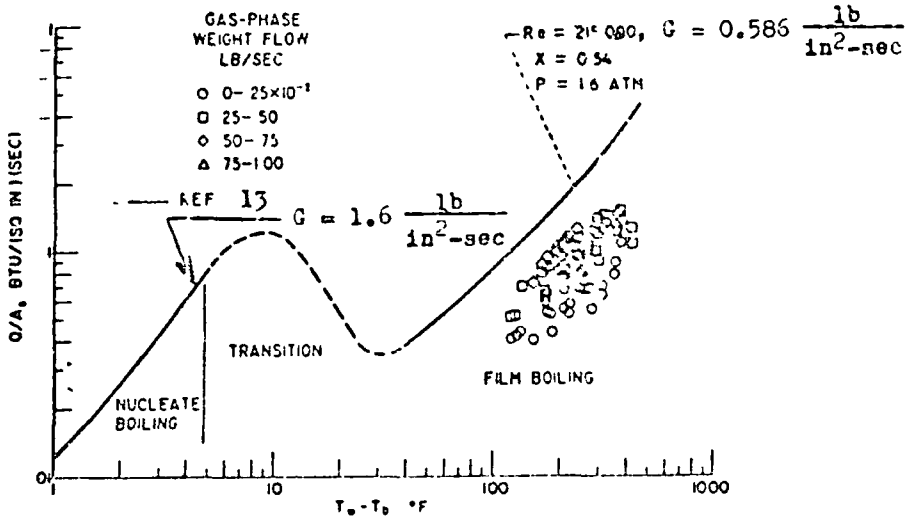

Figure 34 Two-Phase Hydrogen Heat Transfer Regions

the heat flux can be determined from a combination of the properties of the test tube in a lumped system.

$$Q/A = \frac{m}{A}\frac{dh}{dt} = \frac{\rho V}{A} C_p\,(T)\,\frac{dT}{dt} \qquad (7)$$

Using the slope of the cooling data and the known properties, the heat flux can be calculated from Eq 7 If the value of the Biot number is less than 0.1 (Ref 12), the assumption of a lumped system is a reasonable one. Up to a Biot number of about 0 4, Eq. 7 can be used without too much sacrifice in accuracy For values of Biot number greater than 0 4, Eq. 7 is no longer valid. Therefore, the solid should be treated as a distributed system and analytical solutions, which are normally available, should be sought

In the film-boiling region, the Biot number, which can be interpreted as the ratio of internal to external thermal resistances, was calculated by using the experimental $\bar{h}$ in the following relation

$$Bi = \frac{\bar{h}\lambda}{k} = \frac{\lambda/k}{1/\bar{h}} \qquad (8)$$

The calculated Biot numbers are shown on Table 5 . The results of the cooldown test are plotted on Fig 33 through 36 as heat flux versus temperature difference ($T_w - T_B$) between the wall and the bulk fluid temperature on a semi-log paper In the region of film boiling, where $T_w - T_B$ values range from approximately 50 to 400 R, the heat flux decreases slowly with a decrease in ΔT The heat flux decreases very rapidly with a decrease in $T_w - T_B$ below a temperature difference of about 50 R. This is in contrast to the previous experiments carried out with hydrogen (Ref 13 and 14). Figure 34 (taken from Ref 15) indicates that the heat flux increases with a decrease in ΔT between a temperature difference of about 40 to 10 R (transition region) The peak of nucleate boiling is shown to be somewhere between ΔT of 10 to 40 R The discrepancy between the tube cooldown data and the previous experiments (e g., Ref 13 through 15) is attributed to small errors in the tube cooldown data

TABLE 3

BIOT NUMBER FOR SEVERAL TESTS

Run	Material	Thermocouple Number	G, lb/in^2-sec	$T_{b_{avg}}$	Biot No
235	Copper	16	0.259	100	0.0043
235	Copper	16	0.259	400	0.0115
312	Tens-50	16	0.685	100	0.1863
312	Tens-50	16	0.685	400	0.0824
315	Tens-50	16	1.515	100	0.298
315	Tens-50	16	1.515	400	0.130
455	K-monel	16	3.54	100	1.00
455	K-monel	16	3.54	350	0.503
470	Stainless steel	16	4.01	100	0.991
470	Stainless steel	16	4.01	350	0.297

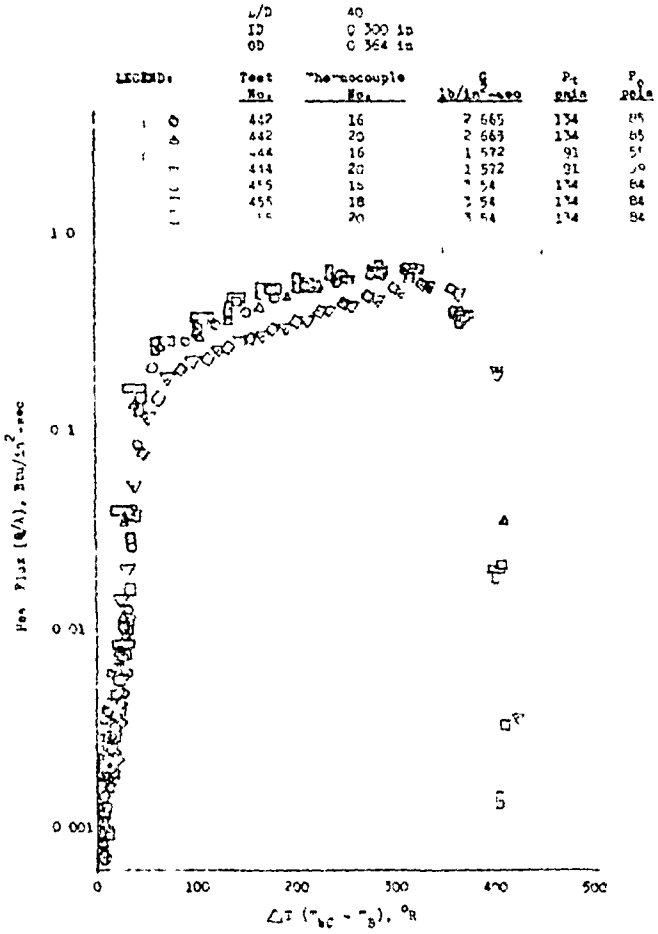

Figure 55. Heat Flux vs ΔT for Chilldown of a k-monel Tube

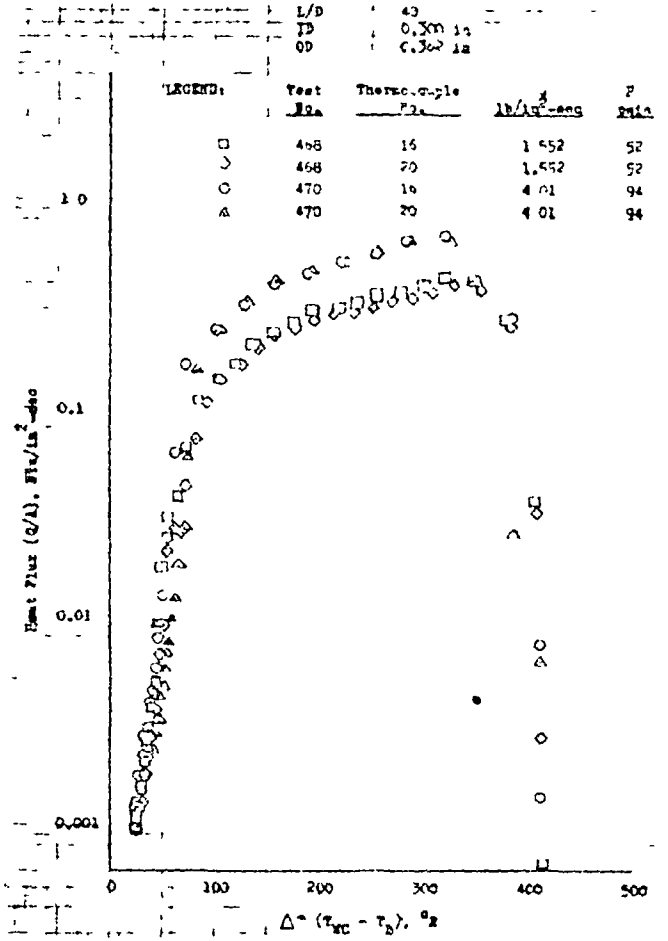

Figure 56. Heat Flux vs ΔT for a Stainless-Steel Tube

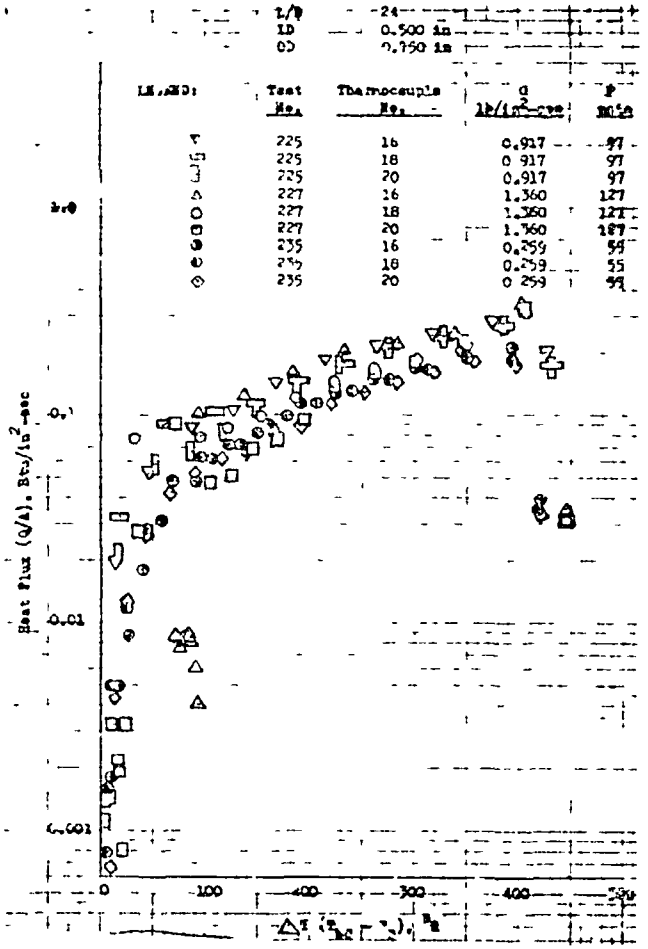

Figure 37. Heat Flux vs ΔT for a Copper Tube

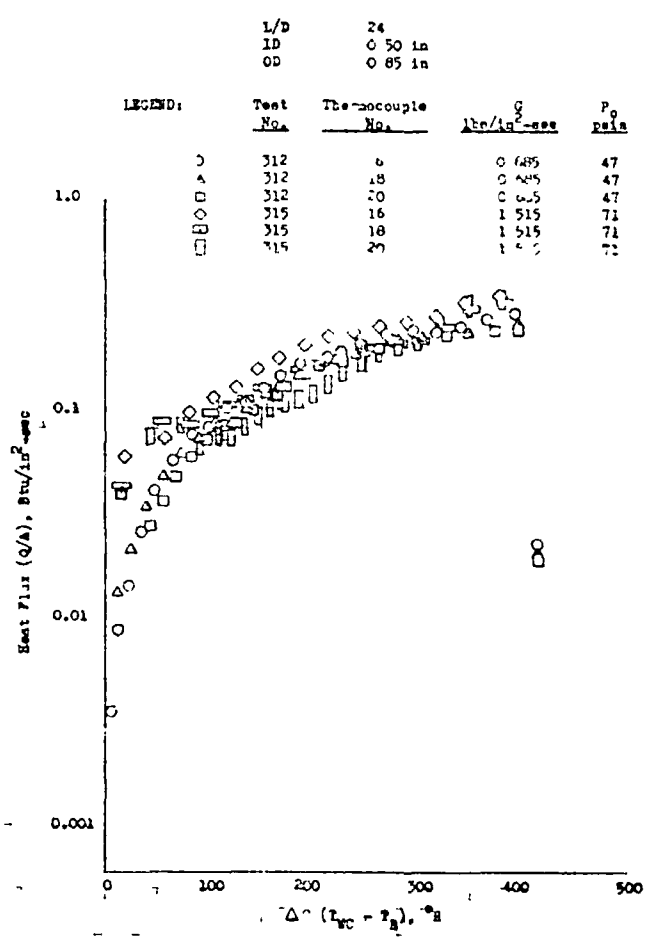

Figure 38. Heat Flux vs Δ T for Chilldown of a Tens-50 Aluminum Tube

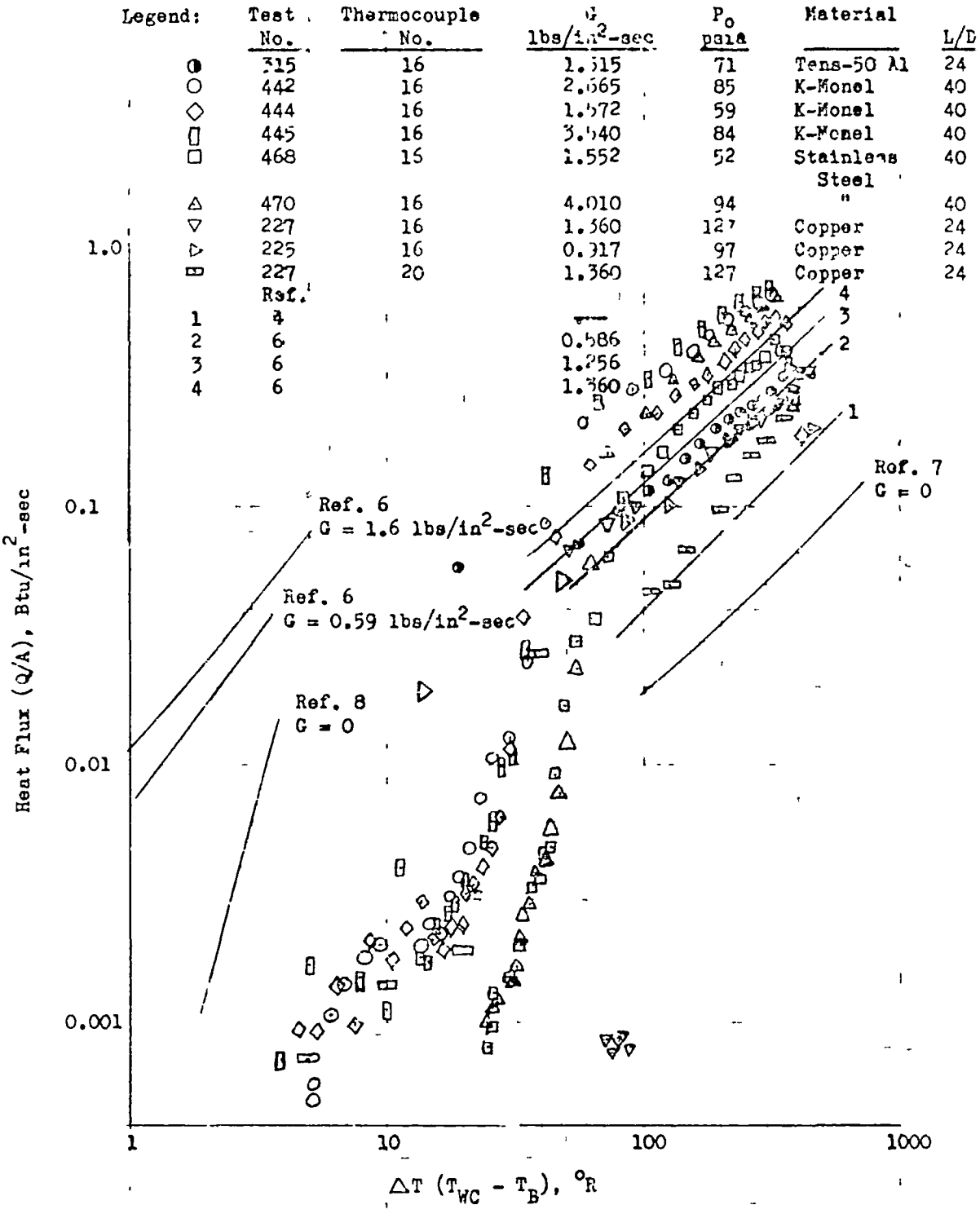

Figure 39 Heat Flux vs ΔT for Chilldown of Various Tubes

The thermocouples located on the outside wall of the tubes were used to determine time-temperature history of the tube wall. The same backwall temperatures were used to compute the heat flux, the inside wall temperature, and the heat transfer coefficients. Therefore, a few degrees error in thermocouple reading could lead to a large error in the heat flux and the heat transfer coefficient. Reference 16 indicates that heat transfer coefficients at the end of cooldown are not valid because experimental errors in temperature measurements are of the same order of magnitude as the temperature difference between the wall surface and the hydrogen Also above a ΔT of about 400 R, a sharp drop in heat flux (Fig. 35 through 38) and heat transfer parameter (Fig 40 through 43) take place. This occurs at about 0.1 second from the start for steels and at about 0.9 second for copper tube and Tens-50 tube. The heat transfer response time is the cause of error at the start of the tests These values are not shown on the remainder of the figures.

The effect of pressure on heat flux is not readily evident in Fig. 35 through 39. This is because the pressure changes are not great and also the pressure changes are accompanied with mass velocity changes. The mass velocity has a greater effect on the heat flux and tends to mask any effect that the pressure might have. The effect of a mass velocity increase is to increase the heat flux For example, at a ΔT of 250 R, the heat flux is about 0.445 Btu/in ^{2}-sec and 0.64 Btu/in ^{2}-sec for a hydrogen mass velocity of about 1 372 lb/in.^{2}-sec, and 3.540 lb/in.^{2}-sec, respectively, for a K-monel tubing of L/D equal to 40 The effect of an increase in L/D is a decrease in heat flux for the same ΔT, however, the effect is not very prominent Perhaps this is because the variation in L/D is not large

Considering a mass velocity of approximately 1.5 lb/in.^{2}-sec, the heat flux at a ΔT of 300 R is about 0.53, 0.38, 0 27, and 0 23 Btu/in.^{2}-sec for K-monel, stainless steel, Tens-50 aluminum, and copper, respectively. The higher values of heat fluxes for a K-monel tube and stainless-steel tube is attributed to nonapplicability of Eq. 7 for Biot numbers higher

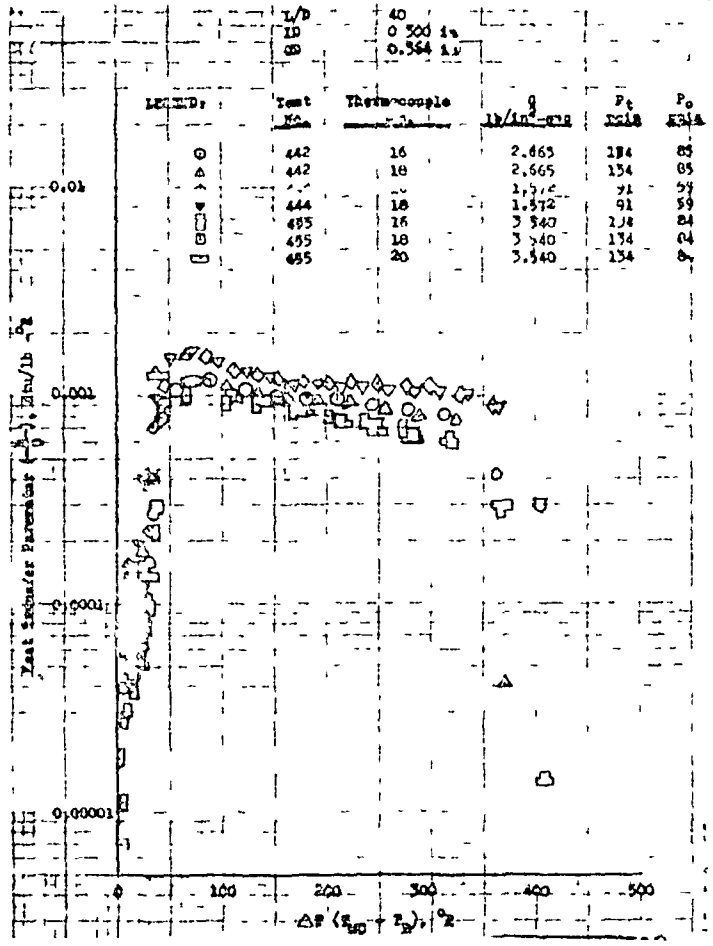

Figure 40. Heat Transfer Parameter vs ΔT for Chilldown of a K-Monel Tube

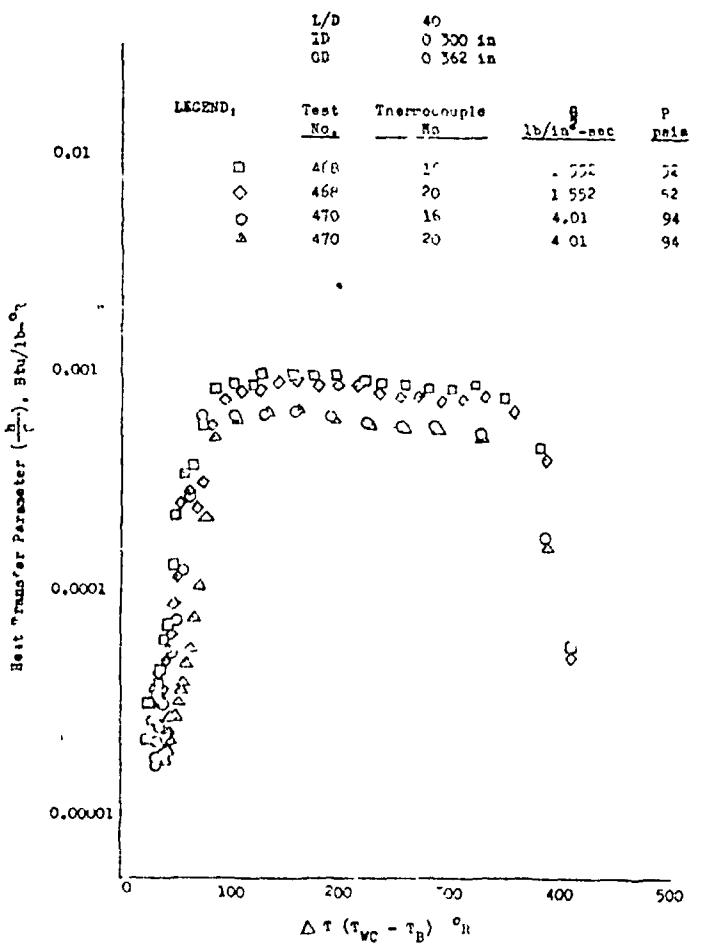

Figure 41. Heat Transfer Parameter vs ΔT for a Stainless-Steel Tube

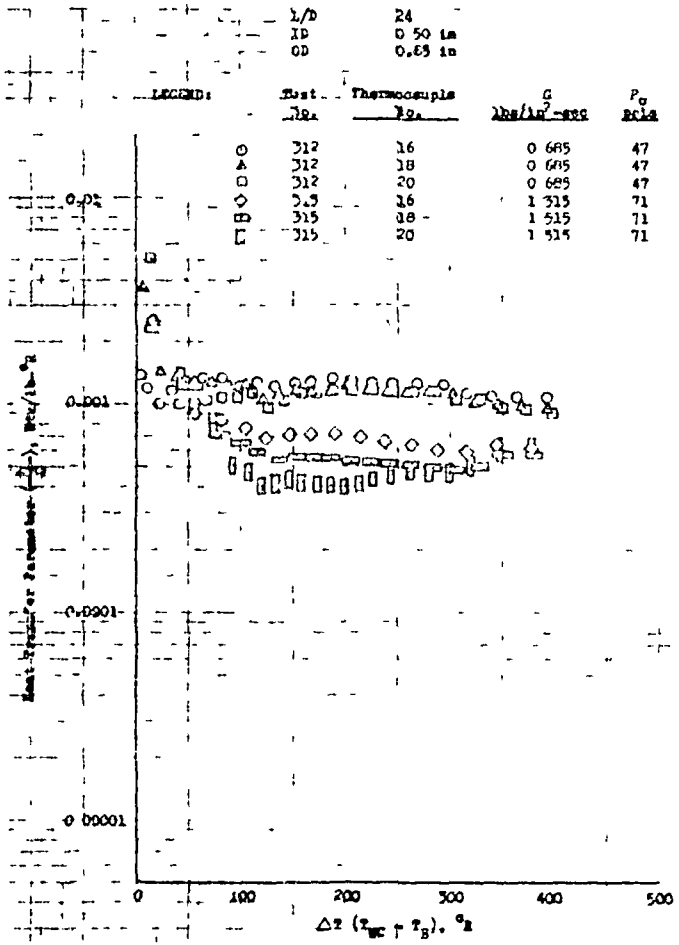

Figure 42. Heat Transfer Parameter vs ΔT for Chilldown of a Tens-50 Aluminum Tube

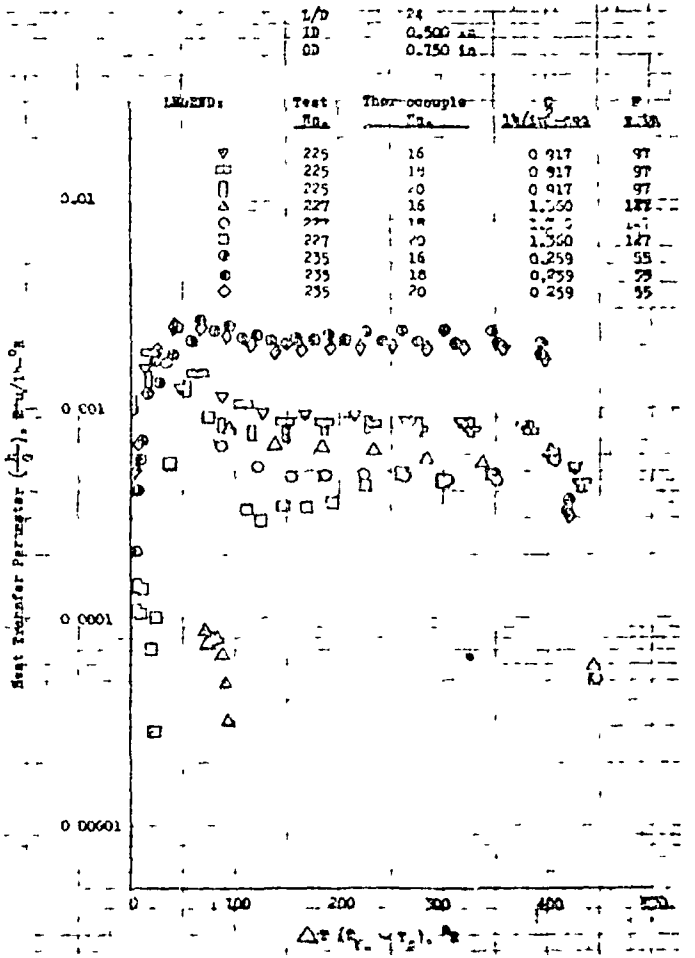

Figure 43. Heat Transfer Parameter vs ΔT for a Copper Tube

than 0.4. Reference 15 indicated that during nucleate boiling of LH_2 the rate of heat transfer at a given surface superheat was as much as 25 times greater from a copper surface than from a stainless-steel surface prepared in an identical manner. The effect of material was not clearly evident in the unheated tube cooldown data. Present tube cooldown experimental data do not appear to extend down to the nucleate boiling region. However, in the convective film-boiling region, the heat transferred from a K-monel surface is higher than stainless steel, Tens-50 aluminum, and copper, in that order, for a comparable mass velocity and diameter. This difference is, however, due to the inaccuracy of the results for K-monel and stainless-steel tubes.

Figure 39 shows a plot of Q/A against $T_w - T_s$ for the unheated tube tests. The results of Ref. 11 and 13 through 15 are also shown on Fig. 39. This figure shows that in the 40 to 400 R ΔT range, the results of the unheated tube tests agree fairly well with the results of Ref. 11 and 13. A straight line with a slope of one can be drawn through the data points. Figure 39 indicates that the heat fluxes for K-monel and stainless-steel tubes are higher than the heat fluxes for Tens-50 aluminum and copper tubes at the same mass velocity. The reason is attributed to the fact that Eq. 7 used for determination of heat fluxes and heat transfer coefficients does not produce accurate results for Biot numbers higher than about 0.4. As it can be seen from Table 4, the Biot number is higher than 0.4 for both K-monel and stainless steel. The results of Ref. 14, which are for film boiling with zero mass velocity, are lower than the results of unheated tubes. The difference is the contribution of the forced convection to the heat flux. In the nucleate boiling region ($\Delta T < 5$), the results of Ref. 15, which are for zero mass velocity, are higher than those of the tube cooldown data. As mentioned earlier, the results of the unheated tubes are not reliable below a ΔT of 40 R.

The existence of two-phase flow during tube cooldown tests was established by the motion pictures taken from the hydrogen at the tube inlet and outlet. However, the absolute value of the H_2 quality was not determined. Reference 11 has used the Martinelli parameter, X_{tt}, as the abscissa to correlate the

TABLE 4

TUBE LH_2 COOLDOWN PARAMETERS

Run No.	P_o', psia	Nominal Bulk Temperature, R	w, lb/sec	G, lb/in^2-sec	Re x 10^{-6}	Initial Wall Temperature, R	Tube Material	ID	OD	L/D	ΔP psi	Flow Stability Remarks
225	97	47.09	0.1807*	0.917	0.94	499	Copper	0.50	0.75	24	***	
227	127	46 58	0.2672*	1.360	1.36	497	Copper	0.50	0.75	24	***	10 cps pressure oscillation 8 to 16 seconds
235	55	42.69	0.051*	0.259	0.22	467	Copper	0.50	0.75	24	***	
312	74	45.63	0.1348*	0.685	0.66	461	Tens-50	0.50	0 85	24	***	Small chugging for first 8 seconds
315	135	47.69	0.2971*	1.515	1.59	454	Tens-50	0.50	0 85	24	***	
442	134	49.04	0.1881**	2.665	1.76	460	k-monel	0.30	0 364	40	11 8**	
444	91	47.09	0.1111**	1 572	0.97	470	k-monel	0.30	0.364	40	***	
455	134	48.18	0.2495**	3.540	2.25	458	k-monel	0.30	0 364	40	6 5	
468	74	45.73	0.1092**	1.552	0.91	456	Stainless Steel	0.30	0 364	40	7.4**	
470	155	48.85	0.2859**	4.010	2 61	453	Stainless Steel	0.30	0.364	40	***	

*Values at 20 seconds from the start

**Values at 5 seconds from the start

***Data not available

data for film-boiling H$_2$ in tubes. The data from transient, as well as the steady-state heated tube, were used in this correlation. The ordinate was chosen as the ratio of experimental to calculated two-phase Nu selt numbers multiplied by the reciprocal of the boiling number raised to the 0.4 power. The equations used in the correlation are

$$Nu_{exp} = \frac{h_{exp} D_t}{k_f} \tag{9}$$

$$Nu_{calc} = 0.023 \left(N_{Re_{tp}}\right)^{0.8} \left(N_{Pr_f}\right)^{0.4} \tag{10}$$

$$N_{Re_{tp}} = \frac{\rho_{fm} V_{av} D_t}{\mu_f} \tag{11}$$

$$\frac{1}{\rho_{fm}} = \frac{\lambda}{\rho_f} + \frac{1-\lambda}{\rho_g} \tag{12}$$

$$N_{Pr_f} = \left(\frac{c_p \mu}{k}\right)_f \tag{13}$$

$$X_{tt} = \left(\frac{1-\lambda}{\lambda}\right)^{0.9} \left(\frac{\mu_g}{\mu_f}\right)^{0.1} \left(\frac{\rho_f}{\rho_g}\right)^{0.5} \tag{14}$$

$$B_o = \frac{q'' A_s}{\lambda W_f h_{fg}} \tag{15}$$

The data are fairly well correlated by this method. No attempt was made to use the above-mentioned correlation in conjunction with the present unheated tube cooldown data simply because the quality was unknown during each test.

Figures 40 through 44 show the heat transfer parameter (h, G) plotted versus ΔT for various tube materials. Although the value of G was changing somewhat from the start of the test, a nominal G shown in table 4 was used

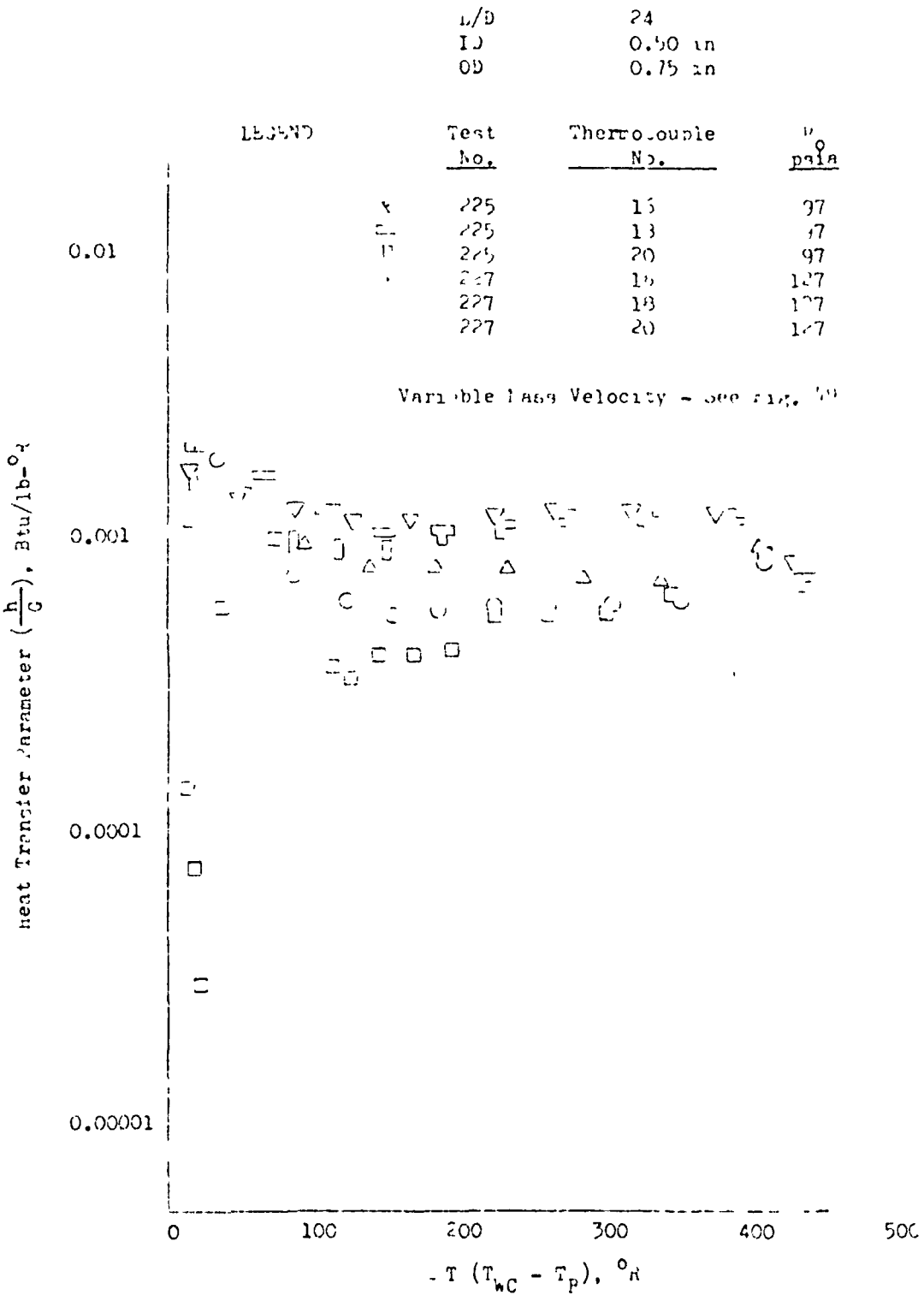

Figure 44 Heat Transfer Parameter vs T for Chilldown of a Copper Tube

for each run. Only for one tube material (copper), the variable G (Fig. 49) was used to compare the results with the constant G (Fig. 43). The use of variable G changed the heat transfer parameter slightly in the very early part of the test (high ΔT), as indicated in Fig. 44 and 45. The heat transfer parameter h/G is generally fairly constant (a slight increase with a decrease in ΔT) in the range of 40 to 300 R value of ΔT This is in very good agreement with results of Ref 13, which also indicated constant h in the range of temperature differences (40 to 300 R) A slight increase in the heat transfer parameter is seen around a ΔT range of 40 to 60 R. The parameter drops very sharply with a drop in ΔT below a $T_w - T_B$ of 40 R If we write

$$(Q/A)_{total} = (Q/A)_{fb} + (Q/A)_{fc} \tag{16}$$

and

$$(Q/A)_{fb} = h_{fb} \Delta T \tag{17}$$

where $(Q/A)_{total}$ is the total heat flux in the convective film boiling region, $(Q/A)_{fc}$ is the heat flux contribution due to the liquid forced convection and can be found by use of a general type forced convection equation (e.g., such as that given for hydrogen by Ref. 17)

$$Nu_{0.4} = 0.023\, Re_{0.4}^{0.8}\, Pr_{0.4}^{0.4} \left(1 + 0.00983 \frac{\nu_h}{\nu_B}\right) \tag{18}$$

The $(Q/A)_{fb}$ is the contribution of film boiling phenomena to the total heat flux If we again write

$$(Q/A)_{fb} = h_{fb} \Delta T \tag{19}$$

or

$$h_{fb} = \frac{(Q/A)_{fb}}{\Delta T} \tag{20}$$

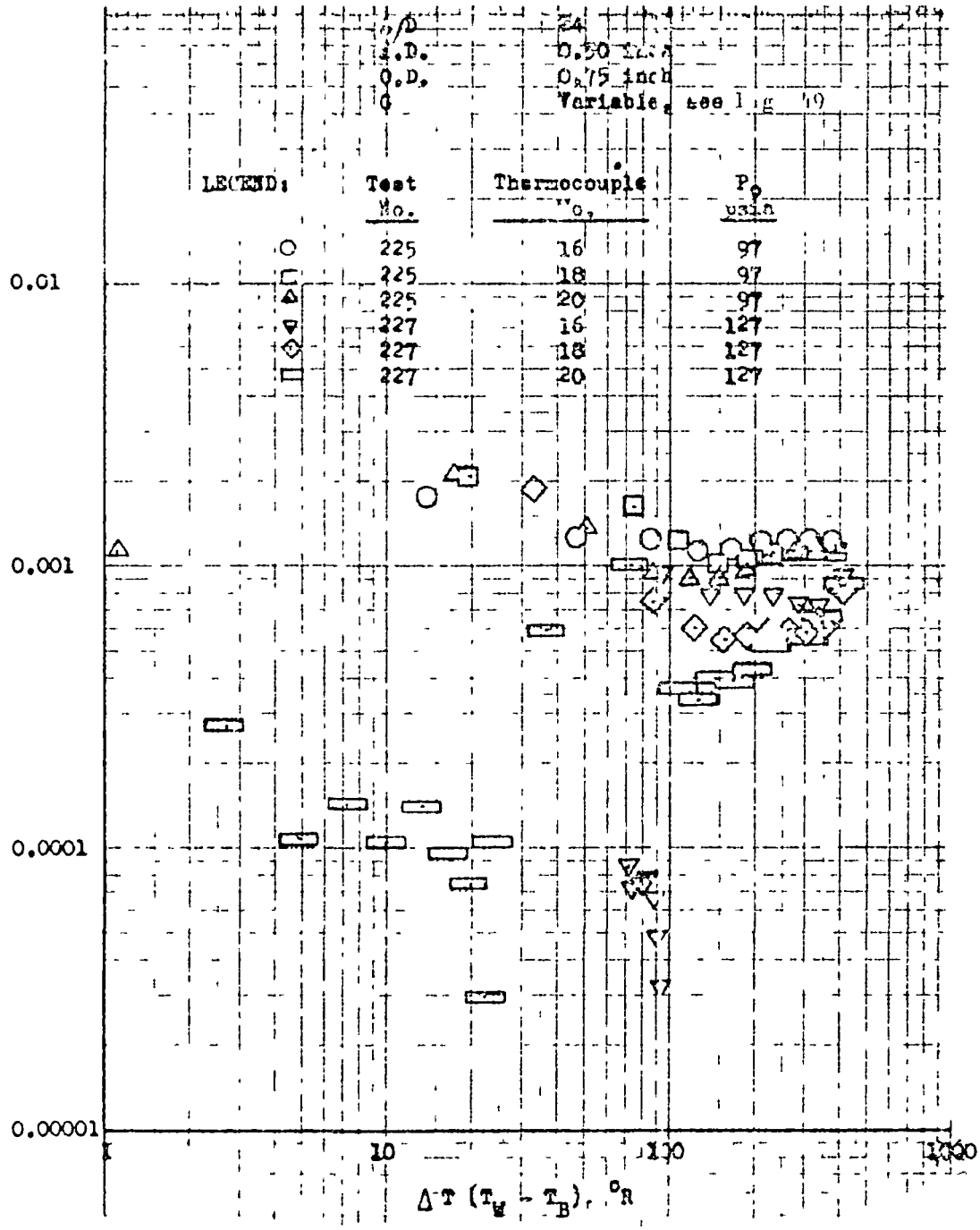

Figure 45 Heat Transfer Parameter vs ΔT for Copper Tube Cooldown Test

it is possible to develop a correlation for the film-boiling heat transfer coefficient similar to Eq 33 of Ref 10 which is for the pool boiling portion of the forced-convection boiling correlation Similarly, the overall (combined) heat transfer coefficient in the forced-convection boiling region (Δt range of 40 to 400 R) can be written as

$$h_{cm} = \frac{(q/A)_{total}}{\Delta t} \tag{21}$$

Figures 46 and 47 are transformed into Fig 48 in terms of heat transfer coefficient versus mass velocity The effect of tube material and surface roughness on the heat transfer coefficient are not quite clear The data of Ref 13 are also shown on Fig 48 for comparison purposes. It is seen that the results of the K-monel unheated tube and the results of Ref 13 (obtained with a heated copper tube) agree fairly well Any difference that exists between the two could be attributed to the differences in the quality of the flowing H_2, the surface conditions of the tubes, in addition to slight error contained in K-monel data (Ref. 12)

Discarding the very small effect of Δt on the heat transfer coefficient in the range of 40 to 400 R temperature difference, the film coefficient for boiling forced convection, with the limited data available, can be written as follows

For a K-monel tubing, this combined h is given as

$$h_{cm} = 0.00125\, G^{0.5} \tag{22}$$

For stainless-steel tubing

$$h_{cm} = 0.0010\, G^{0.5} \tag{23}$$

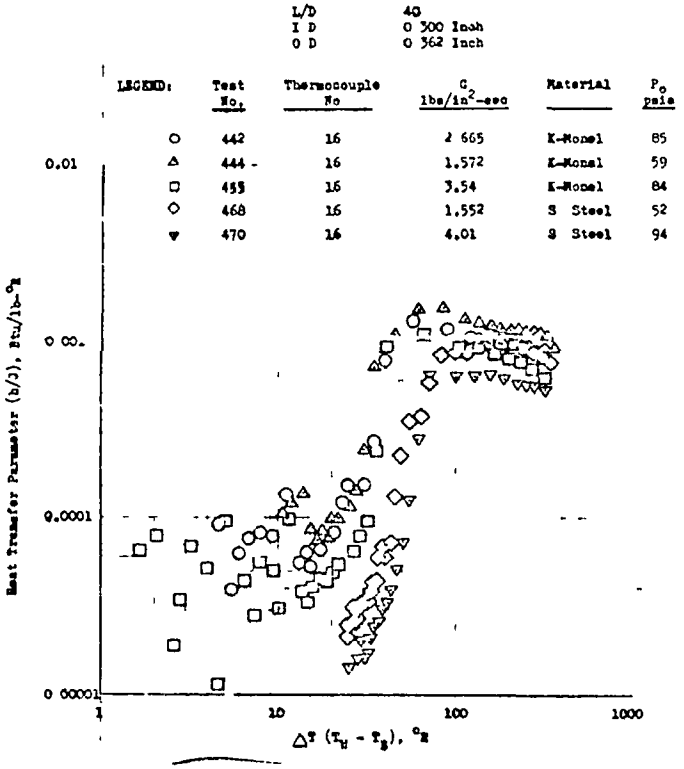

Figure 6. Heat Transfer Parameter vs ΔT for Tube Cooldown

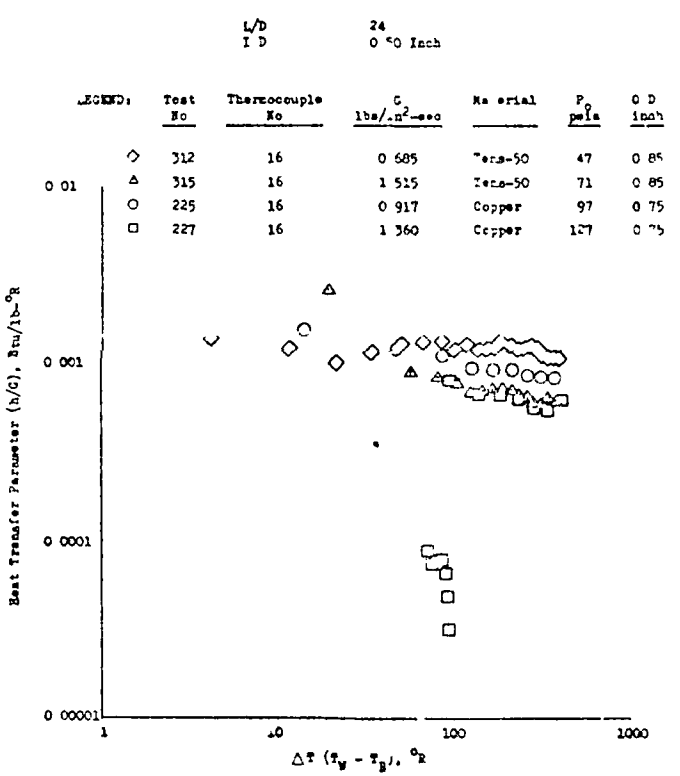

Figure 47. Heat Transfer Parameter vs ΔT for Tube Cooldown

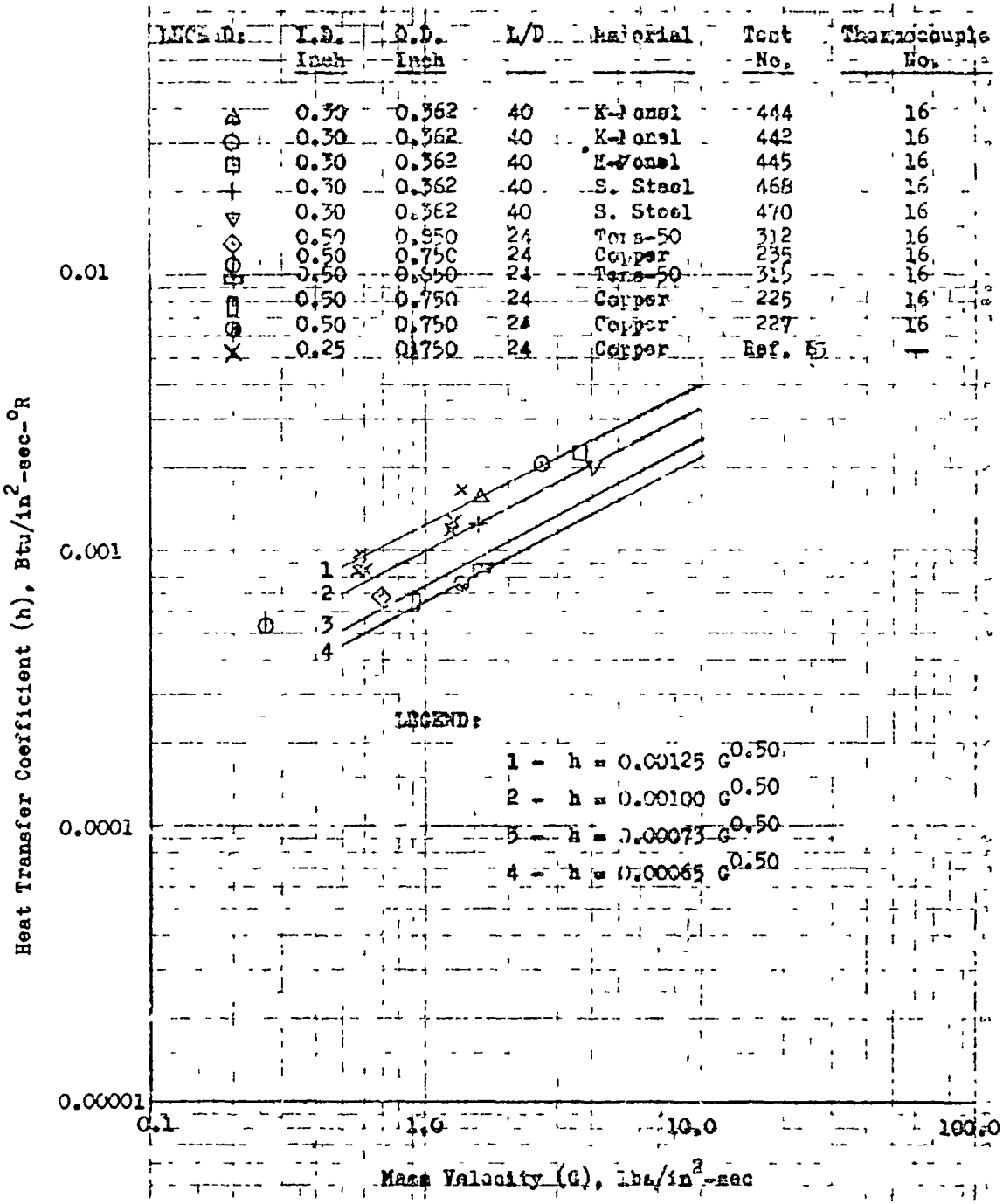

Figure 48. Heat Transfer Coefficient vs Mass Velocity for Various Tube Cooldown Tests

For the Tens-50 aluminum tubing, this combined h is given as

$$h_{cm} = 0\ 0073\ G^{0\ 5} \tag{24}$$

For the copper tubing

$$h_{cm} = 0.00065\ G^{0\ 5} \tag{25}$$

The exponent on the mass velocity G and the constant cannot, however, be accurately assessed for the small range obtained during testing. The accuracy of the equations will be verified if additional data become available. Obviously, there are some pressure, surface conditions, and metal influences on the heat transfer coefficient that are not readily evident from Eq 22 through 25 At this time, no attempt was made to determine the individual or the total influence of the above-mentioned parameters.

In the analysis of the J-2 engine system, use of Eq. 22 through 25 will be made where application is warrented. A plot of H_2 flowrate versus time is shown in Fig. 49 for the cooldown of copper tube It is seen that within the first couple of seconds the H_2 flowrate rises very rapidly with time. The flowrate continues to increase with time but at a very slow rate. Eventually, steady state will be reached if the cooldown time is sufficiently long (not the case here). These flowrates were used to construct Fig 44 and 45 , which show the values of h/G plotted versus ΔT.

The liquid side-wall temperature versus chilldown time is plotted on Fig 50 through 53 for K-monel, stainless steel, Tens-50 aluminum, and copper tubes, respectively. In the case of K-monel and stainless steel, the liquid side-wall temperature drop from about 470 and 460 R to about 75 R in approximately 1.2 and 1 8 seconds, respectively, for a nominal H_2 flowrate of about 1.55 lb/in ^{2}-sec. The effect of higher H_2 flowrate is to reduce the chilldown time requirements. For example, for K-monel

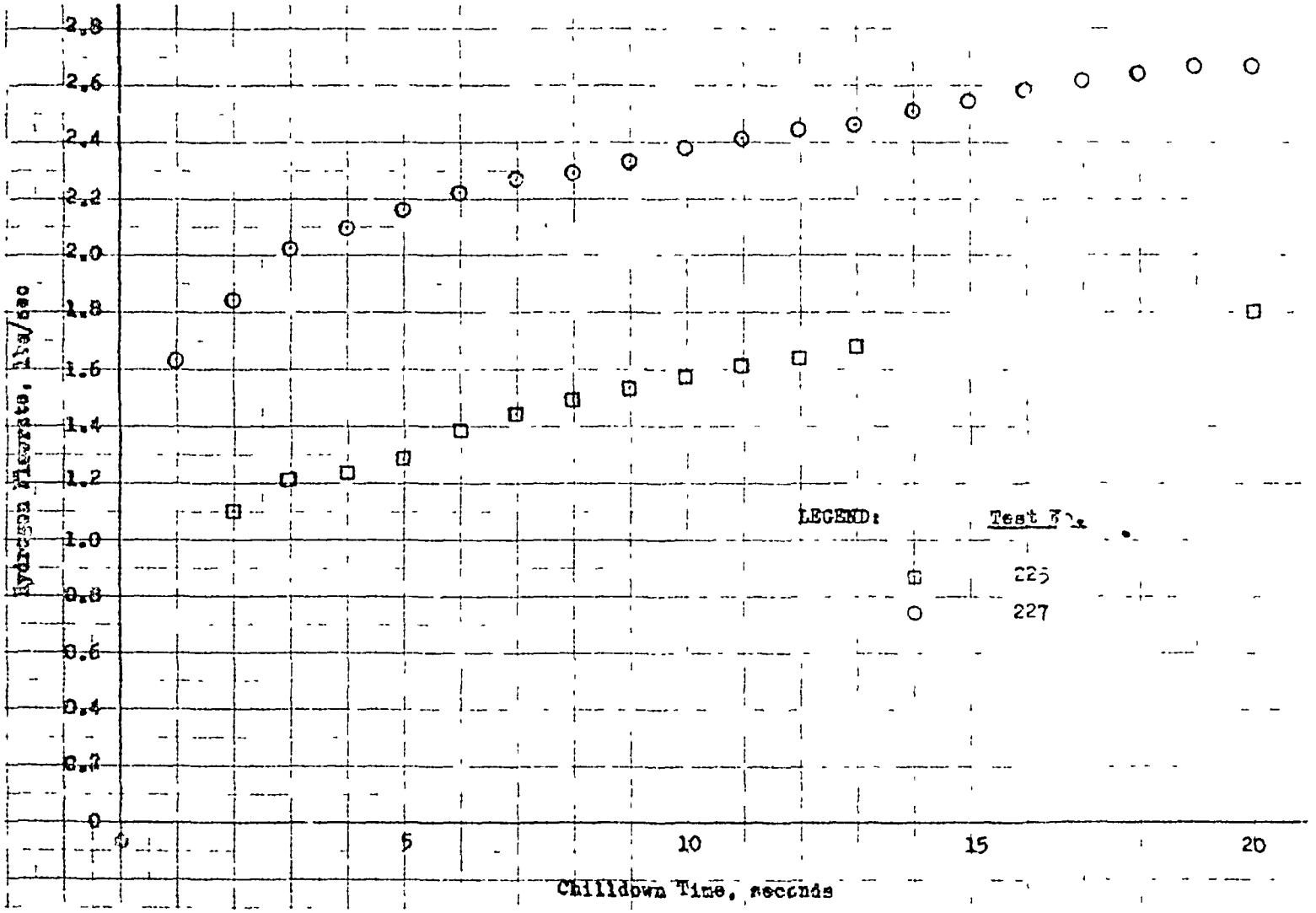

Figure 49. Hydrogen Flowrate vs Chilldown Time for a Copper Tube

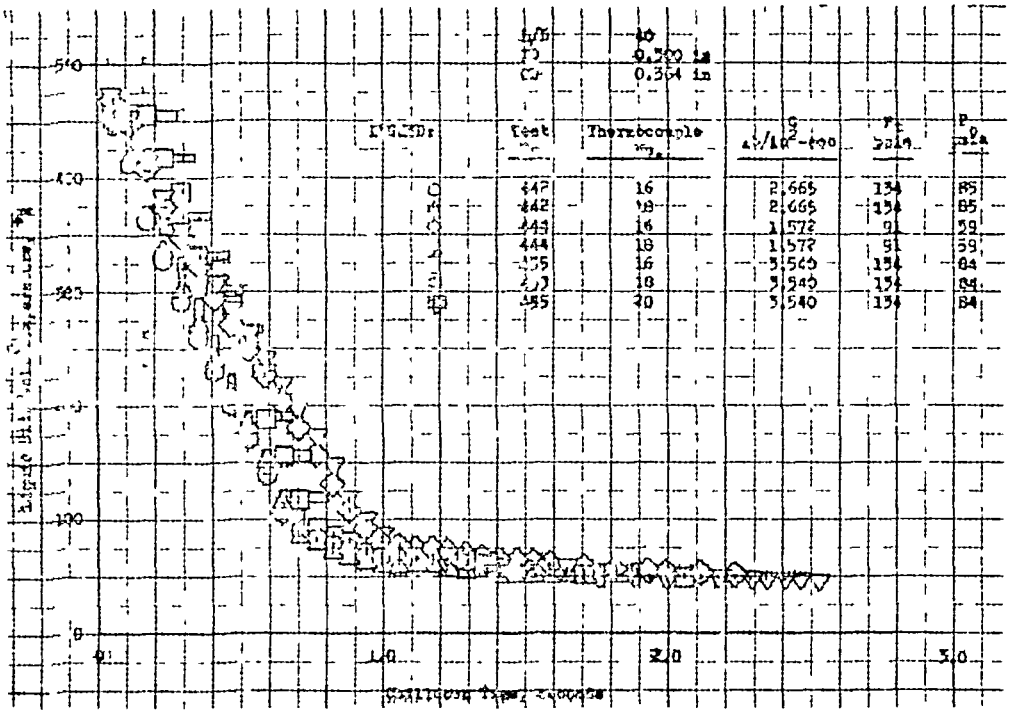

Figure 30 Liquid Side Wall Temperature vs Chilldown Time for a k-monel Tube

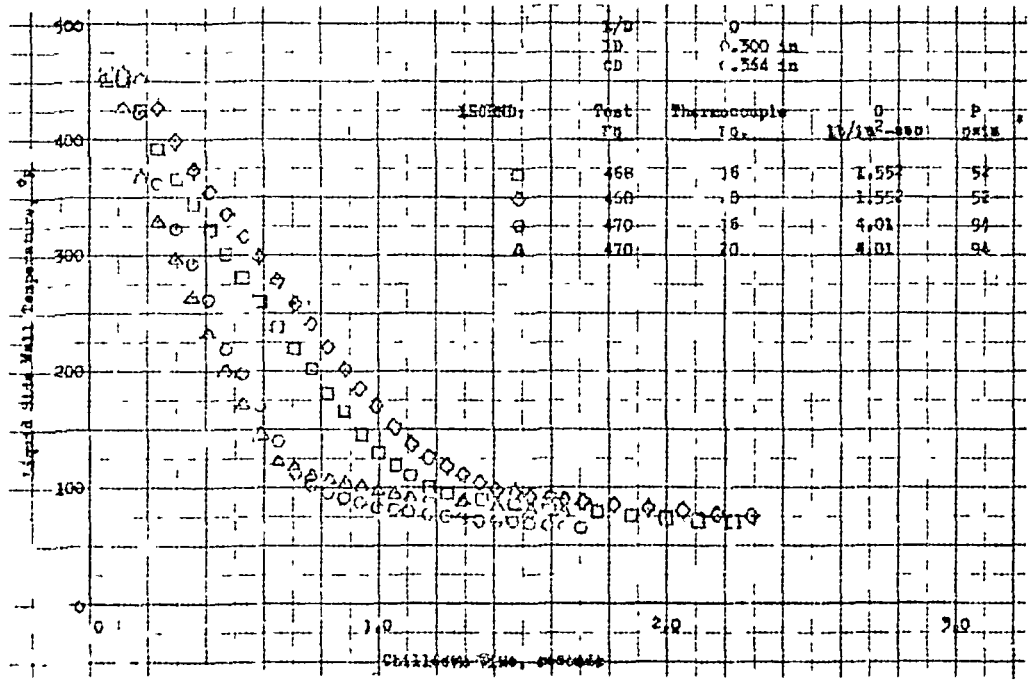

Figure 31. Liquid Side Wall Temperature vs Chilldown Time for a Stainless-Steel Tube

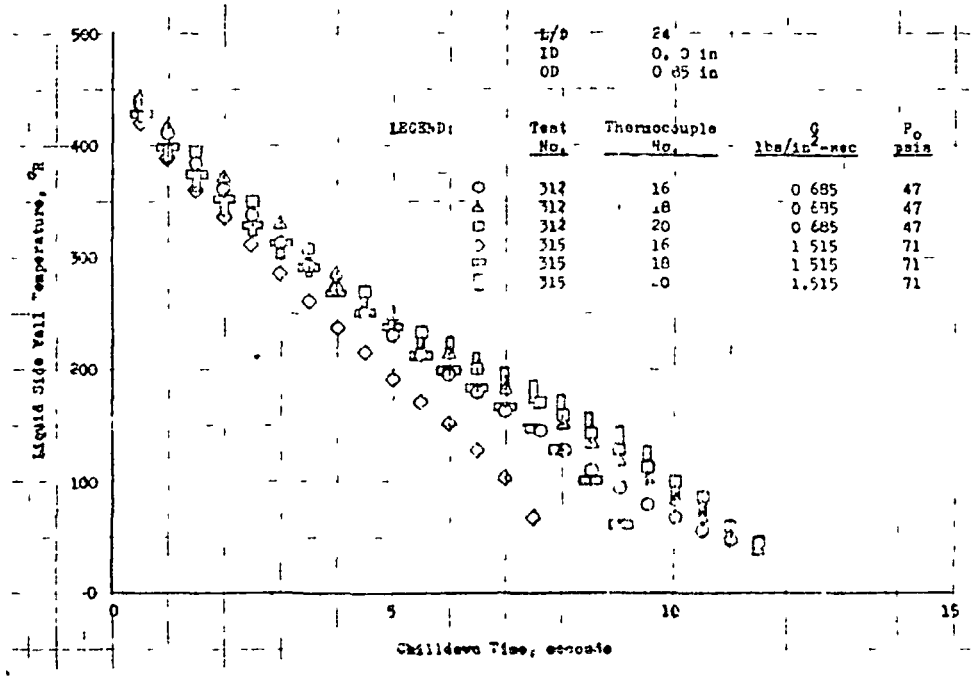

Figure 52. Liquid Side Wall Temperature vs Chilldown Time for a Ten-50 Aluminum Tube

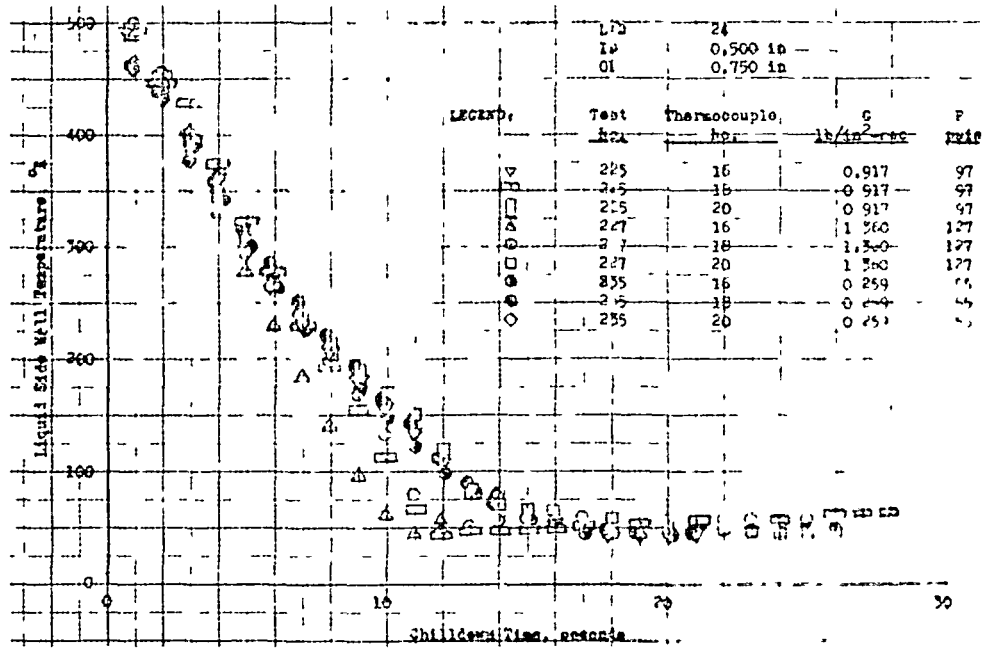

Figure 53. Liquid Side Wall Temperature vs Chilldown Time for a Copper Tube

tubing, the liquid side-wall temperature decreased from an original value of about 465 to 372 R in 1 0 and 1 2 seconds for a mass velocity of 3 54 and 1 57 lb/in^2-sec, respectively.

Figure 54 is a plot of the liquid and the outside wall temperature versus chilldown time for a K-monel tube Both wall temperatures start at about 470 R Immediately after start of chilldown, a temperature difference is created between the two wall surfaces This temperature difference decreases with chilldown time and eventually vanishes if the chilling is continued for a sufficiently long period. Figures 51 and 53 (Tens-50 aluminum) indicate that the outside wall temperatures are not too far behind the liquid side-wall temperatures during a chilldown if the wall is not too thick or the thermal conductivity not excessively low.

Figure 56 shows the outside wall temperature of a titanium tube versus chilldown time There were no liquid side-wall calculations made for titanium due to high Biot numbers, which indicated no accurate liquid side-wall temperature can be determined without having temperature history at two different locations in the wall. However, one can deduce that the liquid side-wall temperature for titanium drops much faster than those of Tens-50 and copper

Comparing the chilldown time of Tens-50 aluminum and titanium, one will notice that for a backside wall temperature of 200 R the H_2 flowrate is about 0.685 and 1 100 lb/in^2-sec and the chilldown time is about 5 9 and 6.3 seconds, respectively. Even though the H_2 flowrate is higher for the titanium tubing, the required cooldown time for the titanium backside wall is still higher than for Tens-50 aluminum. The two tubes have nearly the same total heat content and the difference in the required chilldown time is due to the difference in their thermal conductivities. The thermal conductivity of titanium is lower than Tens-50 aluminum, therefore, the required backside chill time is shorter for Tens-50 aluminum. On the other hand, the liquid side temperature of titanium drops much faster than for the Tens-50 material.

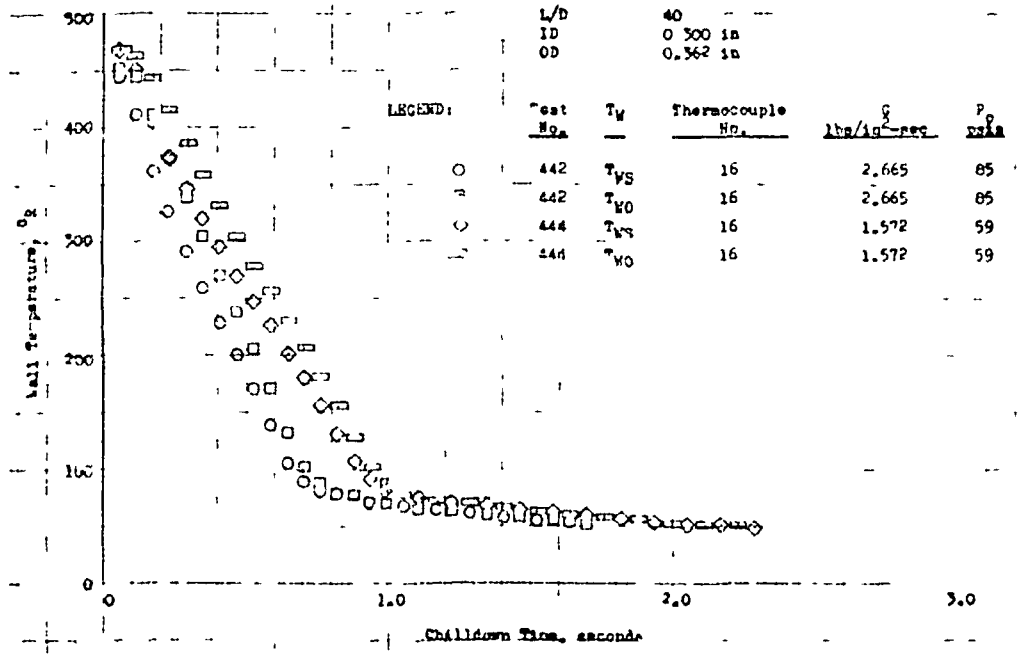

Figure 54. Wall Temperature vs Chilldown Time for a K-monel Tube

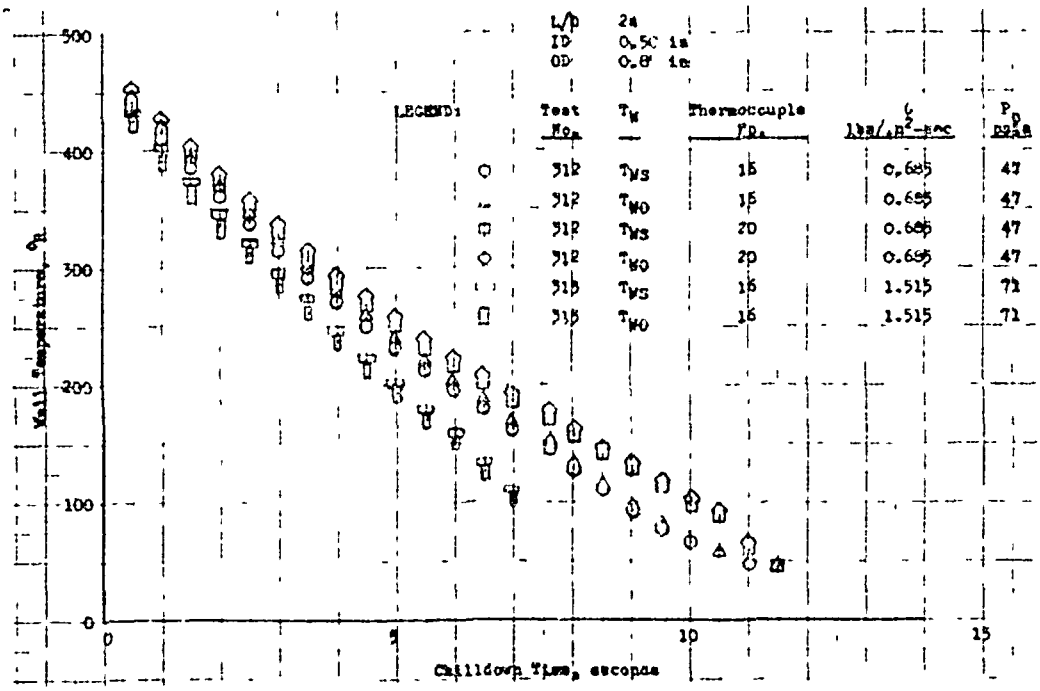

Figure 55. Wall Temperature vs Chilldown Time for a Tens-30 Aluminum Tube

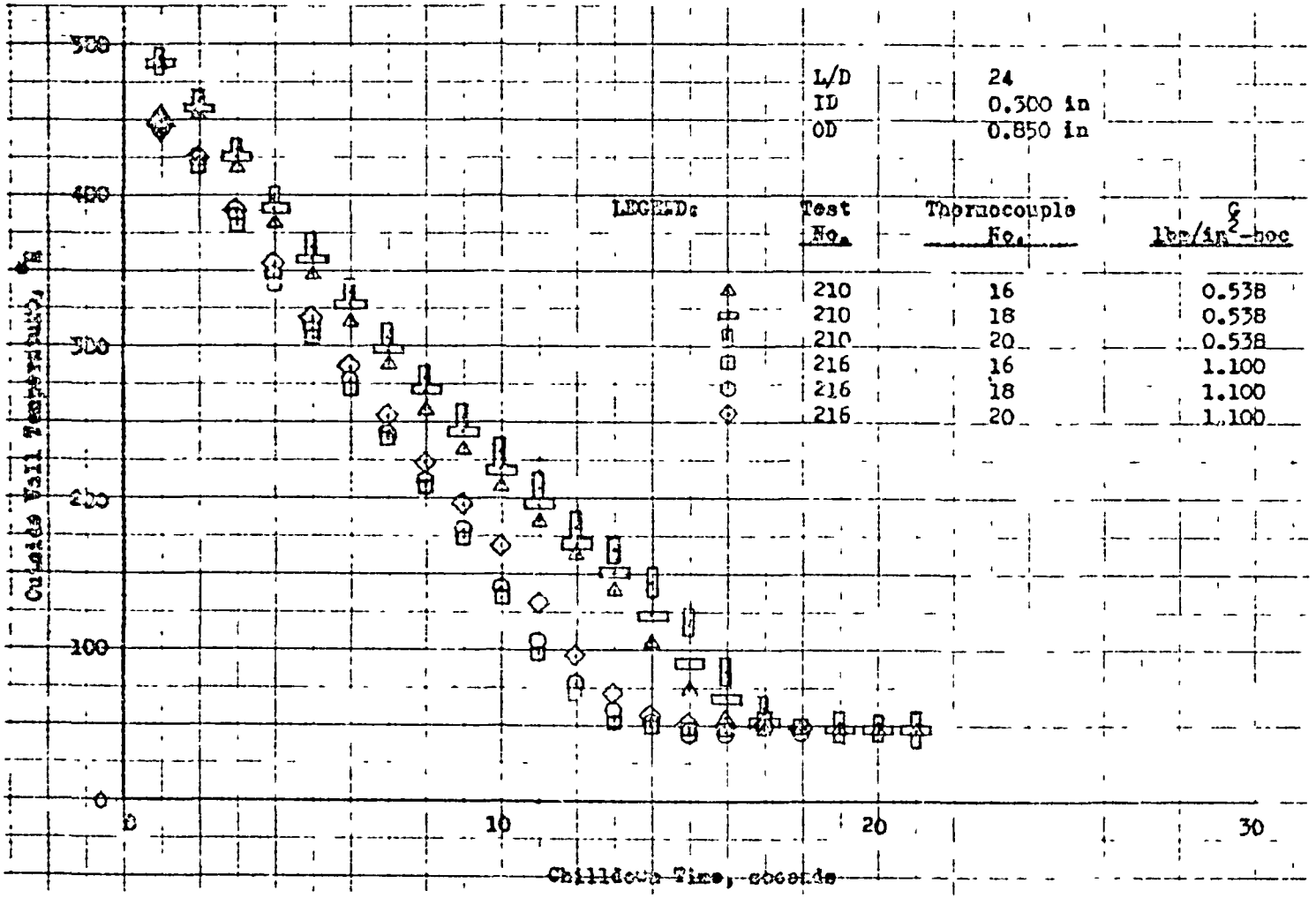

Figure 56 Outside Wall Temperature vs Chilldown Time for a Titanium Tube

The chilldown time for the liquid side-wall temperature of Inco-50 aluminum, titanium, and copper to reach 75 R is on the order of 10 seconds, which is much longer than chilldown time for steels. The longer chilldown time is due to higher original heat content (thicker walls) of the latter three tubes.

During the cooldown tests, H_2 bulk temperature was measured however, no noticeable bulk temperature rise was observed. The bulk temperature increased at the start of chilldown and then immediately dropped to its original value. This is due to very low heat input from the tube to the coolant H_2.

Figure 57 (presented for the reader's interest only) is a typical plot of H_2 bulk temperature versus chilldown time. Because the thermocouples were not calibrated, their accuracy is in doubt.

Reference 18 has presented an extensive theoretical model for determination of two-phase flow heat transfer by using single-phase variable property. Although the theoretical results agree fairly well with the experimental results, the model was not used in the analysis of the J-2 engine system chilldown because of its complexity, iterative procedures involved, and the fact that the model should be programmed to be coupled with thermal analyzer (TAP 51) computer program.

A sophisticated analysis of the J-2 engine system demands the exact knowledge of the local condition of the H_2 during the entire transient chilldown time. At the onset of flow, the LH_2 is heated in the inlet duct, pump, thrust chamber tubes, etc., and by the time it reaches the injector it has picked up a considerable amount of heat so that complete vaporization is accomplished. This means three regions of fluid-flow--LH_2, two-phase flow, and gaseous H_2--take place in the system. As the chilldown time increases, the LH_2 front moves toward the chamber. However, some period of time will pass before all LH_2 will enter the thrust chamber if ignition has not started. Although the thermal analyzer is capable of

Hydrogen bulk temperature, °F
0
10
20
30

handling such intricate problems, the simpler approach to the chilldown analysis will be taken to avoid excessive cost of computing machine time.

Coated Tubes. The cooldown data obtained from the Rel-I coated 321 stainless-steel tube tests (CRL plots) are shown in Fig. 58 through 61. The thermocouple locations are shown on the sketch of the test section in Fig. 62.

For comparison purposes, the data from the uncoated stainless-steel tube is also plotted on Fig. 60. The mass flowrate for the coated and uncoated tube was about 1.14 and 1.55 lb/in^2-sec, respectively. It is seen that the mass velocities are nearly equal, but the backside wall temperature of uncoated tube decreased much faster than the backside wall temperature of the coated tube. Therefore, it is evident that a coating on the inside of the tube will definitely reduce the H_2 requirement for the chilldown of the J-2 engine system. The reason is that the coating has a thermal conductivity that is normally about two orders of magnitude lower than the thermal conductivity of the base metal. Therefore, the coating constitutes a thermal resistance to the flow of heat from the metal wall to the H_2 coolant. The heat stored in the wall will be eventually dissipated into the fluid passing by the wall. However, this heat flow will be at such a slow rate that no, or very little, vaporization of the H_2 will take place.

The determination of the coating thickness requirement for a good thermal barrier is important. If thin coating is applied to the inside of the duct, it is possible to actually increase the heat flux as shown by Ref. 19. Therefore, the coating should be thick enough to be a good thermal barrier and yet not too thick that it will crack because of thermal stresses.

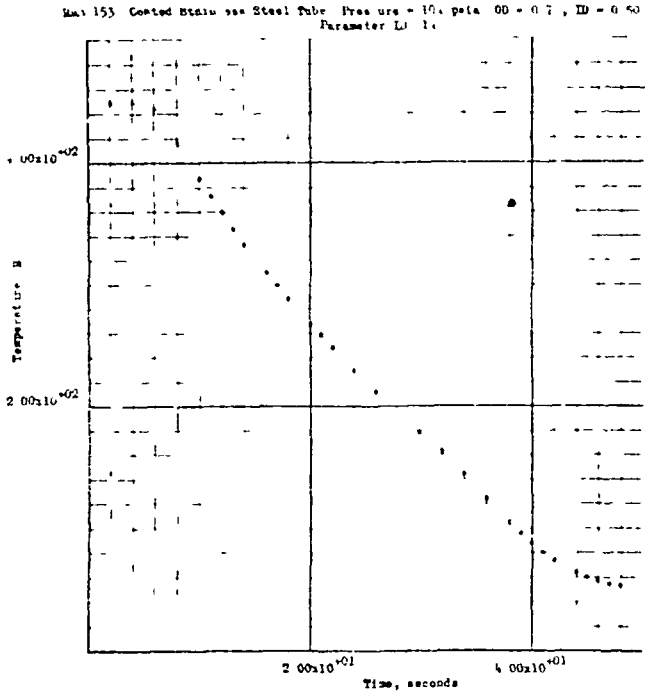

Figure 58. Cooldown of a Kel-F Coated 321 Steel Tube. Run 153. Flowrate 0.223 lb/sec. Reynolds Number 1,130,000. Thermocouple 1.

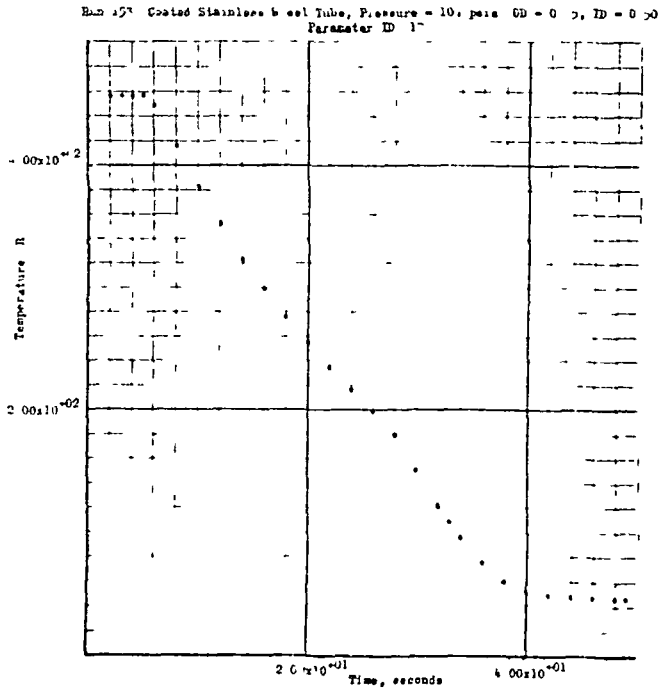

Figure 59. Cooldown of a Kel-F Coated 321 Steel Tube. Run 153. Flowrate 0.223 lb/sec. Reynolds Number 1,130,000. Thermocouple 17

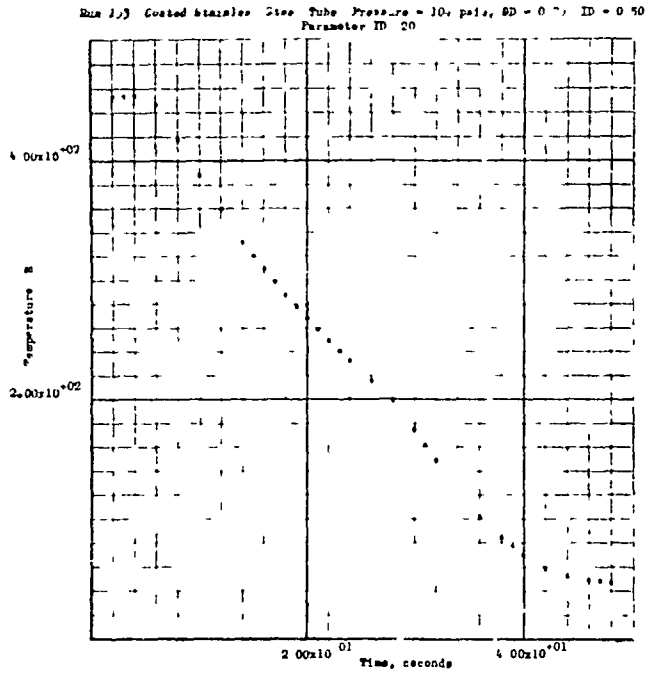

Figure 60. Cooldown of a Kel-F Coated 321 Steel Tube. Run 153. Flowrate 0.223 lb/sec. Reynolds Number 1,130,000. Thermocouple 20

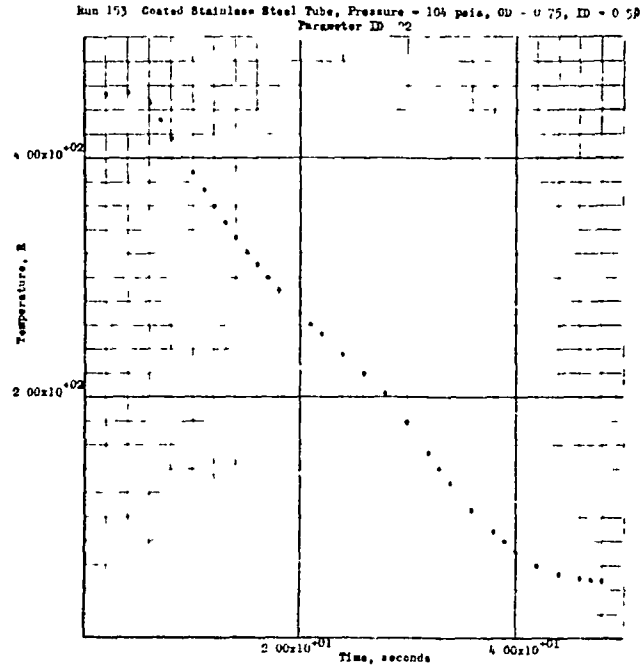

Figure 61. Cooldown of a Kel-F Coated 321 Steel Tube. Run 153. Flowrate 0.223 lb/sec. Reynolds Number 1,130,000. Thermocouple 22

SECTION AA

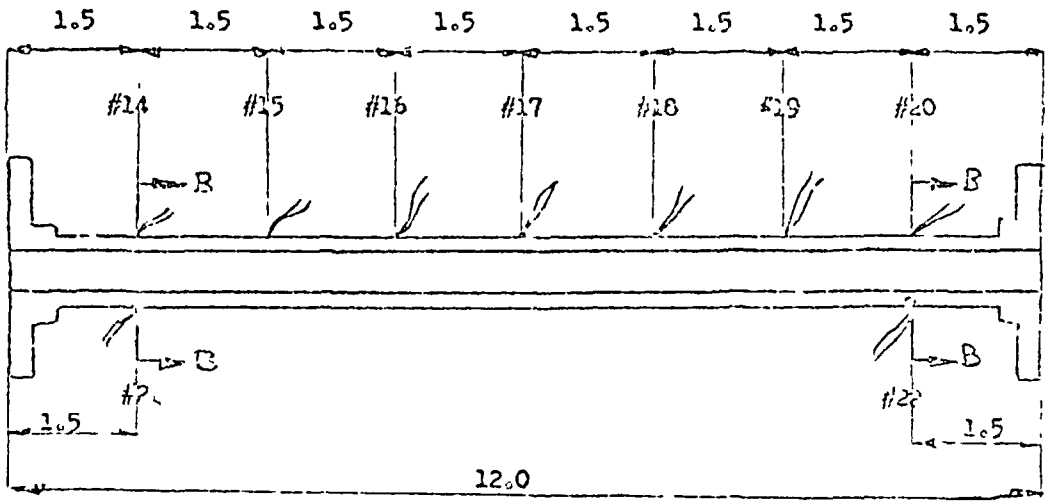

SECTION BB

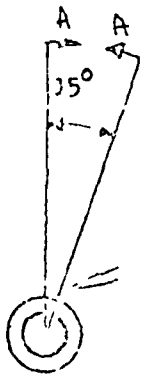

Figure 62 Thermocouple Location and Identification

Warm Pump Operating Conditions

To establish the chilldown requirements of an LH_2 pump, the ability of the pump to deliver pressure and flow while warm must be determined. Therefore, the ratio expressed by Eq. 26 was derived.

$$r = \frac{(dT/dP)_{inlet}}{(dT/dP)_{vapor}} \tag{26}$$

The numerator expresses the LH_2 temperature rise (due to heat transfer at the pump inlet) per unit pressure rise (added by the pump at its inlet). The denominator is the slope of the vapor temperature versus vapor pressure curve at the pump inlet LH_2 temperature. Consequently, if the inlet LH_2 is saturated, a value of r that is less than one will indicate that the flow will remain liquid (Fig. 63) and, therefore, can be pumped. If r is greater than one, vapor will be generated at the pump inlet (Fig. 63) and, therefore, the flow may be difficult to pump.

The pump operating conditions at the warm pumping limit were obtained by setting r equal to one and solving for the rotational speed. This speed is expressed as a fraction of the design speed by Eq. 27.

$$\frac{N}{N_D} = \left\{ \frac{4\, g_c\, NSHA}{\eta' \left(1 - \frac{A_1}{A_2}\right) \frac{\phi_P}{\phi_{FD}}\, \rho_L\, \phi_{TD}\, U_{TD}^3} \left[\frac{\Delta T}{\frac{\rho_L\, C_1}{\rho_V\, (S_V - S_L)} - \frac{1 - \eta'}{\eta'}} \right] \right\}^{1/3} \tag{27}$$

From the tube cooldown test data analysis, the expression for the heat transfer coefficient is (ft/lb-sec units)

$$h = 0.012\, (\rho_L\, U_T)^{0.5} \tag{28}$$

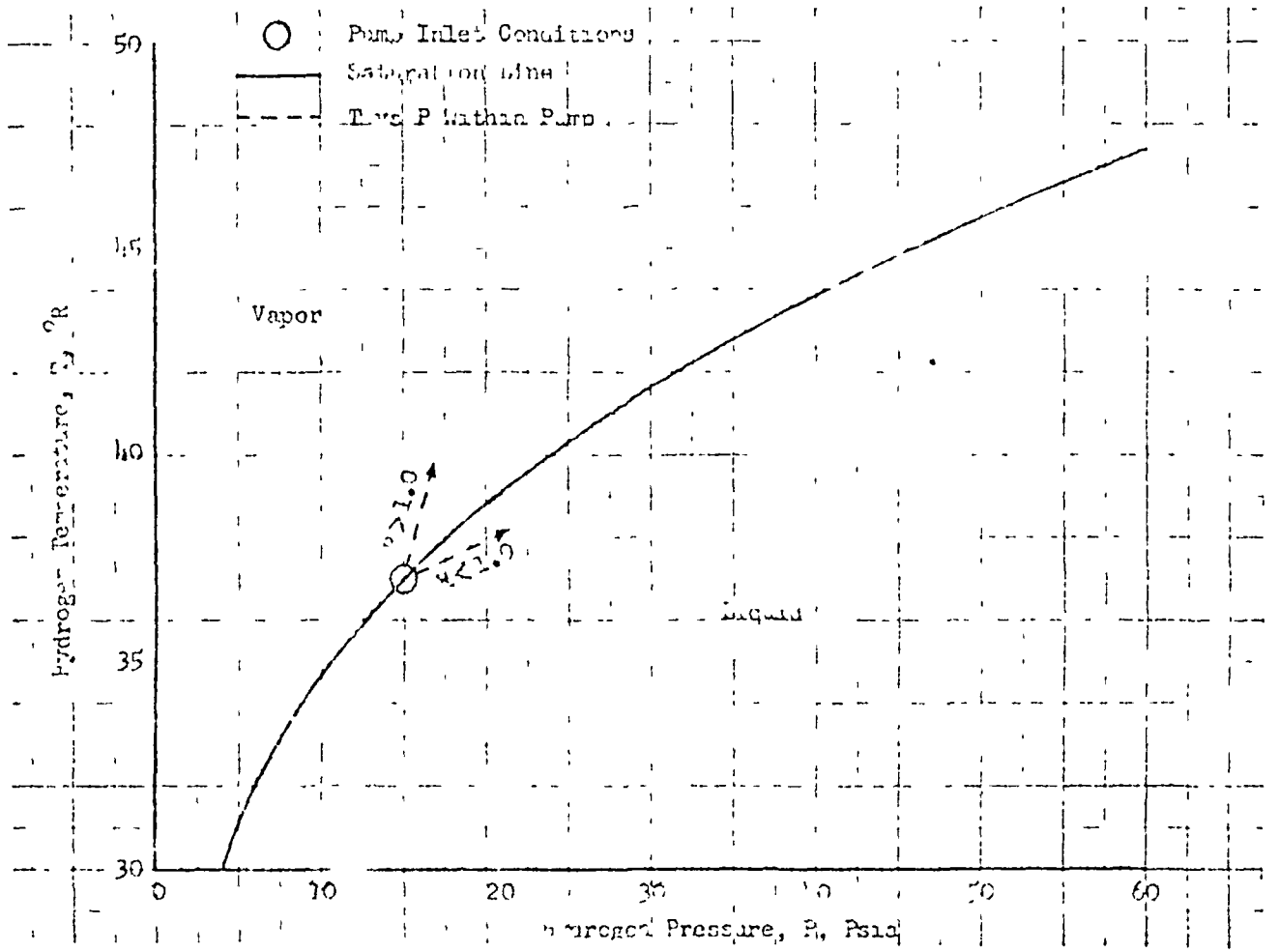

Figure 63 Illustration of "Hot" Hydrogen Pump Pumping Capability Parameter, R

Therefore, substituting into Eq 27, the limiting rotational speed fraction becomes

$$\frac{N}{N_D} = \left\{ \frac{0.0148\, g_c\, JSV}{\eta' \left(1 - \frac{A_1}{A_2}\right) \frac{\phi_1}{\phi_{1D}} \rho_1^{0.5} \phi_{1D}^{0.5} U_{1D}^{2.5}} \left[\frac{\Delta T}{\frac{\rho_1 C_1}{\rho_1 (C_1 - C_{1'})} - \frac{1 - \eta'}{\eta'}} \right] \right\}^{0.4} \quad (29)$$

where the inducer inlet to discharge area ratio is

$$\frac{A_1}{A_2} = \left(\frac{A_1}{A_2}\right)_D \frac{\phi_T}{\phi_{TD}} \quad (30)$$

the inducer efficiency based on static pressure rise is approximated by

$$\eta = \frac{2}{\frac{A_2}{A_1} + 1} - 0.04 \left[\frac{\frac{A_2}{A_1} + 1}{\frac{A_2}{A_1} - 1} \right] \quad (31)$$

and the volume flowrate fraction is

$$\frac{Q}{Q_D} = \frac{\phi_T}{\phi_{TD}} \frac{N}{N_D} \quad (32)$$

For warm inducer blades (i.e., blade temperature = T_b), the factor λ is expressed by Eq 33

$$\lambda = \frac{1}{1 + \lambda} + \frac{\pi}{50\,(1 - \lambda)} \sqrt{\frac{2}{1 + \lambda^2}} \quad (33)$$

and for cold inducer blades (i.e , blade temperature = T), by Eq 34·

$$\lambda = \frac{\pi}{50\ (1 - \lambda)} \sqrt{\frac{2}{1 + \lambda^2}} \tag{34}$$

The hydrogen properties were obtained from the equilibrium flow process correlations and from Ref. 7

These equations were used to predict the operating conditions under which a Mark 15-P pump will pump saturated LH_2. For pump inlet pressures of 15, 30, and 45 psia, these operating conditions are shown on Fig. 64 through 66, respectively, as a function of pump inlet surface temperature and pump inlet flow coefficient. Because inducer blades are thin and therefore chill very rapidly, predictions for both warm and cold blades were made. These curves form the boundaries of the possible operating conditions. For example, referring to the cold blade curve at an inlet static pressure of 15 psia (Fig. 64), a surface temperature of 500 R, and a rotational speed of 15 percent of design, the pump should not generate any vapor due to heat addition if the flowrate is between 10 and 16 percent of design At flowrates beyond this range, vapor may be generated by heat addition within the pump and, consequently, the pumping capability may be impaired. Figures 64 through 66 indicate the inducer blades may require chilling before pumping without vapor generation can begin In addition, the indicated range of pumping capability is greater at lower inlet pressures. This is because the slope of the LH_2 saturation curve (temperature versus pressure) is greater at lower pressures (Fig. 63).

Figure 65 illustrates how surface temperature affects the conditions under which a pump can operate if the inlet pressure is 30 psia. If the inducer blades have the same surface temperature as the flow annulus, the Mark 15 LH_2 pump can be started at 16 percent of design flowrate if the surface temperature is 500 R and at 7 percent if the surface temperature is 100 R Assuming the inducer blades chill very rapidly (which, due to

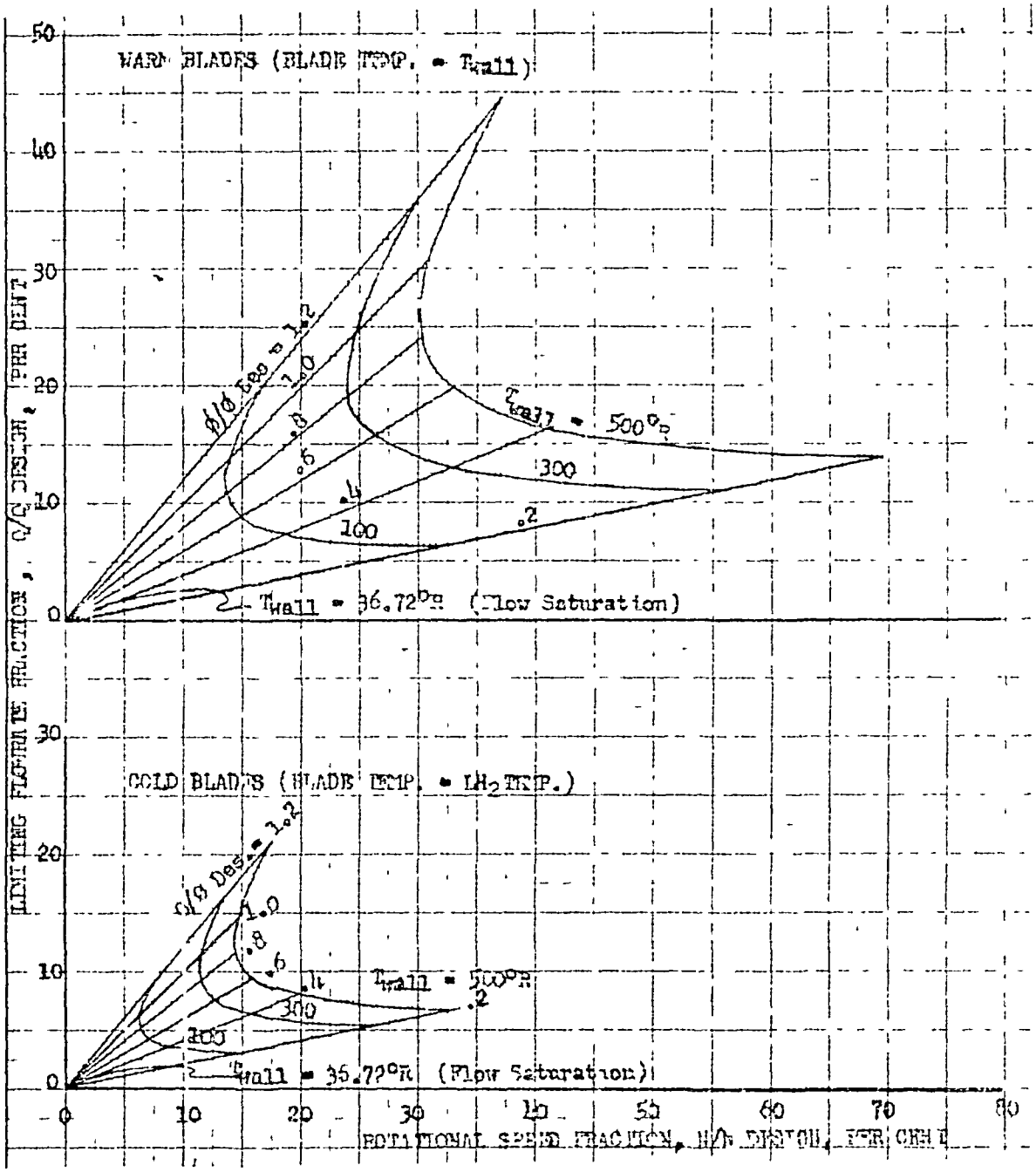

Figure 64 Regions of Pumping Capability for a Warm Mark 15 Pump (Pump Inlet Flow Conditions = Saturated LH_2 at 15 psia)

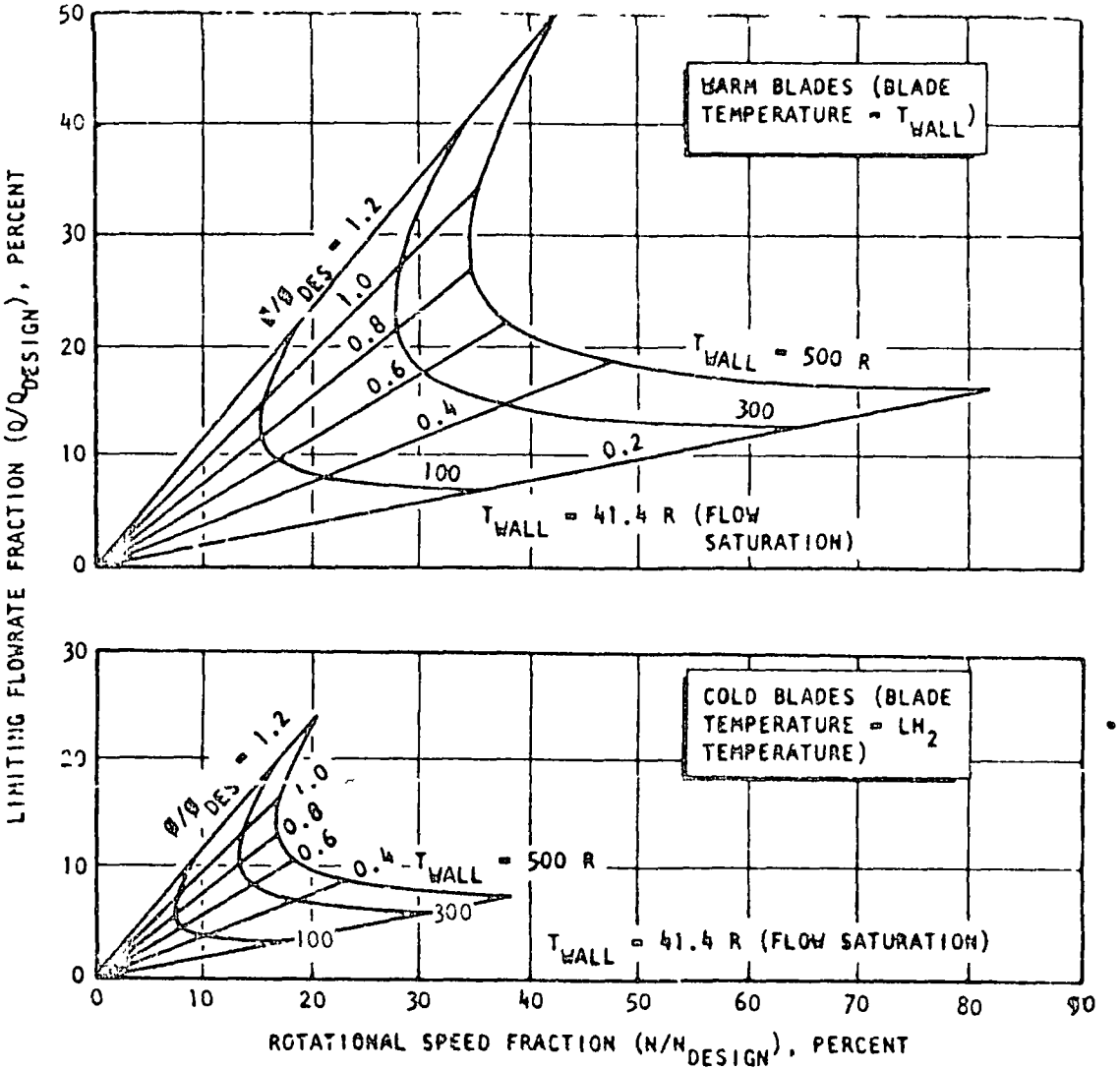

Figure 65 Regions of Pumping Capability for a Warm Mark 15-F Pump (Pump Inlet Flow Conditions = Saturated LH_2 at 30 Psia)

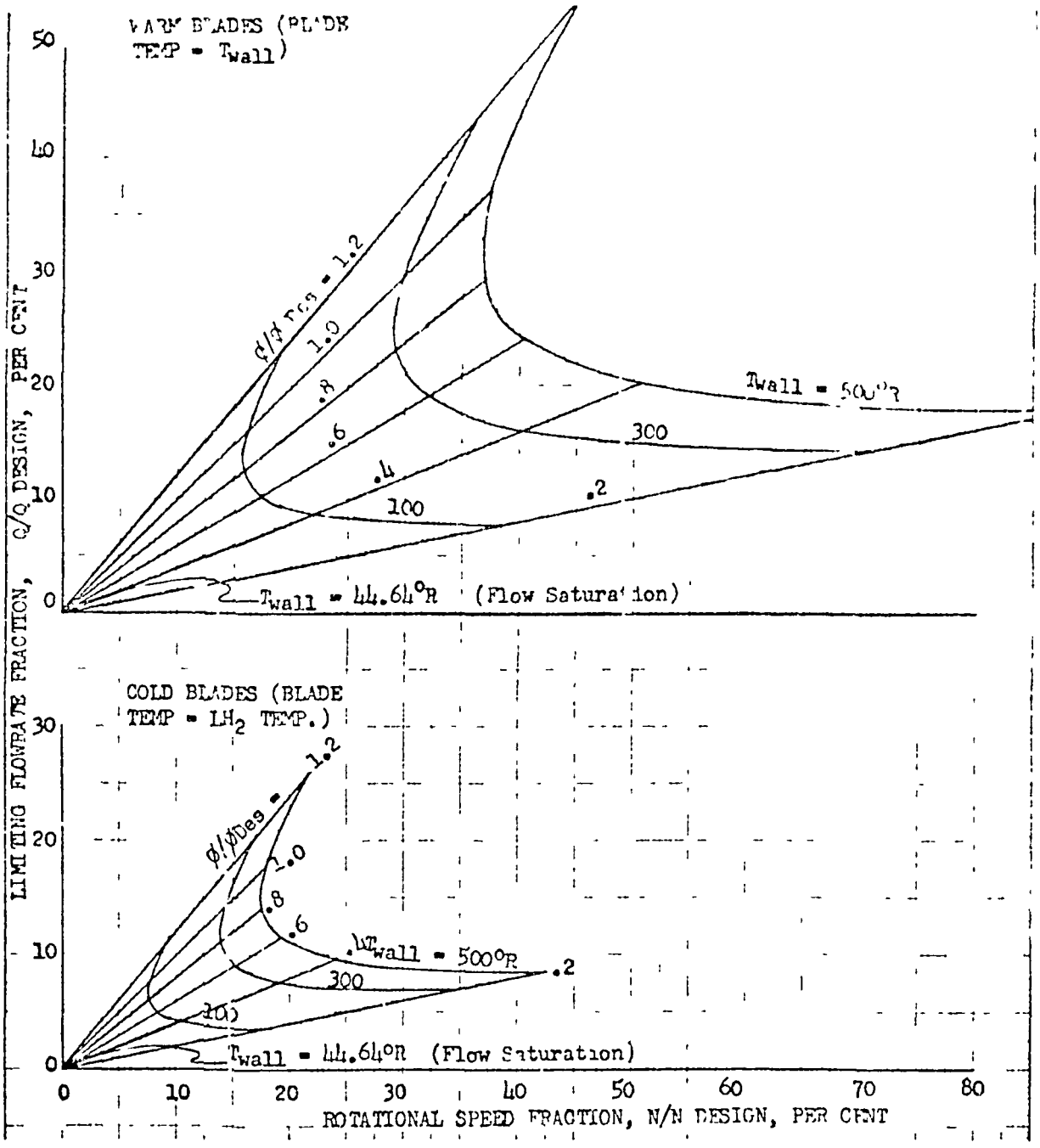

Figure 66 Regions of Pumping Capability for a Warm Mark 15 Pump (Pump Inlet Flow Conditions - Saturated LH_2 at 45 psia)

small thickness may be the case, particularly if coated), the same pump can be started at 8 percent of design flowrate if the annulus surface temperature is 60 R and at only 3 percent if the temperature is 100 R. Because the initial flowrate through the pump is very low because (using tank head idle mode as an example) it depends upon only the tank head, these figures indicate that the pump inlet surface may require chilling to start without vapor generation within the pump.

TWO-PHASE FLOW IN INLET LINE, WARM PUMP

In a warm engine start, the warm inlet line vaporizes some of the flow as it passes through, and the warm pump flow passage surfaces add more heat to the flow so that, under some pump operating conditions, additional vaporization will take place within the pump. Therefore, the analysis for a warm engine start involves a combination of the two previously discussed analyses (cold-pump two-phase flow and warm-pump liquid flow).

An approach to this problem is to predict regions of pumping capability similar to Fig. 65 through 66 with two-phase flow, rather than a saturated liquid entering the pump. The pumping limit could be assumed to occur when the heat added is on the verge of vaporizing additional liquid. Again, due to the lack of warm pumping test data, these predictions would have to be largely analytical.

This portion of the study was not completed because the Mark 25 pump two-phase test data reduction was not completed and, therefore, the limitations on two-phase pumping capability were not yet thoroughly understood. As soon as the two-phase pumping analysis is completed, the two-phase flow warm pump problem will be analyzed and reported.

MARK 29 LH_2 CHILLDOWN ANALYSIS

The theoretical chilldown analysis of the Mark 15 LH_2 pump was carried out, and the results were reported in Ref. 1. The chilldown analysis of the Mark 29 pump was conducted using Fig. 67 as a model, a 5-minute prechill followed by a 2.5-second start transient were considered. The prechill conditions considered were 0, 1.44, and 5 percent of the total flowrate. The first condition assumes that the lines and the pump are filled with -420 F LH_2. Although no LH_2 is flowing through the pump, the pump parts were assumed to be chilled as the LH_2 goes through film and nucleate boiling. During the film-boiling process, the heat flux rate is lower than during the nucleate-boiling process due to low LH_2 film coefficient. As film boiling converts to nucleate boiling, due to drop in temperature difference between the H_2 saturation temperature and the warm pump surfaces, the heat flux rate will increase. The surface temperature decreases, and the heat flows from the internal segment to the surface and, from the surface, heat is absorbed by the LH_2.

The initial temperature distribution was assumed to be 70 F, and the LH_2 bulk temperature was varied in the different locations in the pump, but was kept constant with time. The LH_2 heat transfer coefficients were varied both with time and location in the pump. The determination of the values of these film coefficients for the zero flowrate case as well as the other two cases were based on the data presented in Fig. 4 and Fig. 5 of Ref. 1. The material of the major components of the pump and turbine are identified, and temperature-dependent physical properties tables (thermal conductivity and specific heat) for each material were used. Where the isolation of materials appeared to increase the computer machine time excessively (due to creation of small volume or small time constant), two or more adjacent materials were lumped into one node and their weighted average properties were used.

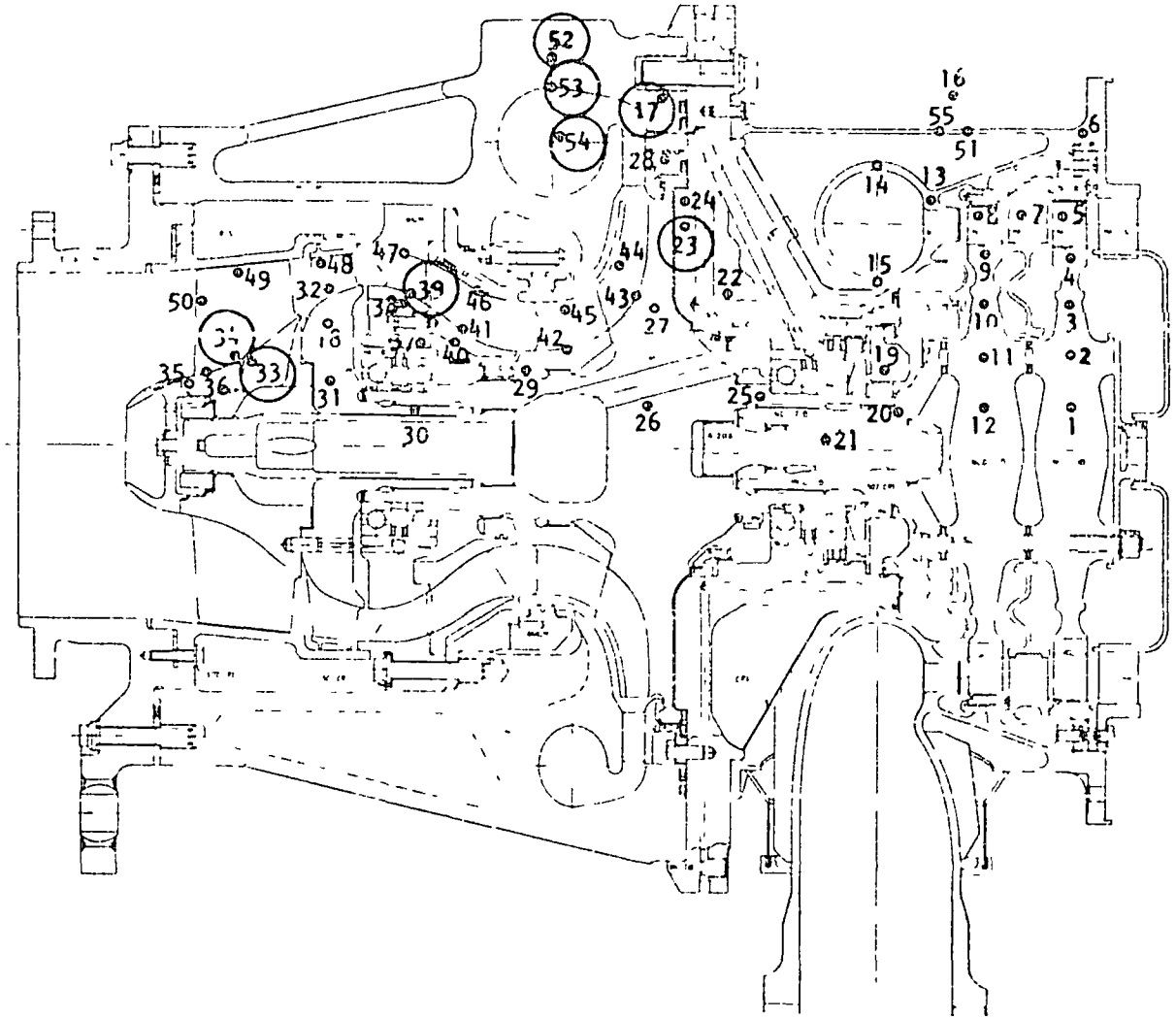

Figure 67. Mark 29 Single-Stage Liquid Hydrogen Turbopump Nodal Point Distribution

The results of the chilldown analysis are plotted on Fig 68 through 70 Figure 68 is a plot of the temperature of the various nodes (internal and surface) as a function of the chilldown time for some critical locations on the inducer, impeller, and volute This zero flowrate condition (it is assumed the pump is full of stagnant LH_2) indicates that the surface temperature of the inducer and support (nodes 34 and 39), which are made of titanium material, drop very rapidly The temperature of node 33, which is an internal node connected to the surface node 34, does not drop as quickly as that of the surface node 34 This is due to resistance between the two nodes Node 33 is cooled at a constant rate during the 180-second prechilling period The rapid temperature decrease in the titanium part is due to low specific heat and density (low heat content) of the material.

For comparison purposes, the temperature distribution of nodes 32 and 33 which are located in the aluminum volute, are also plotted in Fig 68 It is seen that the temperature of these two nodes remains fairly close to the initial condition during the 180-second prechill period. This is in part due to the high heat content of aluminum and in part due to the heat leakage from other nodes (such as node 17) to node 32. Also, the difference in the temperature of the internal node (node 32) and the surface node (node 33) is small because of the fairly high conductivity of the aluminum. However, as the LH_2 film coefficient increases during the start transient, a sharp drop in the temperature of node 33 takes place. During the 180-second prechill, the conductance between internal node 32 and surface node 33 is much higher than conductance between node 33 and the boundary node 34 The heat can peretrate from the inner part to the surface faster than can be rejected from the surface, even though the temperature difference between nodes 33 and 34 is much higher than that between nodes 33 and 32 However, during the start transient, the reverse of the above is true. For example, during the 180-second prechill, the conductance (51) between nodes 32 and 33 is 0.0329 Btu/sec-F, and that (52) between nodes 33 and 34 is 0.0034 Btu/sec-F at 11 secs after start of prechill. On the other hand, the conductances of 51 and

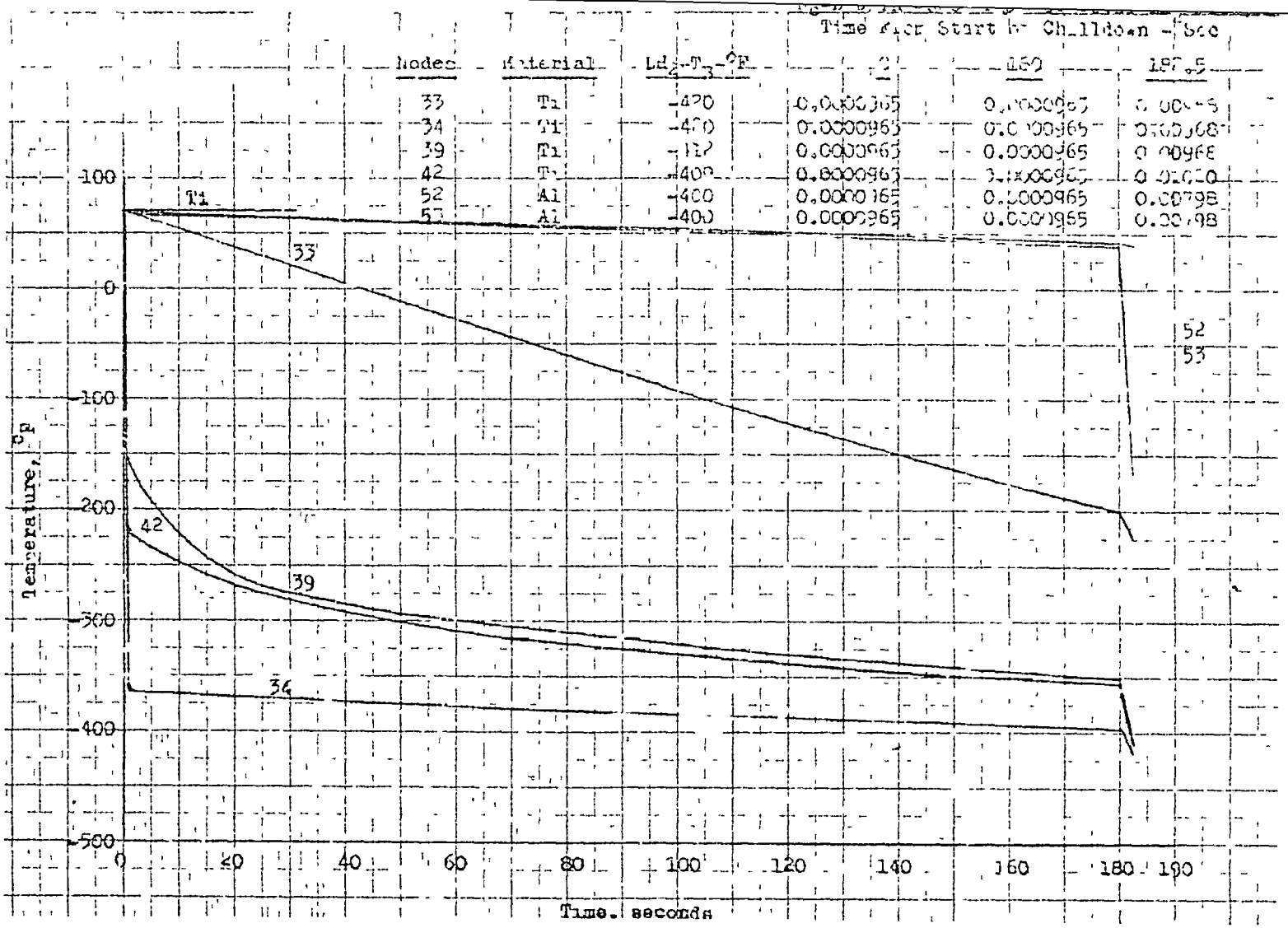

Figure 68 Pump Chilldown Temperature vs Time for the Mark 29 LH_2 Pump

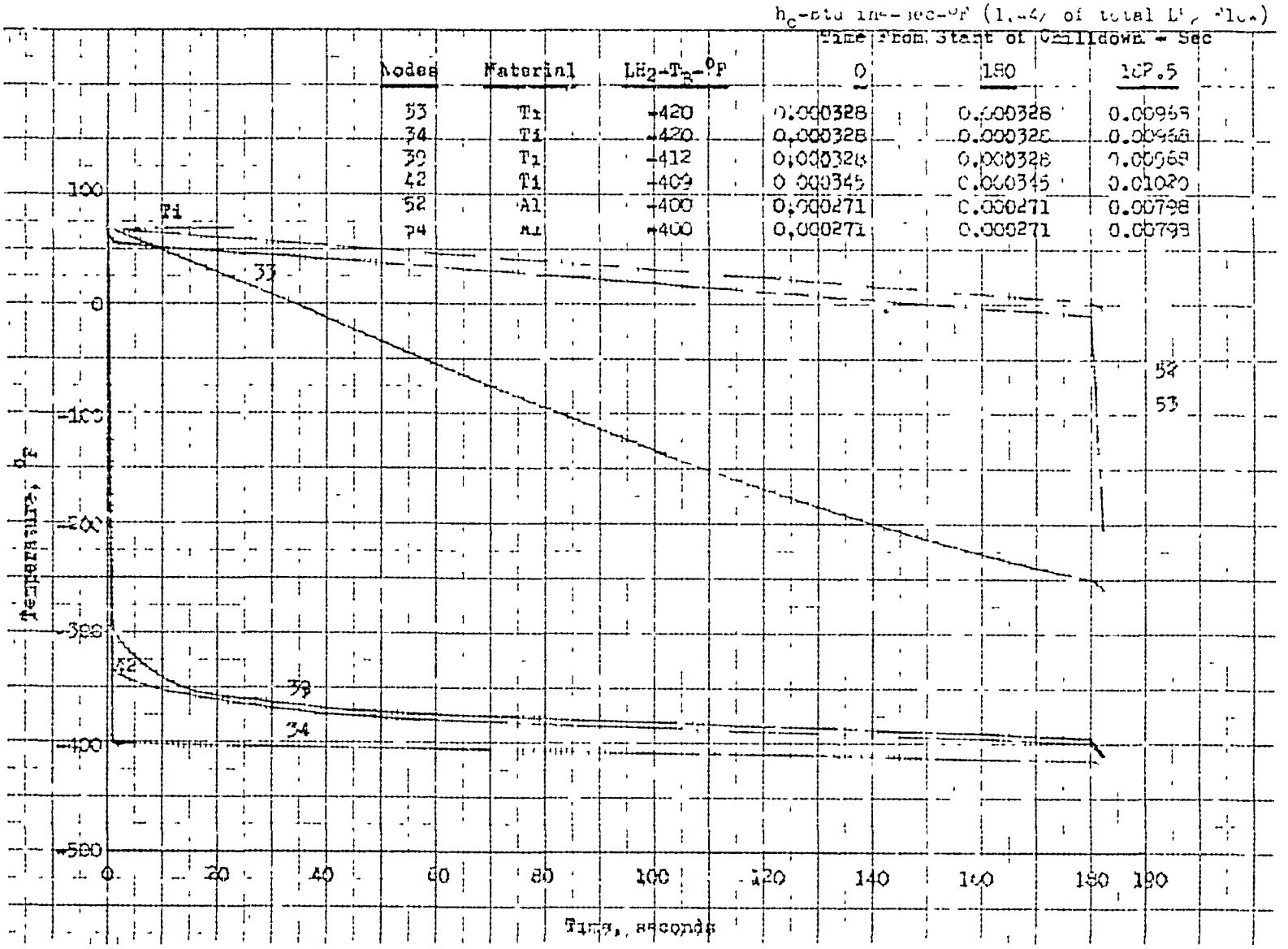

Figure 69 Pump Chilldown Temperature vs Time for Mark 29 LH_2 Pump

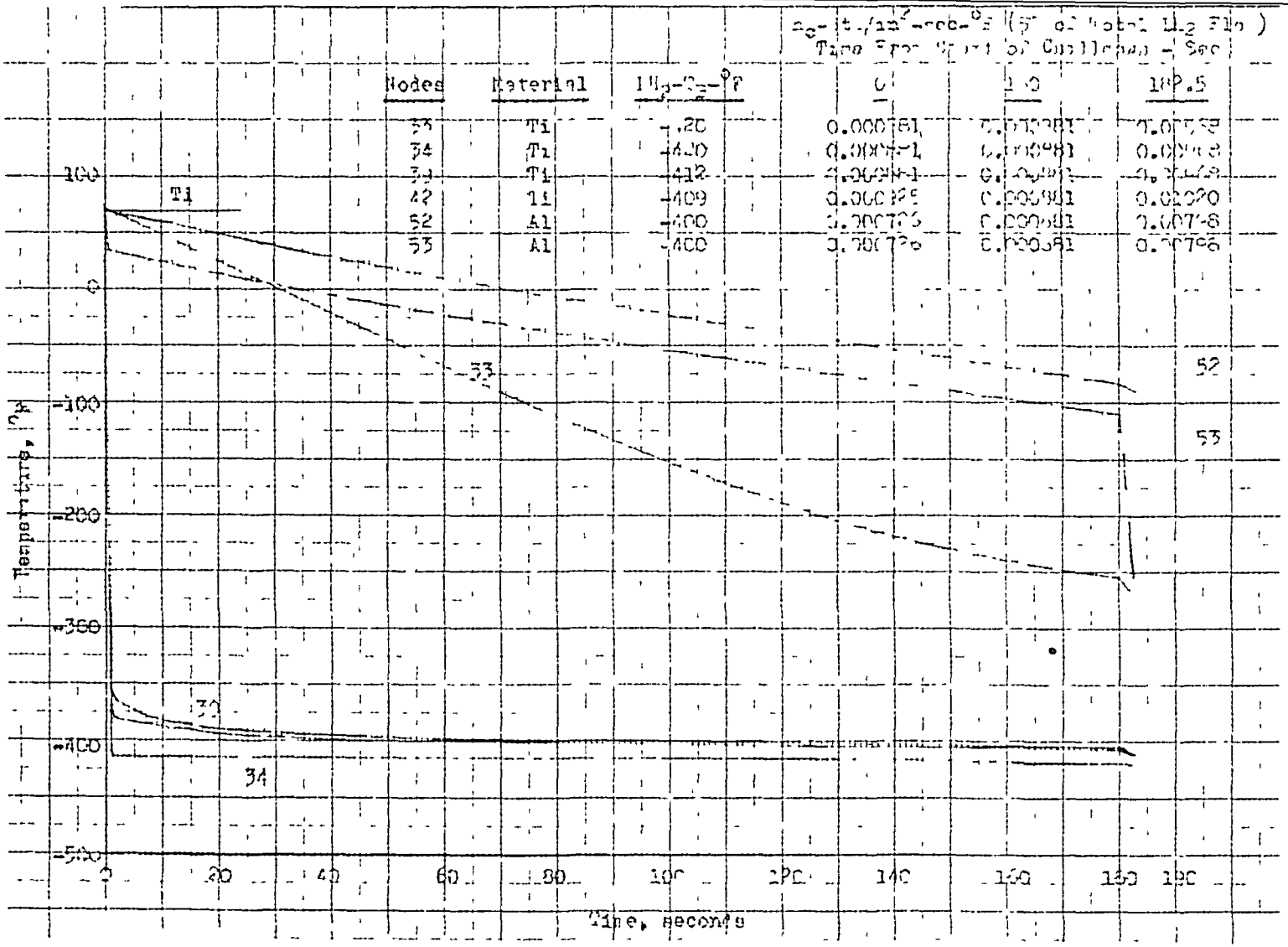

Figure 70 Pump Chilldown Temperature vs Time for the Mark 29 LH_2 Pump

52 are 0 0285 and 0 0281 near the end of the start transient period Since a short time period is required for the inner temperature to respond to that of the boundary, there will be a large temperature difference between nodes 52 and 53 It should be kept in mind that node 52 is receiving heat from node 17, otherwise its temperature would have fallen more in accord with that of node 53

Therefore, it again is observed, as in the case of the 350k LH_2 pump reported in Ref. 1 , that for a quick chilldown, a low-thermal-conductivity, low-density, and low-specific-heat material such as titanium should be selected Other factors such as stresses, created due to sharp temperature variation of the part during the early part of the prechill, also should be considered during selection of pump material. Means of eliminating the thermal stresses were pointed out in Ref. 1 , and will not be repeated here.

Figures 69 and 70 reveal essentially the same picture as Fig. 68 except the temperature of the materials is lowered at a fast rate This is due to the higher film coefficients applied during the 3-minute prechill period

ANALYSIS OF MARK 15 LH_2 PUMP CHILLDOWN TEST DATA

In an effort to obtain maximum experimental chilldown data, tests were conducted complementing the heated H_2 test program under the J-2X program. The heated H_2 tests required the test pump to be chilled prior to testing and, therefore, data on the chilldown characteristics were acquired The testing was conducted at CTL-3, cell 3B facility using a Mark 15 LH_2 pump. The monitored data obtained during these tests consisted mainly of pump skin temperatures, and H_2 coolant flowrate, temperature, and pressure.

The chilldown test data obtained were analyzed in detail for the purpose of determining the chilldown characteristics, and the results indicated that a quick pump chilldown is possible. The pump outlet H_2 bulk temperature dropped to about -415 F within 36 seconds from the start of the

chilldown for the quickest test The pump skin temperature also dropped in the same manner as the H_2 bulk temperature and, at the end of each test, the two temperatures were nearly the same.

Analytical Approach

The analytical approach to the solution of problems involving fluid flow and heat transfer is not too cumbersome if the processes are steady and one dimensional When one of the processe (for example, the fluid flow) becomes transient, the problem becomes much more complex The simultaneous analytical solution of a transient heat transfer and transient fluid flow such as the chilldown of the Mark 15 HH_2 pump becomes increasingly difficult and time consuming (especially when flow oscillations are present) if not formidable. Shapiro (Ref 20) has handled "Unsteady, One-Dimensional Flow with Area Change, Friction, and Heat Transfer or Combustion " In the treatment of this problem, Shapiro has assumed constant heat transfer Reference 21 also has developed the necessary equations for the flow of a cryogenic fluid flowing in a heated transfer line Three different regions (viz , all liquid, liquid and vapor, and all vapor) were distinguished in Ref 21 . However, many simplifying assumptions (such as straight constant-area duct, constant wall thickness, constant density) were used in the derivation of the equations. The cooldown model of Ref. 21 resembles the Mark 15 HH_2 pump in that transient heat transfer and transient fluid flow are involved in both. However, it would be extremely difficult to use the model of Ref 21 in determining the complete solution of simultaneous transient heat transfer and fluid flow. This is due to the complexity of the flow passages and nonuniformity of the wall thicknesses, in addition to numerous materials involved Only when gross assumptions are made is it possible to utilize the work of Ref 21

Some of the simple equations derived and used by Ref 21 for a simplified model are shown below.

$$P_{in} - P_1 = 0.81 \frac{f_\ell \dot{W}_\ell^2}{\rho_\ell D^5} \tag{35}$$

$$P_1 - P_2 = \frac{1.62}{D^4} W_1^2 \left(\frac{1}{\rho_{v_2}} - \frac{1}{\rho_{\ell_1}} \right) \tag{36}$$

$$\left[\pi D \delta C_{P_w} \rho_w \left(T_{w_2} - T_{w_1} \right) + \frac{\pi D^2}{4} \bar{\rho} 2 \phi \lambda \right] \frac{\partial T_1}{\partial t} - \lambda W_1 = 0 \tag{37}$$

$$\frac{\dot{W}_V}{\dot{W}_\ell} = \frac{\frac{D}{4} \rho_{V_2} C_{P\ell_1} + \delta \rho_w C_{P_w \ell_1}}{\frac{D}{4} \rho_{\ell_1} C_{P\ell_1} + \delta \rho_w C_{P_w \ell_1}} \tag{38}$$

$$T_3 = T_2 + (T_a - T_2) e^{-\frac{1}{b} \int a \, \partial t} \tag{39}$$

$$W_\ell = \sqrt{\frac{P_{in} - P_3}{\frac{0.81}{D^5} \left[\frac{X_1 - X_0}{\rho_\ell} f_\ell + \frac{X_3 - X_2}{\rho_{w_3}} f V_3 \frac{\dot{W}_V^2}{\dot{W}_\ell^2} + \frac{1.62}{D^4} \frac{\dot{W}_V^2}{\dot{W}_\ell^2} \left(\frac{1}{\rho_{v_3}} - \frac{1}{\rho_{\ell_1}} \right) \right]}} \tag{40}$$

It is recommended that the reader see Ref. 21 for complete analysis and procedure of application of these equations since the utilization of these equations is very involved and requires many assumptions and iterations. Reference 21 carried out a simple laboratory test, and the results agreed very well with that of the analytical solution. The work of Ref. 21 can be used for analysis of cooldown of simplified ducts

In the case of a simple model (such as a duct of constant cross section, constant wall thickness, simple material of constant density, specific heat, and thermal conductivity), a heat balance equation can be written for the sketch below

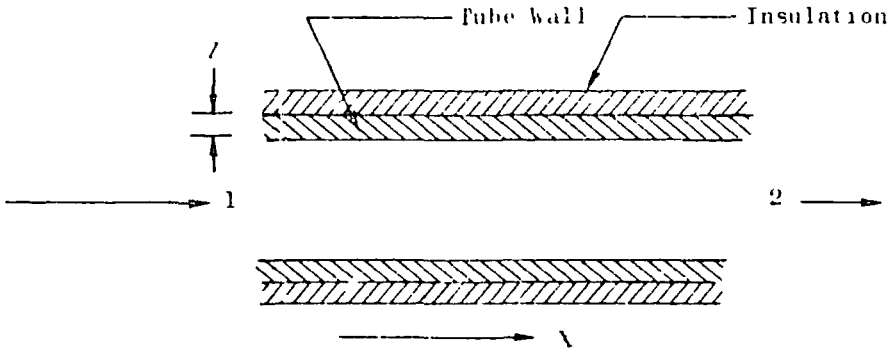

$$-dQ = \left(W C_p\right)_1 \frac{d T_F}{d\theta} - h_c A \left(T_P - T_F\right) = -\left(W C_p\right)_P \frac{d T_P}{d\theta} \quad (41)$$

The momentum equation can be written

$$\Delta P = W \left(\dot{W}\right) \quad (42)$$

At any given time, for a small value of X, one can write

$$\left(W C_p\right)_F \left(T_F - T_{F_1}\right) = \left(W C_p\right)_P \left(T_{P_1} - T_P\right) \quad (43)$$

Solving Eq. 43 for T_F one will get

$$T_F = T_{F_1} + M \left(T_{P_1} - T_P\right) \quad (44)$$

where

$$M = \frac{\left(W C_p\right)_P}{\left(W C_p\right)_F} \quad (45)$$

Substitution of Eq. 44 into Eq 41 will yield

$$h_c A \left[T_{P_1} - M \left(T_{P_1} - T_P \right) - T_{F_1} \right] = -\left(\dot{W} C_p \right)_p \frac{d T_P}{d\theta} \qquad (46)$$

or

$$\int_0^t \frac{h_c A \, d\theta}{\left(\dot{W} C_p \right)_p} = \int_{T_{P_1}}^{T_P} \frac{d T_P}{(1+M) T_P - M T_{P_1} - T_{F_1}} \qquad (47)$$

After integration and substitution of the limits, Eq 47 will yield

$$\frac{h_c A \theta}{\left(\dot{W} C_p \right)_p} = \frac{1}{1+M} \ln \left[\frac{T_{P_1} - T_{F_1}}{(1+M) T_{P_f} - M T_{P_1} - T_{F_1}} \right] \qquad (48)$$

Also

$$h_c = \psi \left(\dot{W}, P, T, D \right) \qquad (49)$$

For example, for H_2 at a bulk temperature below 150 R, the heat transfer coefficient, h_c, under forced convection condition, can be found from (Ref 17)

$$N_{Nu_{0.4}} = 0.0204 \, N_{Re_{0.4}}^{0.8} \, N_{Pr_{0.4}}^{0.4} \left(1 + 0.00983 \frac{\upsilon_{T_{WL}}}{\upsilon_{T_B}} \right) \qquad (50)$$

where the subscript 0.4 indicates that the fluid properties are evaluated at $T_{0.4}$ (Ref. 17).

where

$$T_{0.4} = T_B = 0.4 \left(T_{WL} - T_B \right) \qquad (51)$$

or the H_2 at a bulk temperature greater than 150 R, the heat transfer coefficient can be obtained (Ref 22) from

$$\frac{h_c \left(\frac{T_{wl}}{T_B}\right)^{0.55}}{G\, C_p} = \frac{f/2}{0.92\sqrt{f/2}\left[G(\epsilon^*, Pr) + 8.48\right]} \tag{52}$$

where

$$G(\epsilon^*, Pr) = 4.1 + 0.57(\epsilon^*)^{0.75} \quad 0 < \epsilon^* < 7 \tag{53}$$

$$G(\epsilon^*, Pr) = 5.7(\epsilon^*)^{0.2} \quad \epsilon^* \geq 7 \tag{54}$$

where

$$\epsilon^* = N_{Re}\frac{\epsilon}{D}\left(\frac{f}{2}\right)^{0.5} \tag{55}$$

For low Biot number (less than about 0.4), the simultaneous solution of Eq 42, 44, 48, and 49 will give the required values of fluid temperature, fluid pressure, and wall temperature as a function of time

Briefly, the calculation procedure is as follows

1. A small value of X is specified
2. an increment of time is chosen
3. Total amount of fluid (w) is assumed to have passed through the small value of X during the chosen time increment
4. Assume T_p and find T_f from Eq 44
5. Find h_c from Eq 49 for appropriate fluid using $\left(T_F + T_f\right)/2$
6. Find T_p from Eq 48 if the calculated T_p is equal to the assumed value, go to Step 7, if T_p match is not made, Steps 4 and 5 are repeated until the assumed value and the calculated value agree.

7 Find ΔP from Eq 42

8 Choose another small value of X, and continue until $X = 1$ is reached

9 The sum of ΔP's should equal $P_{in} - P_{out}$ (for nonchoking condition) If not, steps 3 through 11 are repeated until total ΔP's equals $P_{in} - P_{out}$

10 Steps 1 through 11 are repeated for new time increment, and process is continued for as many time increments as desired

The final results gave bulk temperature and pressure of the fluid as a function of time along the pipe length Also, the wall temperatures of the pipe, in addition to the flowrate as a function of time, are part of the solution For example, a plot of the ratio of the outlet bulk temperature to the inlet bulk temperature vs chilldown time should look as shown in the sketch below

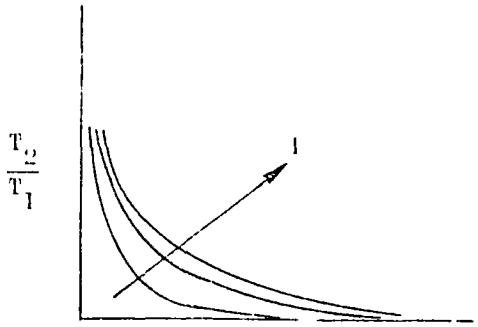

The analytical equations (41 through 54) can be used for two-phase flow as well as single flow as long as the inlet conditions are known However, these equations should be modified to accommodate the heat of vaporization and any other conditions which may be different from those assumed in the derivation of Eq 41 through 54 Also, a nonchoking condition was assumed through the entire pipe length When choking takes place, these equations can still be used as long as proper $P_{in} - P_{out}$ is chosen

It is interesting to examine Eq 48 for various values of M at this time.

A. Very low M value ($M \longrightarrow 0$)

In this case, Eq. 48 can be written

$$\frac{h_c A \theta}{\left(W C_p\right)_P} = \ln \frac{T_{P_1} - T_{F_1}}{T_{P_f} - T_{F_1}} \tag{56}$$

Equation 56 indicates that for a fixed value of $\left(W C_p\right)_P$ the required time for the final H_2 temperature becoming equal to the initial temperature will approach zero

B. Very large M value ($M \longrightarrow \infty$)

In this case, Eq 48 becomes

$$\frac{h_c A \theta}{\left(W C_p\right)_P} \longrightarrow 0 \tag{57}$$

indicating that for very large values of $\left(W C_p\right)_P / \left(W C_p\right)_F$ ratio, the time requirement for the final H_2 temperature becoming equal to the initial temperature becomes very large. From Eq. 56 and 57 it can be seen that the chilldown time θ is

$$\theta \alpha \left(W C_p\right)_F \tag{58}$$

$$\theta \alpha \frac{1}{h_c A} \tag{59}$$

It is obvious, of course, that the lower the weight of the pump, the less the H_2 and the chilldown time requirement. Therefore, any weight reduction of the pump will help reduce the H_2 requirement. Since the verification of the simple analytical solution (even if gross assumptions were used) with experimental data seemed a time-consuming process, no attempt was made to use analytical equations for comparison with the experimental results.

Test Facility and Instrumentation

The testing facility of CTL-3, Cell 3B at Santa Susana Field Laboratory, was used to run chilldown tests on the Mark 15 LH_2 pump. The same facility also was used to run the heated H_2 pumping tests. However, this discussion will be limited to the chilldown tests only. Figure 71 shows diagramatically the plumbing that existed and the modification required to make the facility adaptable for the chilldown tests. Figure 72 depicts the pump inlet and outlet ducting and the instrumentation spools. Figure 10 shows the locations and the distance between the inlet thermocouples, the pressure taps, and the pump. Figure 73 is a cross section of the Mark 15 LH_2 pump depicting the location of the skin thermocouples. Figures 74 and 75 show the chilldown and pump inlet ducting.

The instrumentation was capable of acquiring the following H_2 information:

1. Temperature and pressure just upstream of the feed line flowmeter
2. Flowrate (by means of feed line flowmeter)
3. Temperature and pressure at the pump inlet (about 4.9 feet before the pump inlet flange)
4. Temperature and pressure at the pump out flange
5. Flowrate (by means of pump discharge flowmeter)

Testing Procedure

The testing procedure was to chill down the 4-inch line by closing the chill valve and opening the prevalve and the 2-inch bleed valve. After the H_2 temperature at the chill valve was sufficiently dropped (to about -412 F), the bleed valve was closed. The ducting downstream of the chill valve was pressurized with GH_2 to the same level as the run tank pressure. To begin a chilldown test, the chill valve was opened manually, and when

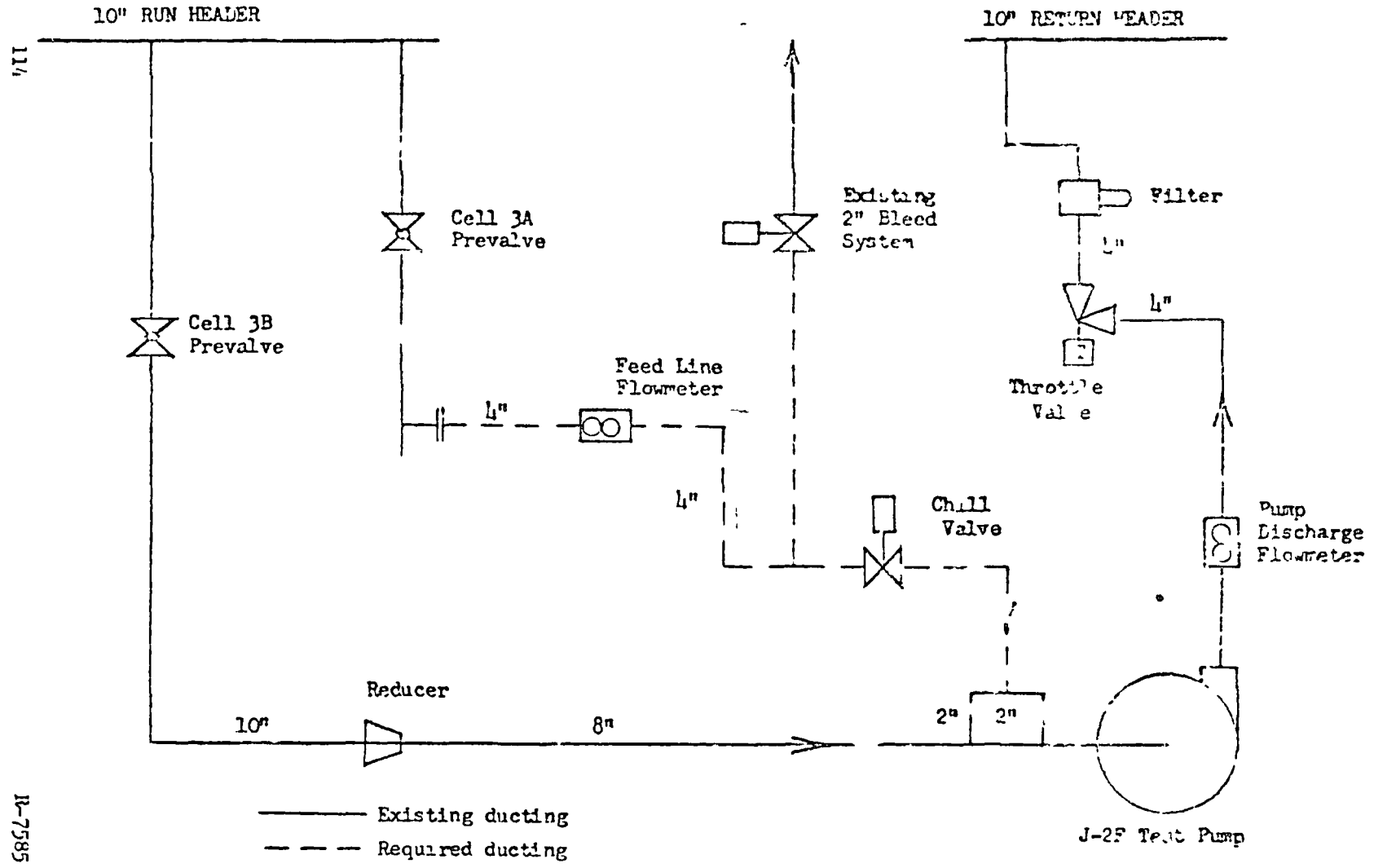

Figure 71. CTL-5, Cell 3B LH_2 Facility Modification

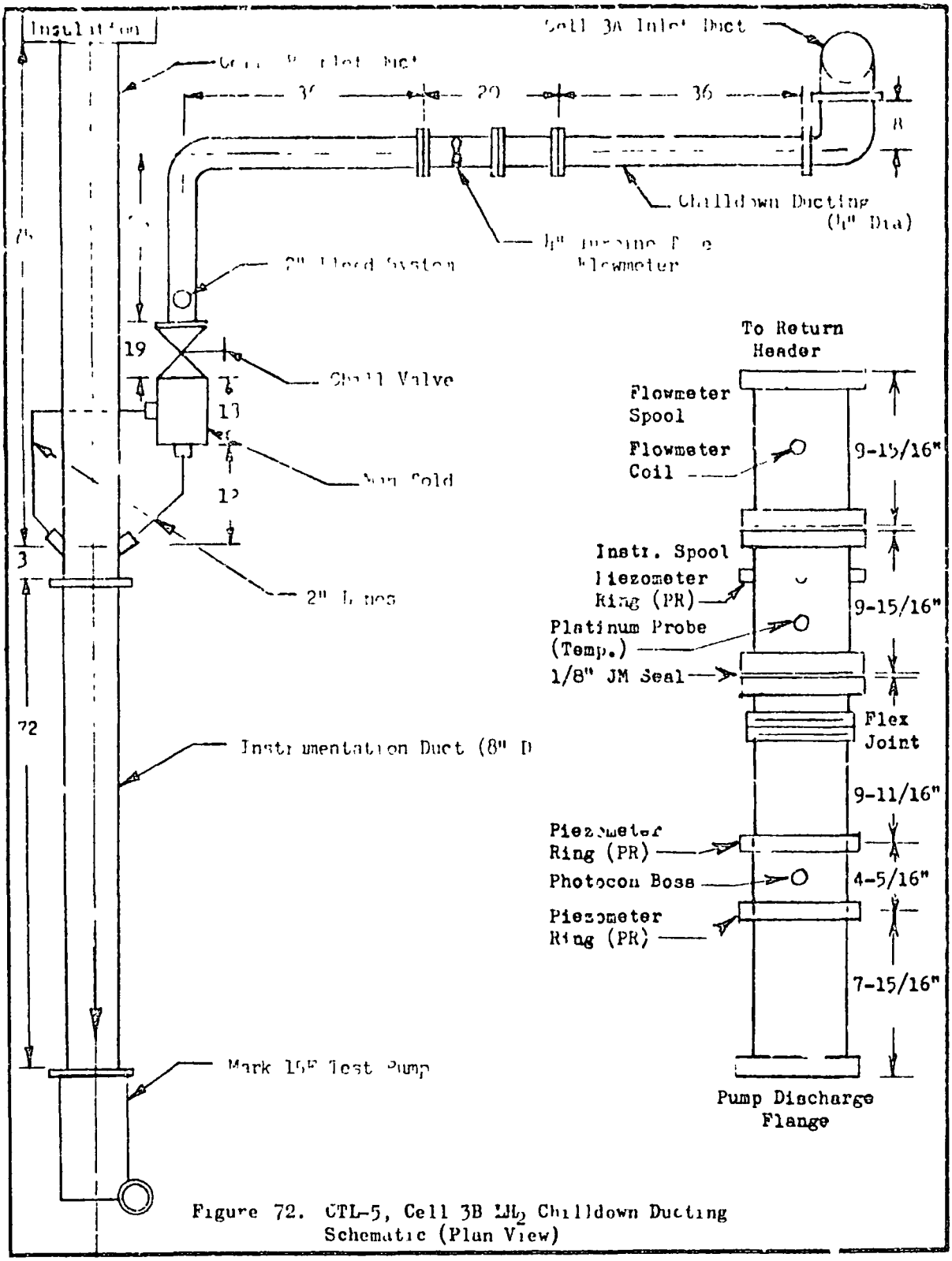

Figure 72. CTL-5, Cell 3B LH_2 Chilldown Ducting Schematic (Plan View)

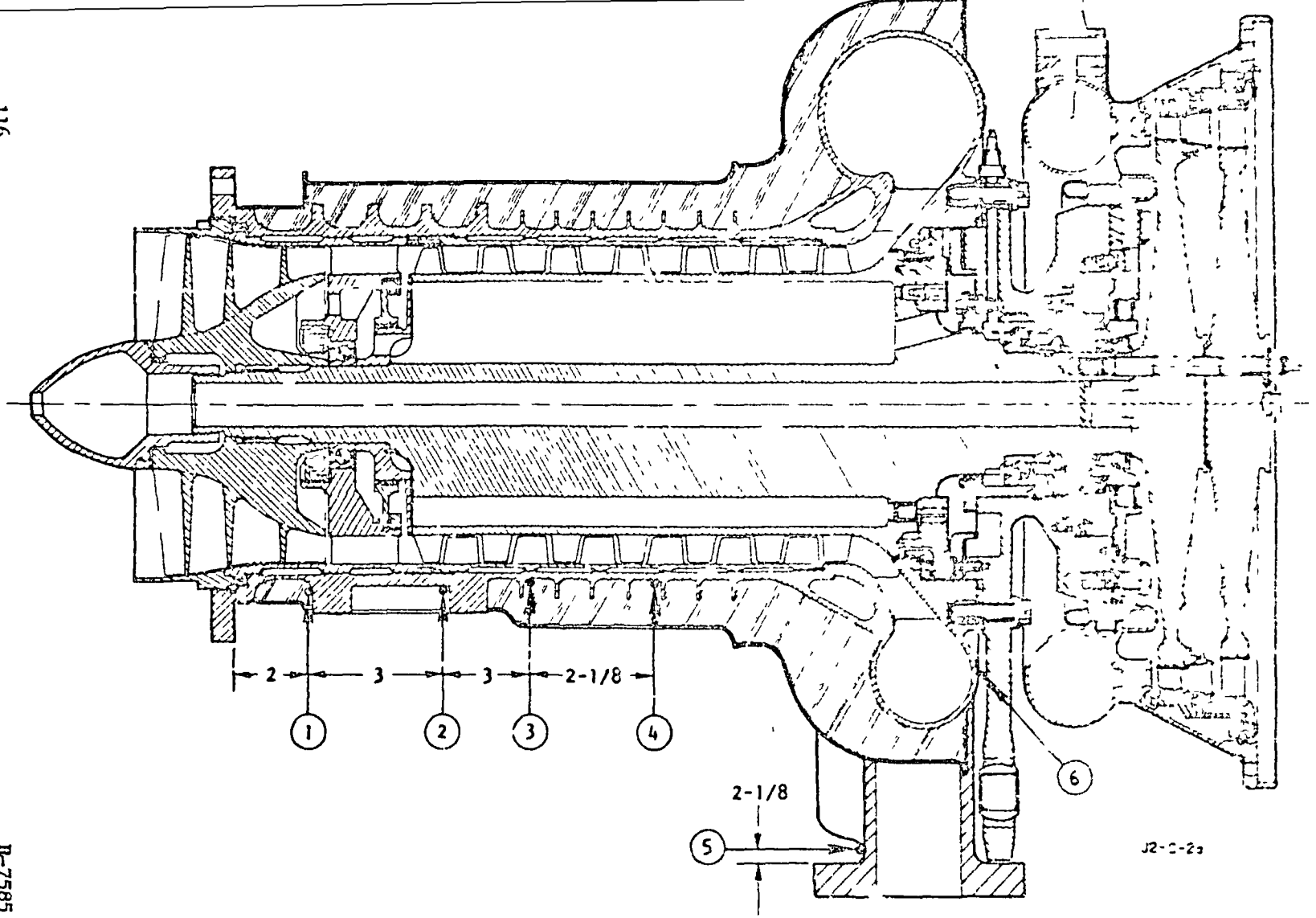

Figure 73. Iron Constantan Thermocouple Locations for the J-2 Fuel Pump (E020-6) Chilldown Studies

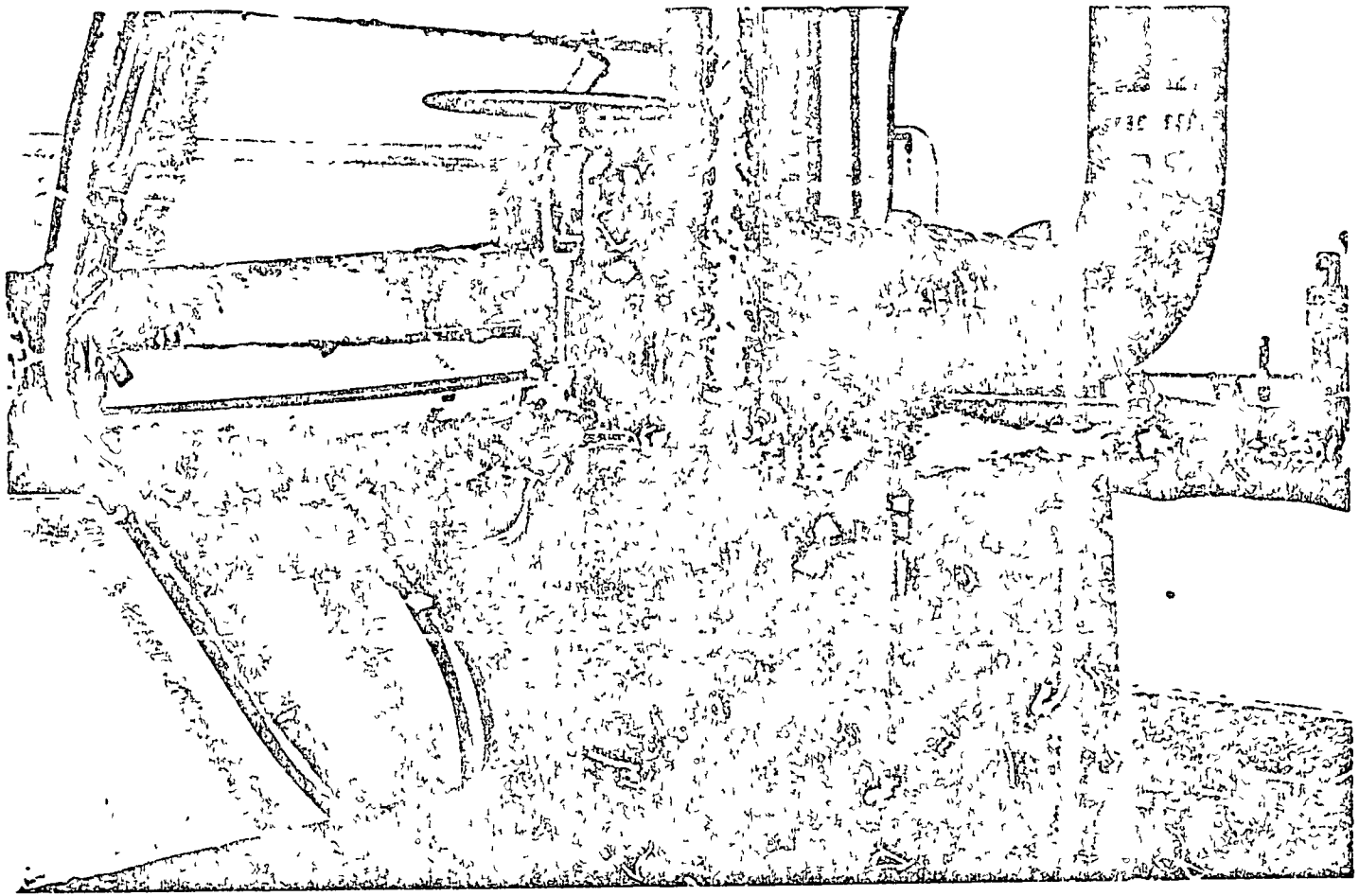

IC753-11/7/67-S1B

Figure 74 CTL-5, Cell 3B Mark 15 LH_2 Pump Chilldown Ducting

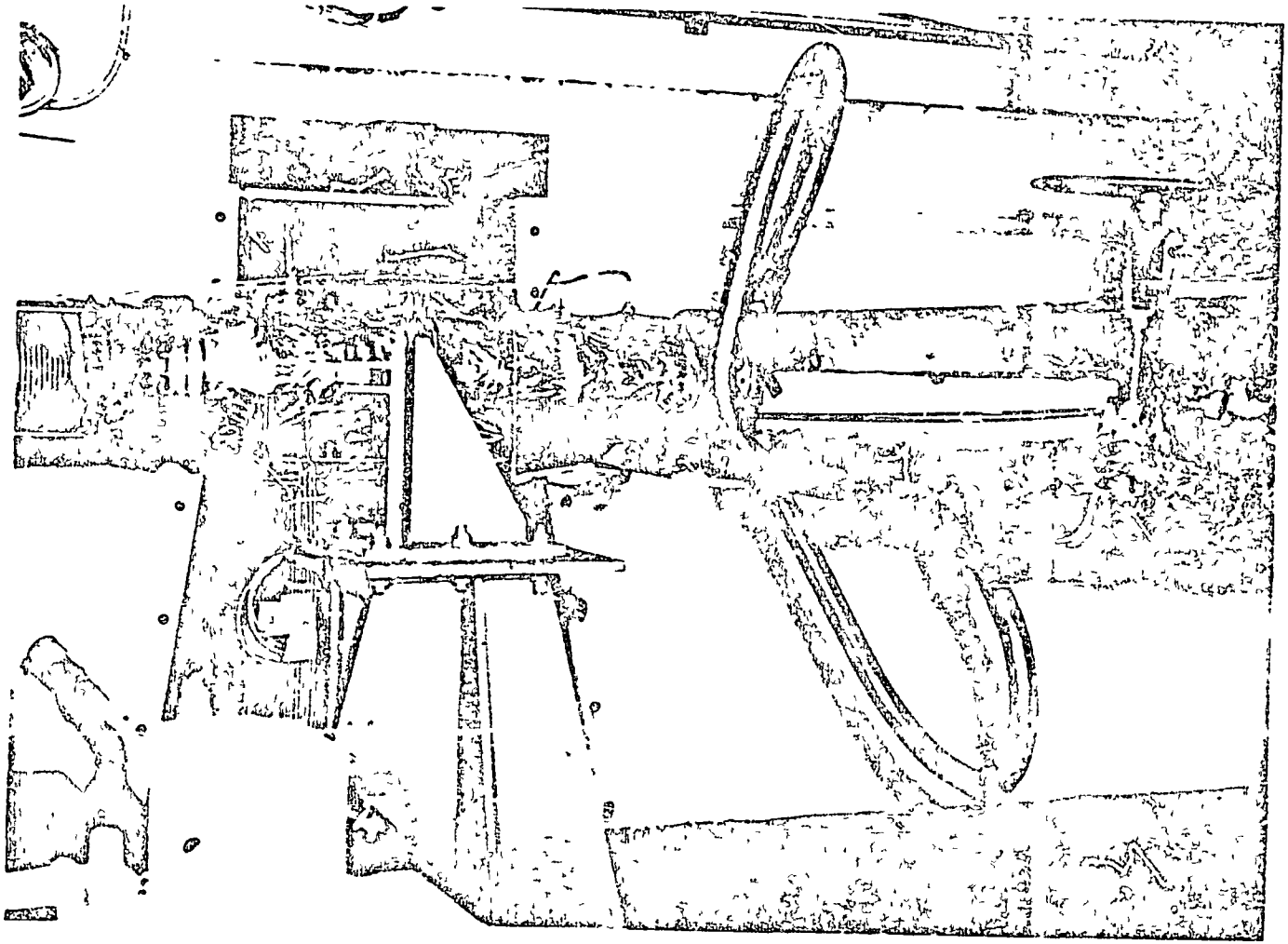

ICI55-11/7/67--1D

Figure 75 CTL-5, Cell 3B Mark 15 LH_2 Pump Chilldown Ducting at Pump Inlet

the operator reached the safety zone, the throttle valve was opened remotely. The rate of H_2 flow, therefore, depended on the run tank pressure and the magnitude of the throttle valve opening. The run tank pressure and the throttle valve opening were varied for each of four tests (No. 118, 121, 122, and 124). Each test duration was long enough so that the bulk temperature of the H_2 leaving the pump had fallen to approximately (at least) -315 F before the test was terminated. Consequently, the test duration depended on the run tank pressure and the throttle valve setting. During each test, all the instruments were recorded on dynalog charts, and automatic printout data were obtained simultaneously. The pump skin temperatures were measured by means of six iron-constantan thermocouples (Fig. 73).

Two tests were run without the chilldown loop (dashed lines of Fig. 71). These two tests (No. 103 and 108) were of long duration (about 1200 to 1400 seconds) and low H_2 flowrate. Low-pressure (about 20 psia) GH_2 was directed from the top of the run tank and passed through the pump for about 500 to 800 seconds. After this time, LH_2 was passed through the pump for about 600 seconds. Although these two chilldown tests were not part of the scheduled chilldown tests and were different from the others, it was decided to utilize all the available data obtained during these two tests.

A further restriction on the upper limit of H_2 flow, especially during the early part of the chilldown tests, was the existence of the pump discharge flowmeter. It was decided to control the H_2 flowrate in such a manner as not to overspin the pump discharge flowmeter. Since this flowmeter had to be used in the main heated H_2 tests which followed every chilldown test, any damage to the flowmeter bearing because of overspinning would have been costly in terms of the test-stand down time in order to repair the flowmeter. Therefore, analytical computations were carried out to investigate the volumetric flowrate of GH_2 under different pressures and temperatures that could be passed safely through the flowmeter.

Figures 76 and 77 show the results of this investigation where the volumetric flowrate in terms of gpm is plotted versus the percent of the total flowrate. The H_2 pressure and bulk temperature were set as parameters. Also, the pump choking condition was established and superimposed on these figures. For example, one can see from Fig. 77 that, at an inlet H_2 pressure of 100 psia and bulk temperature of 200 R, about 2.7 percent of total flow can be used to chill the pump without exceeding the flowmeter rated speed. These figures were used as a guidline to set the run tank pressure and the throttle valve opening for chilldown tests No. 118, 121, 122, and 124. The maximum experimental speed of the downstream flowmeter is shown in Fig. 76 and 77 . It is noticed that no overspeeding of the flowmeter occurred in tests No 103, 108, and 118. Slight overspeeding of the flowmeter was observed during tests No. 121, 122, and 124, which lasted for about 10, 4, and 3 seconds, respectively. However, neither the speed nor the duration of overspinning was excessive enough to cause any damage to the flowmeter bearings. During all of the chilldown tests, the rotor, which was connected to an electric drive for the heated H_2 pumping tests, was locked.

Flow and Pressure Oscillations

Since flow and pressure oscillations were observed in all of the tests, especially test 124, an attempt will be made to discuss some of the causes of flow and pressure oscillation before an analysis of the data is presented. Severe pressure and flow oscillations have been observed in experiments carried out with various fluids in the supercritical thermodynamic region. Such oscillations were reported for ammonia by Schmidt, Eckert, and Grigul (Ref. 23), for water by Goldman (Ref. 24 and 25) and Firstenberg (Ref. 26), for Freon-12 by Holman and Boggs (Ref. 27), for RP-1, diethylcyclohexane, and others, by Hines and Wolf (Ref. 28).

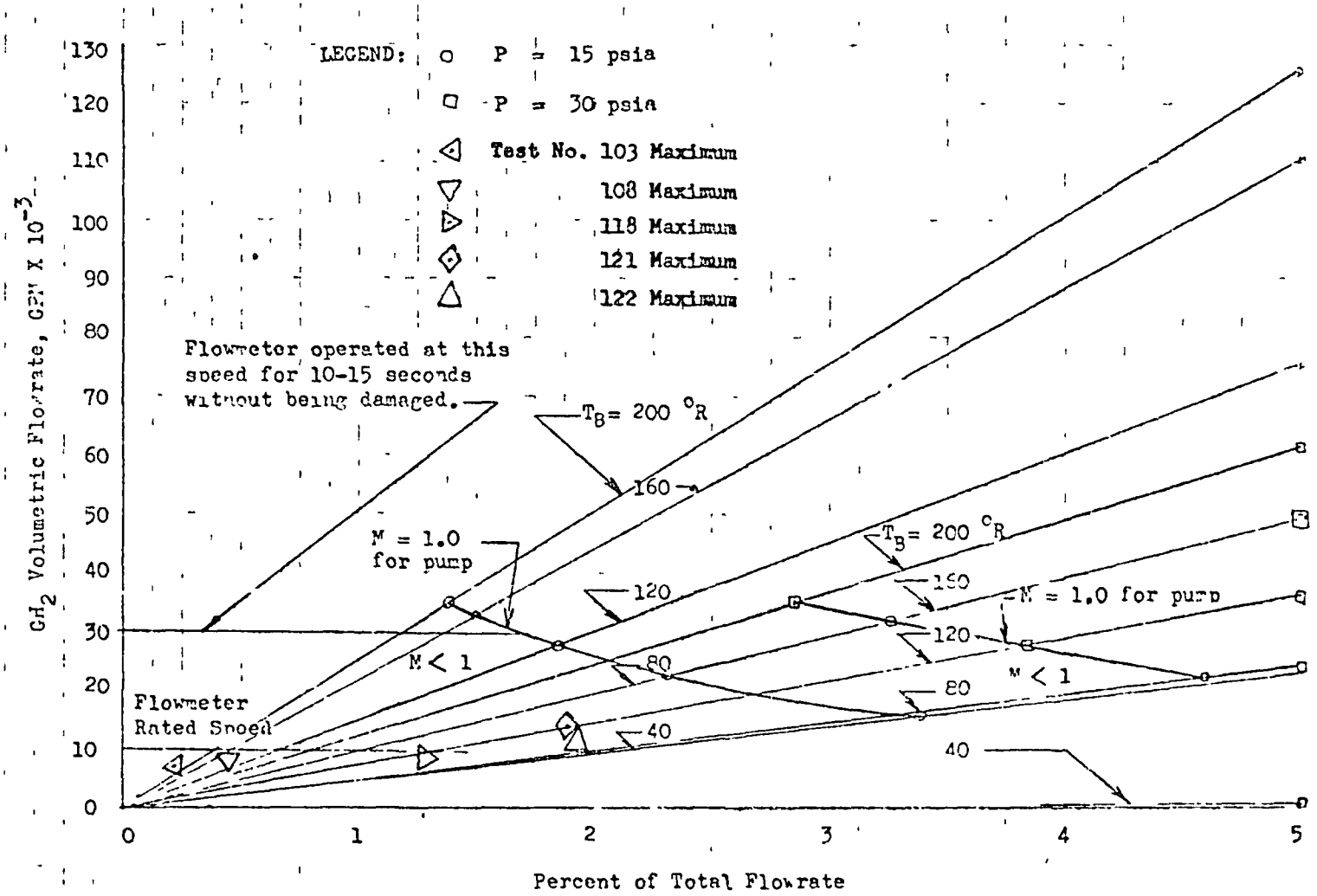

Figure 76. GH_2 Volumetric Flowrate vs Percent of Total Flowrate

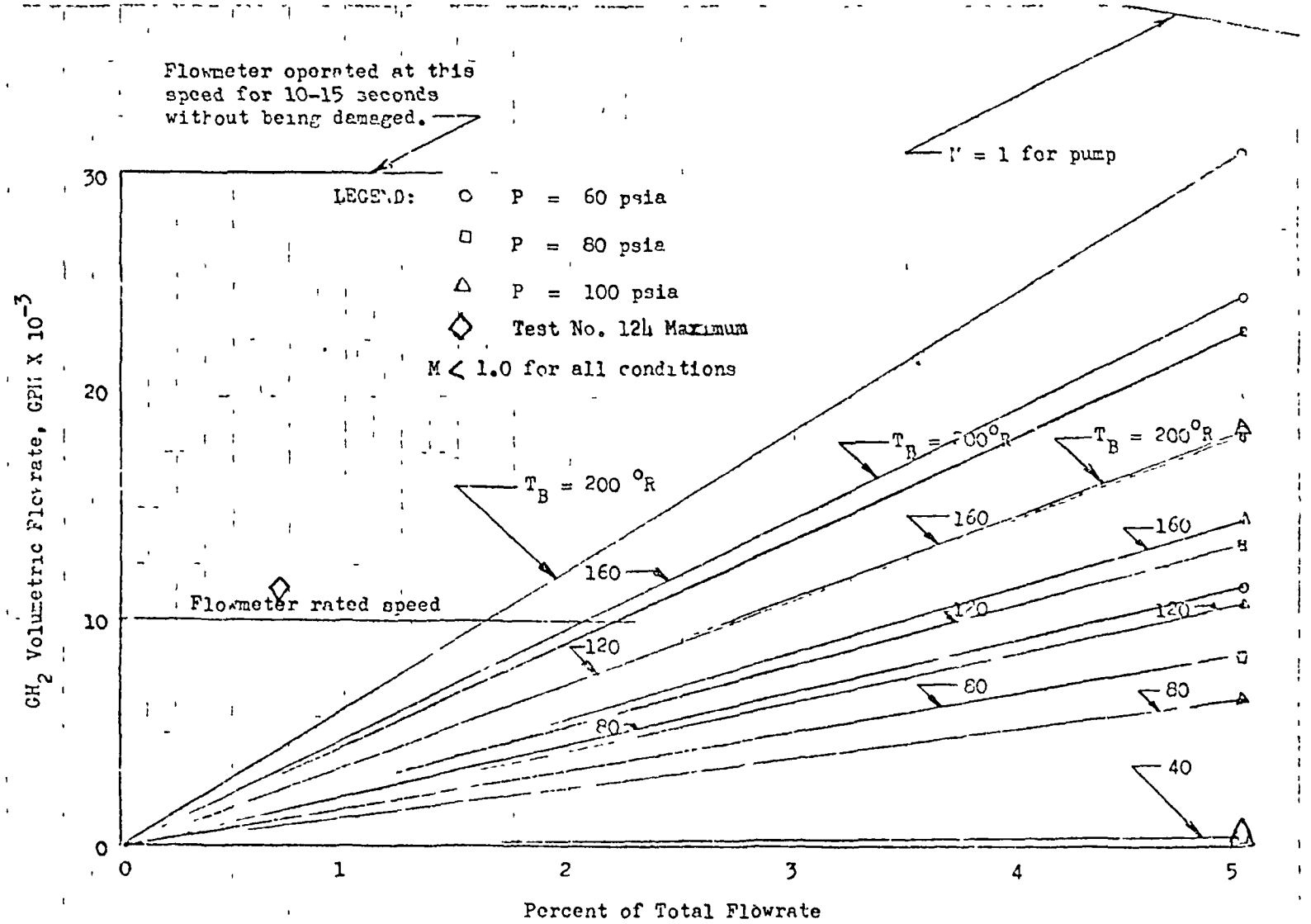

Figure 77. GH_2 Volumetric Flowrate vs Percent of Total Flowrate

There are many mechanisms that can induce thermohydraulic oscillations at near-critical and supercritical pressures. Some of these mechanisms are as follows (Ref. 29):

1. Variation of the heat transfer coefficient at the transposed, i.e., at the pseudo-critical point
2. The effect of large compressibility in the critical thermodynamic region
3. Variation of flow characteristics brought about by variations of fluid density during the heat process
4. Flow oscillations due to low or high inlet subcooling

A quantitative formulation and explanation of the conditions leading to the appearance of the pressure and flow oscillations has not been reported yet, although several qualitative explanations have been advanced. It is, however, generally agreed that the oscillations are caused by the large variations of the thermodynamic and transport properties of the fluid as it passes through the critical thermodynamic region (Ref. 29).

Several investigators (Ref. 30 through 31) note that the appearance of oscillations occurs when the temperature of the heating surface exceeds the 'pseudo-critical" or the "transposed" critical temperatures, i.e., the temperature where the specific heat reaches its maximum value. Oscillations were not observed if the inlet temperature was above this temperature. From this, it was concluded that the mechanism for driving the oscillation occurred only when a "pseudo-liquid' state was present in some parts of the heated duct (Ref. 29).

Firstenberg (Ref. 26) attributes the oscillations to the variations of the heat transfer rates to the fluid, whereas Goldman (Ref. 24 and 25) explains the oscillations as well as the steady-state heat transfer mechanism in the critical and supercritical thermodynamic region as

"boiling like" phenomena associated with nonequilibrium conditions. According to Goldman below the pseudo-critical temperature, the fluid is essentially a liquid, above this temperature, it behaves as a gas. At the pseudo-critical temperature, the density gradient and the specific heat reach maximum values giving an indication of the energy required to overcome the mutual attraction between the molecules. The fluid in the immediate vicinity of the heated wall is in a gas-like state, whereas, the bulk fluid may still be in the liquid-like state. If by means of turbulent fluctuations, a liquid-like cluster is brought into contact with the heating surface, a large amount of energy will flow from the surface to the cluster because of the large temperature difference and because of the high conductivity of the liquid-like fluid. This energy may be large enough to "explode" clusters of the liquid-like state to a gas-like state. Thus, according to Goldman (Ref. 24 and 25), one may visualize the supercritical region as a region where explosions of liquid-like clusters into gas-like aggregates takes place. Goldman considers this process to be similar to the formation of bubbles in liquid during boiling at supercritical pressures (Ref. 29).

Hines and Wolf (Ref. 28) attribute the appearance of the flow oscillations at supercritical pressures to the variations of liquid viscosity. They note that a small change of temperature near the critical point results in a large change of viscosity. Consequently, a sudden increase in wall temperature could cause a thinning of the laminar boundary layer due to variation of viscosity. Thinning of the boundary layer would result in a drop in the wall temperature and a corresponding increase in viscosity. This would cause a thicker boundary layer and produce another rise in temperature, thus repeating the cycle.

At critical and supercritical pressures, as well as in boiling mixtures at subcritical pressures, the heat transfer coefficient is a strong function of pressure. Thus, pressure oscillation may interact with the heat transfer coefficients inducing oscillations of the latter. If these oscillations are in phase, the system may be thermally driven and become oscillatory (Ref. 29).

Still another mechanism that can induce oscillations at subcritical pressure is caused by the change of flow regime which can induce large fluctuations of the mixture density. These, in turn, may induce both oscillations of the flow and of the heat transfer coefficient, thus providing the driving force necessary for maintaining the oscillation (Ref. 29). N Zuber et al (Ref 29) presented a very detailed description and analysis of modes of pressure and flow oscillations

Reference 21 noted that, when a liquid moves in a heated transfer line, the liquid warms up to saturation temperature then evaporates, thereafter, three regimes exist in the transfer line a length of pure liquid called the liquid regime, a length of boiling, saturated liquid-vapor mixture called the two-phase regime, and a vapor regime consisting of pure vapor saturated at the upstream end Flow and pressure surges may occur due to rapid accelerations at first, then decelerations when large amounts of vapor are formed

Analysis of the Data

The data obtained for tests 103 and 108 were not recorded in detail because these tests were part of the routine pump chilldown prior to the main pump test, and only the pump discharge flowmeter was in service. Although turbine-type flowmeters have been utilized successfully in measuring cryogenic fluids such as LO_2 and LH_2, this instrument should be used for the range of flow and density for which it is designed (Ref. 33). Also, this instrument will not produce accurate results when used in two-phase fluid applications The flowmeter used in these chilldown tests were calibrated only for LH_2 flow, but not for GH_2 flow. Therefore, the accuracy of the flow measured during the GH_2 or two-phase flow is questionable. In test 103 as well as test 108, a further complication was evolved because the H_2 bulk temperature was measured by the inlet and the outlet thermocouple The outlet thermocouple almost consistently showed a lower temperature that the inlet thermocouple. These

temperatures are plotted versus chilldown time in Fig. 78 for test 103 and in Fig. 79 for test 108. It is obvious that the outlet thermocouple should have registered higher bulk temperature than the inlet thermocouple due to heat input by the pump. This discrepancy is attributed to the accumulation of warmer GH_2 and formation of a warm pocket of GH_2 adjacent to the inlet thermocouple. This thermocouple was located on top (12 o'clock) of the inlet duct, and nonmixing of the GH_2 in the inlet duct and the pump could have led to the stratification of the GH_2 near the inlet thermocouple. Figures 78 and 79 show that the outlet thermocouple and Rosemount probe measured the same H_2 bulk temperature. However, the same figures show that the inlet thermocouple and the inlet Rosemount probe, which is located on the bottom (6 o'clock) of the inlet duct, measure different temperatures.

This deviation in temperature measurement occurred after LH_2 was used to chill the pump (about 400 seconds from the start of chilldown). The difference in the inlet temperature is further proof of H_2 stratification at the inlet of the pump.

Because of the inaccuracy in the temperature measurements, the enthalpy increase across the pump could not be computed. Also, not knowing the enthalpy increase precluded the determination of the heat rejected by the pump. However, the skin temperatures measured for these two tests seemed acceptable and valid. Figures 80 and 81 show the skin temperatures plotted versus the chilldown time for test 103, and Fig. 82 and 83 show the same parameters for test 108. It can be seen that thermocouple No. 6 indicates a skin temperature below -400 F after about 850 seconds for test 103 and around 830 seconds for test 108. Although the measured flowrate is not accurate, the plot of H_2 flowrate versus chilldown time was prepared (Fig. 84) to present the magnitude of the flowrate for these tests. Also, the accumulated H_2 flow through the pump was prepared and plotted on Fig. 85. These flowrates were determined simply by multiplying the density of H_2, at the pump outlet condition, by the volumetric flowrate as measured by the pump discharge

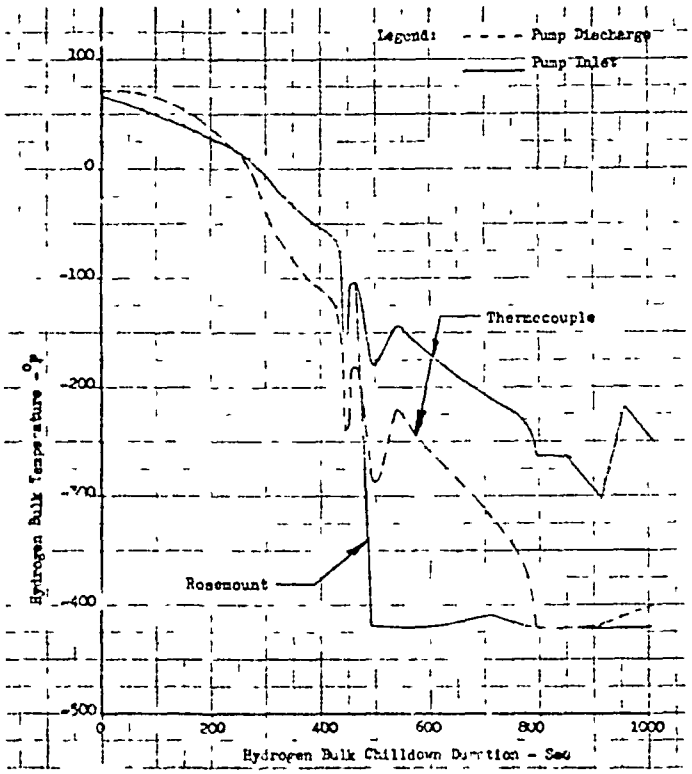

Figure 78. Hydrogen Bulk Temperature vs Chilldown Duration for Mark 15 LH_2 Pump - Run 103

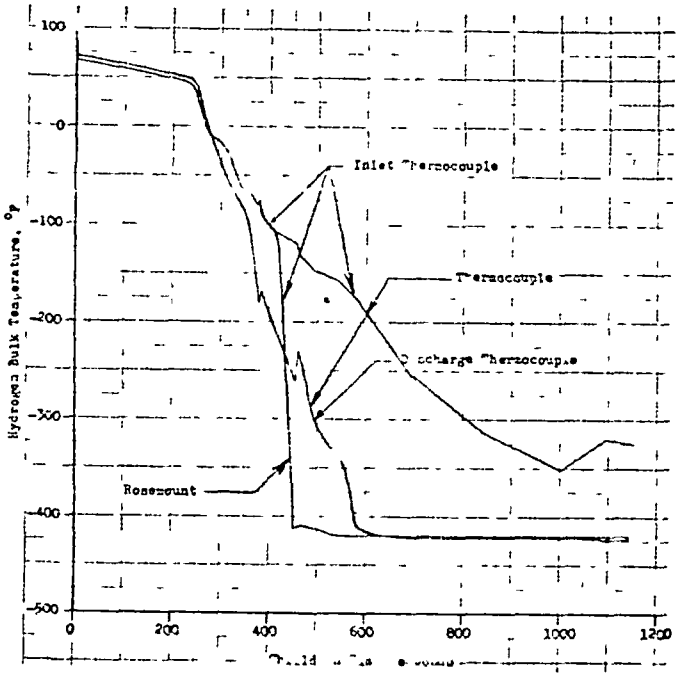

Figure 79. Hydrogen Bulk Temperature vs Chilldown Time for Mark 15 LH_2 Pump - Run 108

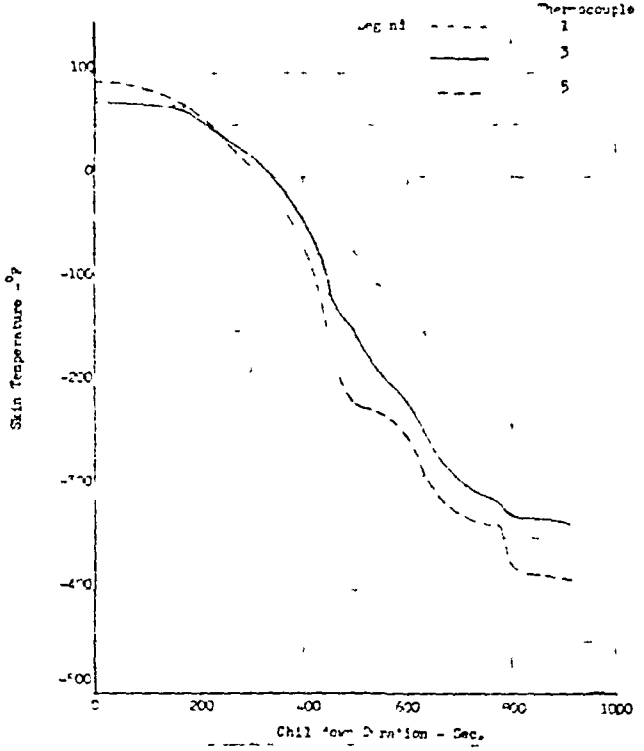

Figure 80. Skin Temperature vs Chilldown Duration for Mark 15 LH_2 Pump - Run 103

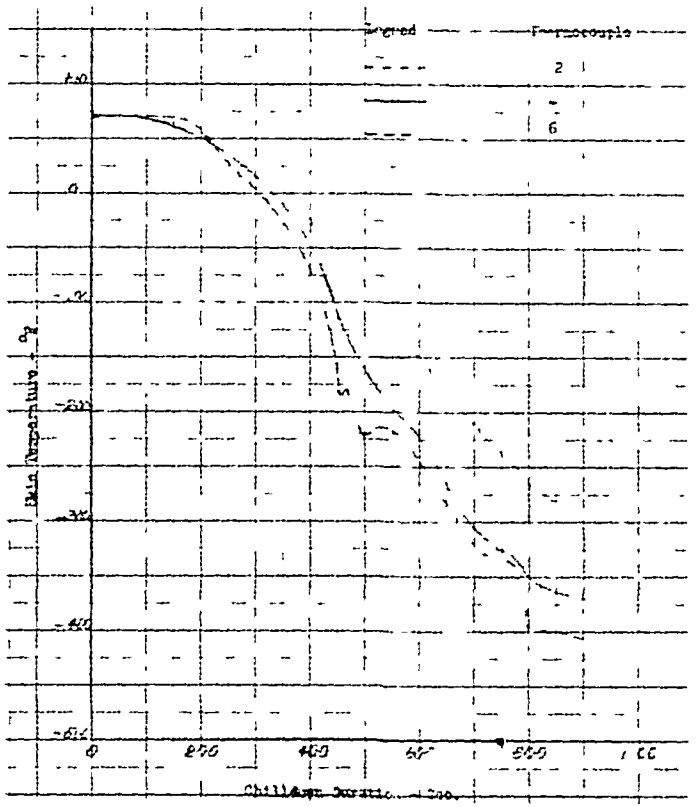

Figure 81. Skin Temperature vs Chilldown Duration for Mark 15 LH_2 Pump - Run 103

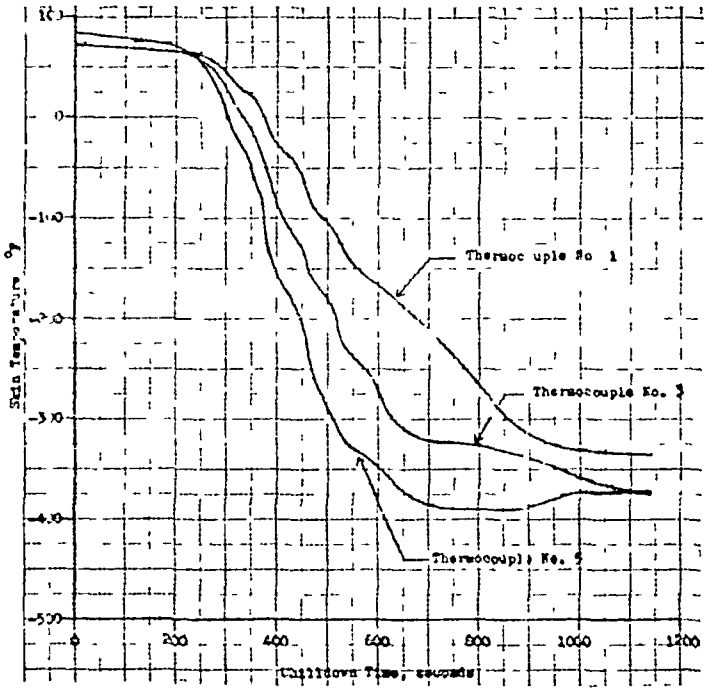

Figure 82. Skin Temperature vs Chilldown Time for Mark 15 LH_2 Pump - Run 108

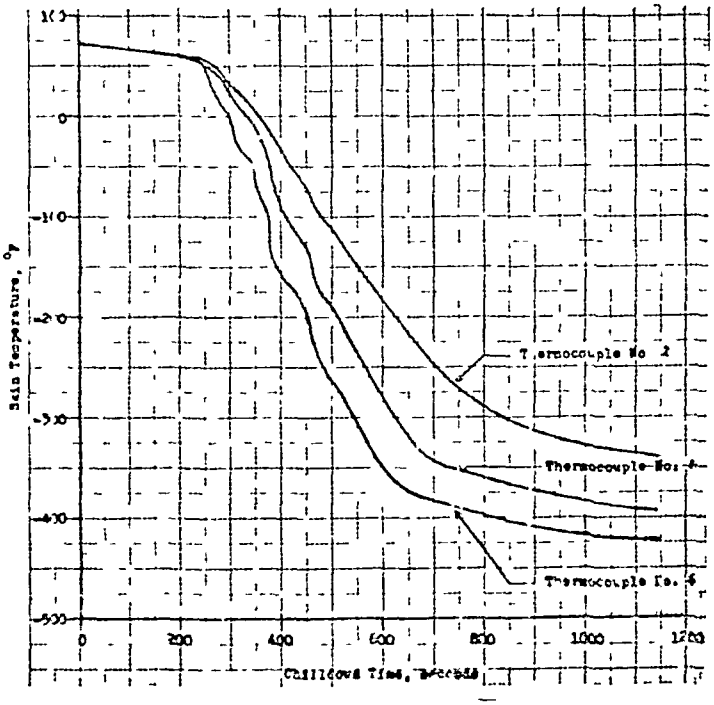

Figure 83. Skin Temperature vs Chilldown Time for Mark 15 LH_2 Pump - Run 108

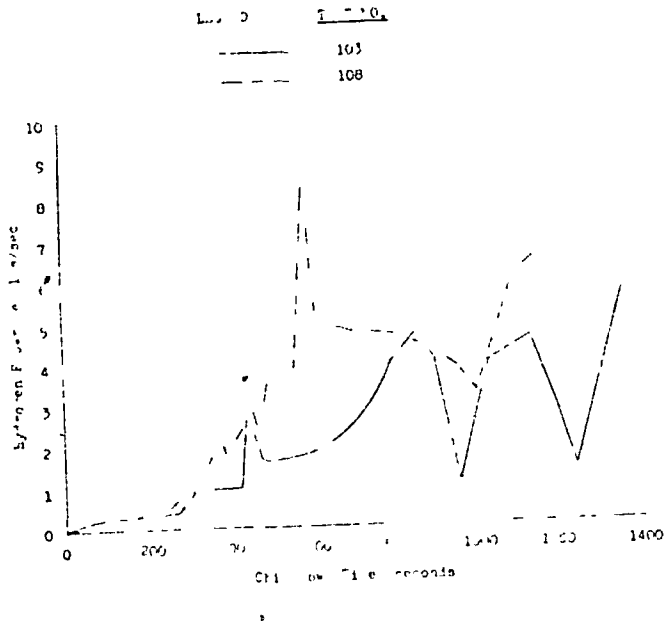

Figure 84. Hydrogen Flowrate vs Chilldown Time for Mark 15 LH_2 Pump

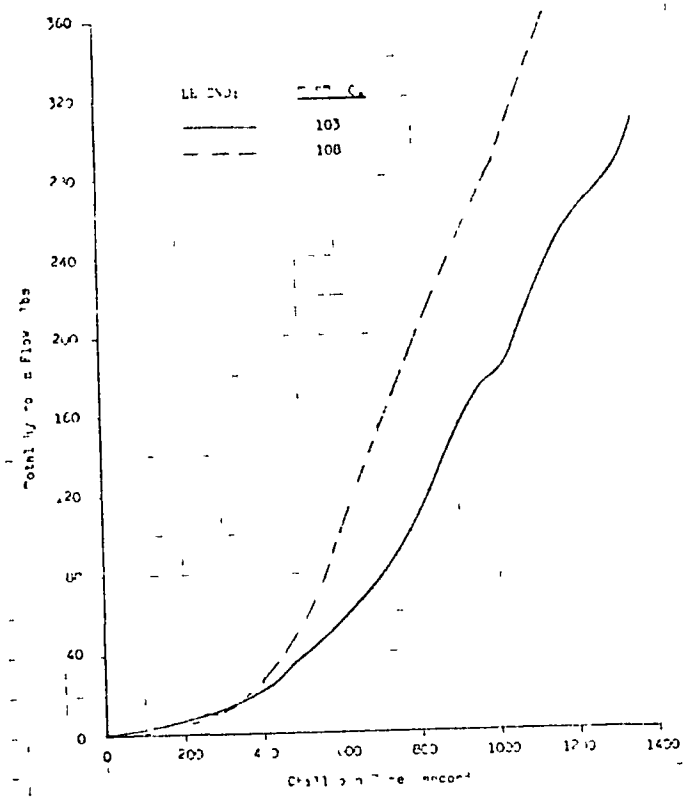

Figure 85. Total Hydrogen Flow vs Chilldown Time for Mark 15 LH_2 Pump

flowmeter. Although there is an error in the flowrate, the magnitude of the error is thought to be about 15 to 20 percent, therefore, it can be seen that less than 300 to 400 pounds of H_2 can be used to chill the pump with a long-term chill.

Test No. 118 was a scheduled chilldown test and lasted about 167 seconds. The difficulty with this test as well as the other tests was that the chilldown loop piping was not chilled sufficiently prior to each test. As a result, the H_2 flowing through the feed line flowmeter was all GH_2 at the beginning, followed by two-phase H_2, and finally all LH_2. Therefore, the difficulty of obtaining an accurate flowrate during gas and two-phase flow existed. Referring to Fig. 86, which is a T-S diagram for H_2, one can see that from the start of the test until about 41 seconds later, only superheated H_2 passed through the feed line flowmeter. For a period of 47 seconds (from 41 to 88 seconds), two-phase H_2 was being metered. The flowmeter received 100-percent LH_2 for only about 45 seconds. Considering the H_2 condition at the pump inlet, one can see that superheated H_2 enters the pump for about 75 seconds. Two-phase H_2 enters the pump from 75 seconds after start of the test (a period of about 47 seconds). The all LH_2 entered the pump for a period of 45 seconds. The H_2 condition at the pump outlet was either all GH_2 or two-phase flow with all LH_2 never leaving the pump. This is understandable even if heat was not added to the LH_2. The pressure drop across the pump is high enough to cause the slightly subcooled LH_2 to become superheated liquid, and result in flashing of the H_2.

The inlet and outlet H_2 bulk temperatures are plotted in Fig. 87. It is seen that in the early part of the test the outlet bulk temperature is higher, as it should be, than the inlet bulk temperature. During this period, the H_2 is in the vapor phase when it enters the pump. At about 46 seconds from the start of the chilldown, a crossover of the bulk temperature takes place, outlet bulk temperature is lower than inlet bulk temperature.

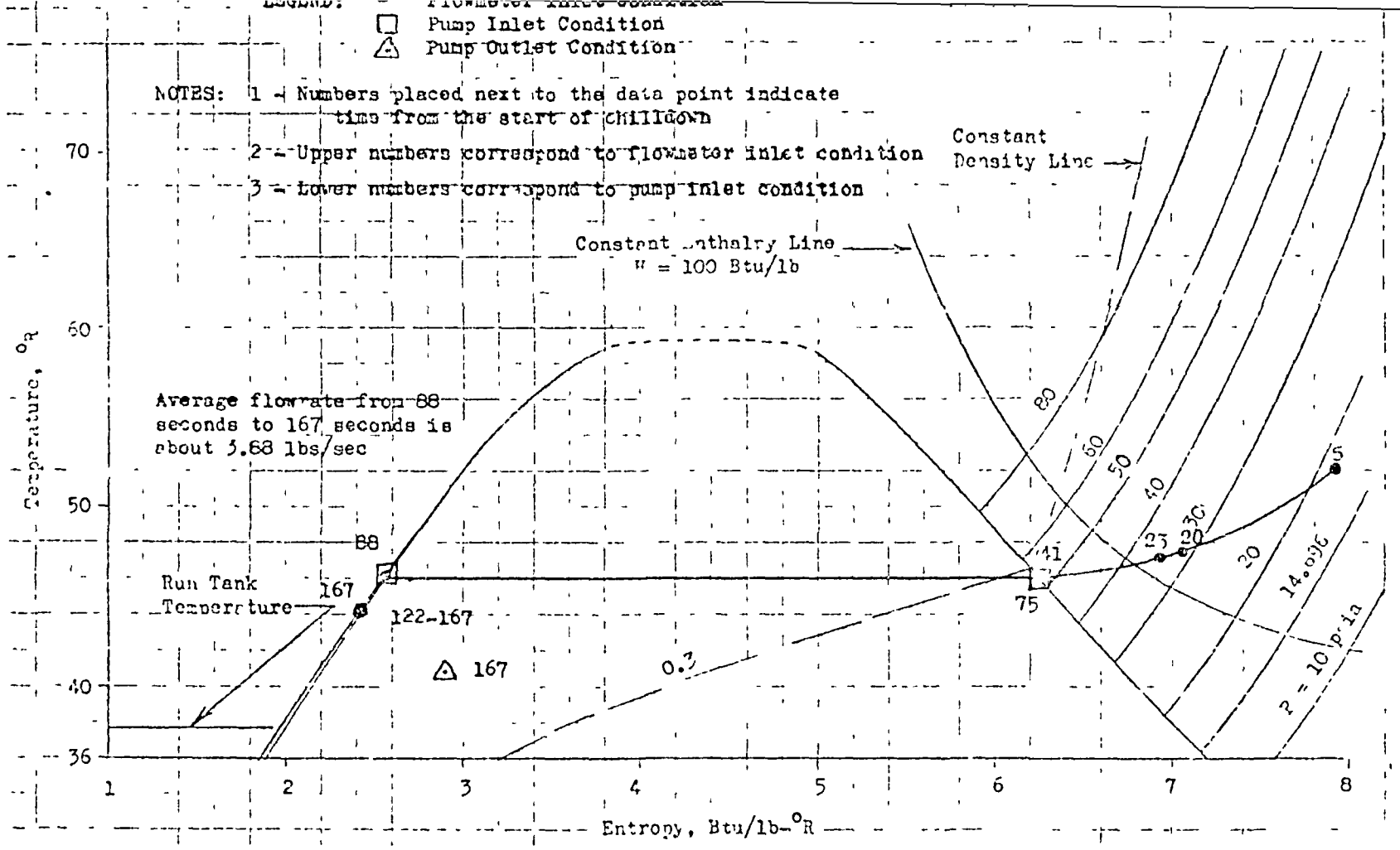

Figure 86. T-S Diagram for Hydrogen - Run 118

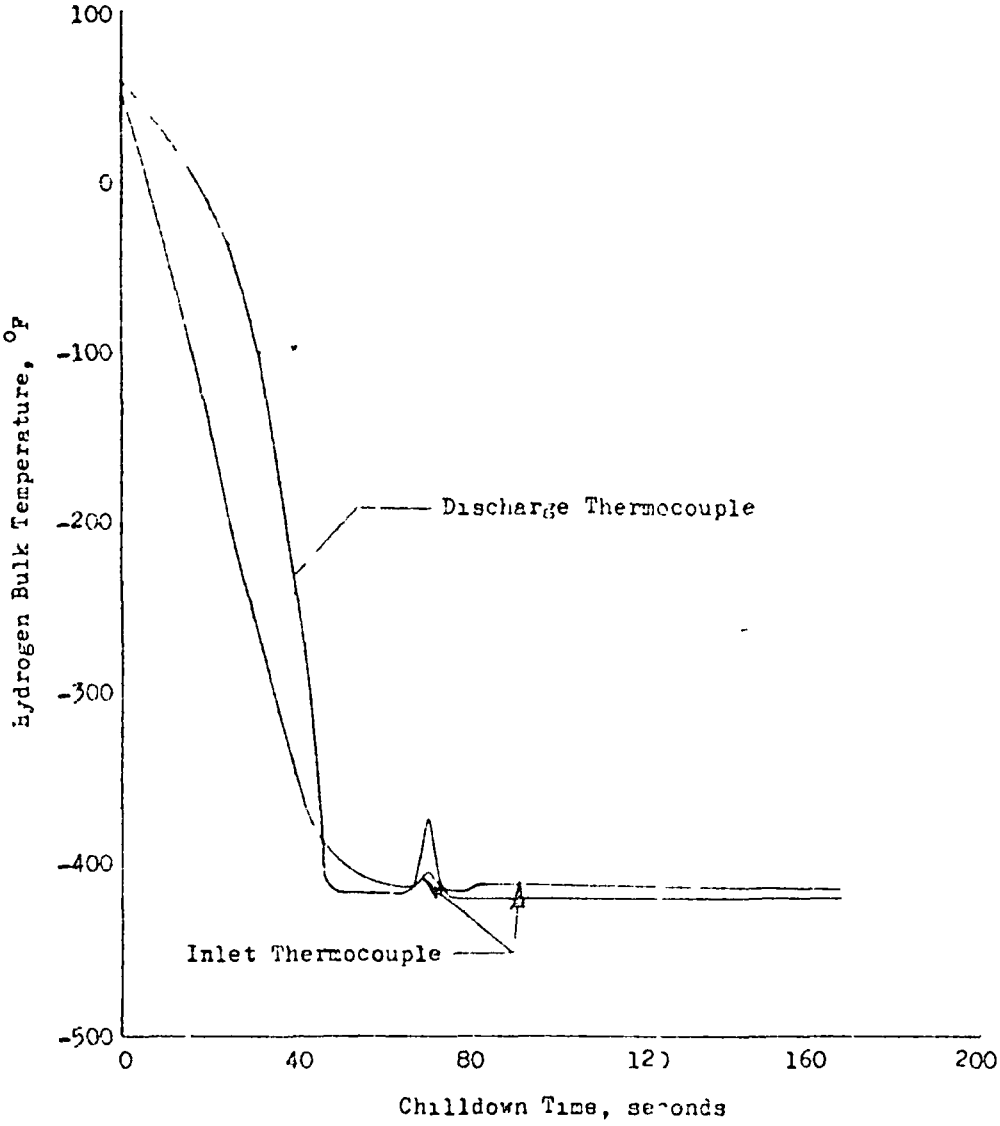

Figure 87 Hydrogen Bulk Temperature vs Chilldown Time for Mark 15 LH_2 Pump - Run 118

During this time, either two-phase flow or 100-percent LH_2 enters the pump. Although some heat is added to the H_2 by the pump, this heat is not sufficient to cause full vaporization of the fluid. The pressure drop across the pump causes the saturated LH_2 entering the pump to flash. The result is a temperature drop of the H_2 as it leaves the pump. As long as saturated LH_2 enters the pump and a large pressure drop (about 30 to 40 psi) takes place across the pump, the H_2 leaving the pump will be in two phase and at a lower temperature than that entering the pump.

Figures 88 and 89 are plots of LH_2 pump skin temperature versus chill-down time for test 118. The thermocouple locations are shown in Fig. 73. The skin temperatures fall rapidly especially for thermocouples 5 and 6. Thermocouples 5 and 6 are located on the discharge flange and volute, respectively. At these locations, the wall is solid and no gap exists between the wetted wall and the wall on which the thermocouples are attached. Therefore, the resistance to the flow of heat is much less at locations 5 and 6 than elsewhere.

The data for all these tests were recorded on one dynalog chart and were printed out simultaneously at different time intervals. Unfortunately, the printed data are missing in the earlier part of the test for all except test No. 124, for which data were acquired every second from the start of the test. No data were printed out for the early part of tests 118, 121, and 122 because of a malfunction to the data acquisition sequencing device.

Tests 12 , 122, and 124 were in general the same as est 118 just described, except for variation i run tank pressure and throttle valve opening. However, during test 121 the thermocouple junction box temperature was in error, resulting in false skin and bulk temperature reading. However, all the bulk temperatures recorded by the Rosemount probe were correct and were used when in range. The inlet and outlet thermocouple readings, although in error, are also shown for the early part of this test (Fig. 90).

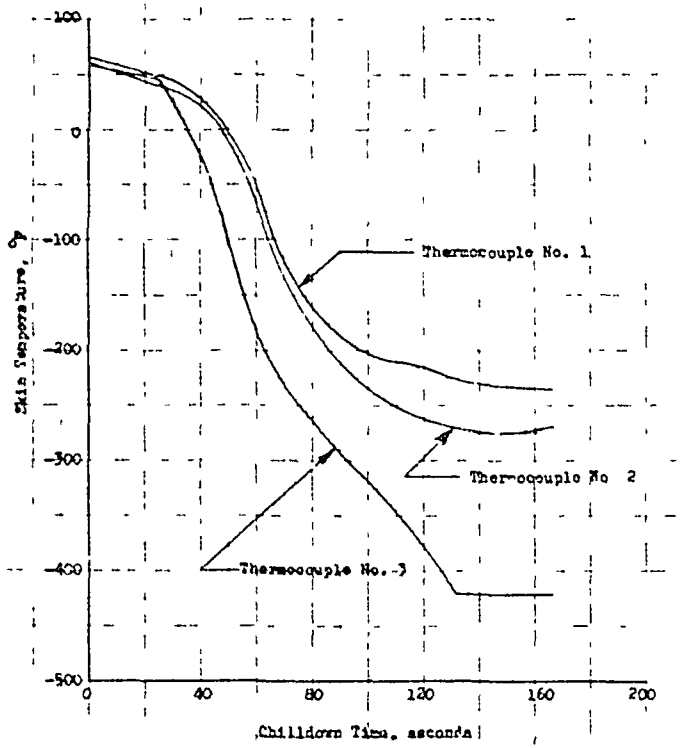

Figure 88 Skin Temperature vs Chilldown Time for Mark 15 HP, Pump - Run 118

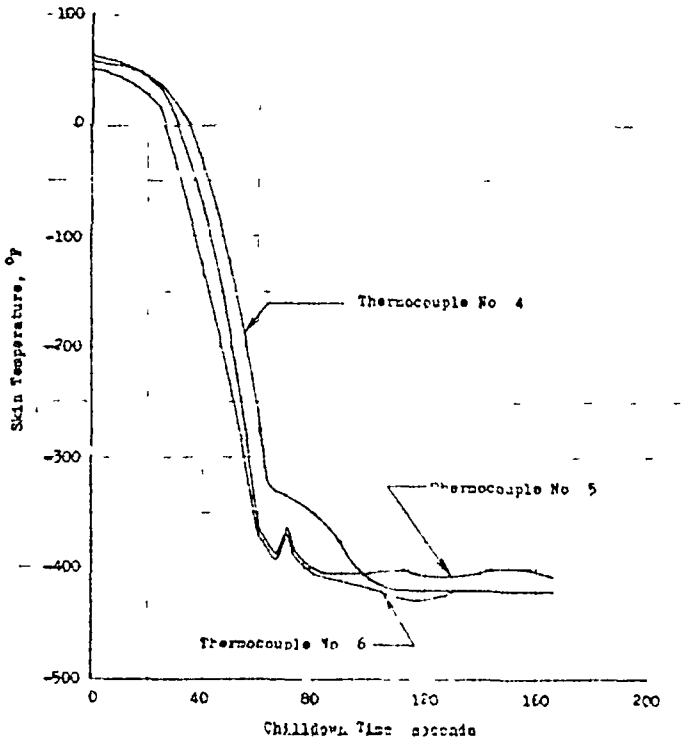

Figure 89. Skin Temperature vs Chilldown Time for Mark 15 HP, Pump - Run 118

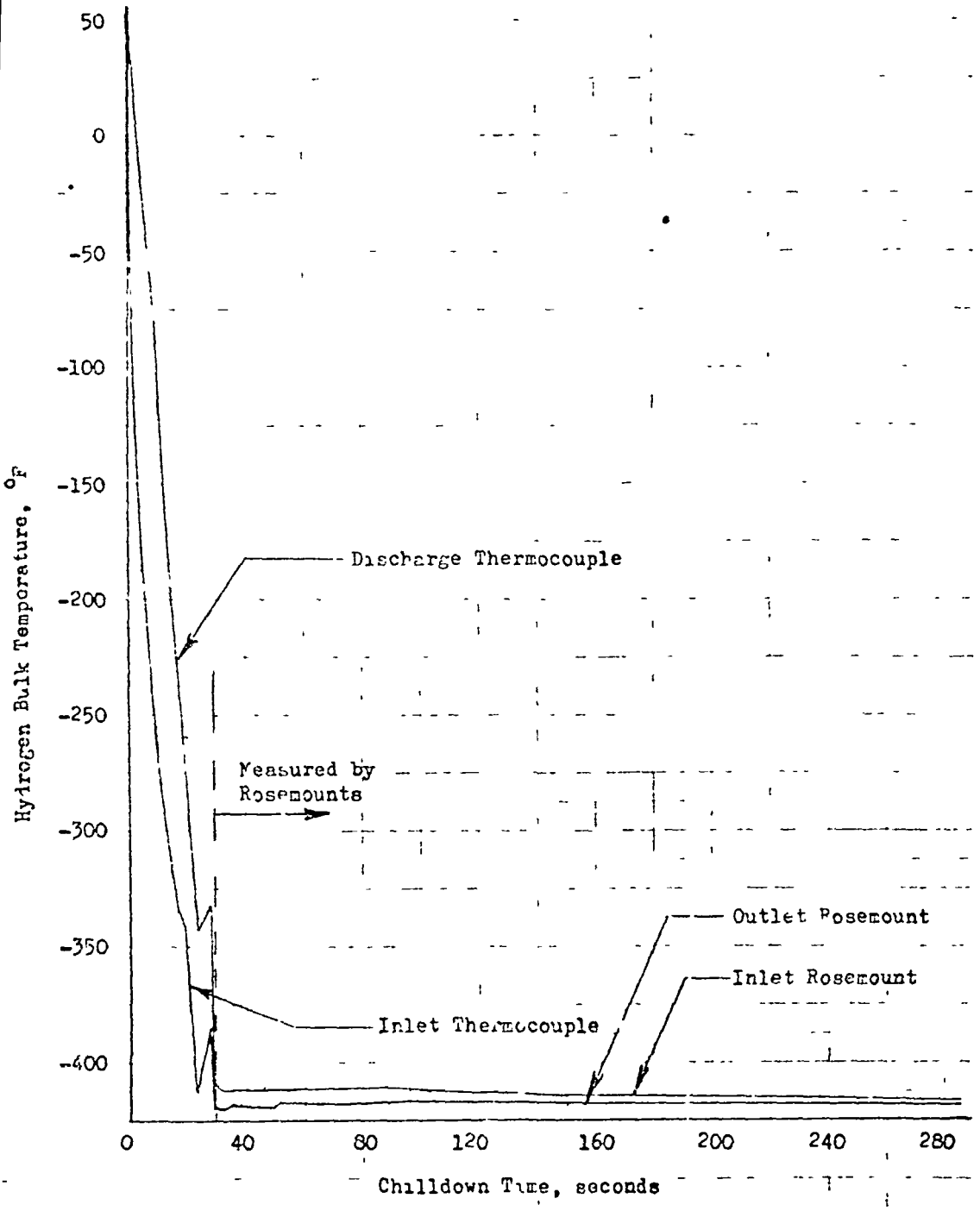

Figure 90. Hydrogen Bulk Temperature vs Chilldown for Mark 15 LH_2 Pump - Run 121

Figures 91 through 99 are for tests 121, 122, and 124, respectively, and are essentially the same as those for test 118 except for minor variation in test durations and temperatures. These figures are self-explanatory and will not be described here.

Figure 100 is a plot of H_2 bulk temperature versus chilldown time for tests 118, 121, 122, and 124. This figure shows how these tests compare with one another. It is seen that in every test the H_2 bulk temperature at the pump outlet falls below -415 F in a relatively short test duration of chilldown time (from 36 to 60 seconds for tests 124 and 118, respectively).

Interpretation of Data

Determination of H_2 flowrate throughout each test was difficult because the feed line flowmeter measured either GH_2 or two-phase flow in the early part of each test. Two choices existed for estimation of the flowrate during this portion of the test. One method was to use the pressure and bulk temperature upstream of the flowmeter and thus determine the density. Using this density and the volumetric flowrate of the flowmeter reading, the mass flowrate was obtained. The second method used assumed that during GH_2 and 100-percent LH_2 flow, the frictional loss and the expansion and contraction loss coefficients are about the same between the flowmeter and the pump inlet. Actually, this is a good assumption since nearly all of the losses occur in the two 2-inch pipes (Fig. 74 and 75). The overall frictional losses between these two points were about 2 percent of the total drop. The main losses are turning, inlet and exit expansion, and contraction losses. Since the pressure drop and flowrate during the all LH_2 flow (near the end of the run) were available, the total velocity head loss was determined by

$$\Delta P = (4f\ L/D + K)\ \frac{V^2 \rho}{288\ g_c} \qquad (60)$$

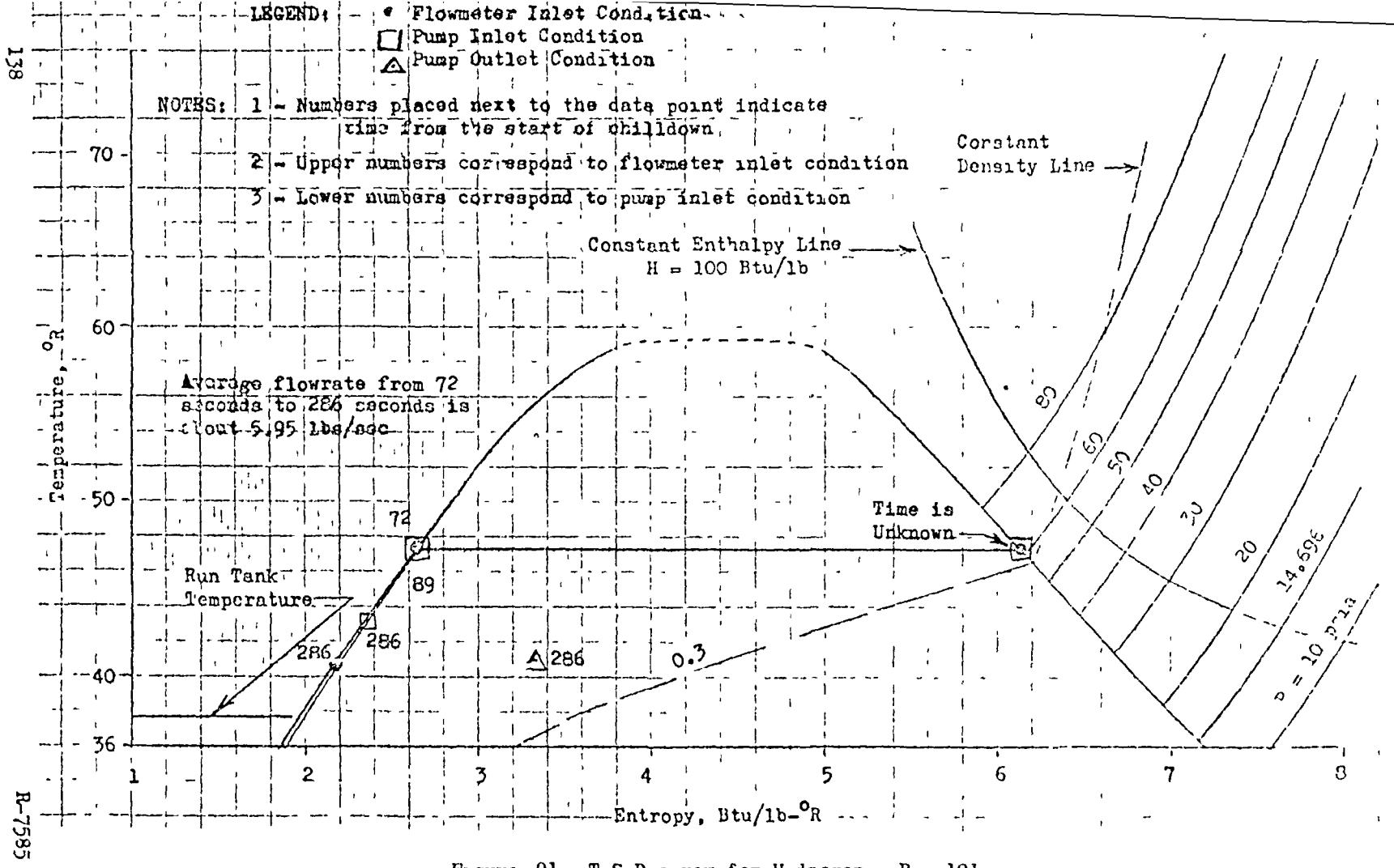

Figure 91. T-S Diagram for Hydrogen - Run 121

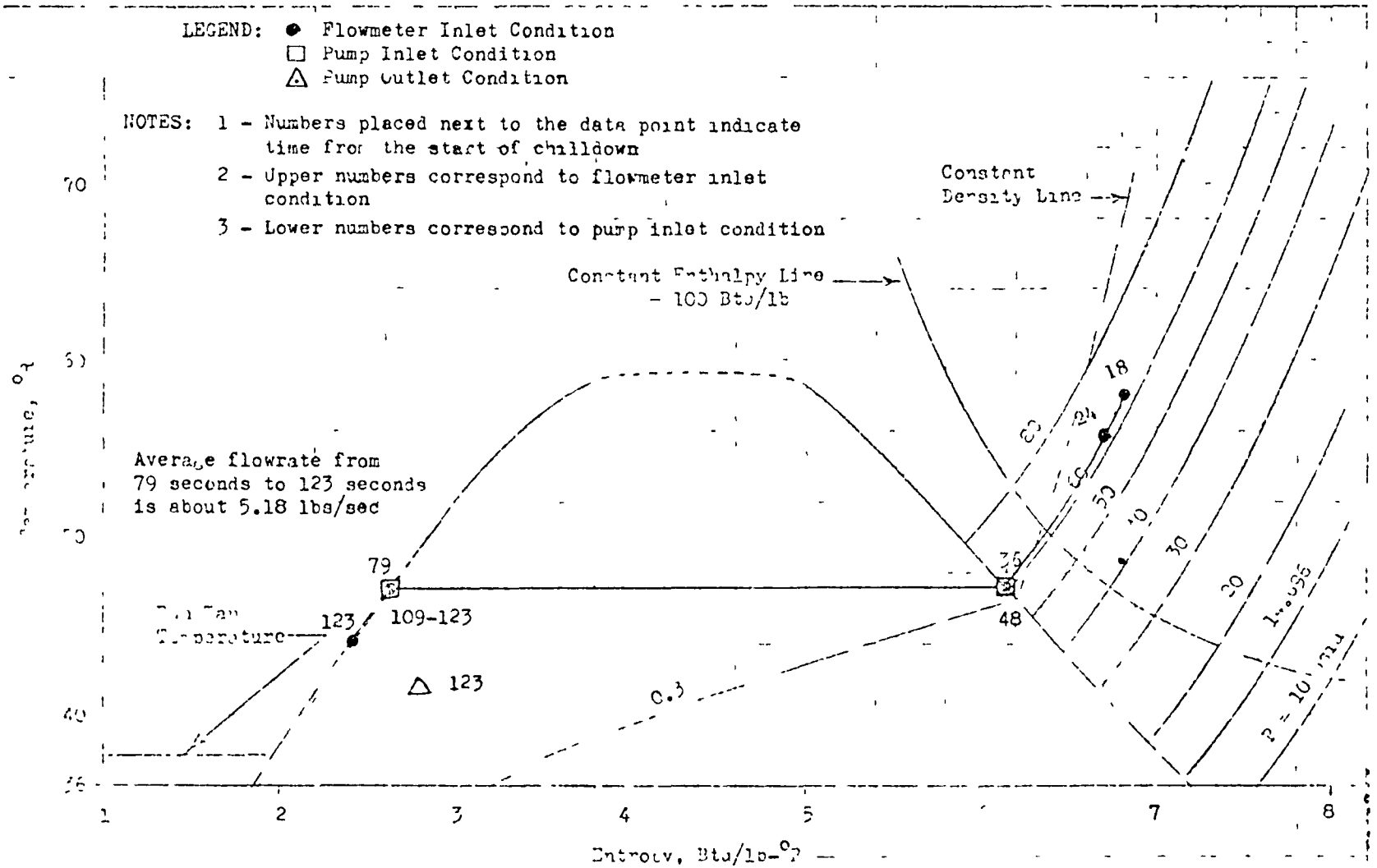

Figure 92. T-S Diagram for Hydrogen - Run 122

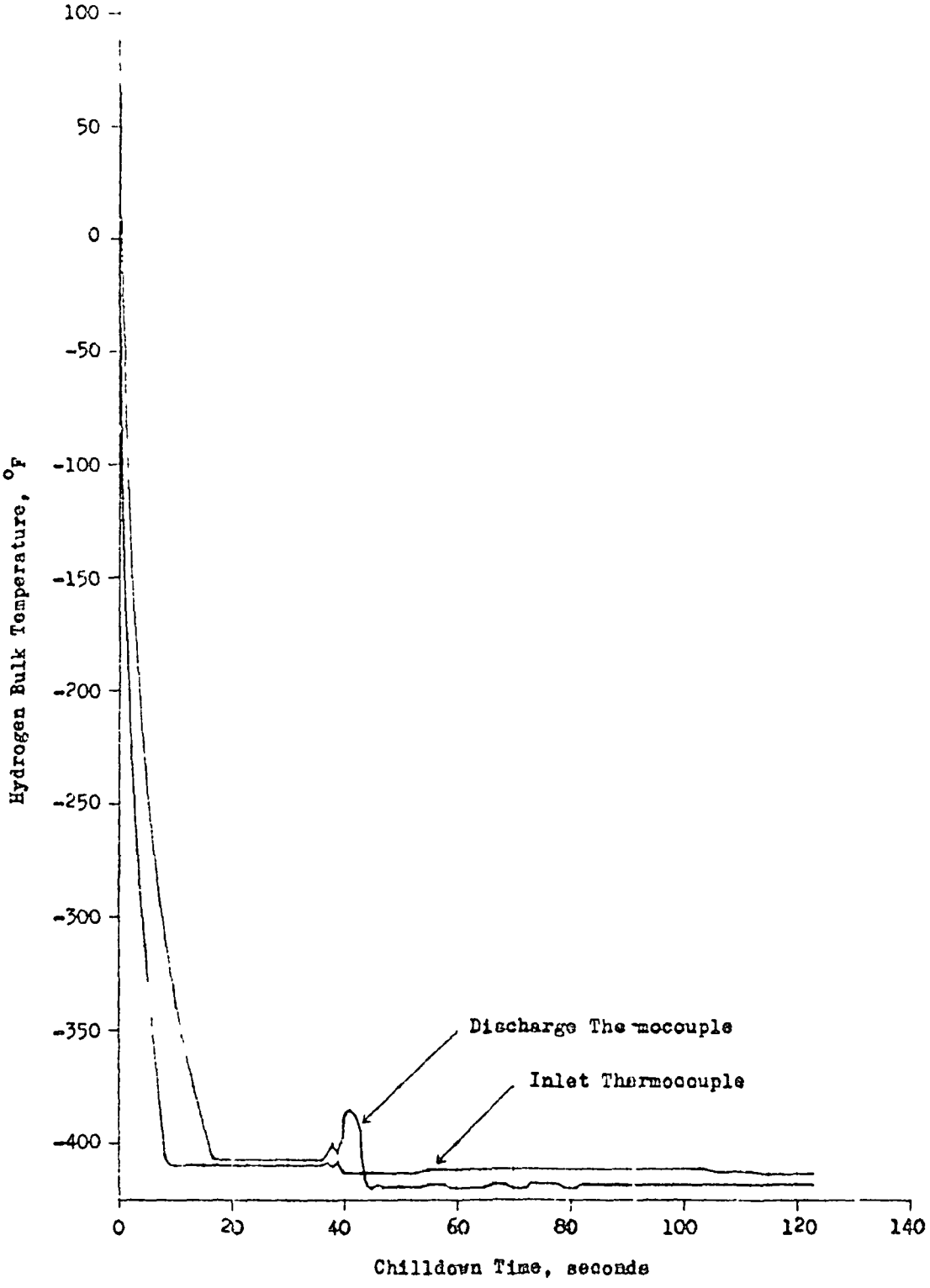

Figure 93. Hydrogen Bulk Temperature vs Chilldown Time for Mark 15 LH_2 Pump - Run 122

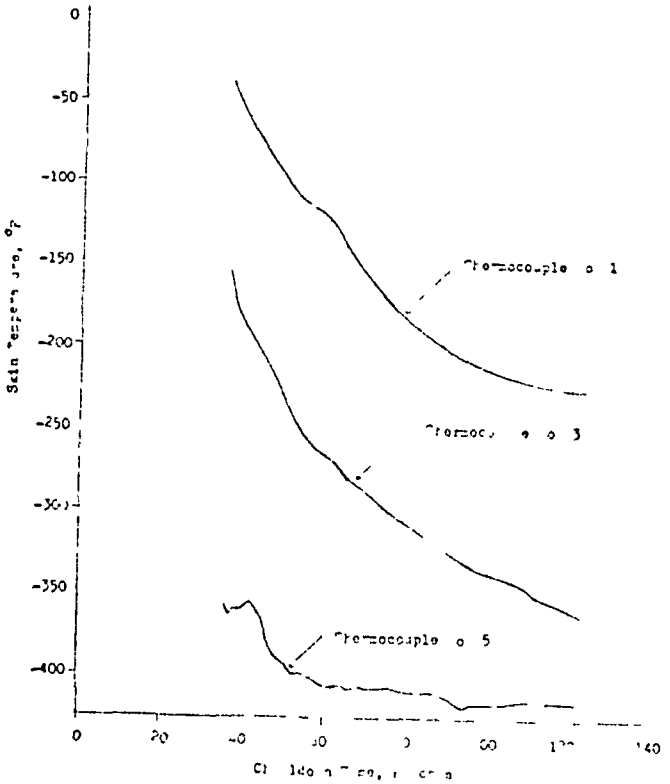

Figure 94. Skin Temperature vs Chilldown Time for Mark 15 LH_2 Pump - Run 122

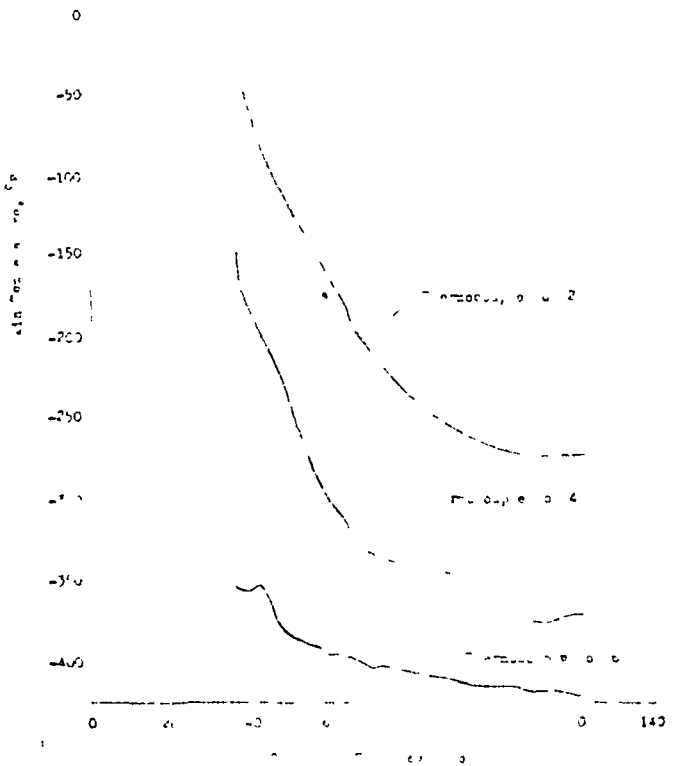

Figure 95. Hydrogen Bulk Temperature vs Chilldown Time for Mark 15 LH_2 Pump - Run 124

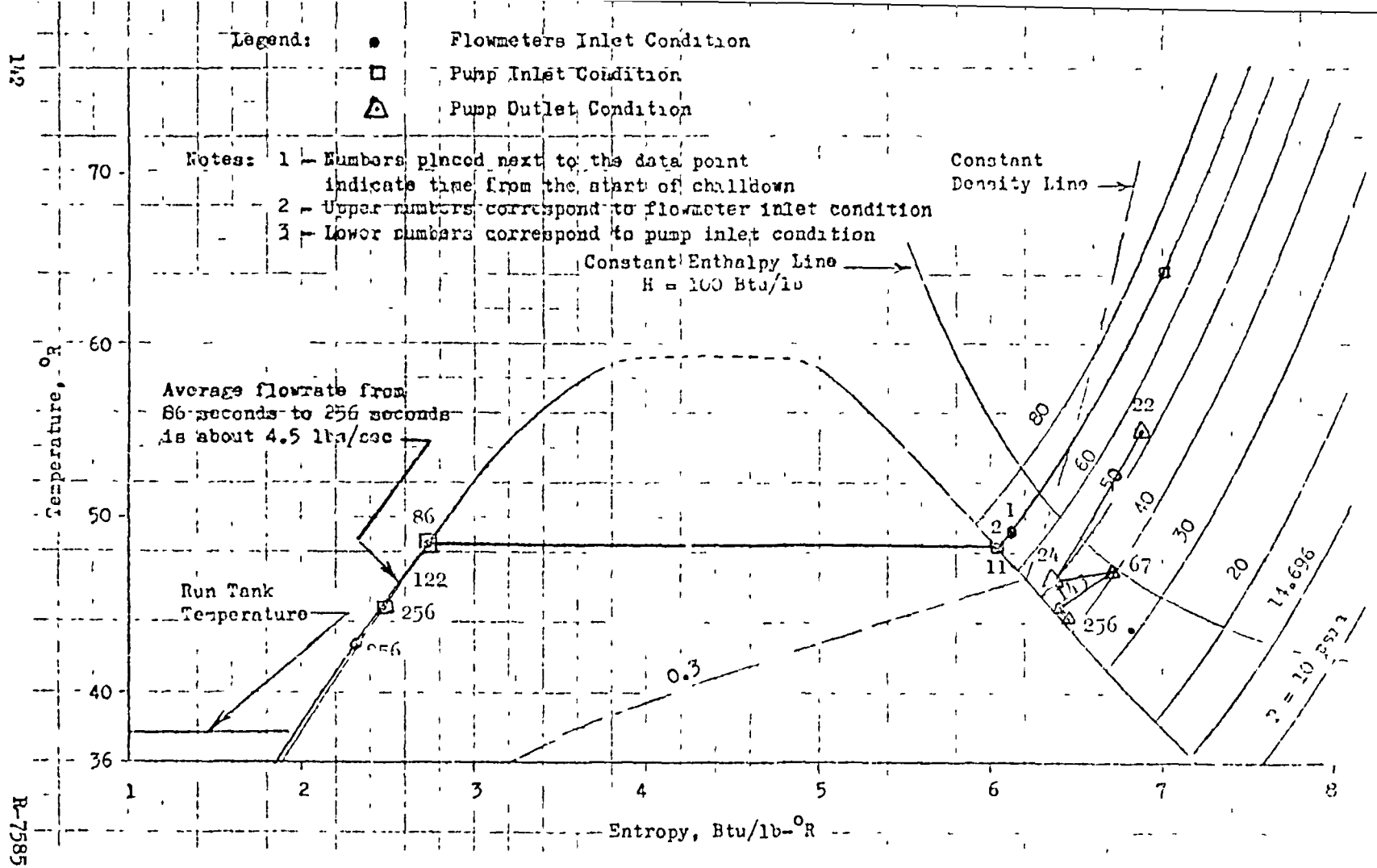

Figure 9o. T-S Diagram for Hydrogen – Run No 12h

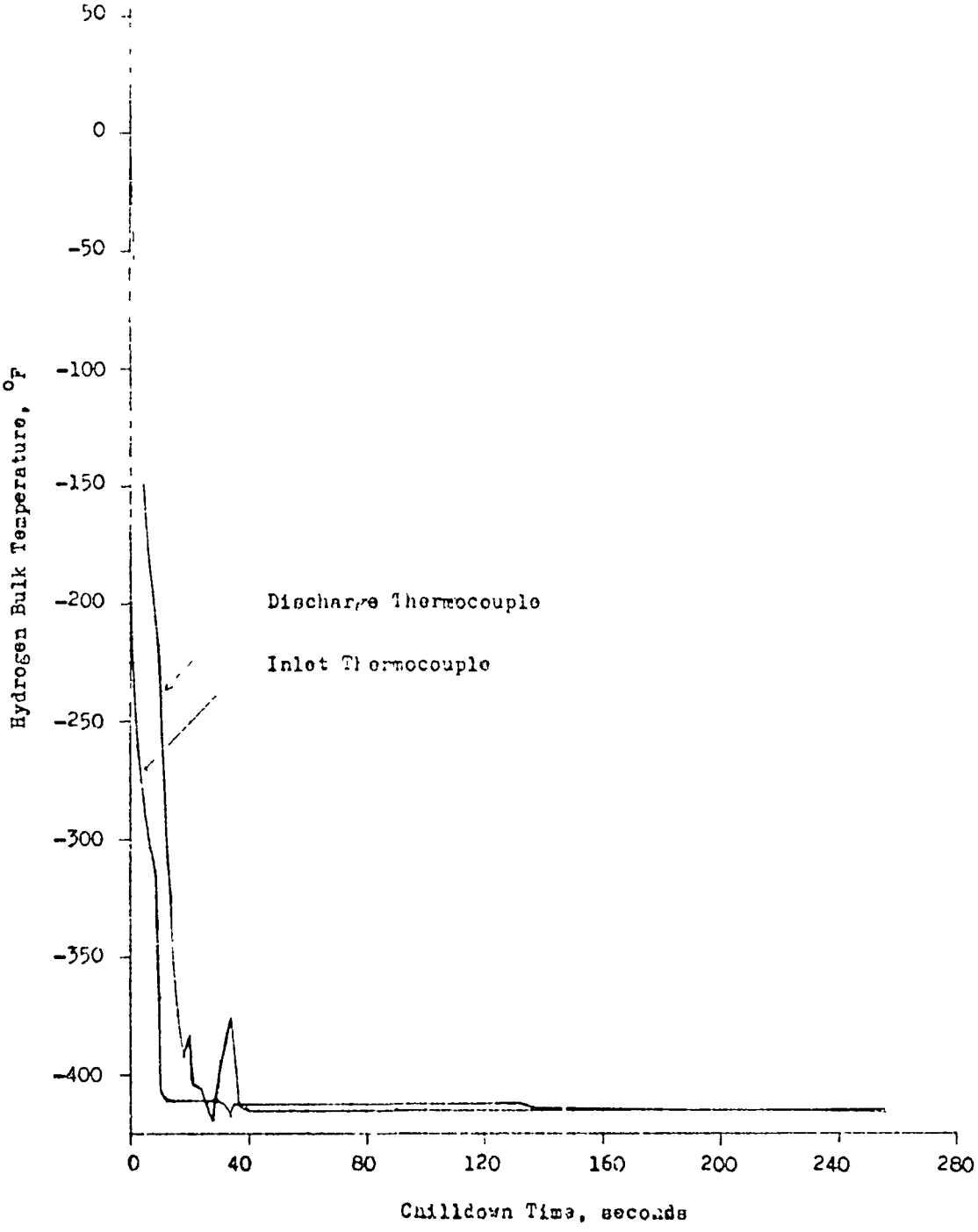

Figure 97 Skin Temperature vs Chilldown Time for Mark 15 LH_2 Pump - Run 124

Figure 98. Skin Temperature vs Chilldown Time for Mark 15 LH_2 Pump - Run 124

Figure 99. Hydrogen Bulk Temperature vs Chilldown Time for Mark 15 LH_2 Pump - Run 124

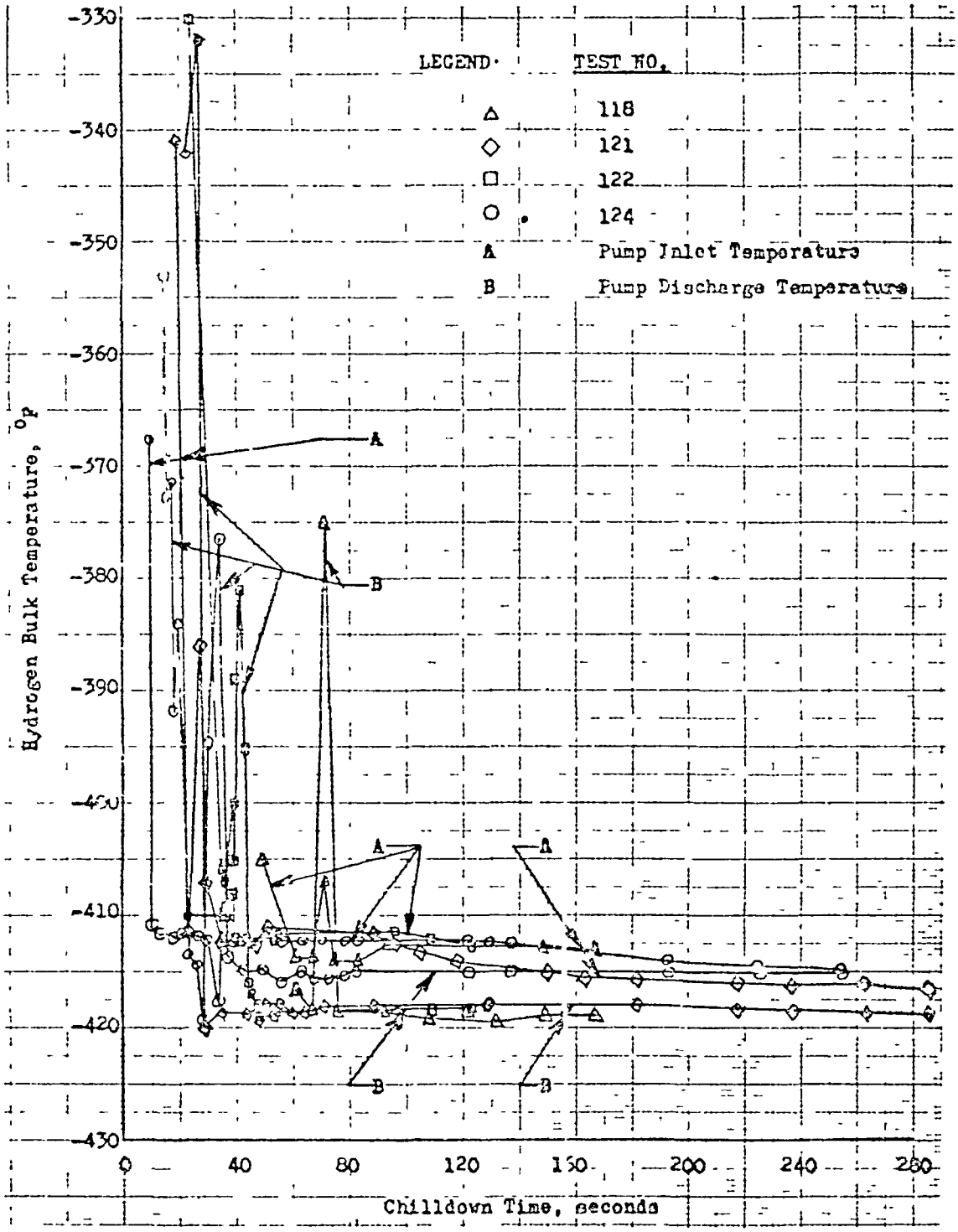

Figure 100. Hydrogen Bulk Temperature vs Chilldown Time for Mark 15 LH_2 Pump

The frictional term was a very small fraction of the total drop (2 percent), and did not change much between LH_2 and GH_2 due to high Reynolds number (about 1.6×10^6 based on 2-inch pipe). Therefore, it was assumed that

$$\Delta P = k \frac{V^2 \rho}{288\, g_c} \tag{61}$$

knowing ΔP, pipe size, and the mass flowrate, the value of k could be found from Eq. 61. An average value of density corresponding to the condition at flowmeter and pump inlet can be used. Method 2 was used to evaluate the flowrate of GH_2 during the early part of the test as it was believed that this method would result in more accurate flowrate than method 1. The turbine-type flowmeters are not to be used for measuring the flowrate of two-phase fluids (Ref. 33).

Since it was assumed that k remains constant, the GH_2 flowrate was found as follows.

Let

$$\Delta P = K \frac{\dot{W}^2}{288\, A^2\, \rho\, g_c} = K \left(\frac{\dot{W}^2}{\rho}\right)_L \tag{62}$$

and

$$\Delta P_g = k \left(\frac{\dot{W}^2}{\rho}\right)_g \tag{63}$$

Then one can write

$$\frac{\Delta P_L}{\Delta P_g} = \left(\frac{\dot{W}^2}{\rho}\right)_L \left(\frac{\rho}{\dot{W}^2}\right)_g \tag{64}$$

Having ΔP_L, ΔP_g, $\dot{W}_L$, ρ_L, and ρ_g, $\dot{W}_g$ thus can be obtained from Eq. 29.

Equation 29 was rewritten for this particular case, which was based on the velocity head in the 2-inch pipe to give

$$W_{GH_2} = 1.181 \sqrt{\Delta P_g \rho_g} \quad \text{lb mass/sec} \tag{65}$$

Equation 65 was used to evaluate the GH_2 flowrate. The flowrate for LH_2 for near the end of the tests was found from the feed line flowmeter readings. Figure 101 shows the pressure drop parameter versus H_2 flowrate for the section between feed stream flowmeter and the pump inlet. Pressure drop across the pump is also plotted in Fig. 101 for all GH_2 and nearly all LH_2. The data seem to correlate very well. Also, prior to the chilldown testing, the pressure drop across the pump was predicted assuming 100-percent LH_2 with a density of 4.2 lb/ft^3. Figure 102 depicts the predicted pressure drop across the pump along with the experimentally obtained pressure drop. There is quite a difference between the two, and the discrepancy can be explained as follows:

1. During actual testing, two-phase H_2 was passing through the pump. The pressure drop for two-phase flow is higher than that of all LH_2. However, the experimental pressure drop seemed to decrease as the quality decreased and the flowrate increased, indicating a trend in direction of the predicted values. Only for test 121 does the pressure drop seem to have become constant. This is obvious since no heat addition takes place in the pump near the end of the test (Fig. 103).
2. The predicted pressure drop does not include the expansion and contraction losses between the rotor and the stator blades, which could be a great percentage of the total pressure drop.

When the H_2 flowrate was plotted versus chilldown time, there was a region for which the flowrate was unknown. This is that portion of the test during which the upstream and downstream flowmeters were measuring two-phase H_2 flow. Since under this condition estimation of the density was

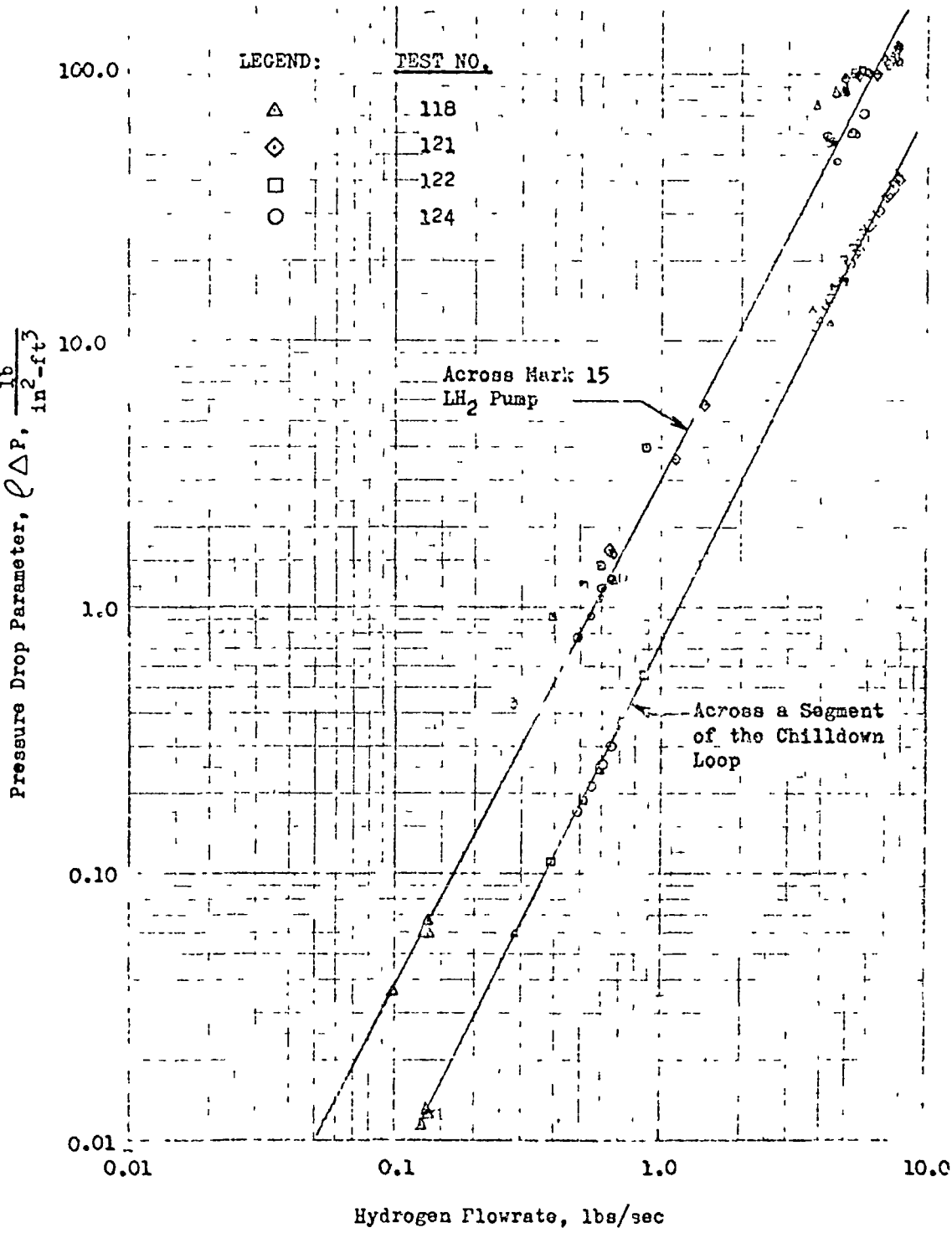

Figure 101. Pressure Drop Parameter vs Hydrogen Flowrate for Mark 15 LH_2 Pump

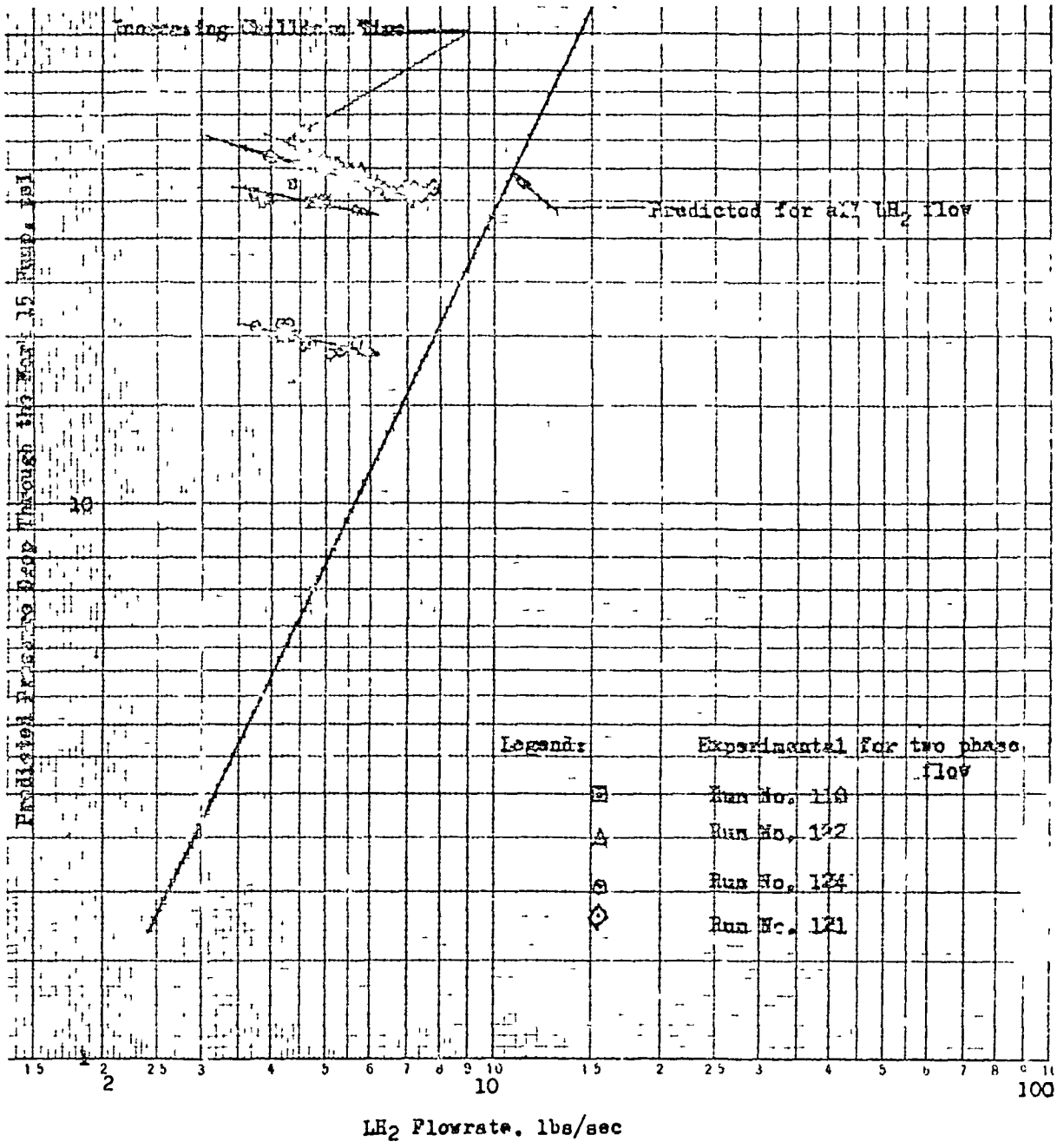

Figure 102. Predicted and Experimental Pressure Drop Through the Mark 15-F Pump vs LH_2 Flowrate for Locked Rotor

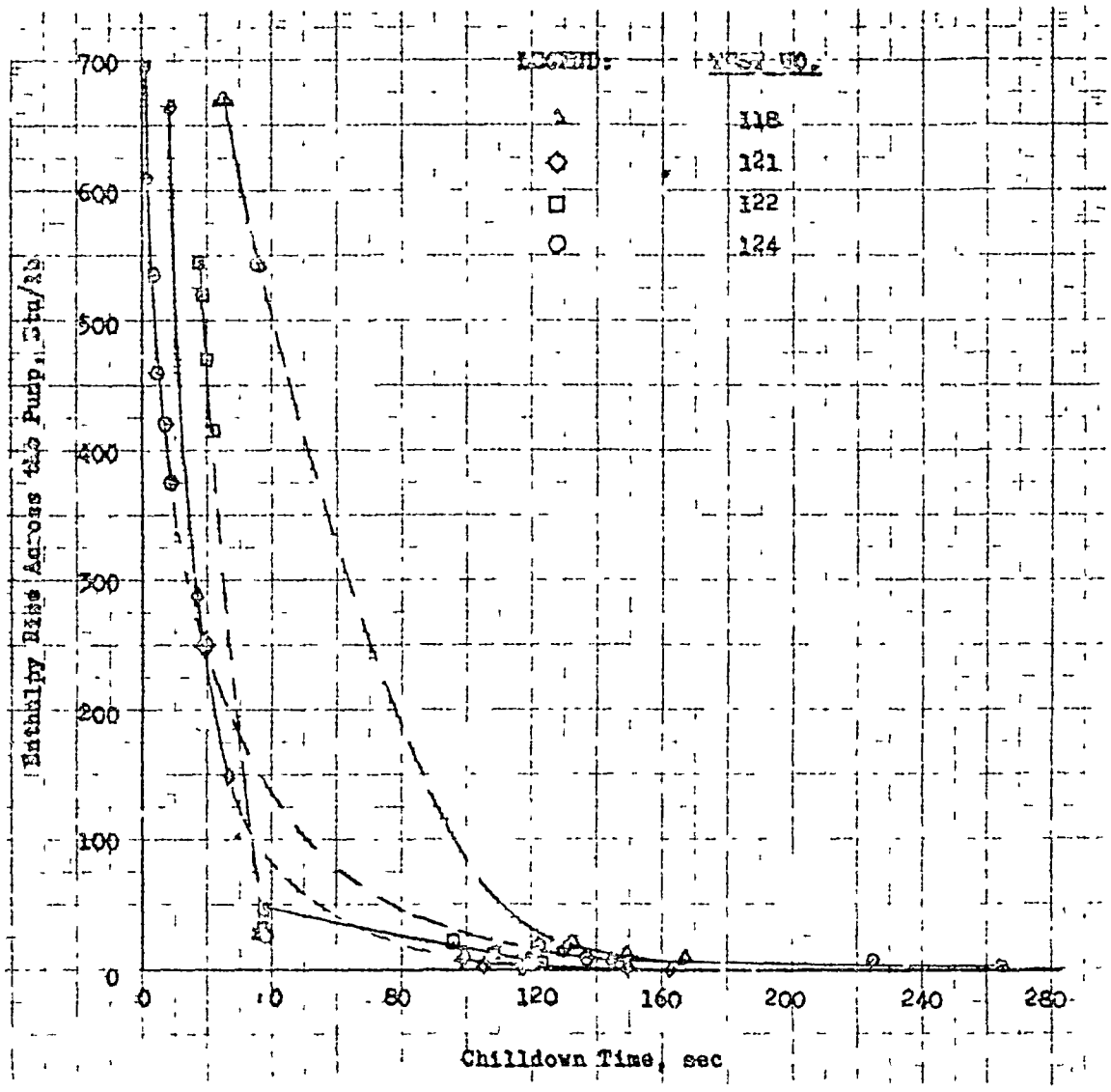

Figure 103. Enthalpy Rise Across the Pump vs Chilldown Time for Mark 15 LH_2 Pump

not possible, the flowrate could not be determined. Consequently, the flowrate during this portion of the test was determined by interpolating by a straight line between the all GH_2 and the all LH_2 data. Figure 104 shows the H_2 flowrate for test 118, 121, 122, and 124 plotted versus chilldown time. The dotted line on these curves indicate the duration of two-phase H_2 flow.

During the latter part of the tests, no changes were made in the pump inlet pressure and throttle valve setting. However, the flowrate seems to be increasing with time, and only for test 121, which is of the longest duration, does the flowrate seem to begin to flatten. Again this increase in flowrate is due to the decrease of the H_2 quality across the pump. The flowrate would have become constant eventually if the heat input had decreased to zero. Figure 105 shows the accumulated H_2 flow versus chilldown time for the four scheduled tests. Again the total flow depends greatly on the test duration and the test condition, i.e., the run tank pressure and the throttle valve setting which were purposely altered to cover a range of conditions. The maximum and the minimum total flow was about 1645 and 385 pounds for test 121 and 122, respectively, at the cutoff time.

The required amount of hydrogen for chilldown purposes, however, is much less than Fig. 105 shows. For example, test 124 indicates that LH_2 enters the pump at about 122 seconds after the start of the test. During this time only about 280 pounds of H_2 has passed through the ducting and the pump. Figures 98 and 99 indicate that the pump is chilled enough to start pumping. Therefore, the H_2 required for chilldown of the pump alone is about 140 pounds. Again, since the pump inlet H_2 temperature was much above that of LH_2, it is possible to still reduce the 140 pounds required H_2 by using cold LH_2 (-423 F). One can conclude that about 50 to 100 pounds of LH_2 may be necessary for the chilldown of the Mark 15 LH_2 pump.

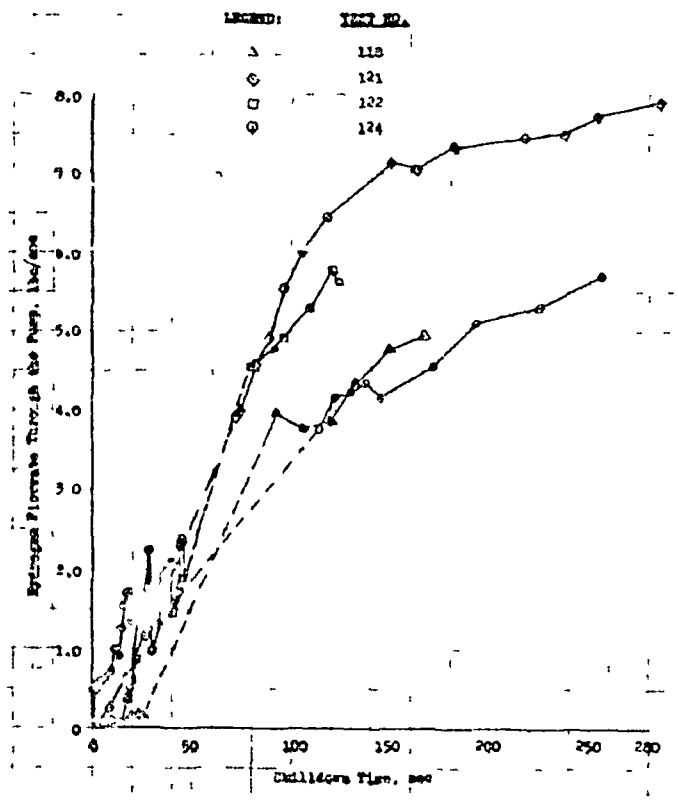

Figure 104. Hydrogen Flowrate Through the Pump vs Chilldown Time for Mark 15 LH_2 Pump

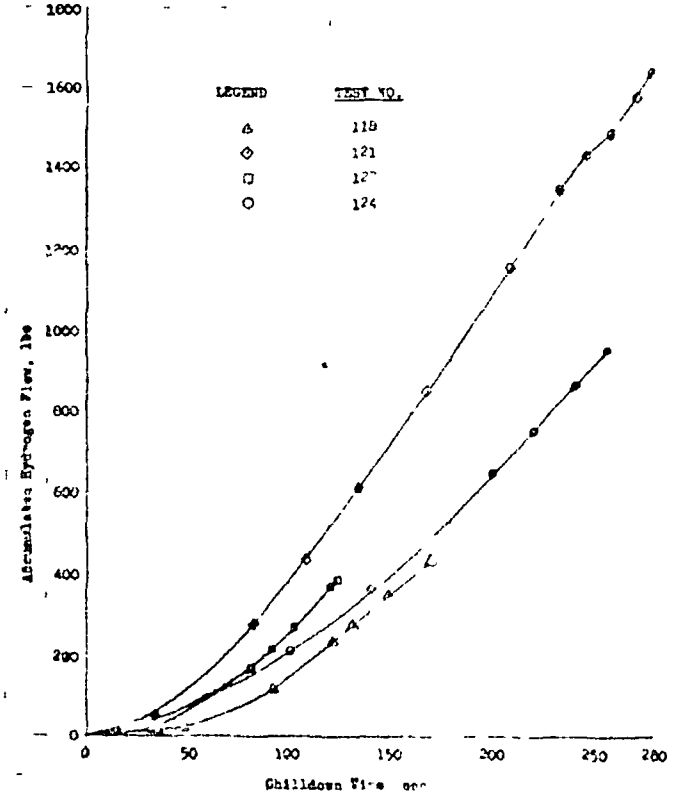

Figure 105. Accumulated Hydrogen Flow vs Chilldown Time for Mark 15 LH_2 Pump

The duration of the test was about the same for tests 121 and 124. However, the total H_2 flow for test 121 is about 83 percent higher than that of test 124. The reason for this large difference in the flow between the two tests is because of the smaller throttle valve opening (88 percent for test 121, and 30 percent for test 124) and the large flow oscillations occurring during test 124. The run tank pressure for tests 121 and 124 is about 75 and 60 psia, respectively. The difference in run tank pressure is not sufficiently high to cause approximately 83 percent difference in the flow. Flow oscillation also is evidenced during other tests, but test 124 was the most severe. For comparison purposes, the dynalog charts for all tests are presented in Fig. 106 and 107, respectively. It can be noticed that the flow oscillation continues for about 119 seconds for test 124, whereas that of test 121 lasted about 60 seconds. During these flow fluctuations, the H_2 flowrate seemed to approach zero for test 124. This is the reason for lower overall total H_2 flow for test 124 than for test 121.

Although some pressure and flow oscillations were noticed in all of the tests, this phenomenon was most severe during test 124. The reason for the severity of the pressure and flow fluctuation is not apparent at this time. One possibility exists, however, that might explain the excessive flow variation for test 124. During this test, the throttle valve setting was the lowest of all tests (30 percent). The restriction downstream of the pump was highest for test 124, therefore, the H_2 flowrate was lowest during this test although the pump discharge flowmeter does not show this. Nevertheless, one can readily observe that the feed line flowmeter fluctuation very definitely proves this claim.

These tests were carried out under subcritical pressure conditions. Reference 29 notes that the nucleation and evaporation at subcritical pressures are rate processes that are affected by the pressure, temperature, and other processes such as the rate of energy transfer, flowrate, etc. Also, Ref. 29 indicates that pressure oscillation is a pressure-dependent phenomenon.

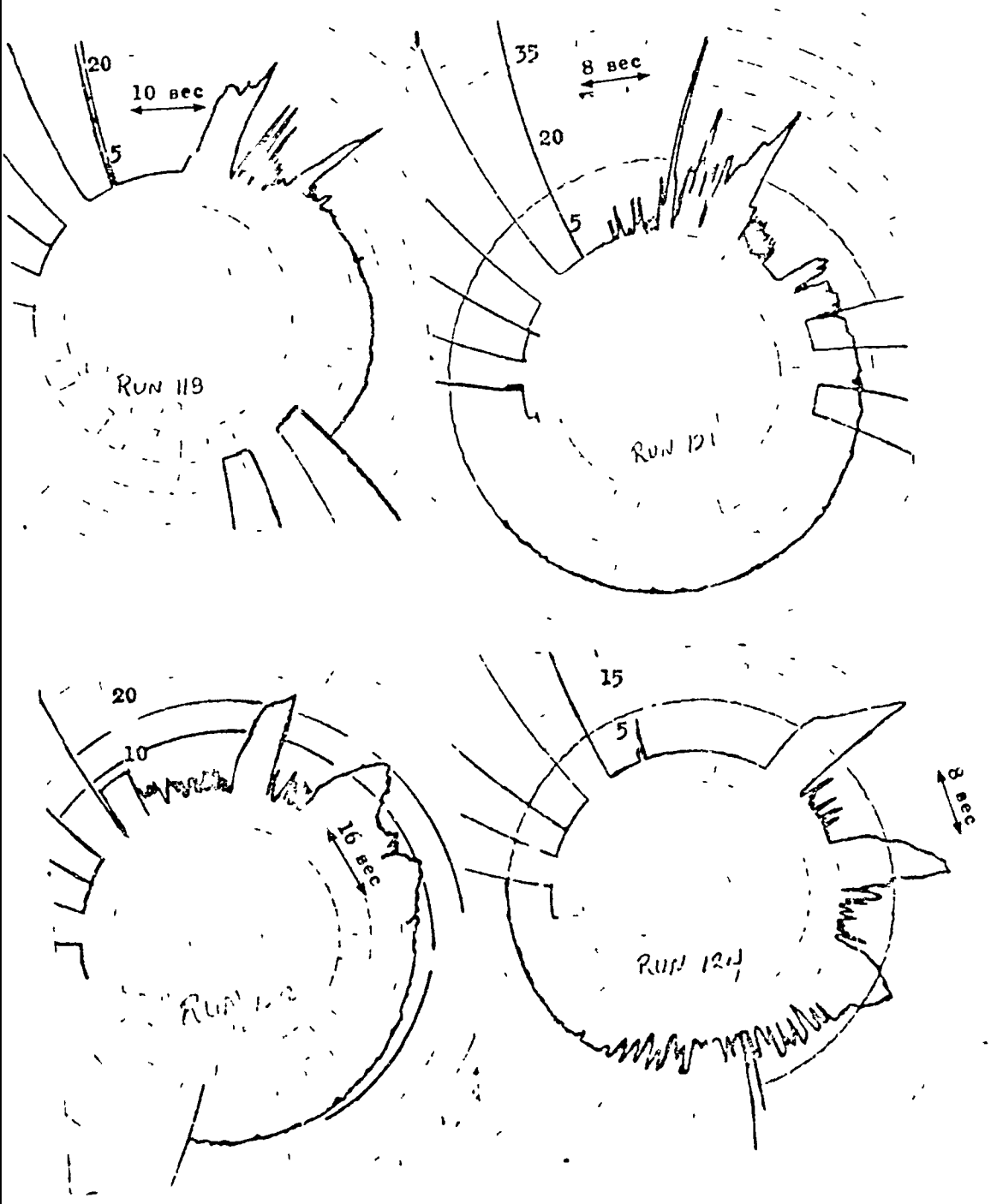

Figure 106. Dynalog Charts of the Feed Line Flowmeter for Mark 15 LH_2 Pump

R-7585

Figure 107. Dynalog Charts of the Inlet Pressure for Mark 15 IR$_4$ Pump

Therefore, the cause of extreme flow and pressure oscillation of test 12 can be attributed to the lower throttle valve setting which, in turn, controls the pump discharge pressure and the H_2 flowrate.

Figure 105 is a plot of the ratio of the downstream to meter speed to the upstream flowmeter speed versus the chamber pressure. This figure indicates slight fluctuations in the speed ratio for tests 11 and 12, but these fluctuations were not significant in test 12. The downstream flowmeter reading was further verified by the measured thrust data. The reason for the high-amplitude fluctuation of test 12 is that the upstream flowmeter reading may contain some cavitating flow during this test. The flow to speed ratio eventually becomes constant after acceleration and decreases slightly, indicating that the pump was decreasing as the pump outlet pressure was approaching zero when the test was terminated by the pump

In the construction of Figure 104, the H_2 flowrate for the early part of the (0 to 2 seconds) of test 12 was based on the pump inlet pressure reading rather than the local flowmeter readings which were too oscillatory and would have made the determination of the flowrate difficult. Figures 106 and 107 show a comparison of the flowmeter and inlet pressure readings for various tests. It is seen that the pressure and flow fluctuation are more drastic in test 12 than the other three test

The determination of the enthalpy across the pump encountered the same difficulty in the evaluation of the H_2 flowrate through the pump for the start and the end of each run when the H_2 condition at the inlet to the pump was either all GH_2 or all LH_2, the evaluation of the enthalpy was simple. At the pump outlet, the H_2 was either two-percent GH_2 or in two-phase flow. The enthalpy of the GH_2 was found easily from a Mollier diagram. During two-phase flow, especially for the mid portion of each test, there was no way of knowing the enthalpy of the H_2 since the density and the quality were unknown. However, the enthalpy of two-phase H_2 at the pump outlet was determined by assuming that the ratio of the

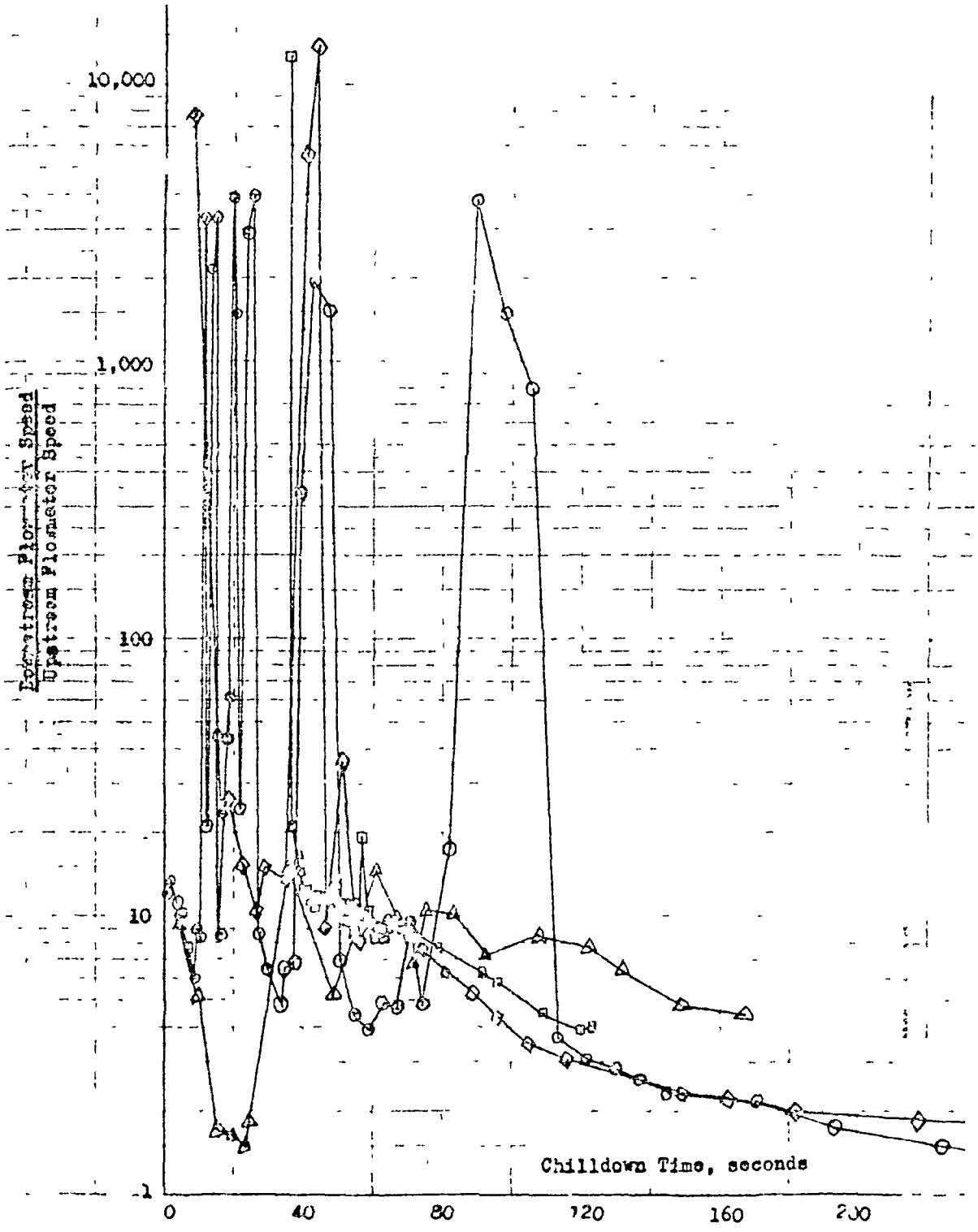
Downstream Flowmeter Speed
Upstream Flowmeter Speed
10,000
1,000
100
10
1
0
40
80
120
160
200
Chilldown Time, seconds

II-7545

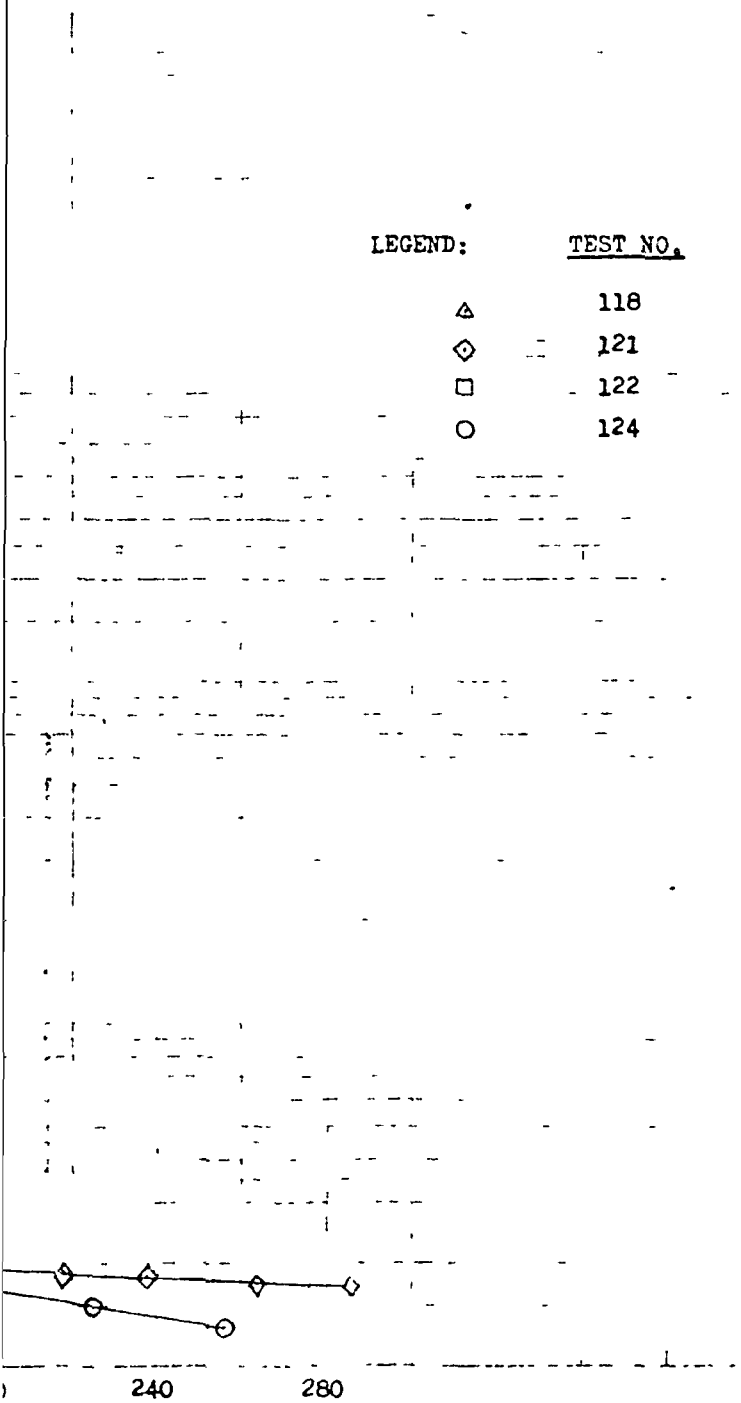

Figure 108. Ratio of Downstream Flowmeter Speed to Upstream Flowmeter Speed vs Chilldown Time for Mark 15 LE_2

density at the pump inlet to the density at the pump outlet was the same as the ratio of the pump discharge flowmeter to the feed line flowmeter Some heat was added to the H_2 between the pump outlet and the pump discharge flowmeter, but the exact amount could not be determined because the condition of H_2 was unknown at the inlet to the flowmeter. Therefore, the density at the flowmeter inlet is slightly lower than the density at the pump outlet. The two flowmeters had he same calibration factors Knowing the ratio of two flowmeters and the LH_2 density at the pump inlet, the density of two-phase H_2 was found This density and the measured outlet bulk temperature fixed the quality of the H_2. The enthalpy of the H_2 then was found by utilization of the following equation

$$H_{T.P.} = \text{Quality } (H_V) + (1 - \text{quality}) (H_L) \qquad (66)$$

The enthalpy rise across the pump is simply the difference between the outlet and inlet enthalpies, and the results are plotted in Fig. 103 for tests 118, 121, 122, and 124. The dotted line interpolates the data during the two-phase flow when determination of enthalpy was impossible. Figure 103 shows that the enthalpy increase is maximum during the very early part of the test, decreases with time, and finally approaches zero. During the first seconds of each test, the H_2 entering the pump was in the all-gaseous state and the flowrate was the smallest. The pump at th s time is at ambient temperature, therefore, there is a great difference between the wetted surface temperature of the pump and the bulk temperature of the H_2. Although the flowrate is lowest, the heat transfer coefficient is highest for the given flowrate at a bulk temperature between about 150 to about 500 (Ref. 17). Consequently, the high ΔT and high heat transfer coefficients result in a maximum enthalpy rise across the pump. As the chilldown time increases, the flowrate and the heat transfer coefficient increases. The difference between the wetted wall and the bulk temperature has decreased with time, and eventually the wetted surface temperature will be that of the bulk temperature. Actually, the thermal conductivity of the material, which drops rapidly with a decrease in the material temperature, becomes the controlling resistance to the flow of heat. The result is a lower enthalpy rise across the pump.

This process continues until no heat is left in the pump. The amount of heat rejected by the pump to the H_2 was determined easily from the following simple equation

$$Q = w \Delta H \tag{67}$$

Figure 109 shows a plot of Eq 67 vs time for various tests. Again, the dotted lines are used to interpolate the data in the region where the flowrate of H_2 was unknown. To determine the total amount of heat rejected by the pump to the H_2 in each run, the area under each curve of Fig. 109 was determined by using small time intervals. The results are plotted in Fig. 110. The total heat rejected by the pump for the four tests is not too far apart. Figure 110 also depicts a straight line with zero slope, which represents the total available heat within the control volume that could be rejected to the H_2. Figure 110 indicates that in all of the tests the rejected heat approached the limit line, and on the average about 64 percent of the total heat was removed by the H_2. The skin temperature thermocouples indicate that there is still some heat left in the pump casing, and that not all of the heat is removed from the thick rotor section. The total heat rejected was about 11,300, 11,800, 10,500, and 13,200 Btu for tests 118, 121, 122, and 124, respectively. The total available heat was approximately 18,500 Btu.

To determine the available heat content of the pump, its stand, and the inlet ducting, it was assumed that the temperature would drop from 530 to 40 R. Also, different parts of the pump made of the same material were lumped together, and integrated enthalpy difference was used in the computation of the pump heat content.

When the weight of the pump and its adjoining ducting was being determined, it was found that the weight of the inlet ducting and some non-flight weight of the pump was about as much as that of the pump itself.

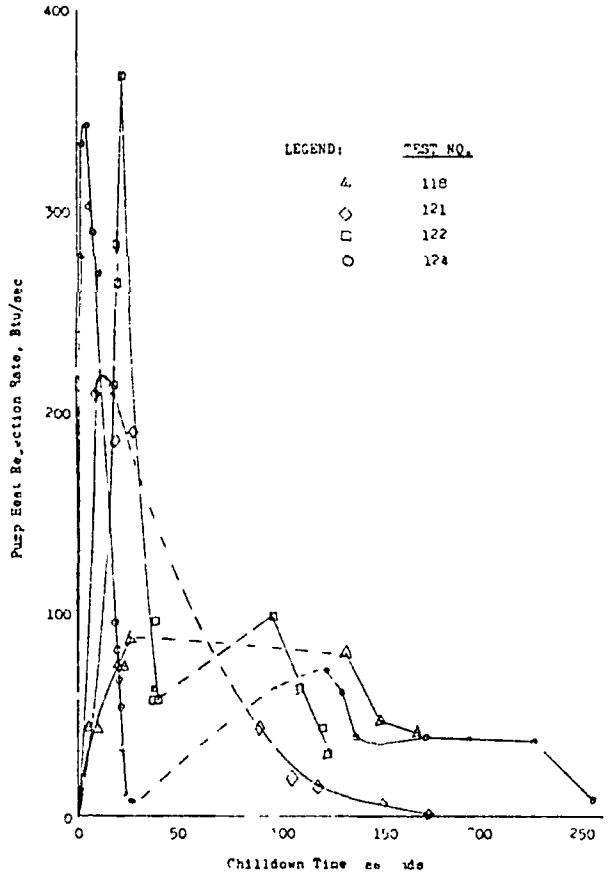

Figure 109 Pump Heat Rejection Rate vs Chilldown Time for Mark 15 LH_2 Pump

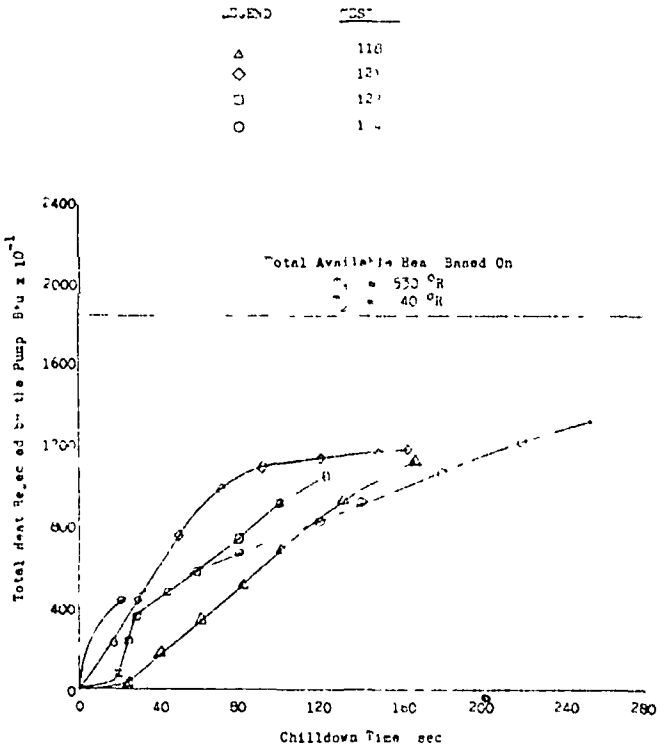

Figure 110. Total Heat Rejected by the Pump vs Chilldown Time for Mark 15 LH_2 Pump

(the pump weighed about 238 pounds, and inlet ducting, etc , weighed around 264 pounds). The inlet ducting was, of necessity, included in the computation because the inlet thermocouple was located about 4 feet upstream of the pump inlet flange (Fig. 10) Table 5 shows the weight of the individual material and its heat content for the pump and the inlet ducting.

Flowrate Limitations

The Mark 15 LH_2 pump stator and rotor present a fairly complex flow passage for the coolant H_2. The fluid, after entering the pump, must undergo a number of sharp-angle turns to flow between the stator and rotor blades. The fluid undergoes expansion and contraction between the blades. Therefore, the flow picture is not analogous to a simple pipe flow.

The analysis of the chilldown test data was continued by determining the number of velocity head losses through the pump. The pressure drop was assumed to be given by

$$\Delta P = K \frac{V^2 \bar{\rho}}{288\, g_c} \tag{68}$$

Rearranging Eq. 68, one can write

$$\frac{\dot{W}}{A} = \frac{96.2}{K^{0.5}} \sqrt{\Delta P \bar{\rho}} \tag{69}$$

The flow area of the inducer was substituted for A in Eq. 69. Since $\dot{W}$, A, ΔP, and $\bar{\rho}$ were known, a plot of pressure-drop parameter across the pump versus mass velocity was prepared and shown in Fig. 111 . The value of the head loss coefficient K for the best-fitted line through the data was about 32.5, whereas the predicted value of K (which is also shown in Fig. 111) was about 11.8. The difference between the two K values was probably caused by expansion and contraction of H_2 between the rotor and stator blades. Another reason for higher experimental K value was because of the irreversible work done on the liquid by the gas (Ref. 34) in a two-phase fluid passing through the pump during chilldown testing.

TABLE 5

WEIGHT AND HEAT CONTENT OF DIFFERENT PARTS OF MARK 15 LH_2 PUMP AND INLET DUCTING

Material	Weight, pounds	ΔH, Btu/lb	Heat Content Between 530 R and 40 R, Btu
Inlet Ducting			
A-286 CRES	36 2	35 0	1,268
321 CRES	162.7	37.5	6,100
Invar 36	65 4	35.0	2,285
Total	264 3		9,553
Mark 15 LH_2 Pump			
310 CRES	112.36	37.4	4,220
K-monel	101.00	37 5	3,790
INCO-713	7.88	37.5	296
A-286-CRES	2.67	35.0	93.5
440 CRES	1.56	37.5	58.5
Bearium	2.78	36.0	100.0
CRES Alloys	6.30	37 5	236.5
Nickel Alloys	4 09	38.0	155 2
Total	238.64		~8,950
Grand Total	~503.00		~18,503

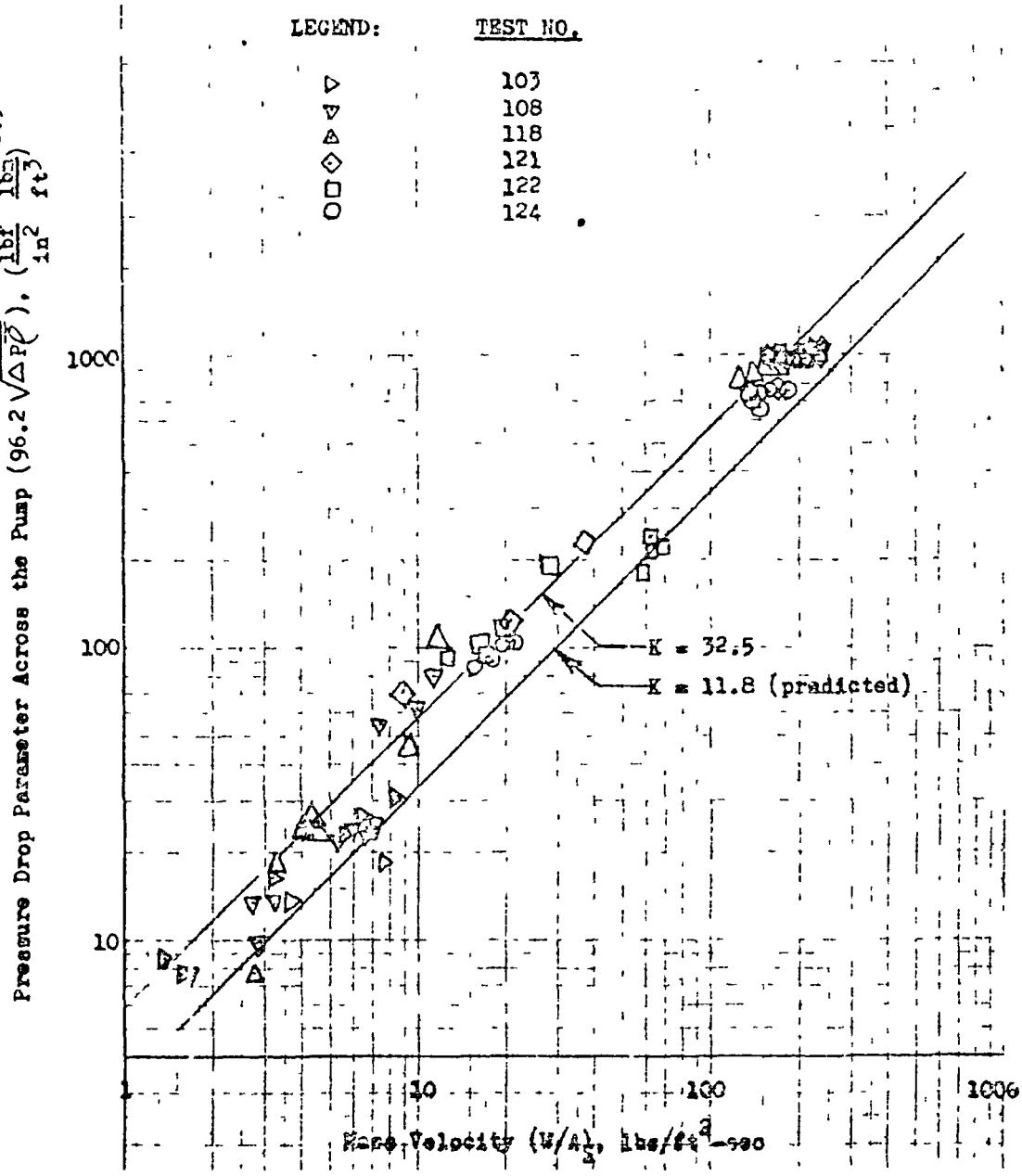

Figure 111. Pressure Drop Parameter Across the Pump vs Mass Velocity for Mark 15 LH_2 Pump

Gaseous Hydrogen Flow Limits

The maximum GH_2 that could be passed through the pump in the early part of the tests was investigated. The Mach numbers for all the tests were computed, and it was found that choking did not take place in any of the tests even though the pressure ratio (the ratio of exhaust pressure to supply pressure) was below the critical value. The maximum Mach number was about 0.882, occurring at a pressure ratio of about 0.461 during the early part (36 seconds from the start of the test) of test 122. To compare the maximum flow of H_2 under isentropic flow conditions and that of the actual condition, Eq. 4.16 of Ref. 20 was used to evaluate the mass flowrate for the isentropic flow.

$$\left(\dot{W}/A\right) = \sqrt{\frac{K}{R}} \frac{P_o}{\sqrt{T_o}} \frac{M}{\left(1 + \frac{K-1}{2} M^2\right)^{\frac{K+1}{2(K-1)}}} \qquad (70)$$

A constant K value equal to 1.4 was used for H_2 in Eq. 70. The result is plotted in Fig. 112 as H_2 flow parameter versus exhaust pressure to supply pressure. Also, the results of the experimental chilldown tests were superimposed on Fig. 112. Two curves were drawn through the data points, one curve for a K (K and 4f L/D are equal quantities) value of 11.8, as had been predicted, and one curve for a K value of 32.5, as was found experimentally from Fig. 111. For a friction factor equal to 0.003, the equivalent frictional L/D of the pump becomes about 2500. It is seen that the data are well encompassed by the two curves. Figure 112 shows that although at the choking condition for the isentropic flow the H_2 flow parameter is about 0.14, the same parameter is about 0.0352 under actual conditions (K = 32.5). Also, Fig. 112 shows that the pump will not choke until a pressure ratio of about 0.135 is reached. This pressure ratio is much less than the critical pressure ratio, however, the H_2 flow through the pump is accompanied by friction and other losses in addition to being heated. Figure 112 is quite similar to Fig. 69a of Ref. 20, which is for a fluid with a k value of 1.4.

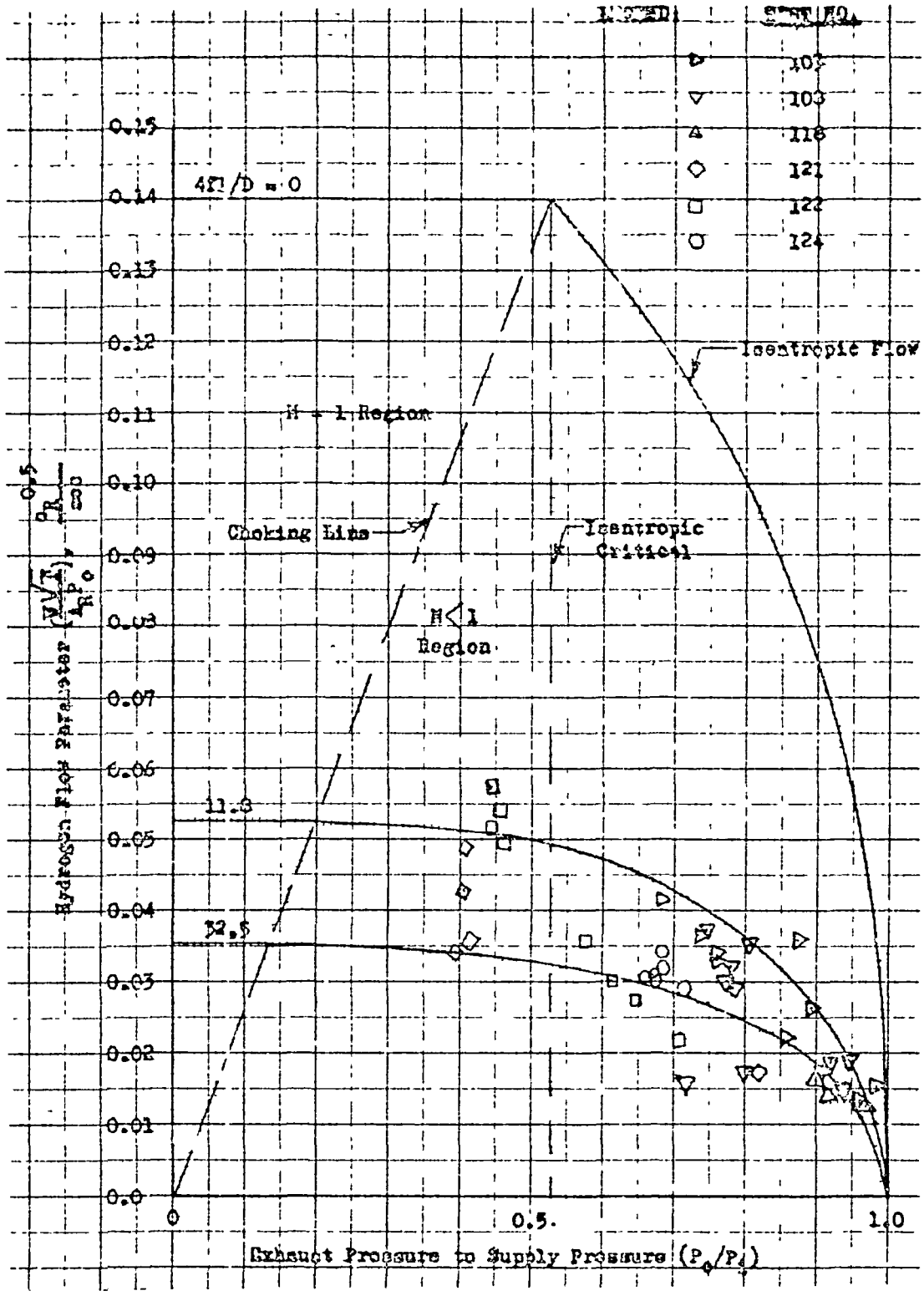

Figure 112. Hydrogen Mass Flow Parameter vs Exhaust Pressure to Supply Pressure for Mark 15 LH_2 Pump

Figure 112 is a useful tool in that one can determine the expected H_2 flow through the pump when the inlet and outlet conditions are known. Conversely, if one desires to know what pressure ratio is required to pass a certain predetermined H_2 flowrate, this figure can be used again to find the unknown pressure ratio.

The overall results of the Mark 15 H_2 pump chilldown tests were very encouraging, and the data in general correlated very well. For comparison purposes, a summary of the test conditions and results are presented in Table 6. The minimum chilldown time of the pump was fairly short (~ 36 seconds), and this time may be reduced further with proper cooling methods and ducting modifications. Unfortunately, no actual pump start test was performed to assess the short chilldown merits in conjunction with a rapid start. The H_2 bulk temperature at the pump outlet dropped to about -415 F within 36 seconds from the start of the test, and the wetted surface temperature was expected to be close to that of the bulk temperature. The wetted surface of the pump should be fairly well chilled (about -410 to -415 F) for a rapid pump start. High H_2 flowrates should be used for a short period of time, followed immediately by the pump start. In this manner, the pump wetted surfaces are cooled sufficiently without extracting too much heat from the body of the pump, and the result is a low total H_2 flow through the pump. Figure 113 shows the accumulated H_2 flow versus chilldown time for various skin temperatures, as measured by thermocouples 5 and 6 (Fig. 73). It is seen that the required amount of H_2 is less for a pump chilldown if high flowrates are used. It is possible that severe thermal stresses be set in the pump during a fast chill. Therefore, a compromise between slow and fast chill may be necessary. The allowable thermal stresses should be investigated by using the actual temperature distribution of various parts during a rapid chill.

TABLE 6

SUMMARY OF THE MARK 15 LH_2 CHILLDOWN TESTS

Test No	Time,* seconds	Run Tank Pressure, psia	Run Tank Temperature, F	Pump Inlet Pressure, psia	Pump Inlet Temperature, F	Pump Outlet Pressure, psia	Pump Outlet Temperature F	Flowrate lb/sec	ΔP across the Pump psi	Inducer slip Speed percent
103	169	18.9	-423 56	16 0	34 5	14 6	49 9	0 [illegible]	1 4	13 1
103	774	23 1	-423 50	23 1	-230.5	16 4	-361 9	0 370	6 7	25 9
103	1356**	23.2	-423 20	23 4	-420 6	15 4	-420 6	-	8 0	25 9
108	242	18 5	-423.60	16 9	41 1	15 8	47 6	0 0[illegible]	1 1	9 5
108	536	25.0	-422.10	24 2	-420 0	16 3	-335 7	0 [illegible]	6 9	35 6
108	1141**	24.1	-423 30	24 0	-420 4	15 0	-422.7	-	9 0	35 6
118	25	44 2	-422.70	43 5	-203 3	42 1	-37 7	0 132	1 4	7 4
118	83	55.6	-422 60	55 8	-413 9	27 1	-418 6	-	26 7	67 4
118	167**	65 1	-422 60	61 0	-413 1	26 1	-418 9	4 940	34 9	91 9
121	9	63 1	-423 60	61 6	-254 0	50 6	-81 0	0 275	11 1	18 8
121	96	74 7	-423.50	69 3	-412 7	39 2	-417 9	5 550	39.1	88 5
121	286**	74 7	-423 50	64 6	-416 5	27 7	-418 6	7 650	36 9	88 4
122	36	63 5	-422 9	61 2	-410 7	28 4	-407 0	1 920	32 8	100 0
122	61	74 8	-422 8	70 0	-411 4	26 4	-418 7	-	43 6	100 0
122	123**	74 9	-422 8	69 1	-412 7	29 4	-418 1	5 630	39 7	100 0
124	1	68 8	-423 4	67 1	-235 0	47 7	-56 0	0 490	19 4	26.2
124	71	68 5	-423 4	65 3	-412 1	41 5	-415 3	-	23 8	30 7
124	256**	68 9	-423 3	63 1	-414 9	43 8	-415 1	5 700	19 3	30 8

*Time from the start of the test
**End of test

NOTE Flowrate could not be calculated due to two-phase condition of the flow

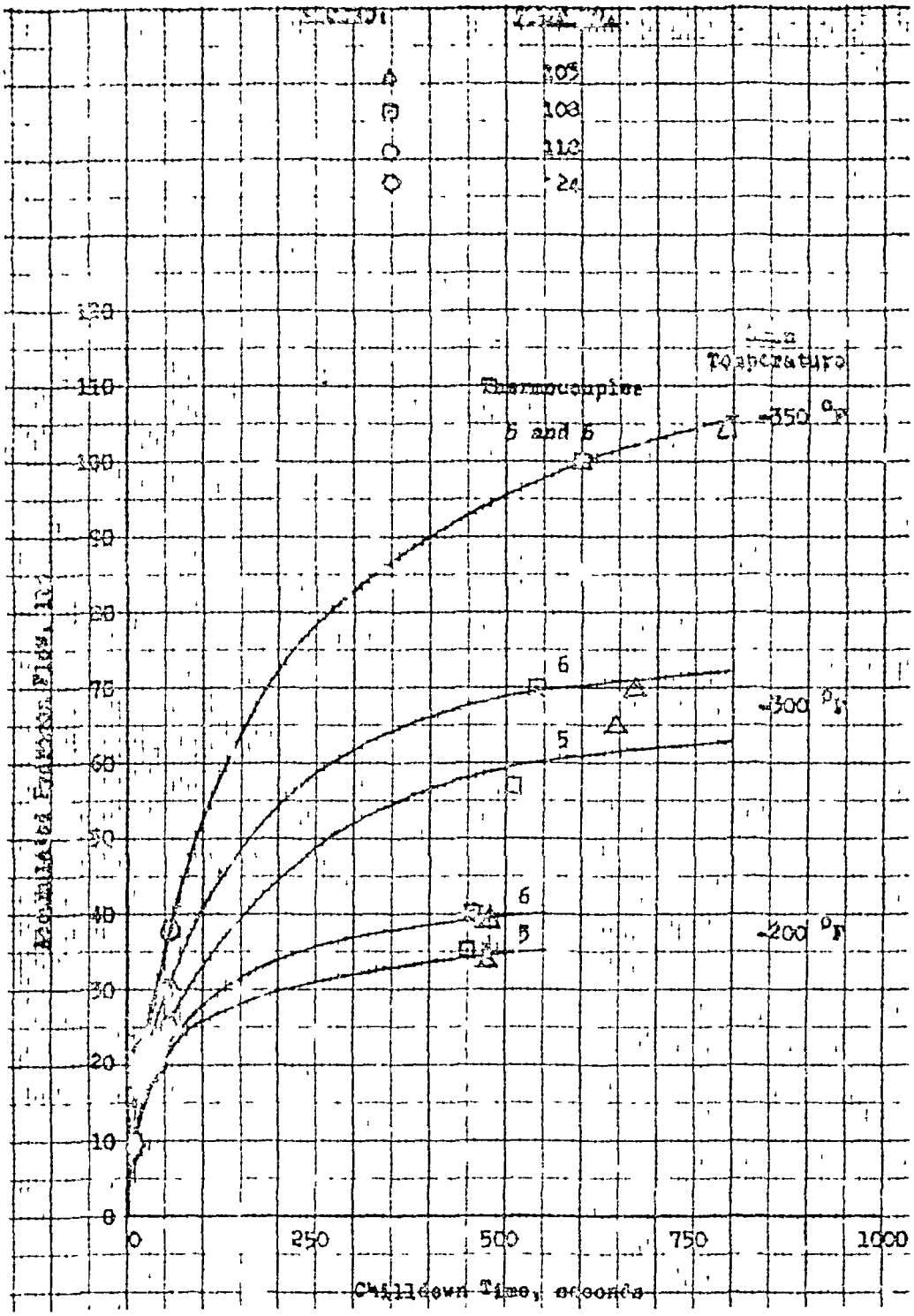

Figure 113. Accumulated Hydrogen Flow vs Chilldown Time for Mark 15 LH_2 Pump

J-2 ENGINE SYSTEM CHILLDOWN

To evaluate the chilldown characteristic of an engine system, other fuel system components upstream and downstream of the LH_2 pump must be analyzed together with the pump. The critical items in the fuel system include I/D of the lines, material properties, hydrogen flow conditions, and component masses. The J-2S engine system was transformed into a simplified chilldown model, and an analysis was conducted to determine the hydrogen heat transfer coefficient for large values of ΔT between the wall and coolant.

This analytical chilldown study used both the Mark 15 and Mark 29 LH_2 pumps and the results indicated that the warm engine system can be chilled down, especially the wetted pump surfaces within 45 seconds using about 35 to 40 pounds of hydrogen.

Integrated Engine System

A thermal system model involving the critical parameters of the fuel system was established to calculate the interaction between the hydrogen flow and the relatively warm fuel system components during the transient start operation. Figure 114 shows a schematic of the J-2S engine system, which was used as a reference system to establish a basis for optimizing engine chilldown characteristics. This system differs from the J-2 and the J-2X engine in that separate motor-driven pumps for prestart circulation chilldown are used. Table 7 shows its corresponding starting sequence. The engine system has been divided into seven sections (Table 8) from the hydrogen tank to the injector face. The material thermal properties (c_p, k, h) fluid properties, Reynolds number, flowrate, and temperature, all of which are time dependent, have been specified through the engine system.

Analytical Chilldown Study

To carry out the chilldown analysis of the J-2S engine system in an appropriate manner, a simplified model was prepared for the IBM 360 computer.

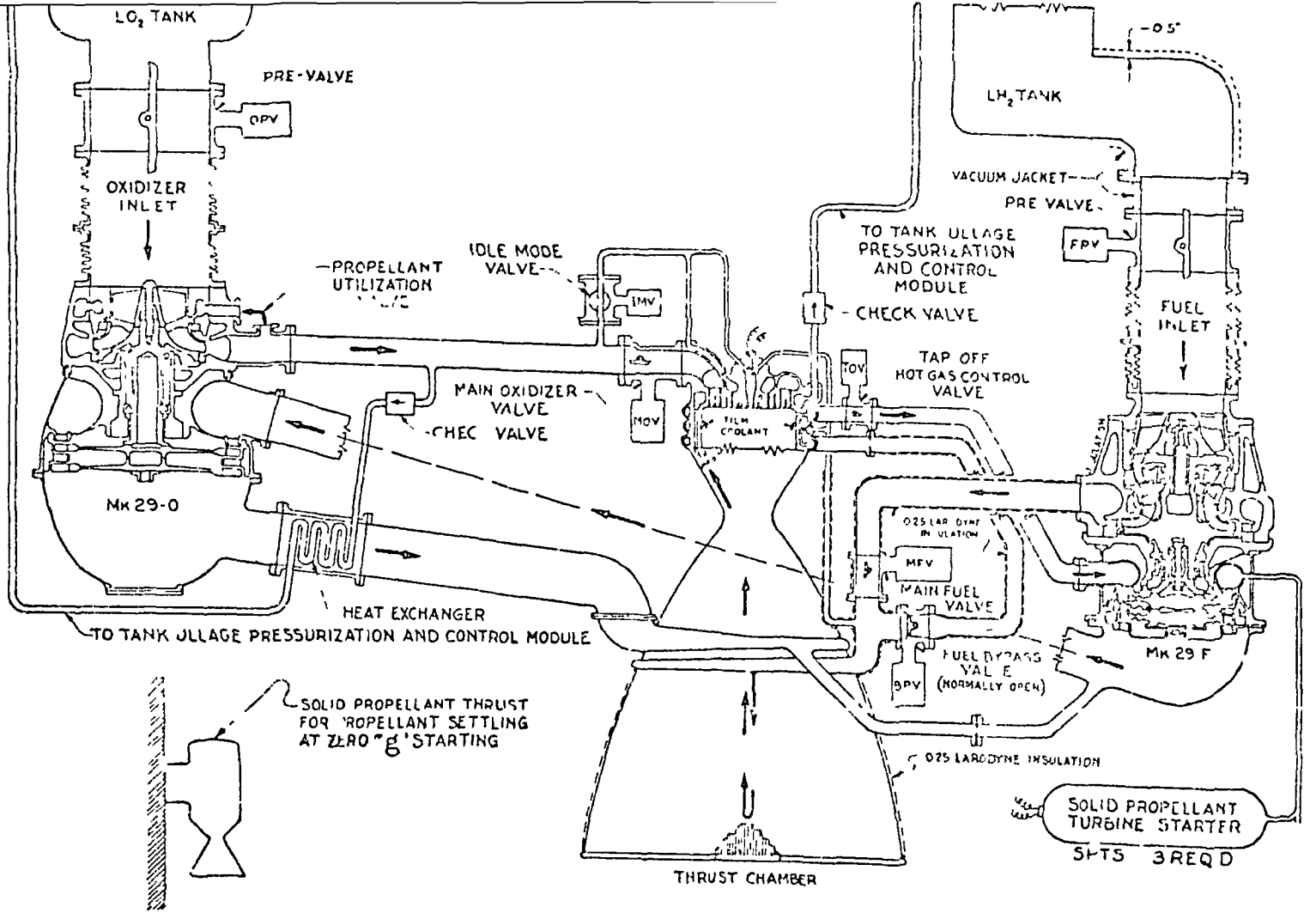

Figure 114. Schematic of J-2S Engine Feedline and Component Installation

TABLE 7

J-2S ENGINE START SEQUENCE

	Prestart and Shutoff	Pump Chill	Idle Mode	Mainstage Ignition
Spark Ignition (SI)	Off	Off	On	Off
Solid Propellant Turbine Starter (SPTS)	Off	Off	Off	On
Fuel Prevalve (FPV)	Closed	Open	Open	Open
Oxidizer Prevalve (OPV)	Closed	Open	Open	Open
Fuel Bypass Valve (BPV)	Open	Open	Open	Closed
Main Fuel Valve (MFV)	Closed	Closed	Open	Open
Main Oxidizer Valve (MOV)	Closed	Closed	Open	Open
Idle-Mode Valve (IMV)	Closed	Closed	Open	Open
Tapoff Hot-Gas Control Valve (TCV)	Closed	Closed	Closed	Open

NOTE. Thrust Chamber Injector is divided into two sections, a central section and a mainstage section.

TABLE 8

ZONE BREAKDOWN FOR CHILLDOWN ANALYSIS OF TOTAL J-2S ENGINE SYSTEM (FIG 115)

Zone	System Section
A	Hydrogen tank to pump inducer inlet
B	Pump inlet to pump discharge (for prediction of hydrogen flow and pressure drop through pump)
C	Pump and turbine (for chilldown analyses)
D	Pump discharge flange to thrust chamber inlet manifold flange
E	Thrust chamber fuel inlet manifold to injector fuel inlet manifold
F	Injector fuel inlet manifold to injector fuel discharge face
G	Bypass valve inlet to injector fuel inlet manifold

This model (Fig. 115), which is for the J-2 system, includes the Mark 15 LH_2 pump in the system rather than Mark 29 LH_2 pump and no bypass line.

Each component was isolated and treated individually. The thick parts (e.g., pump casing, rotor, etc.) were broken down in smaller nodes for better accuracy. Other parts, such as ductings where walls were not too thick, were lumped into one node to reduce the computer machine time. Extensive physical property tables (thermal conductivity and specific heat as a function of temperature) for the materials and the coolant hydrogen were used throughout these analyses. It was assumed that the hydrogen in the fuel tank was at -423 F and 32 psia. The rest of the system was assumed to be at 70 F. Node 1 of the simplified J-2 engine system breakdown (Fig. 116) represents the LH_2 tank condition and remains constant with chilldown time. All other node temperatures were made time dependent. The LH_2 temperature and pressure varies with time and position in the system.

The computation of the heat transfer coefficient for all parts of the J-2 system, except the injector posts, was based on the experimental tube cooldown data (from the Research Division). The heat transfer coefficient was determined through the use of the following equation:

$$h = 0.001\, G^{0.5} \tag{71}$$

To avoid excessive usage of the computer time, phase change or two-phase flow pressure-drop were not considered in these analyses. The heat transfer coefficient for the injector posts was determined by the use of Eq. 10-11(a) of Ref. 35. The pressure drop was determined with the aid of the following equation:

$$\Delta P = K \frac{W^{2.0}}{\rho} \tag{72}$$

Experimental values of K were used for the pump, thrust chamber manifold, thrust chamber tubes, and the injector. For the pump inlet and outlet

Note: Zone C = Turbopump = Pump and Turbine

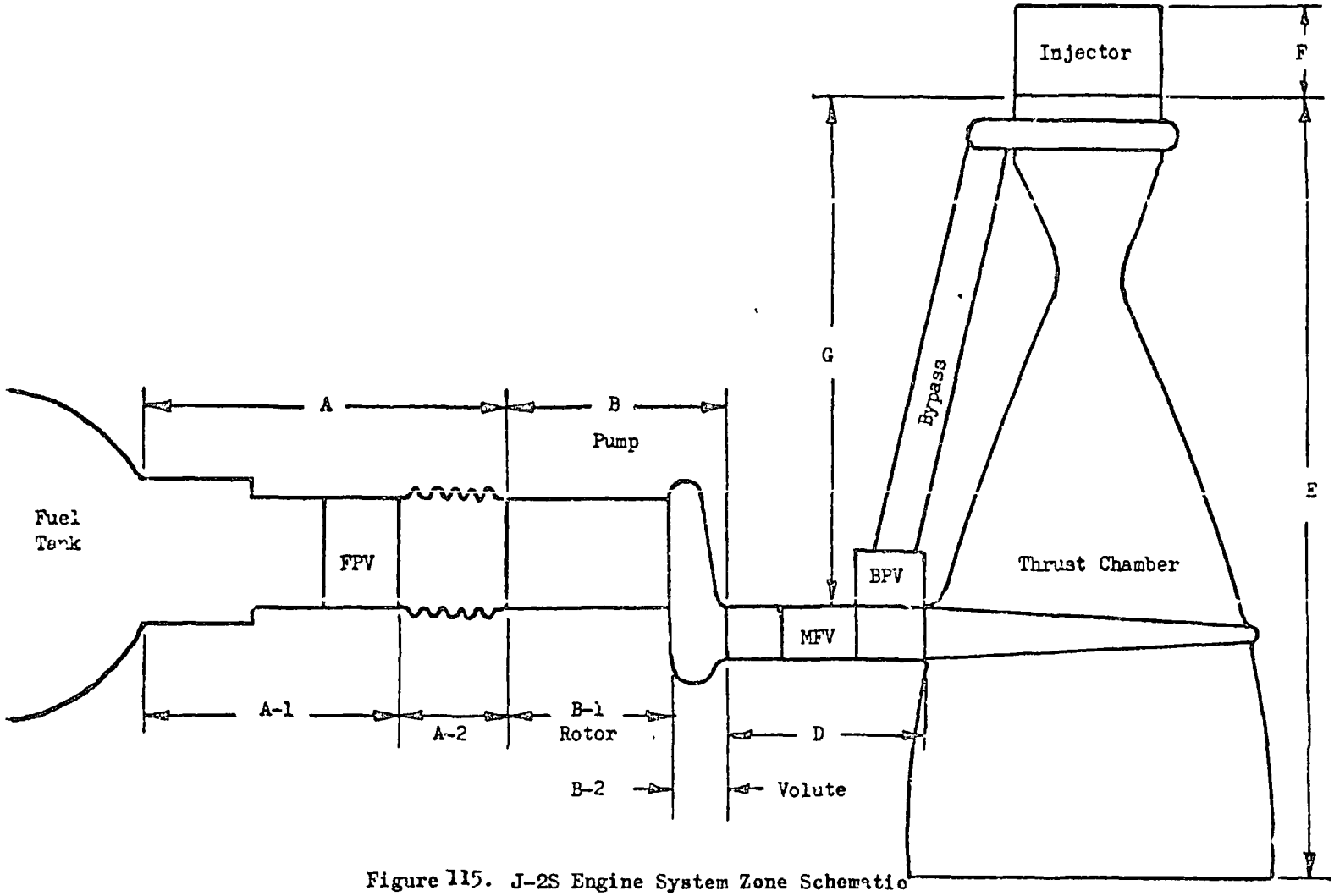

Figure 115. J-2S Engine System Zone Schematic

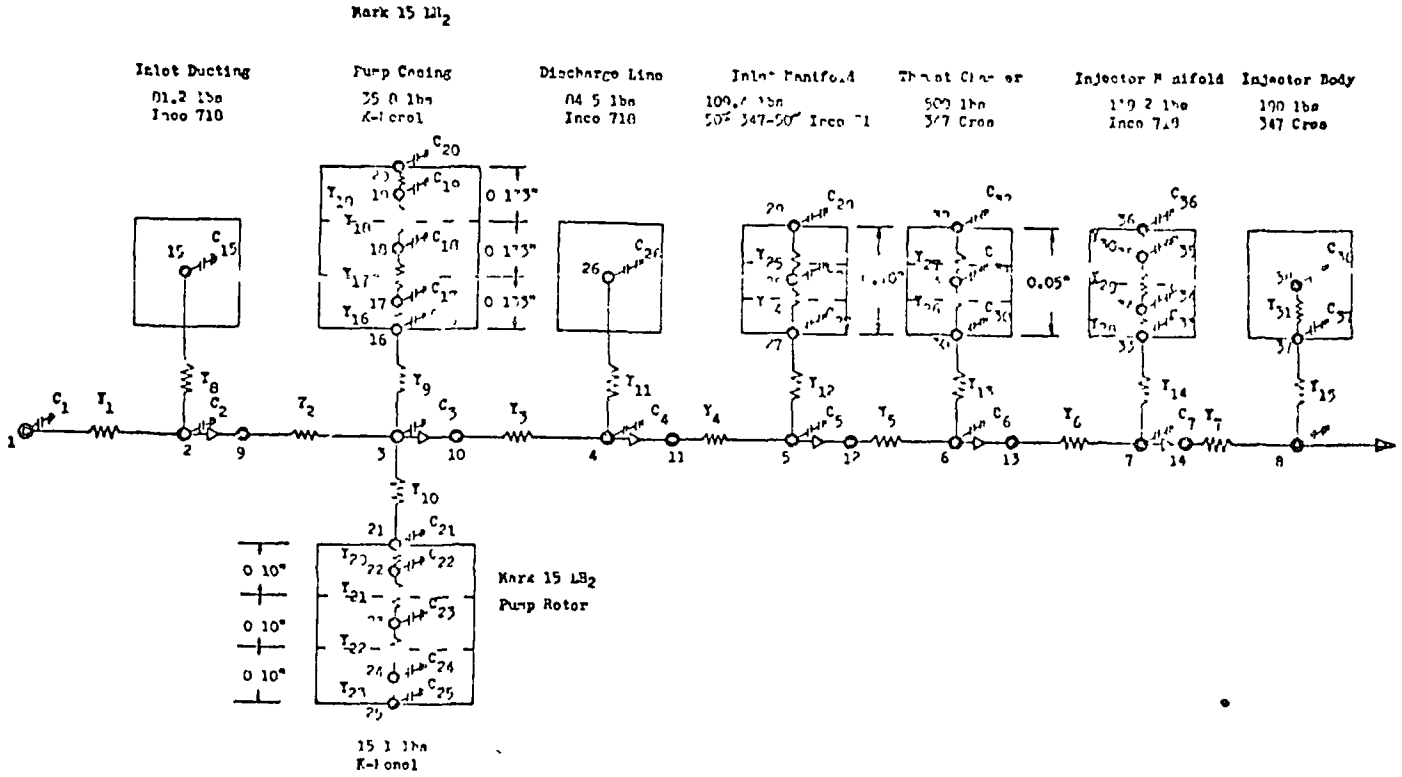

Figure 116. Simplified J-2 Engine System Component Breakdown for Chilldown Study

duct, a friction factor of 0.003 was assumed and used in the following equation:

$$\Delta P = 4f \frac{L}{D} \frac{V^2 \rho}{(2g_c)(144)} \qquad (73)$$

Through application of appropriate L/D, cross-sectional flow area, and f equal to 0.00?, Eq. 73 was transformed into Eq. 72. Only frictional pressure drops were considered here and the momentum pressure drops were assumed to be about 20 percent of total frictional pressure drop.

The chilldown analysis was an iterative process and hydrogen flowrate as a function of time was assumed and used. The calculated total pressure drop in the system was checked against the available pressure drop between the fuel tank and the thrust chamber. If the pressure drop did not agree, a new hydrogen flowrate as a function of time was assumed and the chilldown analysis was resumed. The process was continued until a satisfactory pressure drop agreement was obtained.

Engine System Analysis (Mark 15 LH_2 Pump). At first, the Mark 15 LH_2 pump was assumed to be in the engine system and a 1-minute chilldown analysis was carried out. The two final assumed hydrogen flowrates as a function of chilldown time are shown on Fig. 117. The last two iterations are shown on these figures to indicate the variation of pressure drop in the system with flowrate. The calculated total system pressure drop for the flowrates of Fig. 117 is shown on Fig. 118, where it is seen that the pressure drop is between 20 to 30 psia during the 1-minute chilldown time period. The available pressure drop was about 32 psi. Therefore, when the momentum pressure losses were added to the calculated pressure drop, the system predicted and the available pressure drops were nearly the same. Consequently, no further refinement of the assumed flowrate was made.

Figure 119 depicts the temperature of the hydrogen at various locations (Fig. 116) in the system as a function of the chilldown time. The temperature of the wetted surfaces of the system is shown in Fig. 120.

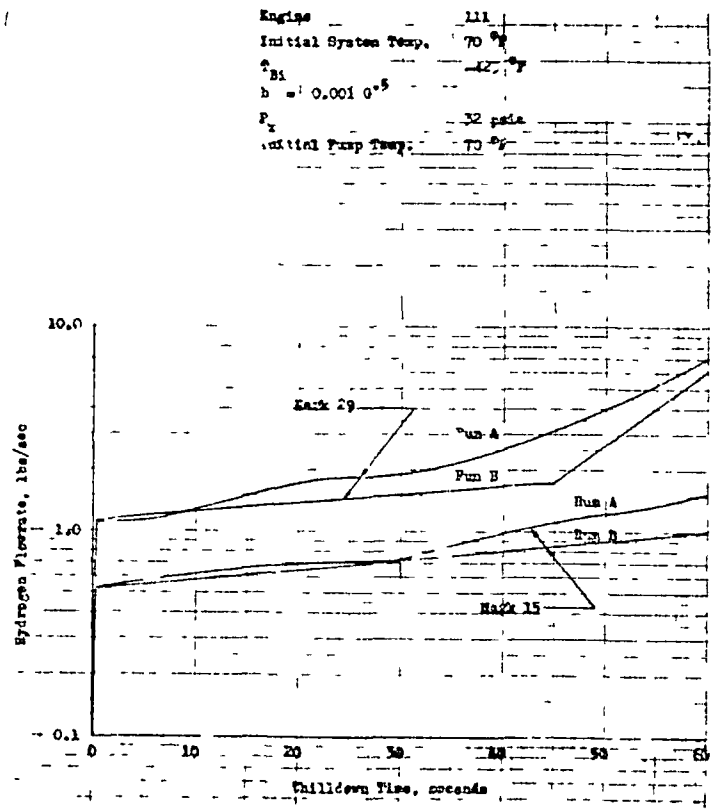

Figure 117. Hydrogen Flowrate vs Chilldown Time for the J-2 and J-2S Engine System

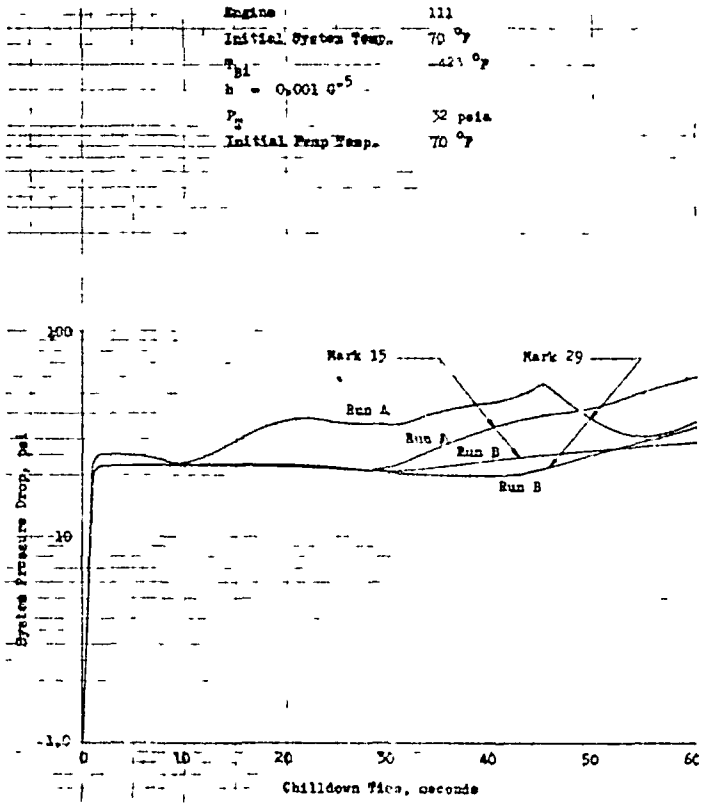

Figure 118. System Pressure Drop vs Chilldown Time for the J-2 and J-2S Engine System

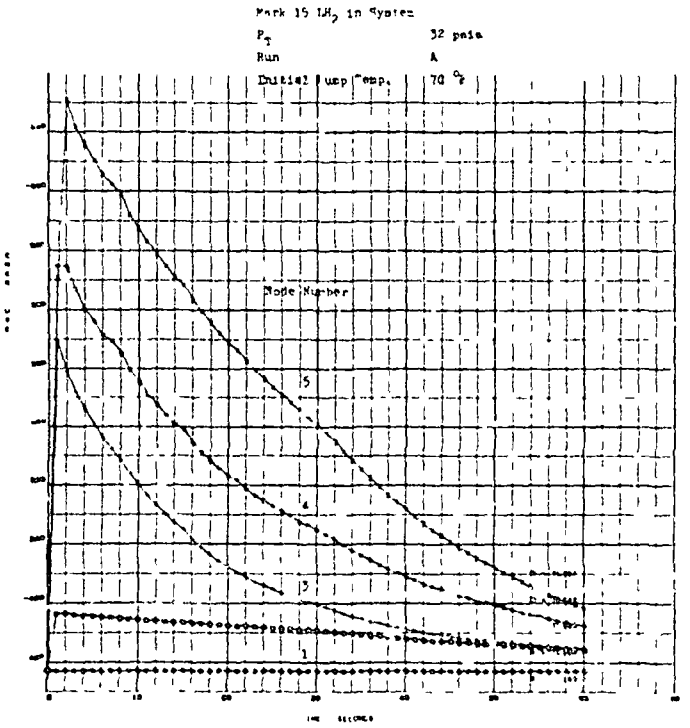

Figure 119 Hydrogen Bulk Temperature vs Time for the J-2 Engine System

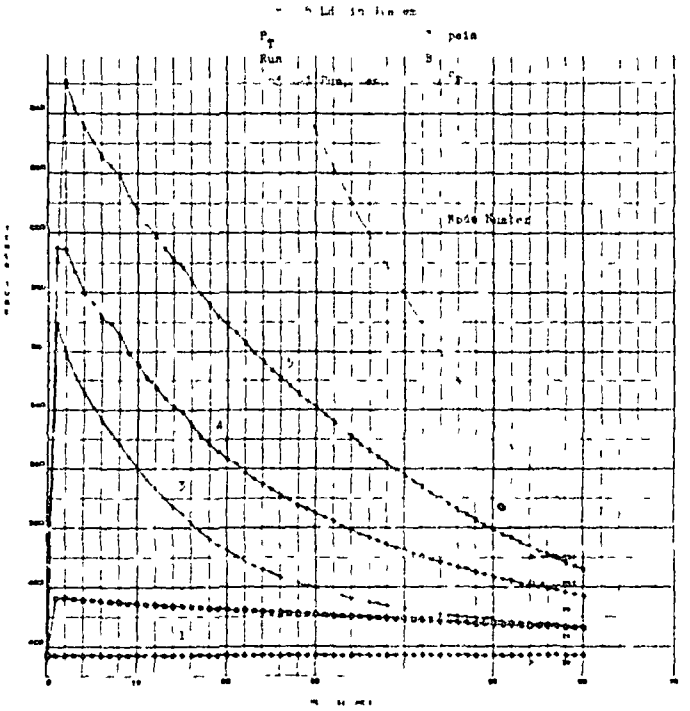

Figure 120. Hydrogen Bulk Temperature vs Chilldown Time for the J-2 Engine System

Figure 119 shows the hydrogen bulk temperature in the inlet duct, pump, outlet duct, inlet manifold, and the thrust chamber tubes. At first, the bulk temperature increases very rapidly and then decreases with time as the system components temperatures drop. At the end of 60 seconds of chilldown, the bulk temperature of the hydrogen leaving the thrust chamber tubes is about -378 F. It is interesting to observe the hydrogen bulk temperature at the pump exit which is about -311 F (after 1 second of chilldown) drops to about -413 F (after 60 seconds of chilldown)

Engine System Analysis (Mark 29 LH_2 Pump) The appropriate physical dimensions and properties pertaining to Mark 29 LH_2 pump were assigned to the nodes shown in Fig. 116 for the pump casing, rotor, and volute. The aluminum volute was handled separately. Various hydrogen flowrates were assumed and the chilldown analysis was continued until the system pressure drop was in good agreement with the available pressure drop. The last two assumed hydrogen flowrates (shown on Fig. 117) are higher than those of Mark 15 case. This is because the pressure drop in the Mark 29 is much less than the pressure drop in the Mark 15. Figure 118 also depicts the pressure drop in the system with Mark 29 pump. It is seen that a slight variation in the hydrogen flowrate affects the system pressure drop. The hydrogen bulk temperature for the two flowrates given in Fig. 117 are shown on Fig. 119 and 120 for the Mark 15 pump and Fig. 121 and 122 for Mark 29 pump. The bulk temperatures are slightly higher for the lower and final hydrogen flowrates. Figures 123 and 124 show the wetted surface temperature of the system with Mark 15 as the fuel pump. Very little difference can be noticed between the two figures as far as the pump casing and rotor are concerned. However, slight surface temperature increase is noticed elsewhere in the system (Nodes 26, 27, 30, and 37) for the lower hydrogen flowrate. It is noticed that the surface temperature of the rotor (Node 16) and casing (Node 21) dropped very sharply from 70 F to about -410 and -412 F, respectively. This indicates that in about 60 seconds of chilldown, the wetted surface temperature of the Mark 15 H_2 pump is nearly the same as the coolant bulk temperature. The total LH_2 used during the 60 seconds of chilldown time was about 45 pounds. This is in good agreement with the results of the Mark 15 LH_2 pump chilldown test data.

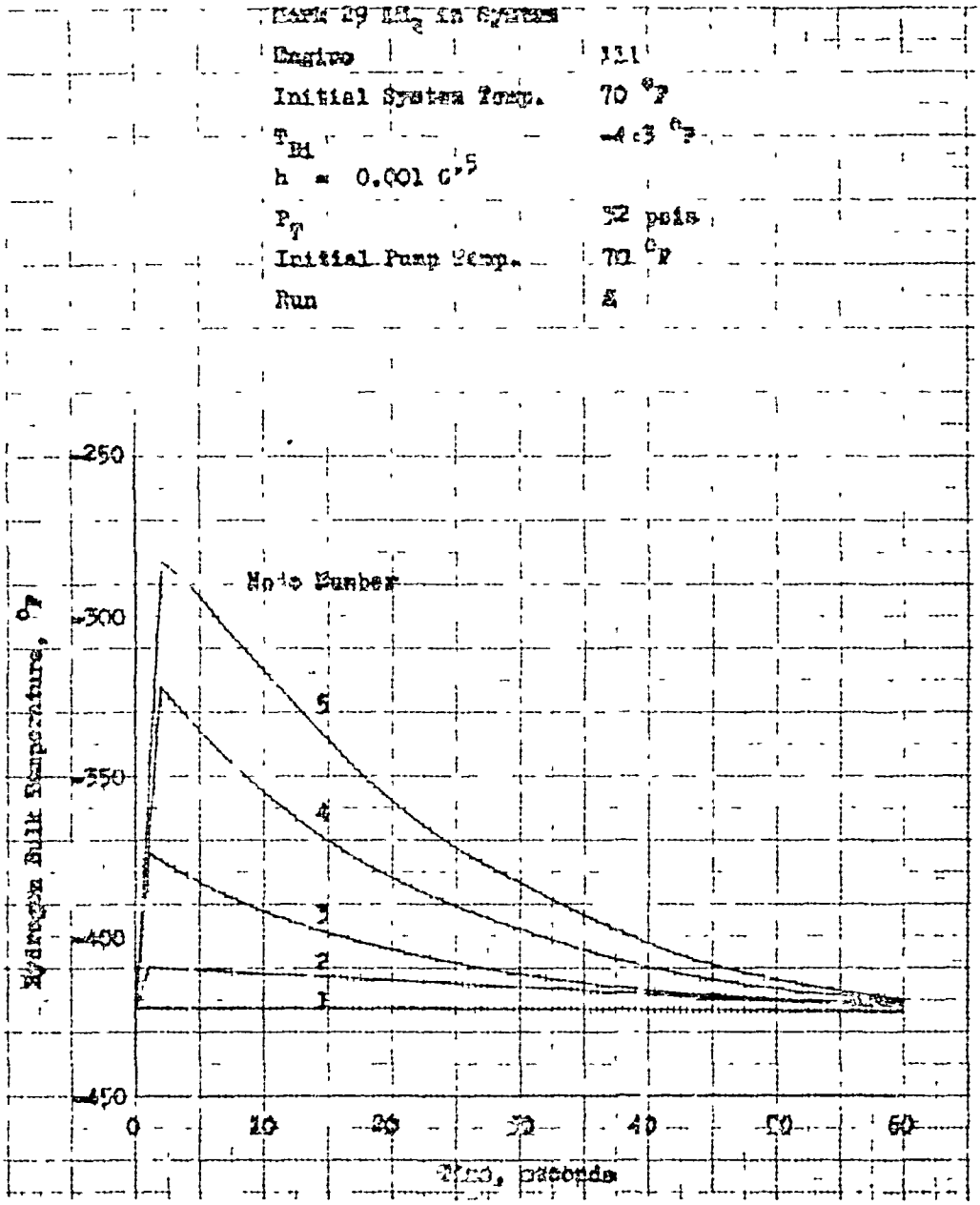

Figure 121. Hydrogen Bulk Temperature vs Time for the J-2S Engine System

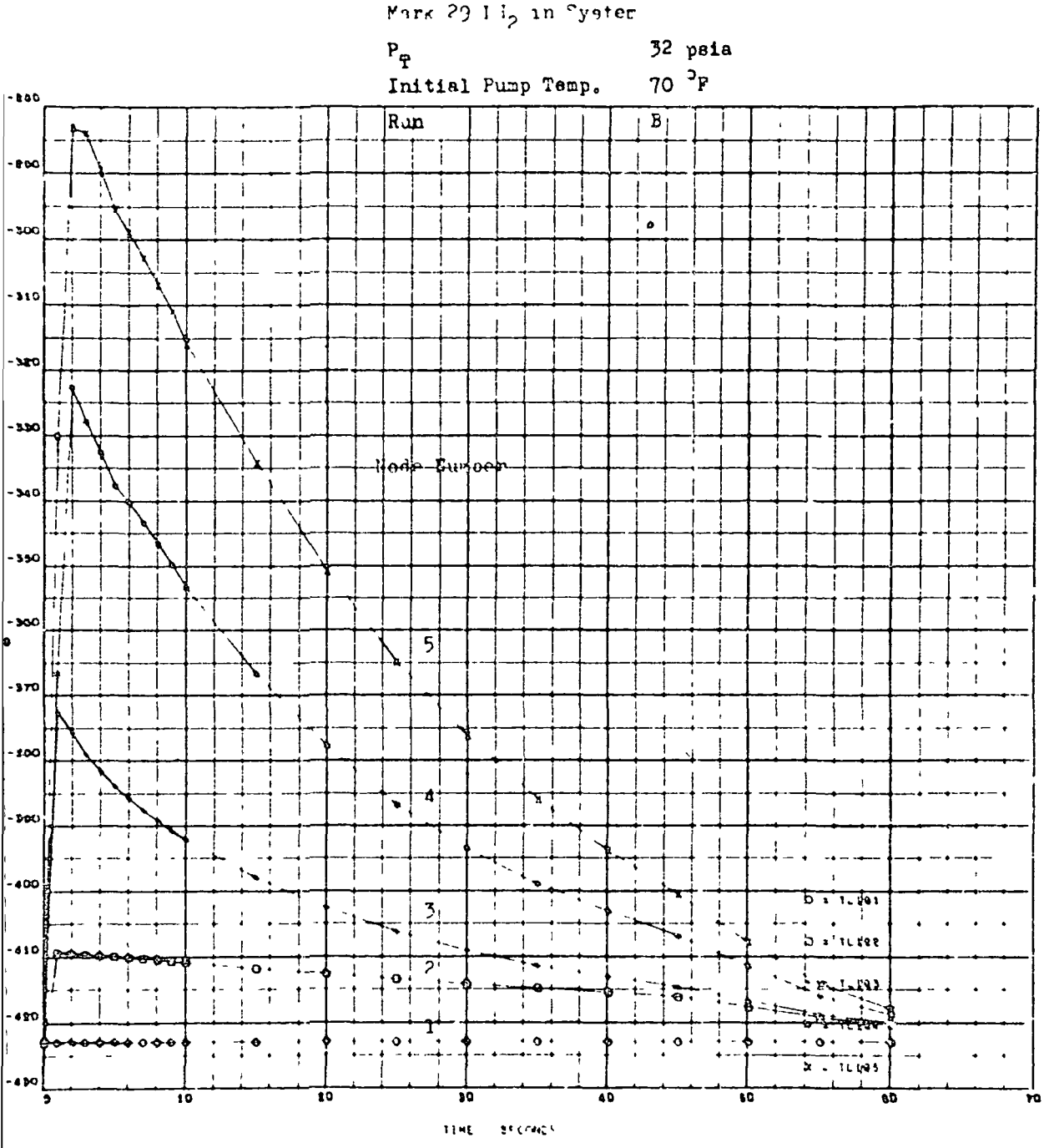

Figure 122. Hydrogen Bulk Temperature vs Time for the J-2S Engine System

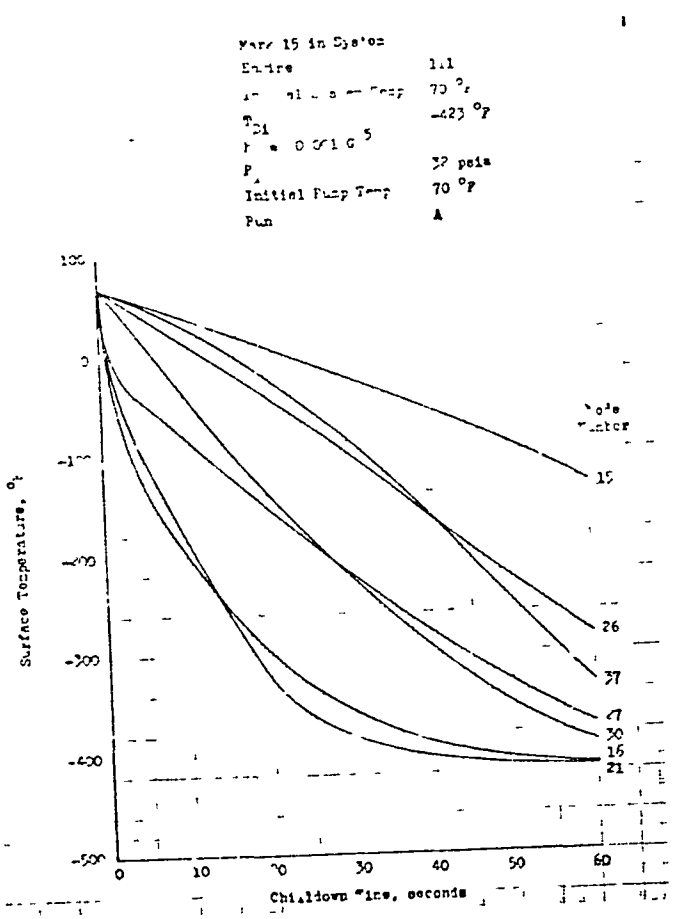

Figure 123. Surface Temperature vs Chilldown Time for the J-2 System

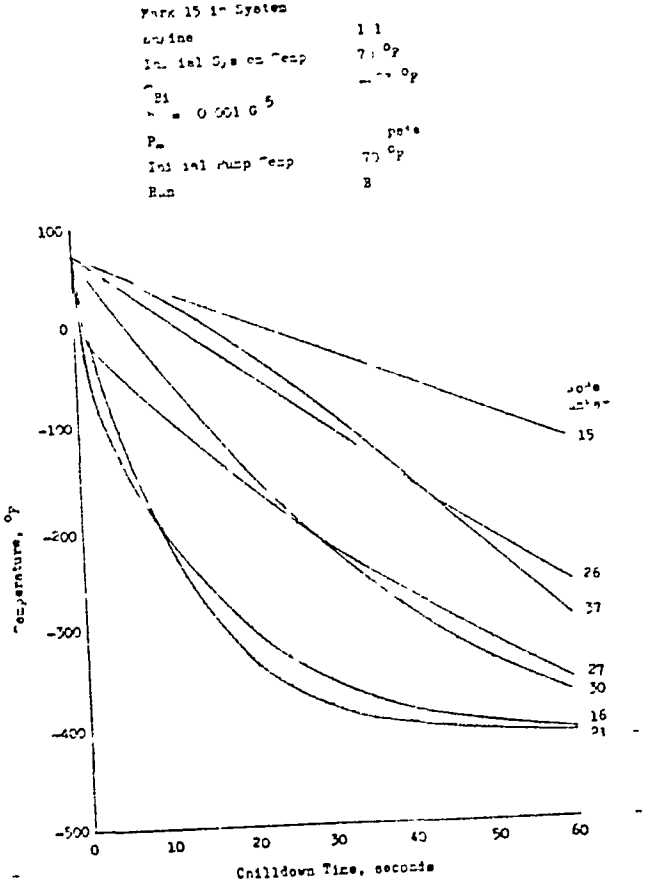

Figure 124. Temperature vs Chilldown Time for the J-2 Engine System

Figure 125 is a plot of the wetted surface temperature versus chilldown time for various components of the J-2S system with Mark 29 but no bypass line. It is seen again that the Mark 29 impeller and casing surface temperatures dropped sharply in about 40 seconds and are about -400 and -390 F, respectively. The H_2 bulk temperature in the pump (Node 3) was about -414 F and upon comparison of Fig. 124 and 125, one will learn that there was very little difference between the two although the H_2 flowrate was much higher in the case of Mark 29 (Fig. 125). However, the flowrate alone was not the determining factor in the chilldown rate of the two pumps and other paremeters should be considered. For example, aside from physical properties differences between the two pumps, one major influencing factor in chilldown rate is the weight to wetted surface ratio. When these two parameters are compared, it was observed that the weight-to-surface ratio of the Mark 29 is higher (9 lb/ft^2 for the rotor and 0.4 for the casing) than that of Mark 15 (2.1 lb/ft^2 for the rotor and 6.31 for the casing). Therefore, the excess LH_2 flowrate in the case of Mark 29 is offset by the higher mass to surface area ratio of the pump. This clearly points out that for a fast chilldown, a very low mass to wetted surface ratio is mandatory. The reason for the hydrogen bulk temperature in the Mark 29 (Node 3) being lower (-414 F) than the H_2 bulk temperature in Mark 15 (40 F) is, of course, because of the higher H_2 flowrate in the case of Mark 29. It then becomes obvious that a high H_2 flowrate is desirable for a fast chilldown and attainment of LH_2 in the pump inlet in a short time.

Figure 126 shows the breakdown of the J-2S engine system, which includes the bypass line. It was assumed that the initial temperature was about 70 F and that the initial bulk temperature of the H_2 was -423 F. Chilldown analysis was run for this case using the same H_2 flowrate as the previous case without the bypass line (Fig. 117). The results of the LH_2 bulk temperature changes are plotted versus chilldown time (Fig. 127). This figure shows that the H_2 bulk temperature in the pump (Node 3) drops to about -410 F in approximately 30 seconds. The bulk temperature in the

Mark 23 in water (no bypass ine)	
Engine	111
Initial System Temp.	70 °F
T_{Bi}	-423 °F
$h = 0.001\ G^{0.5}$	
P_T	32 psia
Initial Pump Temp.	70 °F
Run	8

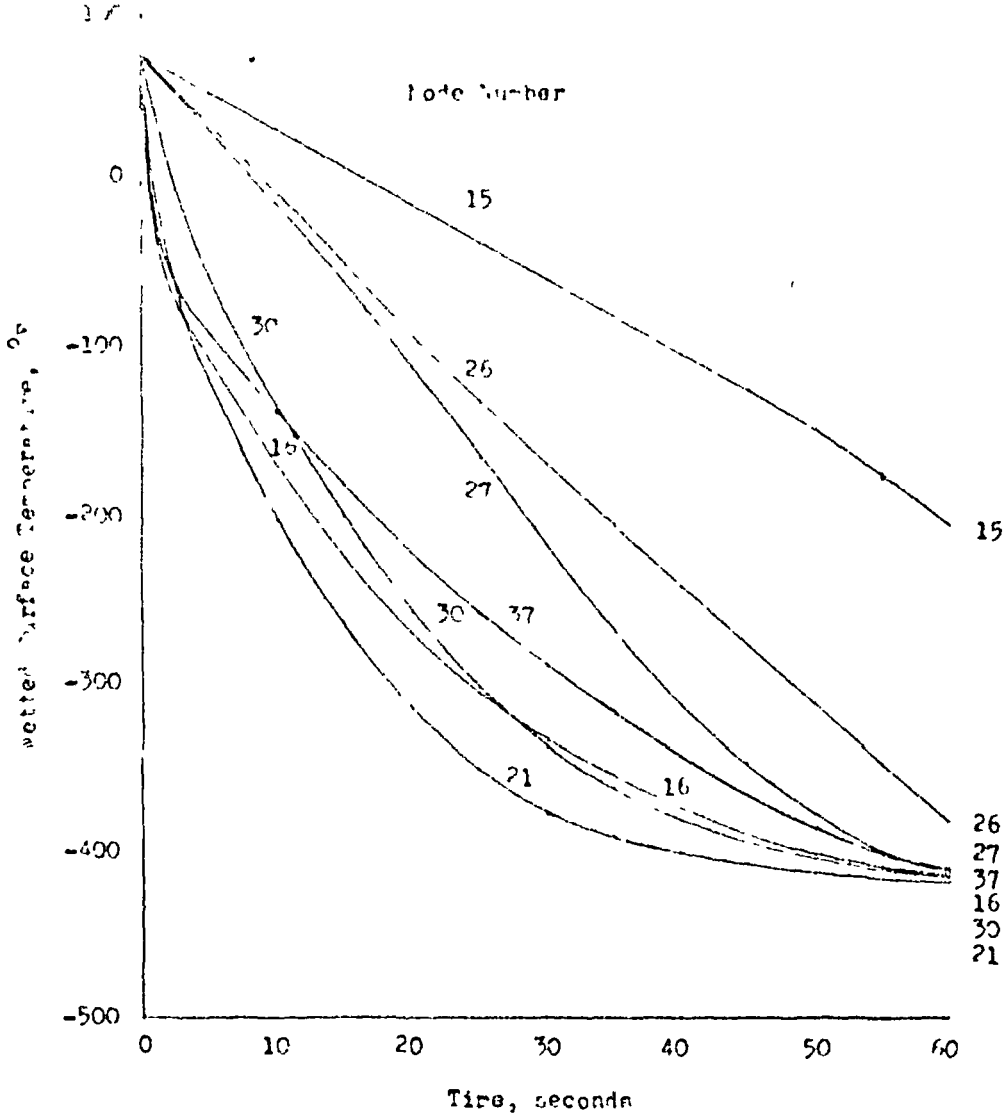

Figure 125. Wetted Surface Temperature vs Time for the J-2S Engine System

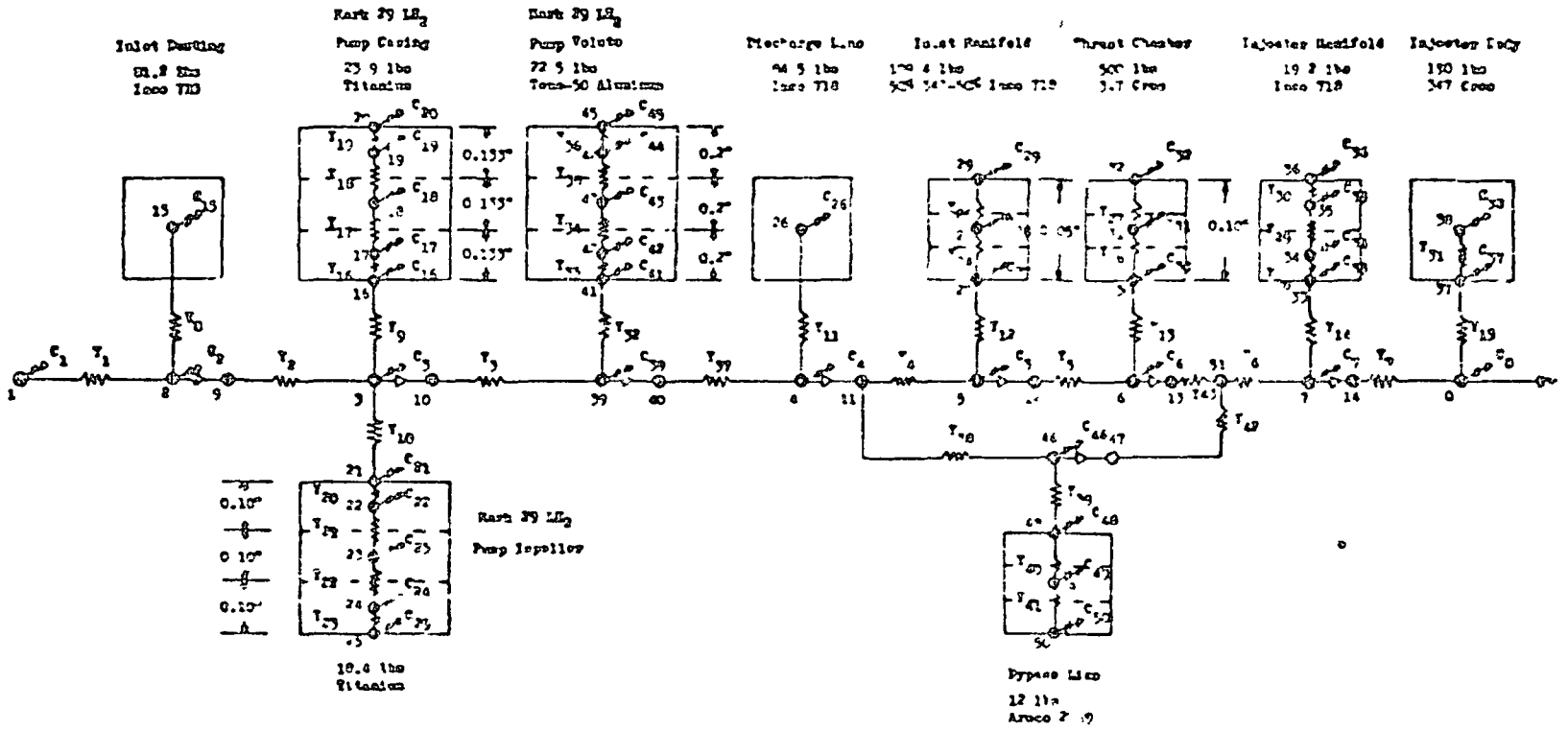

Figure 126 Simplified J-2S Engine System Component Breakdown for Chilldown Study

Mark 29 in System	
Engine	111
Initial Water Temp.	[illegible] °F
T_{sat}	[illegible] °F
$h = 0.001 G^{0.5}$	
P_T	32 psia
Initial Pump Temp.	70 °F

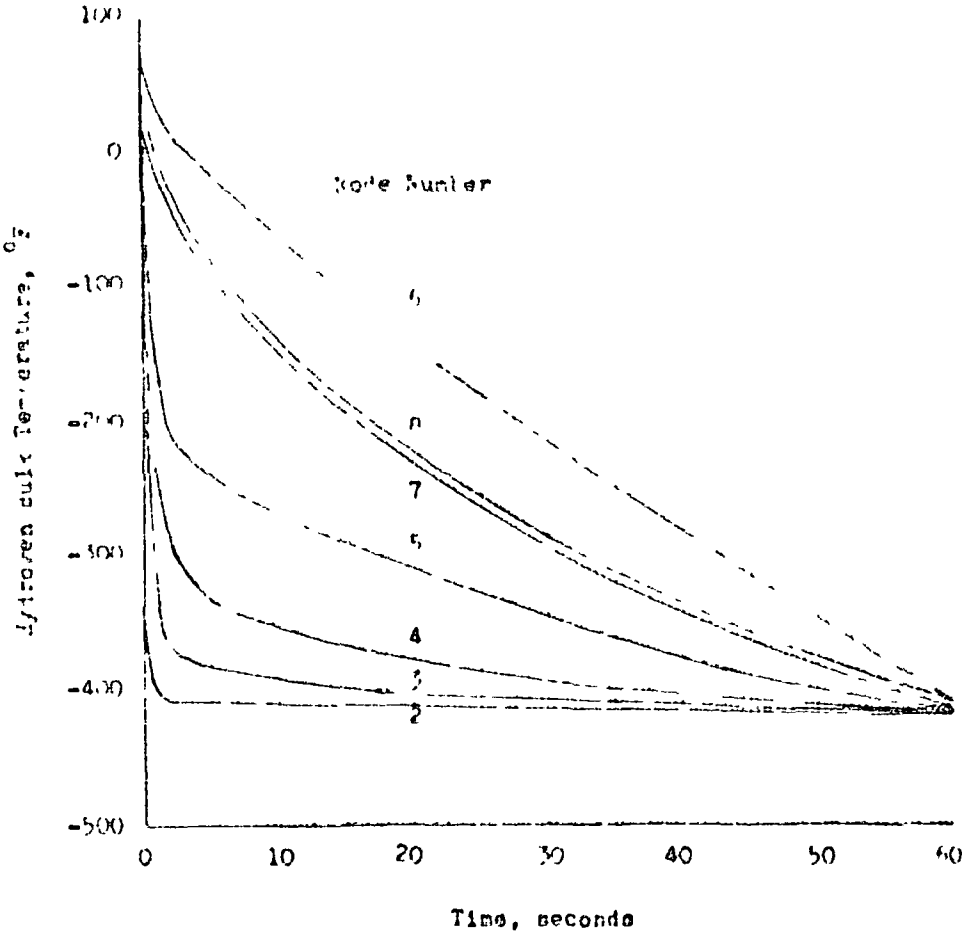

Figure 127 Hydrogen Bulk Temperature vs Time for the J-2S Engine System

reaches -240 F in about 45 seconds. However, it is seen that the H_2 bulk temperature in the injector manifold and in the injector is rapidly decreasing. The H_2 bulk temperature in the thrust chamber tubes (Node 6) is higher than the H_2 bulk temperature in the injector manifold (Node 7). The reason is that most of H_2 (about 65 percent by weight) is flowing through the bypass line and is mixed in the injector manifold with the H_2 flowing through the tubes of the thrust chamber.

Figure 128 shows the temperature of the wetted surfaces for various components in the J-2S system. No difference exists between the surface temperatures of the pump when Fig. 125 and 128 are compared. This is because the H_2 flowrate in this area is the same for both cases and the changes only take place downstream of the inlet to the bypass line. For example, temperature of Nodes 2, and 30 (surface temperatures of the inlet manifold and thrust chamber tube) are quite different between 10 and 30 second of chilldown time. These temperatures are lower for the case of no bypass because in this case all of the H_2 flows through the tubes.

Figure 129 shows the total H_2 flow through Mark 29 H_2 pump versus chilldown time. This total hydrogen flow was obtained by integrating the area under curve of Fig. 117(test B for Mark 29). Figure 130 depicts the H_2 enthalpy rise across the pump and the heat rejection rate of the pump versus time. It is seen that the maximum enthalpy rise and heat rejection rate take place a very short time (about 1 second) after the start of the chilldown. During this period, the temperature difference between the wetted wall and the H_2 bulk is maximum.

Figure 131 shows the total heat rejection by the Mark 29 H_2 pump versus time during the 60-second analytical chilldown study. The total heat rejected by the pump is about 2440 Btu. However, in this analysis, the entire pump was not considered. Only up to a certain depth from the wetted surfaces was analyzed as is shown on Fig. 126. The weight of the pump under consideration (Fig. 126) was about 64.8 pounds whereas the total weight of Mark 29 H_2 pump is about 297.7 pounds. It is seen that the

Engine	111
Initial System Temp.	70°F
T_{Bi}	-423 °F
$h = 0.001\ C^{.5}$	
P_T	32 psia
Initial Pump Temp.	70 °F

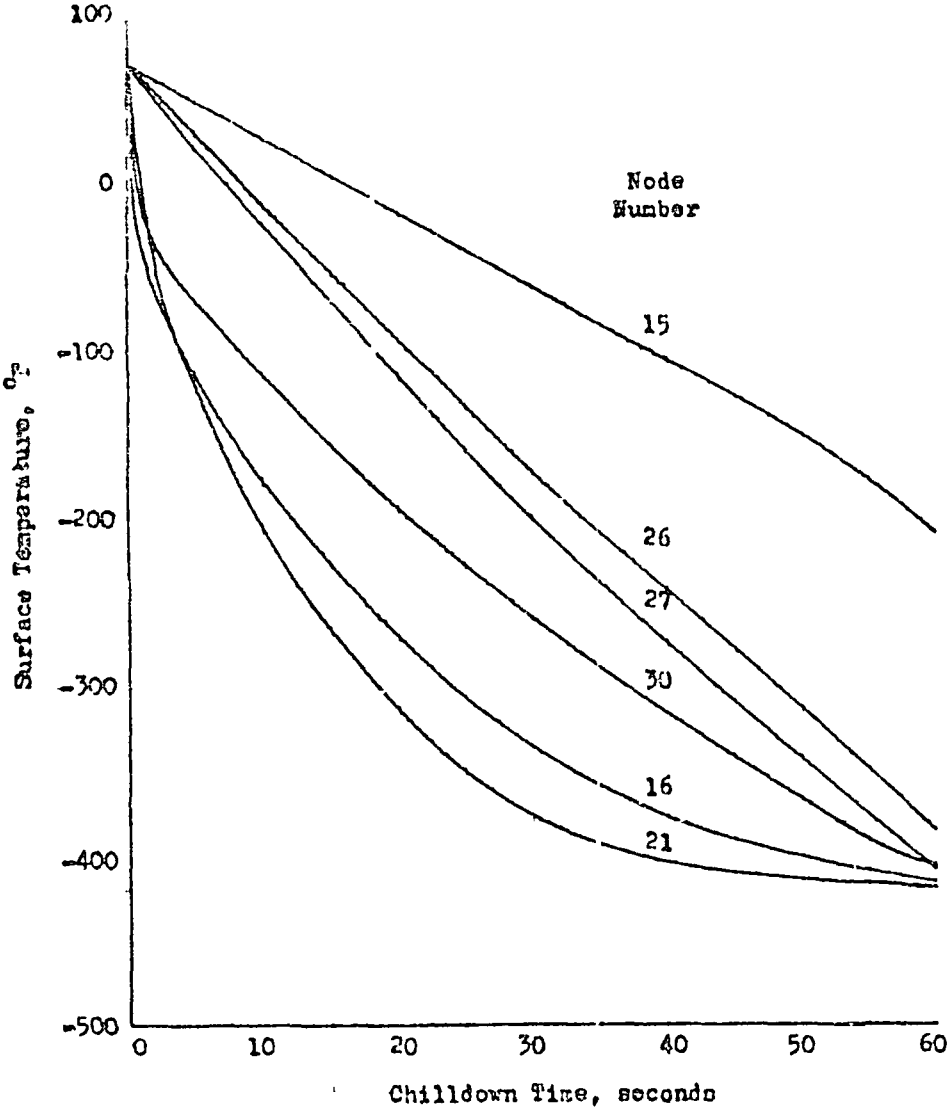

Figure 128 Surface Temperature vs Chilldown Time for the J-2S Engine System

Engine	11
Initial System Temp.	70 °F
T_{Bi}	-4.3 °F
$h = 0.001\ \theta^{.5}$	
P_T	32 psia
Initial Pump Temp.	70 °F

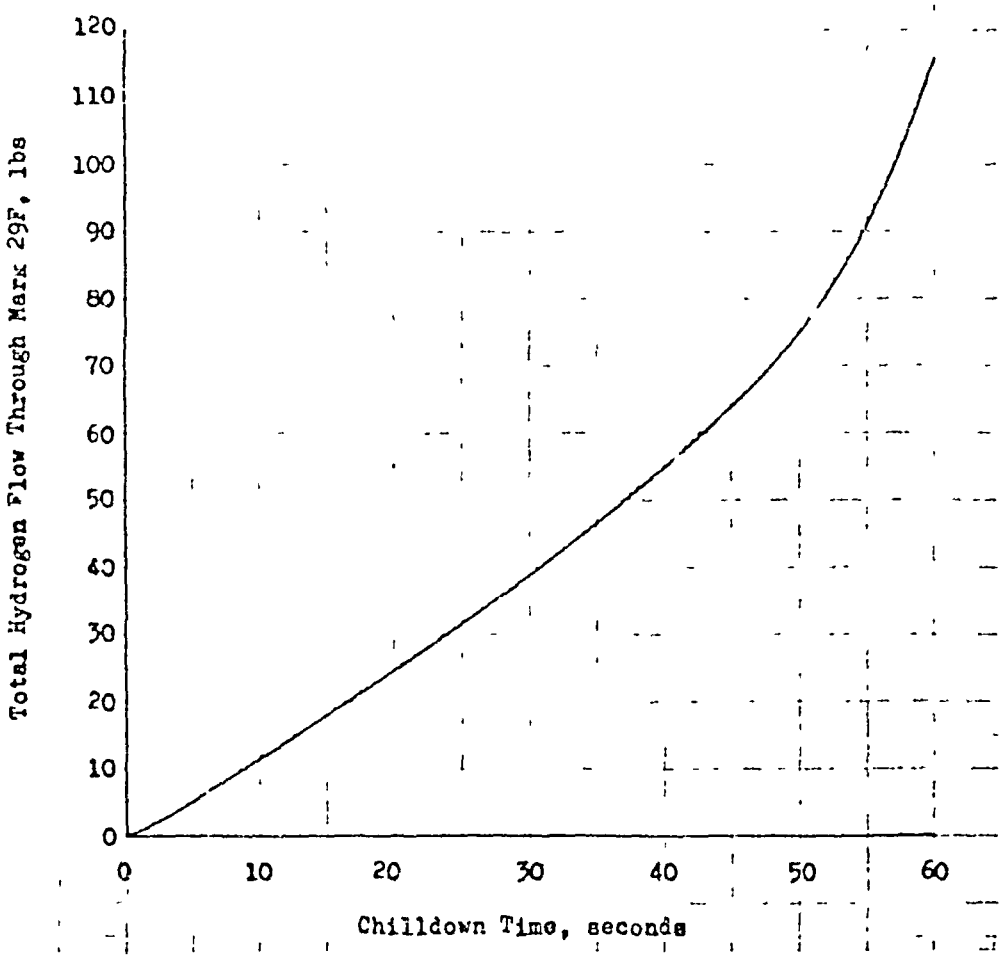

Figure 129. Total Hydrogen Flow Through Mark 29-F vs Time for the J-2S Engine System

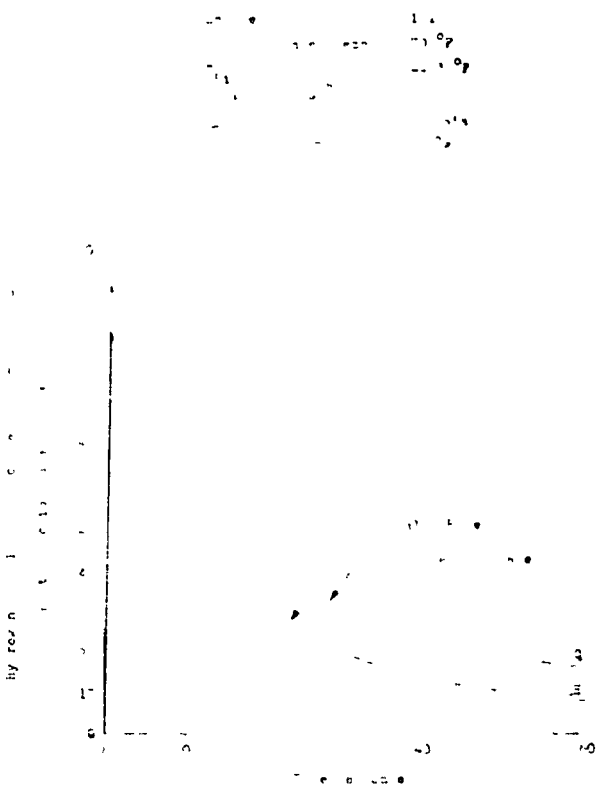

Figure 130 Hydrogen Enthalpy Rise Across the Pump and Heat Rejection Rate vs Time for the I-2S Engine System

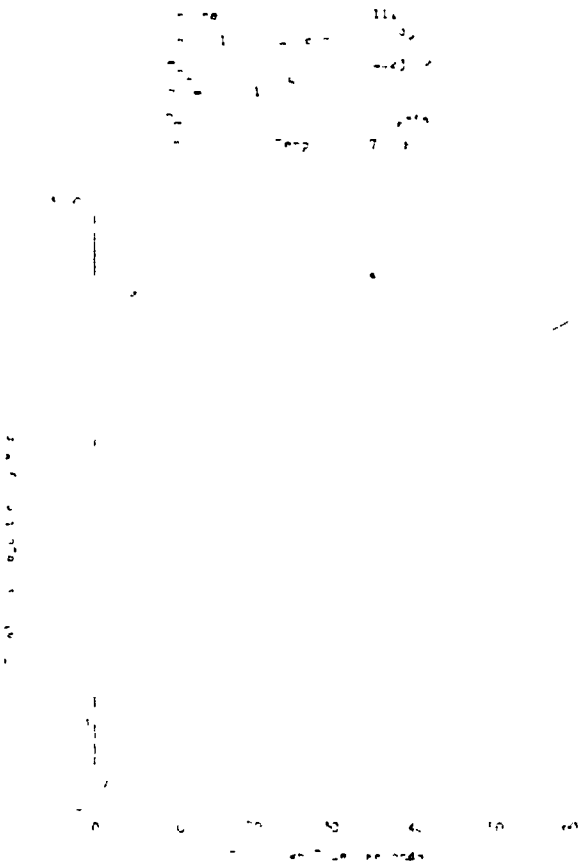

Figure 131. Total Heat Rejection by Mark 29-I vs Time for the I-2S Engine System

content of the pump is shown on Fig. 126 was about 2550 Btu of which 2440 Btu was removed in 60 seconds by about 117.5 pounds (Fig 129) of H_2.

In the absence of the experimental data, the flow breakdown between the tubes and the bypass line was based on the I/D and cross-sectional flow area. It was further assumed that the density is the same in both of the passages (not so in actuality). A friction factor of equal to 0.003 was assumed for both lines, and the pressure drop is equal in both passages then the flowrate is proportional to the resistances in each line. It is seen from these analytical investigation that the Mark 29 H_2 pump of the J-2S engine system can be chilled with fairly small amounts of LH_2 in a short time (30 to 40 seconds). If the resistances downstream of the pump are reduced, the LH_2 flowrate under tank head pressure will increase and cause a further reduction of the chilldown time.

Experimental Data Analysis

While the analytical chilldown study of the J-2S engine system was in progress, tests were run on the J-2S engine system that consisted of a period of idle mode followed by a mainstage operation. The data obtained for tests 6, 8, and 9 are presented here on Fig. 132 through 138. In all tests, the Mark 29 H_2 pump was filled with H_2 by opening the fuel prevalve (FPV) and having the main fuel valve (MFV) closed. The pump was chilled for about 45 minutes to 1 hour before the idle-mode start. The rest of the system was at an ambient temperature. Test 6 was a 1-second, idle-mode duration followed by the mainstage. Tests 8 and 9 were of 8 seconds idle mode followed by the mainstage. The test conditions during the idle modes were the same in all of these tests, that is to say preconditioning of the pump and tank pressure (driving force during idle mode) were about the same. The objective of these tests were investigation of various parameters during mainstage.

All the mainstage tests were accomplished without any difficulty, indicating that the short-duration idle modes were sufficient for the engine system

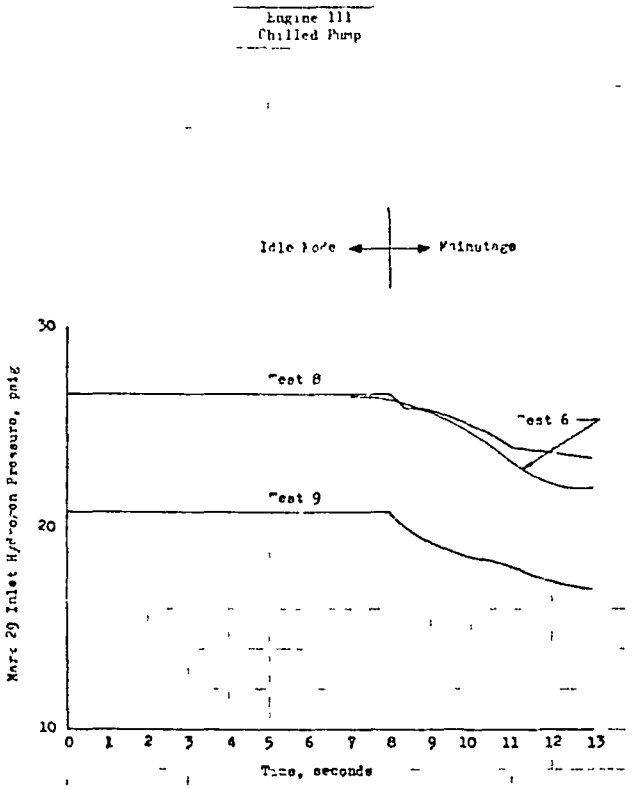

Figure 132. Mark 29 Inlet Hydrogen Pressure vs Time for the J-2S Engine System

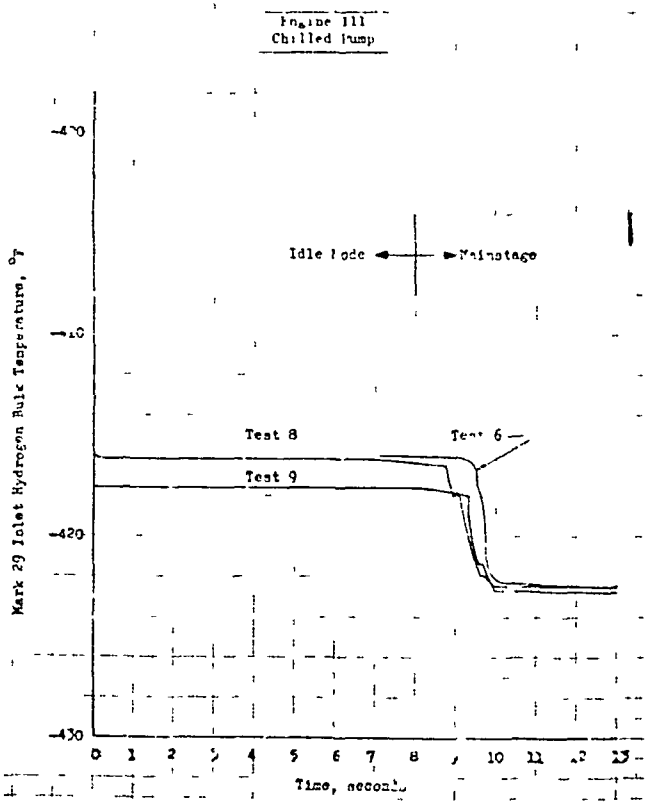

Figure 133. Mark 29 Inlet Hydrogen Bulk Temperature vs Time for the J-2S Engine System

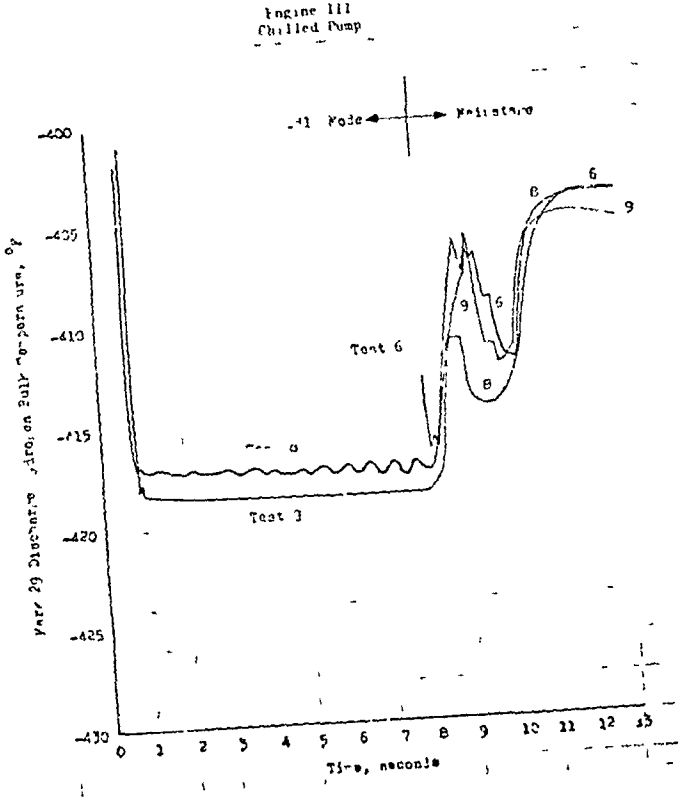

Figure 134. Mark 29 Discharge Hydrogen Bulk Temperature vs Time for the J-2S Engine System

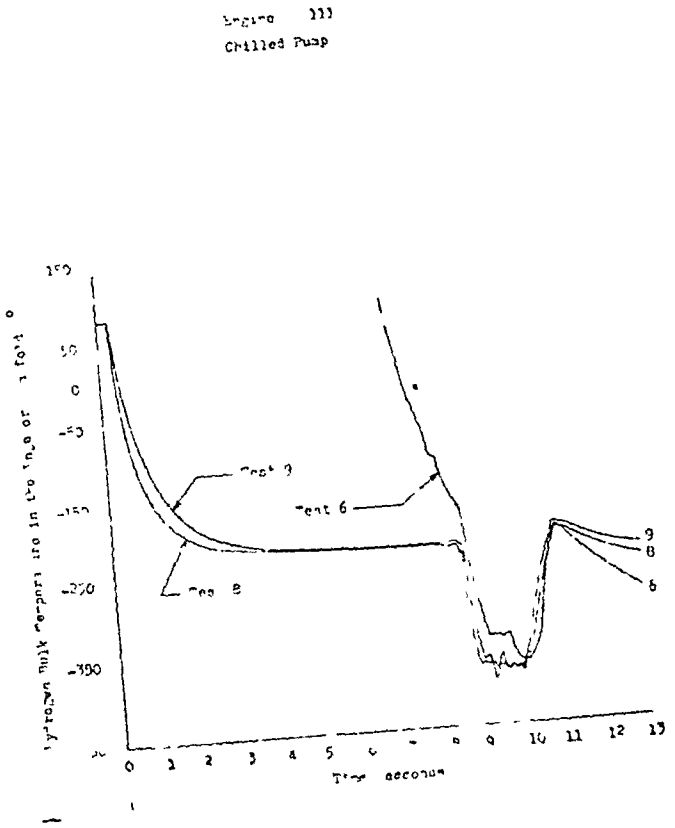

Figure 135. Hydrogen Bulk Temperature in the Injector Manifold vs Time for the J-2S Engine System

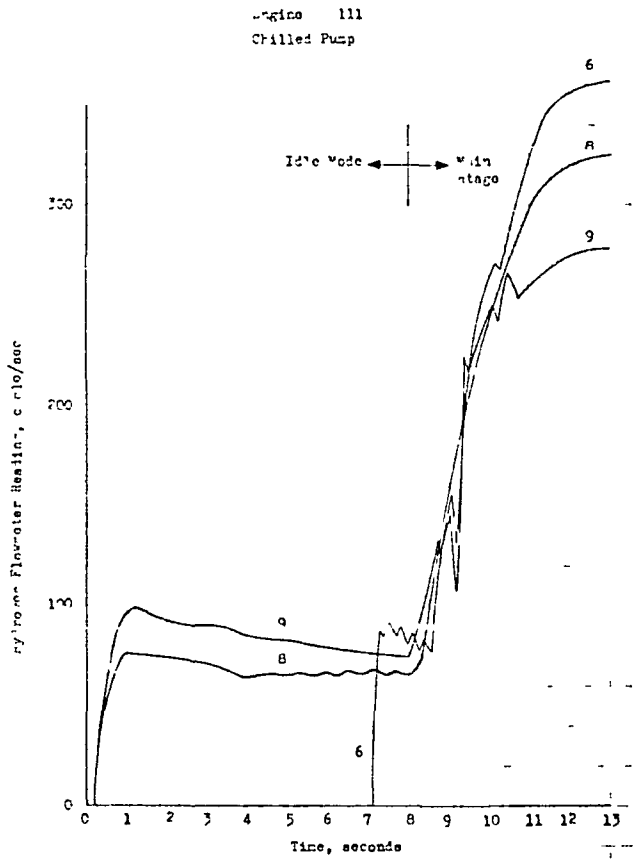

Figure 136. Hydrogen Flowmeter Reading vs Time for the J-2S Engine System

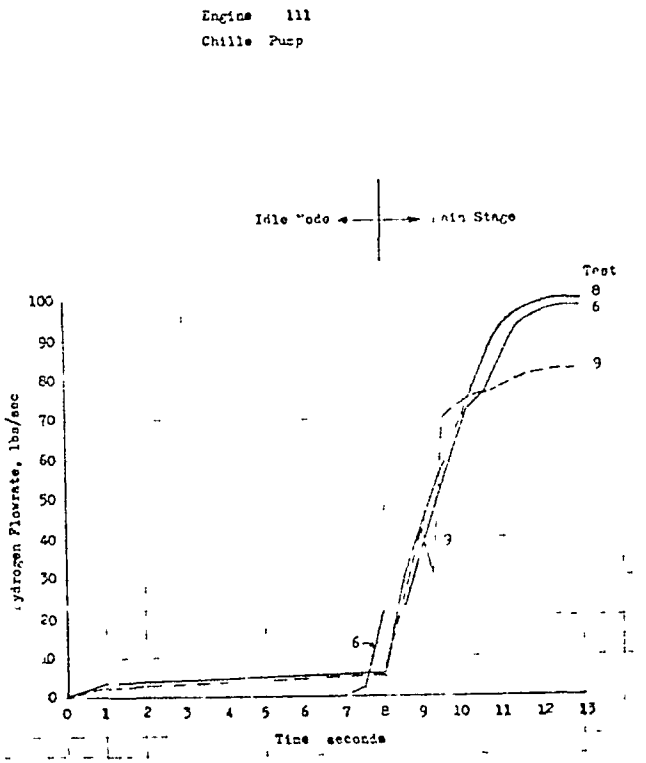

Figure 137. Hydrogen Flowrate vs Time for the J-2S Engine System

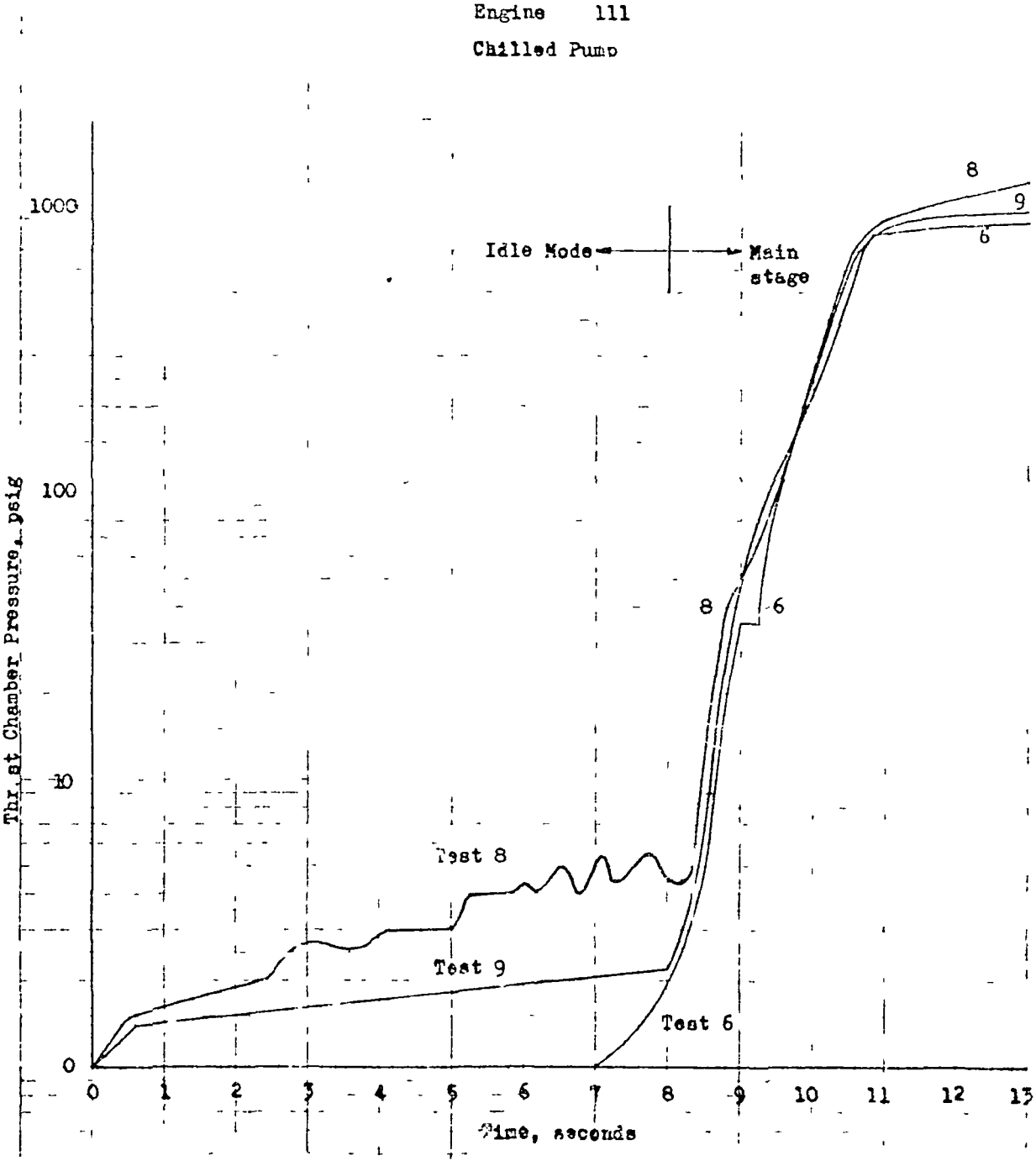

Figure 138 Thrust Chamber Pressure vs Time for the J-2S Engine System

(downstream of the pump) chilldown. The reason for 8 seconds idle mode for tests 8 and 9 was that during test 7, which was a 1-second idle mode followed by the mainstage, the main fuel valve was cracked and hydrogen leaked out. Because of the crack, it was decided to increase the duration of idle mode to chill down the valve more slowly to reduce the thermal stresses. It is, therefore, established that the Mark 29 pump can develop the necessary head after being filled with LH_2 for approximately 45 to 60 seconds

The data of tests 6, 8, and 9 were analyzed and the results are presented in Fig. 139 through 141. The H_2 enthalpy increase between the pump discharge and the injector manifold is shown in Fig. 139. It is seen that the enthalpy increase is highest at about 1 second after the start of the idle mode. Maximum heat input from the structure to the H_2 coolant takes place at this time. The heat input reduces until a fairly steady heat input is established after 3 seconds of idle mode. After 8 seconds of idle mode, the pump is started and an increase in H_2 flowrate takes place, which reduces the enthalpy increase per pound of H_2 although the total heat input increases. During the first 2 seconds of mainstage, the thrust chamber pressure rises slowly (Fig. 138) as does the heat input from the combustion gases to the H_2. The thrust chamber pressure rises sharply after 2 seconds of mainstage followed by an increase in the gas-side heat transfer coefficient and high heat input rate (Fig. 139). Finally, at about 4 seconds after mainstage, the thrust chamber pressure starts leveling off and a steady-state operation is established and the enthalpy rise tends to become steady. This holds true for tests 6, 8, and 9 except that test 6 is of 1-second idle-mode duration. The variation of heat input after 3 seconds of mainstage is attributed to differences in H_2 flowrate (Fig. 137) and mixture ratio.

Figure 140 is a plot of the heat rejection rate versus time for tests 6, 8, and 9. To obtain the heat rejection rate, the flowrate was simply multiplied by the enthalpy rise. However, determination of flowrate during the idle-mode portion of the test was not easy. During this

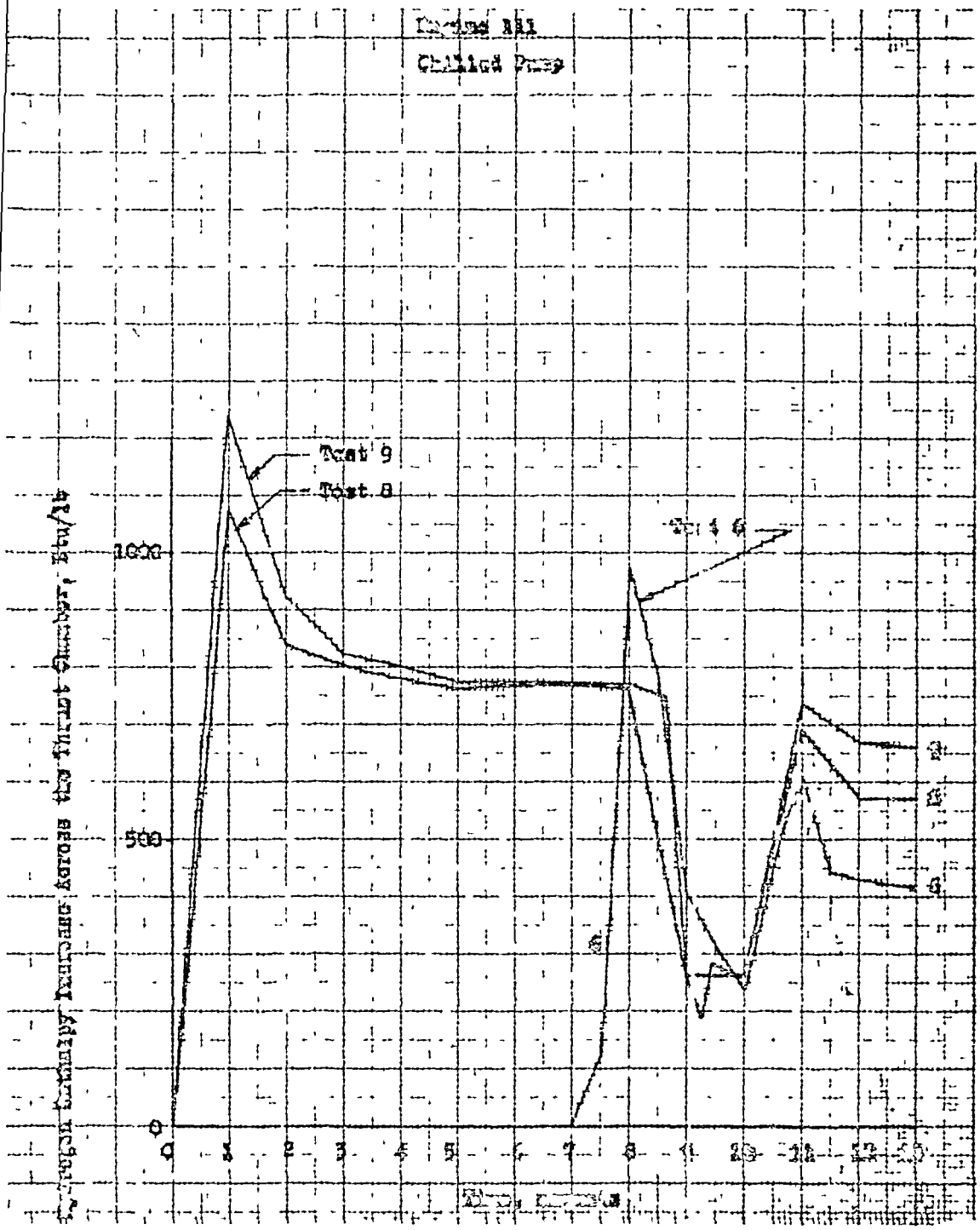

Figure 139 Hydrogen Enthalpy Increase Across Thrust Chamber vs Time for the J-25 Engine System

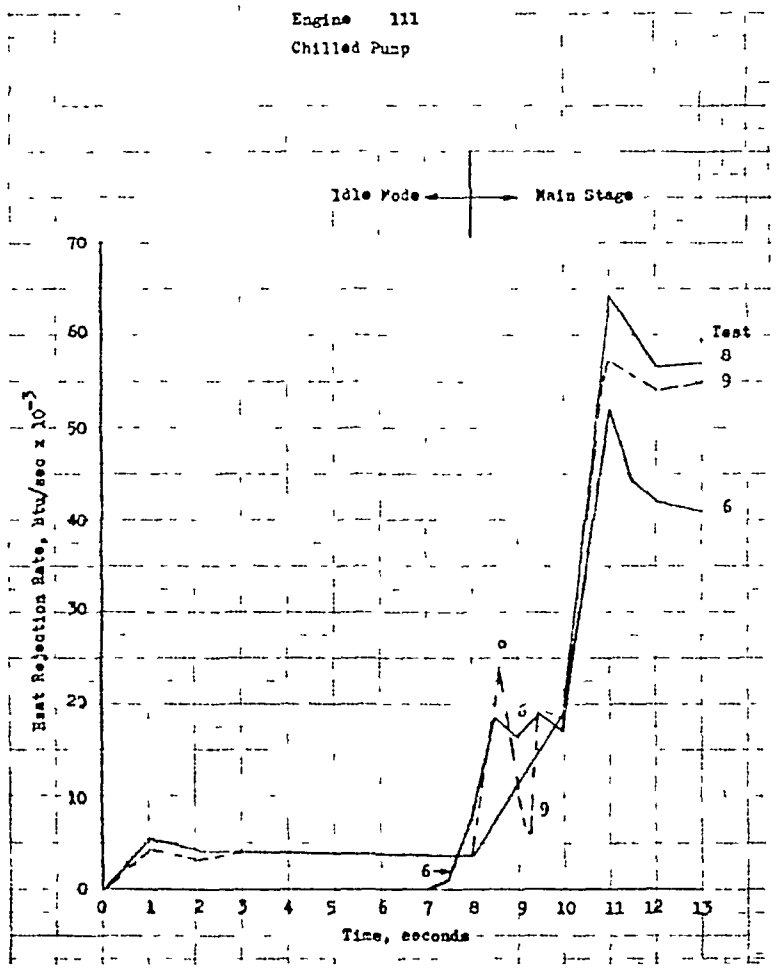

Figure 140. Heat Rejection Rate vs Time for the J-2S Engine System

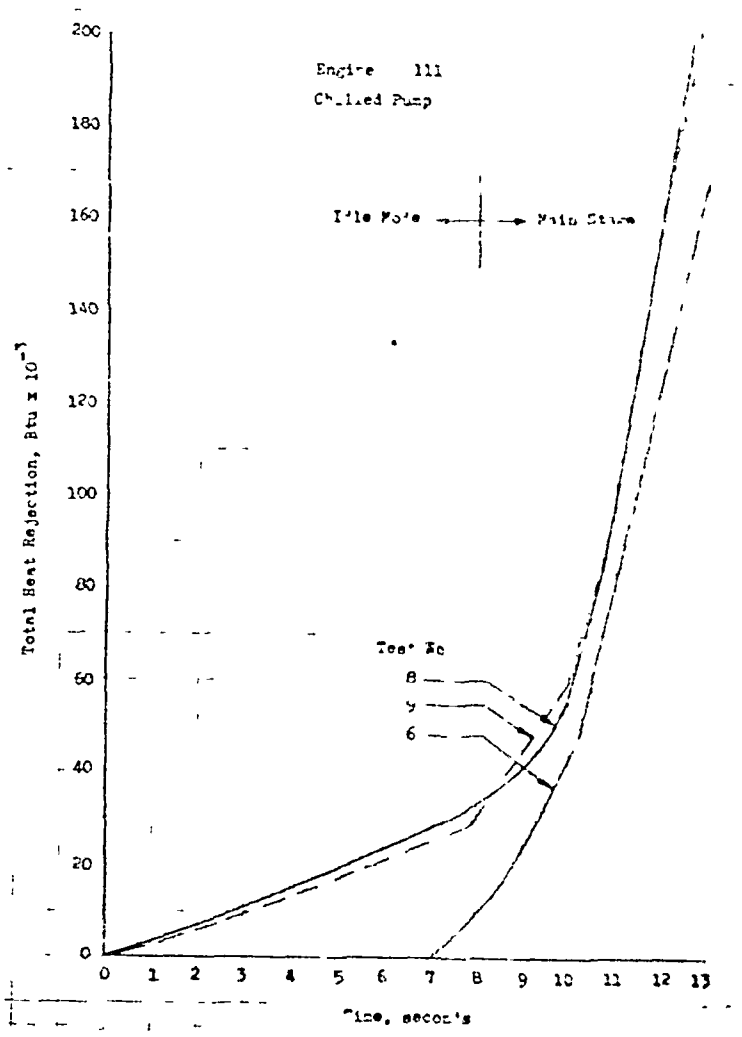

Figure 141. Total Heat Rejection Rate vs Time for the J-2S Engine System

segment of the test, two-phase H_2 (about 30 percent volume of vapor) flows through the pump and the flowmeter. Therefore, the flowmeter reading cannot be used to define the flowrate because the density is not known and that the flowmeter is not calibrated for measurement of two-phase fluid. Consequently, the pressure drop across the pump, which was nearly constant and was about 4.8 psi, was used in conjunction with the experimental data (Fig. 142) to estimate the H_2 flowrate during the idle-mode portion of the test. This estimated H_2 flowrate was about 5.8 lb/sec. During mainstage, subcooled LH_2 flows through the flowmeter, thus the flowrate is known. Figure 140 shows good agreement between tests 8 and 9. Test 6 varies slightly from the other two tests, this discrepancy is attributed to differences in mixture ratio. Figure 143 shows the integrated total heat rejection for the three tests.

One longer duration (about 195 seconds) test was run on the J-2S engine system while the analytical chilldown study was in progress. Prior to the start of the test, the entire J-2S engine system, including Mark 29, was at ambient temperature. This test was not followed by a mainstage test. The data obtained from this test are plotted in Fig. 143 through 145. Figure 143 shows the pressure at various positions in the J-2S engine system. It appears that the system has reached steady operation after 164 seconds of idle mode. The thrust chamber pressure is about 10 psig (23.8 psia), and remains constant till the end of the run.

Figure 144 is a plot of temperature versus time for various parameters. The pump inlet and outlet temperatures are nearly the same after about 14 seconds. The main fuel injector temperature drops rapidly from that of ambient to about -437 F in about 80 seconds and remains constant throughout the rest of the test. Obviously, this temperature reading is in error, and is attributed to inaccuracy of the thermocouple. However, it is seen that this temperature is about the same as the pump outlet temperature because most of the H_2 flows through the bypass line and receives very little or no heat. Additionally, the rear bearing temperature was measured as shown on Fig. 144. From 0 to 80 seconds, the rear bearing temperature is out of range of the measuring device but the temperature

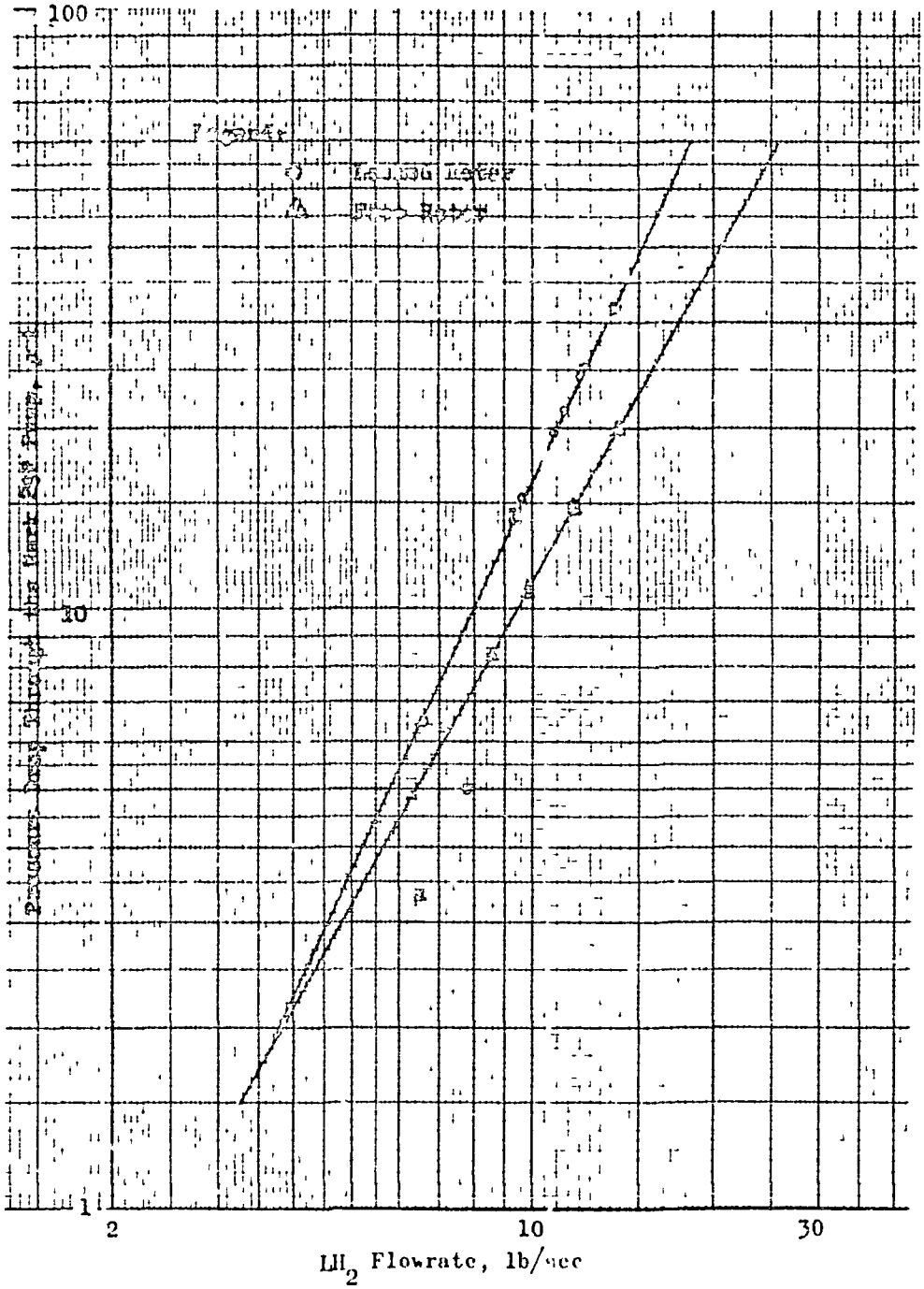

Figure 142. Pressure Drop Through the Mark 29F Pump vs LH_2 Flowrate

Engine	111
Test	16
Local Pressure	13.8 psia
Initial Pump Temp	92 °F

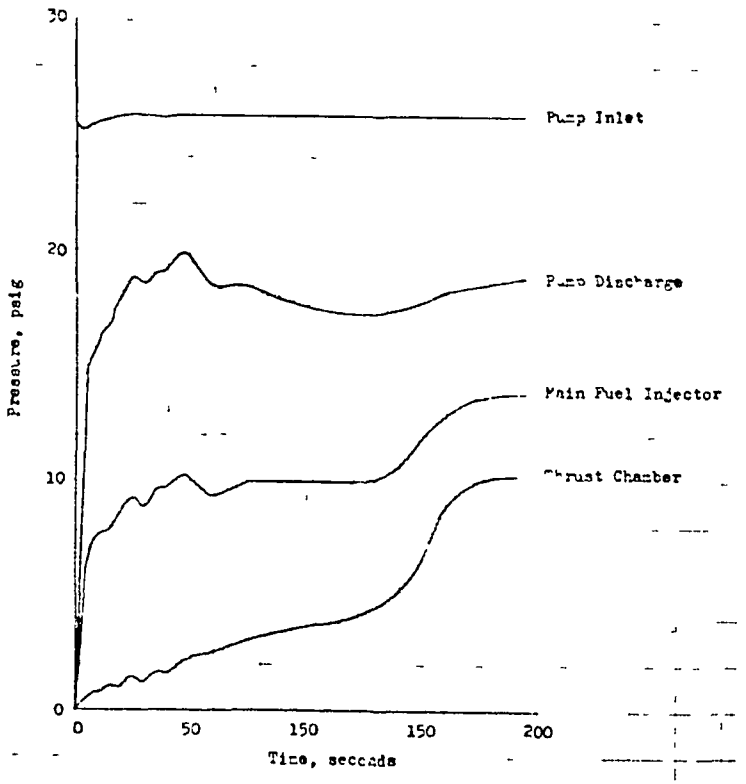

Figure 143. Pressure vs Time for the J-2S Engine System During Idle Mode

Engine	111
Test	16
Local Pressure	13.0 psia
P_T	40 psia
Initial Pump Temp.	92 °F

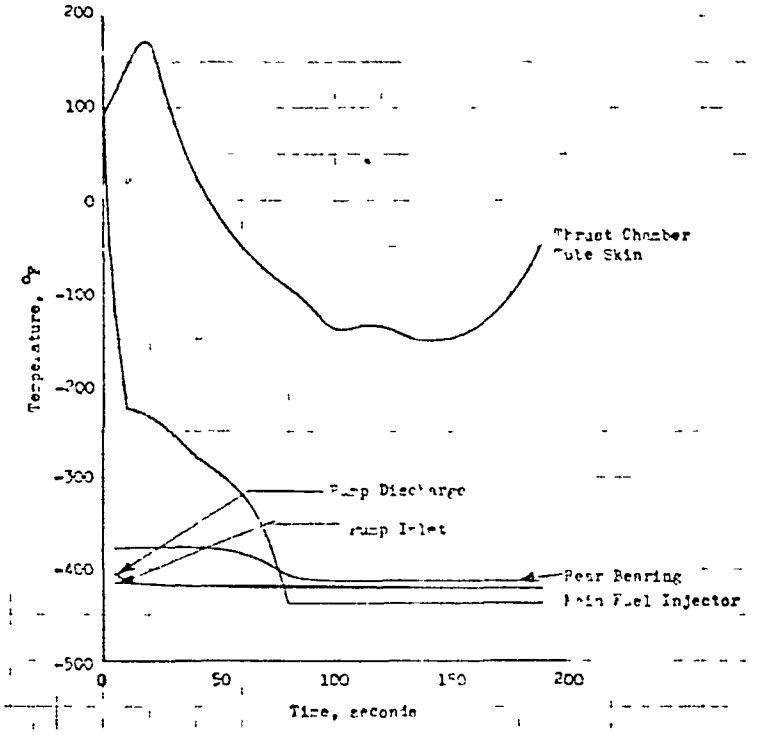

Figure 144. Temperature vs Time for the J-2S Engine System During Idle Mode

is valid for the rest of the test. It is indicated that the rear bearing temperature decreases slowly and approaches the pump discharge temperature.

A thermocouple was also located on the back side of the thrust chamber tube near the throat. This temperature (Fig. 144) shows that some heat is being added to the LH_2 as it flows in the tube. This heat is released by the combustion gases and since only a small portion of the fuel flows through the tubes, the bulk temperature of the H_2 is high. This is the reason for such a large difference between the thrust chamber tube skin temperature and the main fuel injector temperature.

During this test, a quality meter was located upstream of the pump and the H_2 quality (percent liquid by volume) is plotted on Fig. 145. This figure shows that two-phase fluid enters the pump, which is initially at ambient temperature and it is seen that the quality of H_2 reaches all liquid phase after 60 seconds of idle-mode operation. The quality of H_2 leaving the pump was not measured, but it is obvious that two-phase flow leaves the pump for some time after saturated LH_2 enters the pump. This is because heat is added to the H_2 by the pump body and to the pressure drop through the pump.

Consequently, an accurate determination of the flowrate throughout the test was not possible but the H_2 flowrate was predicted during the beginning of the test. Saturated LH_2 begins to leave the pump after about 70 seconds of idle-mode operation. The hydrogen flowrate versus time for the test is plotted on Fig. 146. The dotted portion of the curve indicates the time during accurate measurement of flowrate was not possible because two-phase fluid was flowing through the flowmeter. The total H_2 flow versus time is plotted on Fig. 147, and it is seen that about 1429 pounds of hydrogen has passed through the pump. Figure 148 shows the enthalpy difference across the pump and the thrust chamber (including the bypass line, and inlet manifold) approaches zero indicating the pump is completely chilled in 195 seconds. The enthalpy difference across the thrust chamber should eventually reach steady state because of the heat input by the hot combustion gases.

Engine 111
Test 16
P_c 40 psia
Initial Pump Temp 92 °F

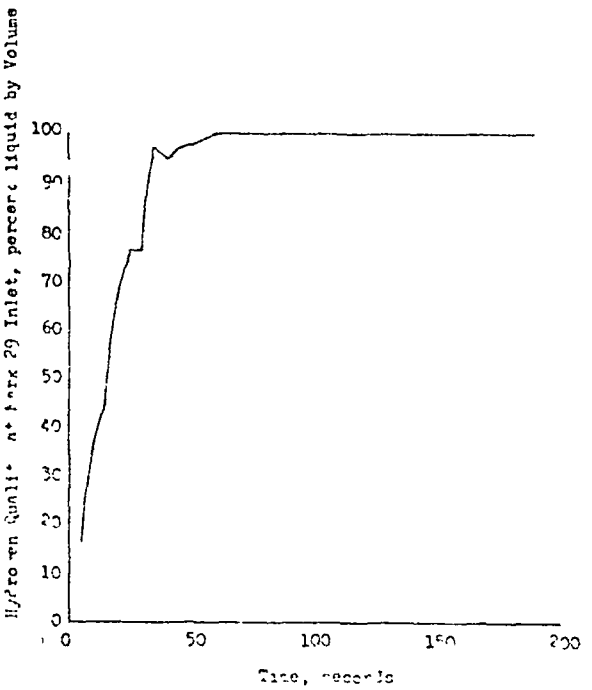

Figure 145. Hydrogen Quality at Mark 29 Inlet vs Time for the J-2S Engine System

Engine 111
Test 16
P_c 40 psia
Initial Pump Temp 92 °F

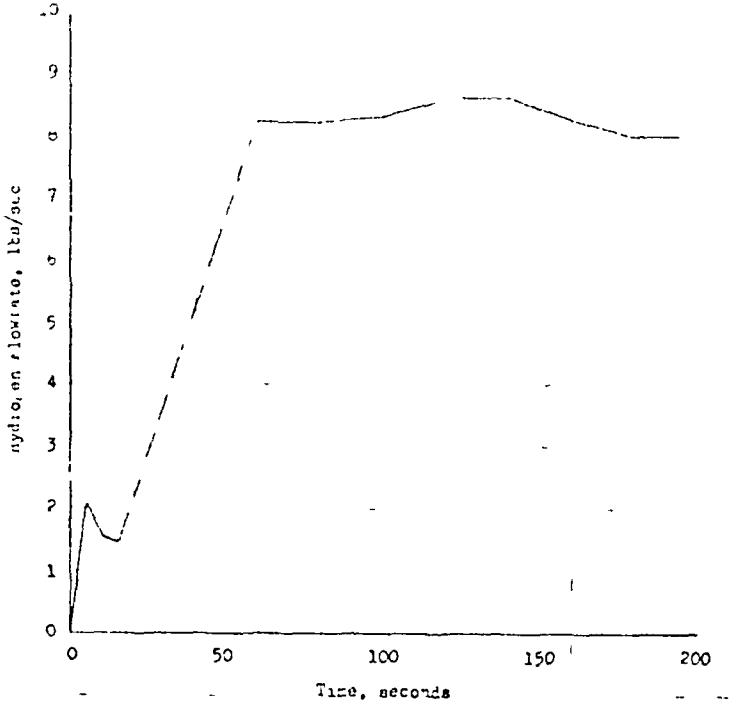

Figure 146 Hydrogen Flowrate vs Time for the J-2S Engine System

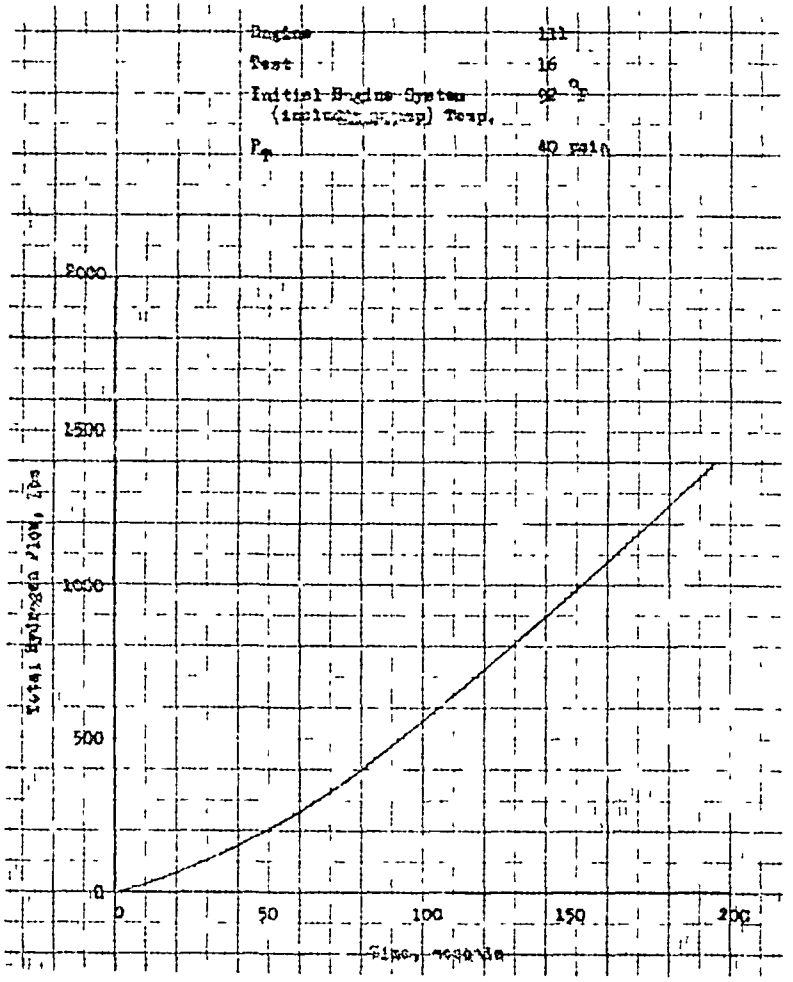

Figure 147 Total Hydrogen Flow vs Time for the J-2S Engine System

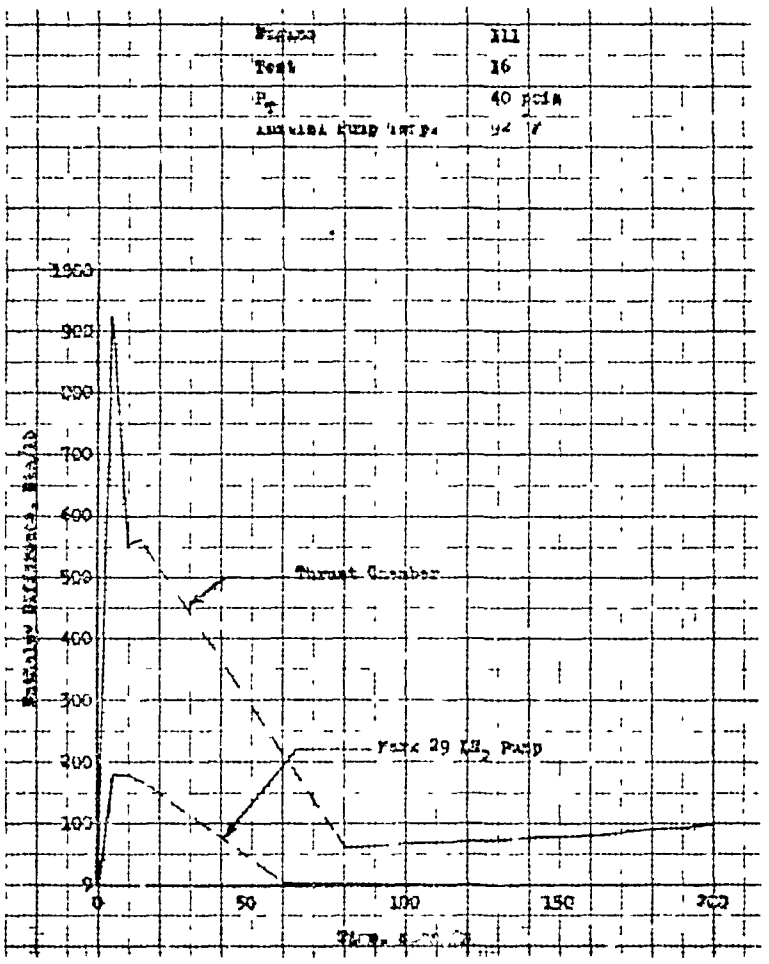

Figure 148 Enthalpy Difference vs Time for the J-2S Engine System

Figure 149 is a plot of heat rejection rate versus time for the pump and the thrust chamber and it is seen that this rate has become zero after 195 seconds of idle-mode operation. Figure 150 is a plot of total heat rejected by the pump and the thrust chamber versus time. The maximum amount of heat rejected by the pump is about 15,700 Btu. The estimated heat content of the pump between -418 and 80 F is about 15,500 Btu. Some additional heat is also released by the inlet and outlet duct and turbine parts. Any inaccuracy involved should be attributed to the lack of accurate knowledge about the H_2 flowrate during the two-phase flow period. In general, the test data agrees well with the predicted heat content of the pump.

After about 70 seconds of idle mode, nearly 100-percent LH_2 leaves the pump and the pump can even be started before this time because the pump is capable of developing the necessary head when H_2 quality is about 65 percent liquid by volume, or more, at the pump inlet. It can be seen from Fig. 145 that it takes about 20 seconds of idle-mode operation before the pump inlet quality reaches 65 percent liquid by volume.

Comparison of Analytical and Test Results

Comparison between analytical and experimental chilldown results were modified (Fig. 126) to agree with that of test 8. It was assumed that the pump was chilled and contained H_2 at -417 F. Analytical studies were conducted for a duration of 8 seconds, the same as the test 8 duration and assumptions were made that the heat input from the combustion gases were small. The H_2 flow was to be 63 percent through the bypass line and 37 percent through the tubes. Various flowrates were assumed and the analysis was carried out with the aid of a computing machine using the following equation for determination of the heat transfer coefficient:

$$h = 0.001\ F^{0.5}$$

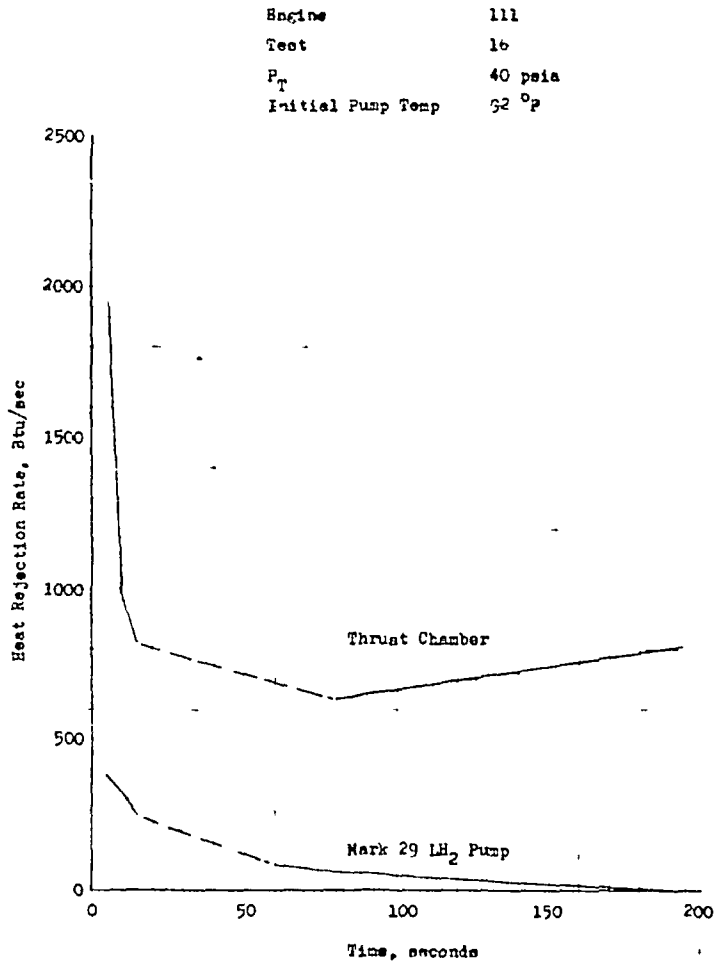

Figure 149 Heat Rejection Rate vs Time for the J-2S Engine System

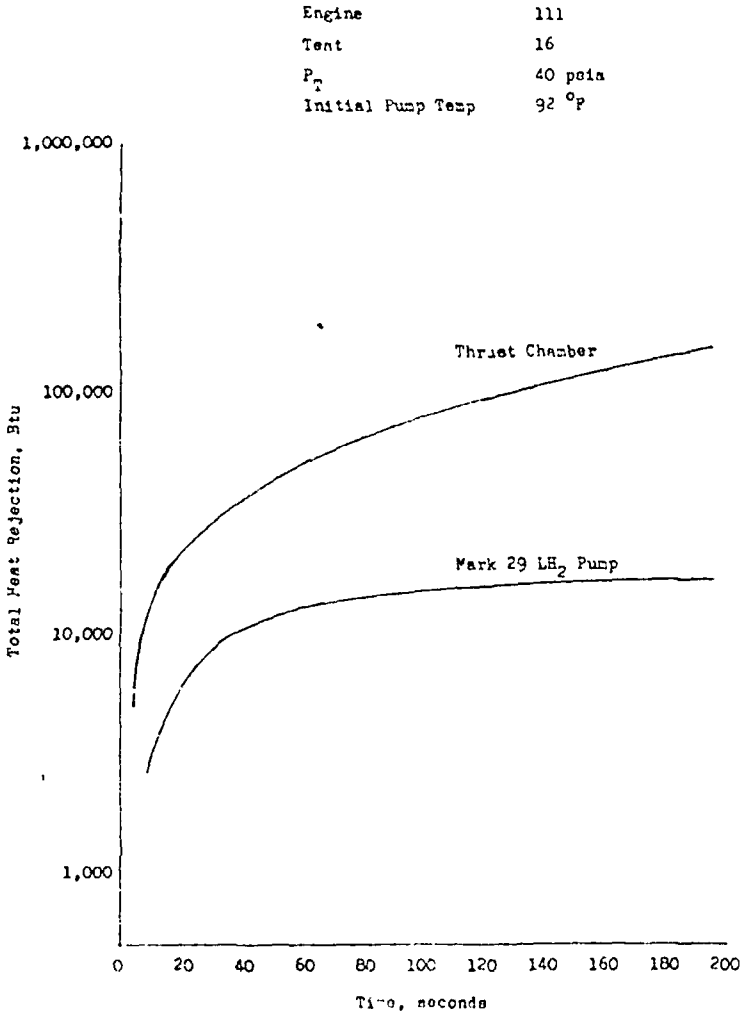

Figure 150 Total Heat Rejection vs Time for the J-2S Engine System

It was found that to duplicate the measured injector manifold H_2 bulk temperature, a flowrate should be used that causes an excessive pressure drop in the system (higher than available during test 8). Therefore, the heat transfer coefficient was found through the use of

$$h = 0.00065\ G^{0.5}$$

This equation was developed for copper tubes during the analysis of tube cooldown test data and is more accurate than $h = 0.001\ G^{0.5}$, which was obtained from the analysis of the stainless-steel tube cooldown data The H_2 flowrate versus time is plotted on Fig. 151. The J-2S engine system pressure drop (pump inlet duct through injector) for the flowrate of Fig. 151 is plotted on Fig. 152. The system pressure drop for test 8 is also plotted on Fig. 152. There is a difference between the two pressure drop curves and this difference can be reduced by assuming slightly lower flowrates for the analytical case. The H_2 bulk temperature at different locations of the system is plotted versus time on Fig. 152(see Fig. 126) and was measured in the injector manifold during test 8. This temperature is also plotted on Fig. 153, and is in good agreement with the result of test 8 and that of analytical chilldown studies. It is evident that the equations developed through the analysis of tube cooldown data can be used successfully to estimate the chilldown behavior of the J-2S engine system.

Figure 154 shows the wetted surface temperature of the engine system for the flowrate of Fig. 151 and because it was assumed that the pump was at -417 F, no surface temperature for the pump or inducer and impeller is plotted on Fig. 154. Node 48 corresponds to the temperature of the bypass line through which most of the H_2 flows (about 67 percent by weight). For this reason, the temperature of this surface decreases much faster than temperature of other nodes.

THRUST CHAMBER AND ENGINE SYSTEM CHILLDOWN INFLUENCE FACTORS

The ability for H_2-fueled engine systems to throttle over a wide range and the ability to accelerate rapidly to mainstage conditions under widely

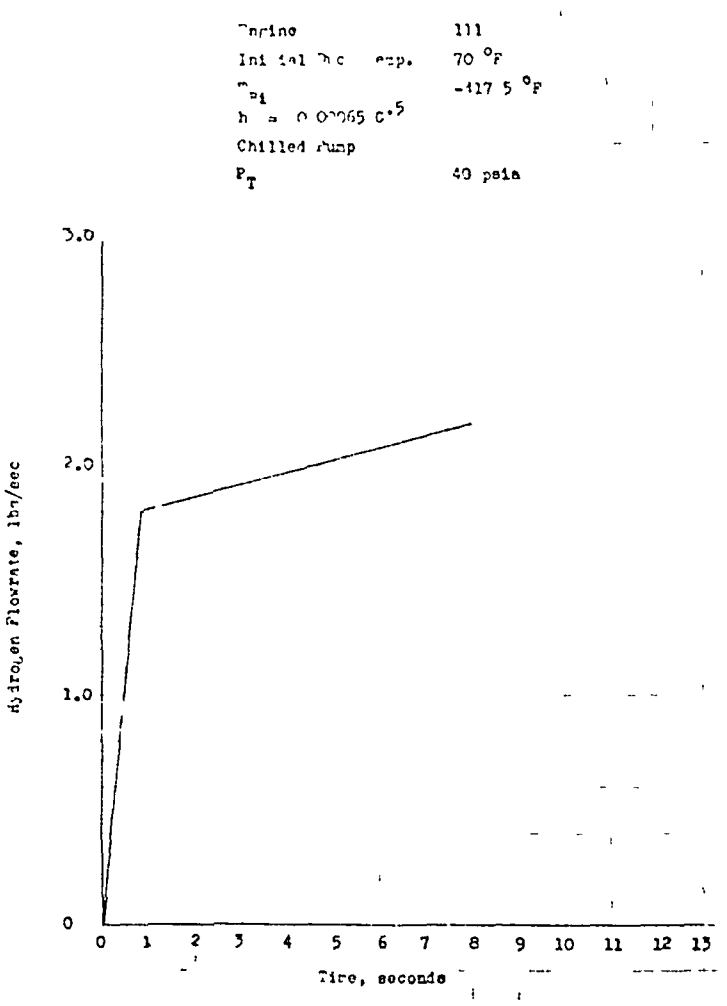

Figure 151. Hydrogen Flowrate vs Time for the J-2S Engine System

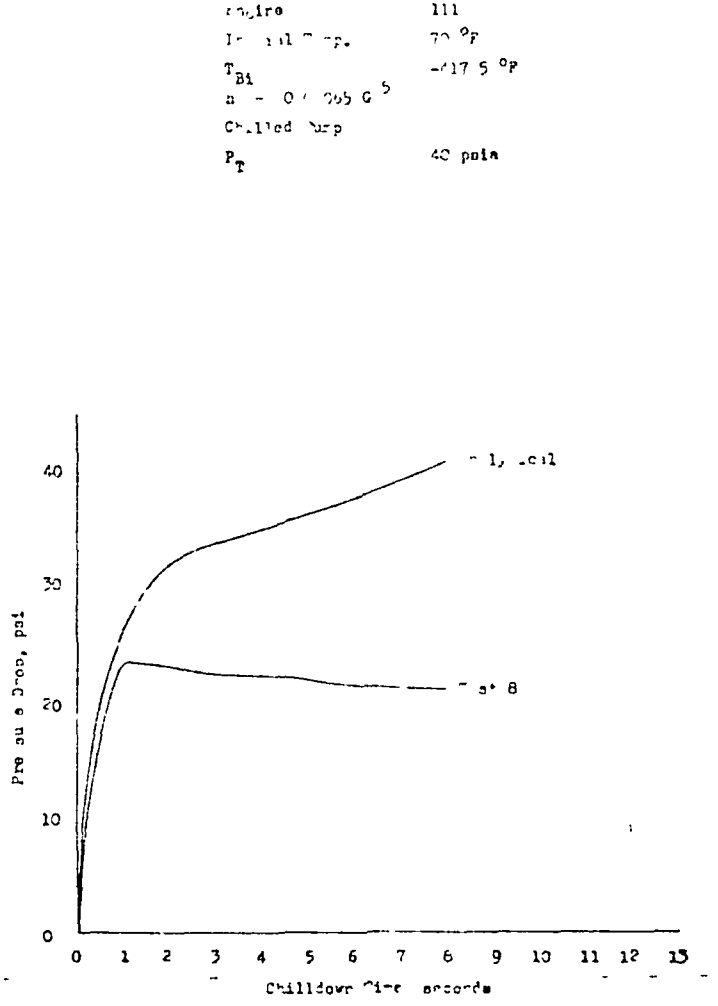

Figure 152. Pressure Drop vs Chilldown Time for the J-2S Engine System

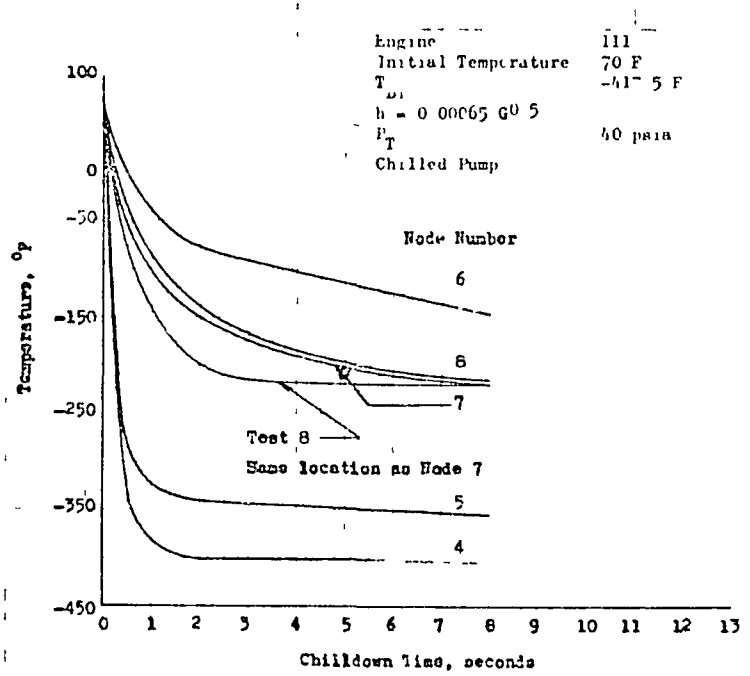

Figure 153. Hydrogen Bulk Temperature vs Chilldown Time at Various Locations of the J-2S Engine System

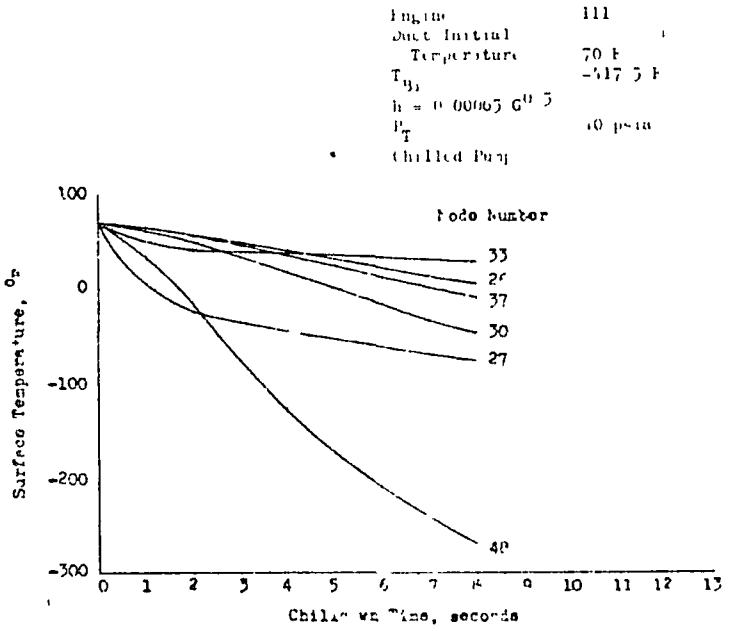

Figure 154 Surface Temperature vs Chilldown Time for Various Locations of the J-2S Engine System

varying pump and thrust chamber initial temperature conditions are desirable goals to be attained. Present H_2 engine system characteristics are such that extensive pump and thrust chamber preconditioning is required to ensure LH_2 within the entire fuel feed system. The current study is evaluating the necessity of chilling the entire pump body as opposed to a chilling of the H_2-wetted surfaces only. The latter approach leads to a reduction in fuel flow and a shorter chill period before pump spinup can be initiated. Analytical and experimental studies provided by Ref. 1 indicate pump, line, and thrust chamber configurations of low mass, large flow area, and short L/D are of necessity if a large chill flow is to be passed through the feed system in a short chill time. Commensurately, high H_2 tank pressures are desirable to provide a high chilldown flow. Study of the pump and thrust chamber components indicates these can be conceivably designed for broad band temperature operation. Similarly, thrust chamber design approaches for higher coolant side-wall temperatures and less coolant flow resistance are being reviewed; these are discussed herein.

The problem of engine system startup under the situation of a warm thrust chamber injector and feed line downstream of the pump results from the near linear thrust chamber operating line in terms of pressure and flow that results when a near choked gas flow is passed. Under a situation where the LH_2 pump is accelerating with a LH_2 flow, the possibility of pump stall or surge will result if the resistance downstream of the pump is greater than that indicated by the pump "stall" line.

Figure 155 illustrates the typical intersection points resulting from different stall line and thrust chamber (gas) operating lines. Illustrated are high- and low-resistance thrust chamber operating lines and low, intermediate, and high stall margin pump lines A comparison of the moderate stall margin line with the high- and low-resistance thrust chamber operating lines shows that a reduction in the stall pressure (severity) point (D to B) occurs with a low-resistance flow line. With a high stall margin line as shown, no intersection occurs, illustrating the allowance for a

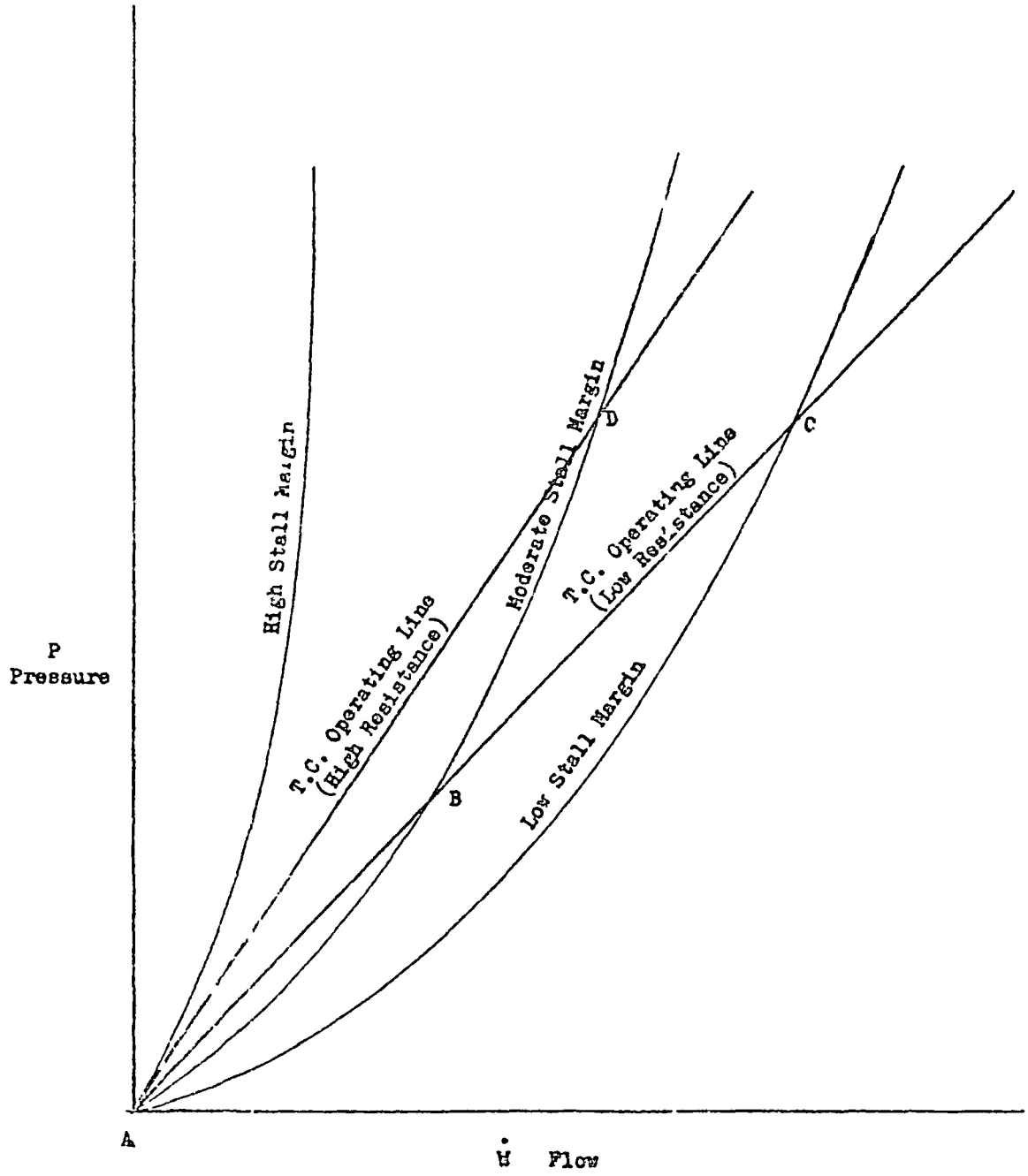

Figure 155 Comparison of Stall Margin and Operating Line Intersections

wide throttling range and thrust chamber startup under a wide range of environmental temperature conditions. With a low stall margin line as shown, even with a low-resistance thrust chamber operating line severe stall problems may be expected to be encountered during startup and for throttling.

Thrust-Chamber Coolant Area Influences

The most restrictive portion of the fuel flow area in the region downstream of hydrogen pump occurs in the thrust chamber of a regenerative design (Table 9), particularly in the throat and combustion zone regions where heat loads and commensurate cooling mass velocity requirements are the greatest. From a system start (and cooldown) standpoint, a reduction in throat coolant passage area resulting from an attempt to achieve a minimum throat gas-side wall temperature will require an increased stall margin on the pump design. As a result, the enlargement of the coolant passages to values allowing a maximum wall temperature commensurate with the prescribed tube thermal fatigue life requirement is desirable.

During this study, a review of the J-2 and J-2S throat region coolant passage area and wall temperature parameters was made. A heat balance of the convective heat input and rejection influences was made to develop the relationship between the coolant passage area and chamber throat hot-gas flow area. This balance can be made by considering the following equations:

$$h_c \left(T_{wC} - T_C\right) = h_g \left(T_{AW} - T_{wG}\right) \tag{74}$$

$$\frac{h_g}{G_g C_p} \equiv N_{ST_g} \qquad G_g = \frac{\dot{w}_g}{A_g} \tag{75}$$

$$\frac{h_c}{G_c C_{p_c}} \equiv N_{ST_c} \qquad G_c = \frac{\dot{w}_c}{A_c} \tag{76}$$

$$\left(\frac{T_{wC} - T_C}{T_{Aw} - T_{wG}}\right) = \left(\frac{G_g^*}{G_c^*}\right)\left(\frac{C_{p_g}}{C_{p_c}}\right)\left(\frac{N_{ST_g}}{N_{ST_c}}\right) = \left(\frac{A_c^*}{A_g^*}\right)\left(\frac{\mu_g}{\mu_c}\right)\left(\frac{C_{p_g}}{C_{p_c}}\right)\left(\frac{N_{ST_g}}{N_{ST_c}}\right) \quad (77)$$

$$\left(\frac{A_c^*}{A_g^*}\right) = \left(\frac{T_{wC} - T_C}{T_{Aw} - T_{wG}}\right)\left(\frac{1}{1 + MR}\right)\left(\frac{C_{p_c}}{C_{p_g}}\right)\left(\frac{N_{ST_c}}{N_{ST_g}}\right) \quad (78)$$

TABLE 9

COMPARATIVE J-2 AND J-2S FEED SYSTEM FLOW AREAS

Passage Location	Flow Areas, sq in.	
	J-2	J-2S
Pump Inlet	41.2	50.2
Pump Inducer	4.96	4.1
Staging (Rotor)	4.45	4.97
Staging (Stator)	8.55	--
Volute Exit	12.5	12.6
Thrust Chamber Tube Inlet	13.4	12.7
Thrust Chamber Throat Tube	10.2	8.1
Thrust Chamber Tube Exit	19.1	13.3
Injector Orifice Area	25.8	19.2

It is seen that higher wall temperatures (gas side and coolant side) and a higher coolant Stanton number will result in a more-favorable, larger, coolant-side cross-sectional flow area. A graph of this relationship with J-2S O_2-H_2 thrust chamber conditions imposed is shown in Fig. 156. With the throat region curvature and moderate coolant surface roughness

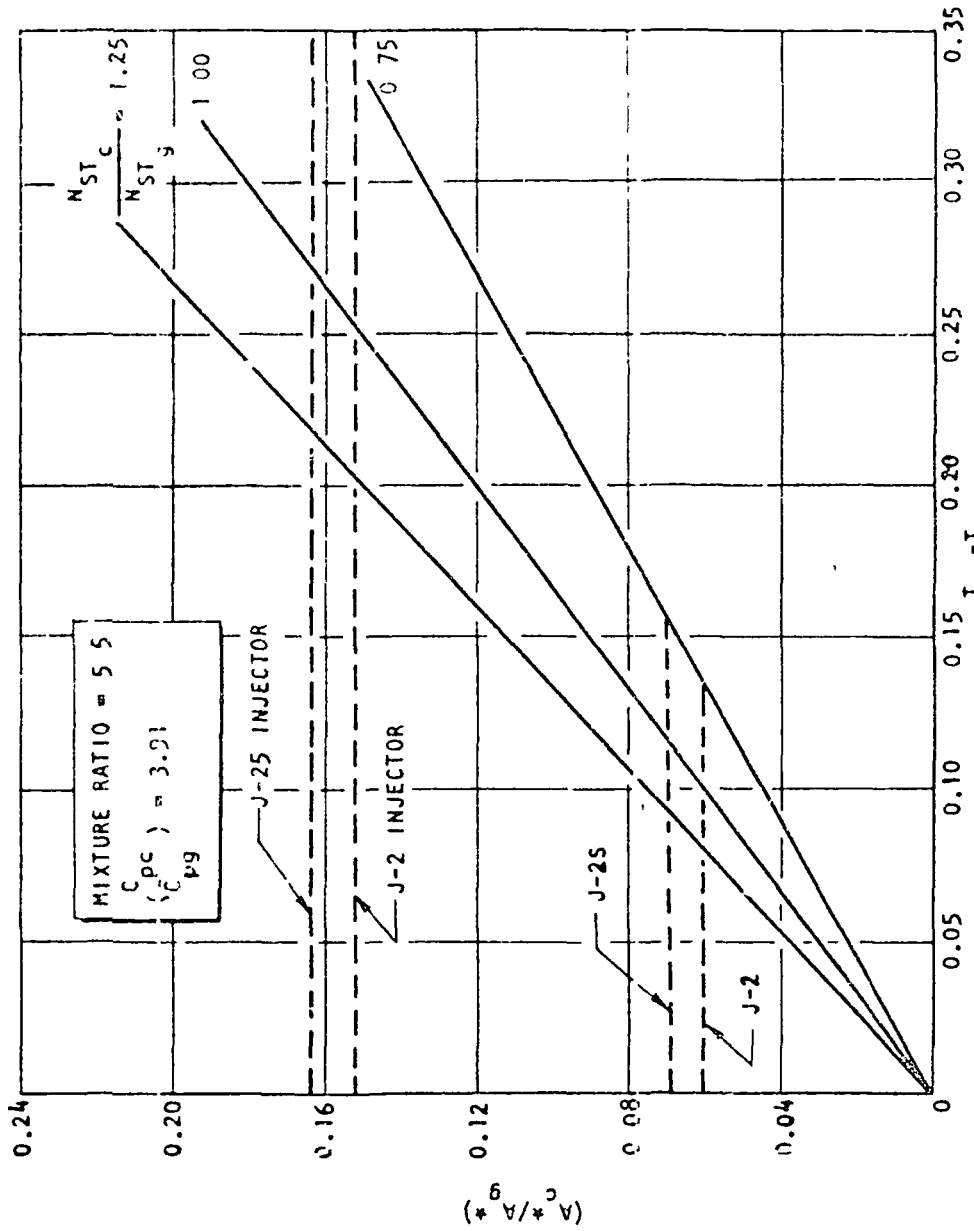

Figure 156 Coolant Passage to Throat Area vs Temperature Ratio

and high Reynolds number influence, a Stanton number ratio of approximately 1.0 is obtainable. An allowable increase in the coolant-side and gas-side wall temperature is shown to have the beneficial effect of allowing a coolant passage flow area increase toward the next size limiting flow area; the injector orifice area.

A translation of an increased wall temperature on the J-2S thrust chamber is shown in Fig. 157. It is seen that a 45-percent throat region area increase would be allowed by a 200 F wall temperature increase. This would result in a calculated wall temperature of 1500 F for the increased area condition (A_c = 11.7 in.^{2}). Influences of the increased wall temperature on thrust chamber life would have to be assessed through test experiment. Increases of 25-percent coolant passage area can be seen in Fig. 158 to reduce materially the pressure point for incipient stall. Typically, the J-2S thrust chamber without a chilldown (T 520 R) with a throat passage area increase from 8.1 to 10.2 in.^{2} could probably avoid an intersection with the stall line. Similarly, a 40-percent increase in J-2 throat region coolant passage area could result in safe wall temperatures (<1600 F) and a significantly reduced stall possibility. For example, for a no chilldown thrust chamber case, a 40-percent increase in passage area should allow a stall line interception at about point A on Fig. 158 (Mark 15-F).

The approach of providing a bypass line during thrust chamber blowdown and start on the J-2 and J-2S engines to provide an equivalent by larger fuel coolant passage area during start transients simulates the larger throat passage area which could possibly be built into the J-2S thrust chamber by a permanently enlarged throat coolant passage area. Enlargement of this area by 20 to 40 percent or larger is possible but would necessitate qualification of the thrust chamber and engine system to determine the change effect on chamber tube life aspects. The elimination of the fuel bypass valve, controls, and line plumbing would appear to be a worthwhile goal.

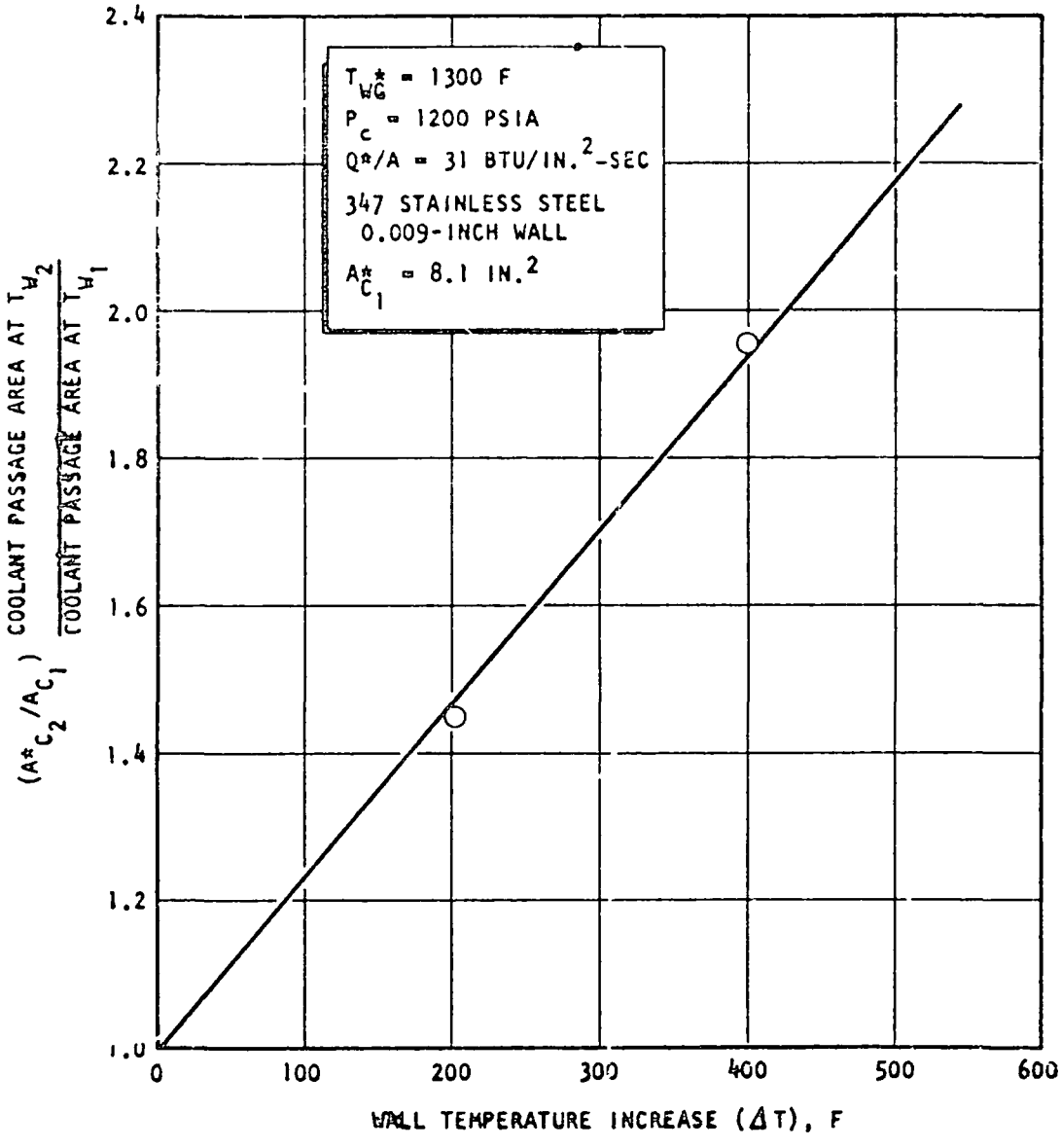

Figure 157. Coolant Area Ratio vs Wall Temperature Increase

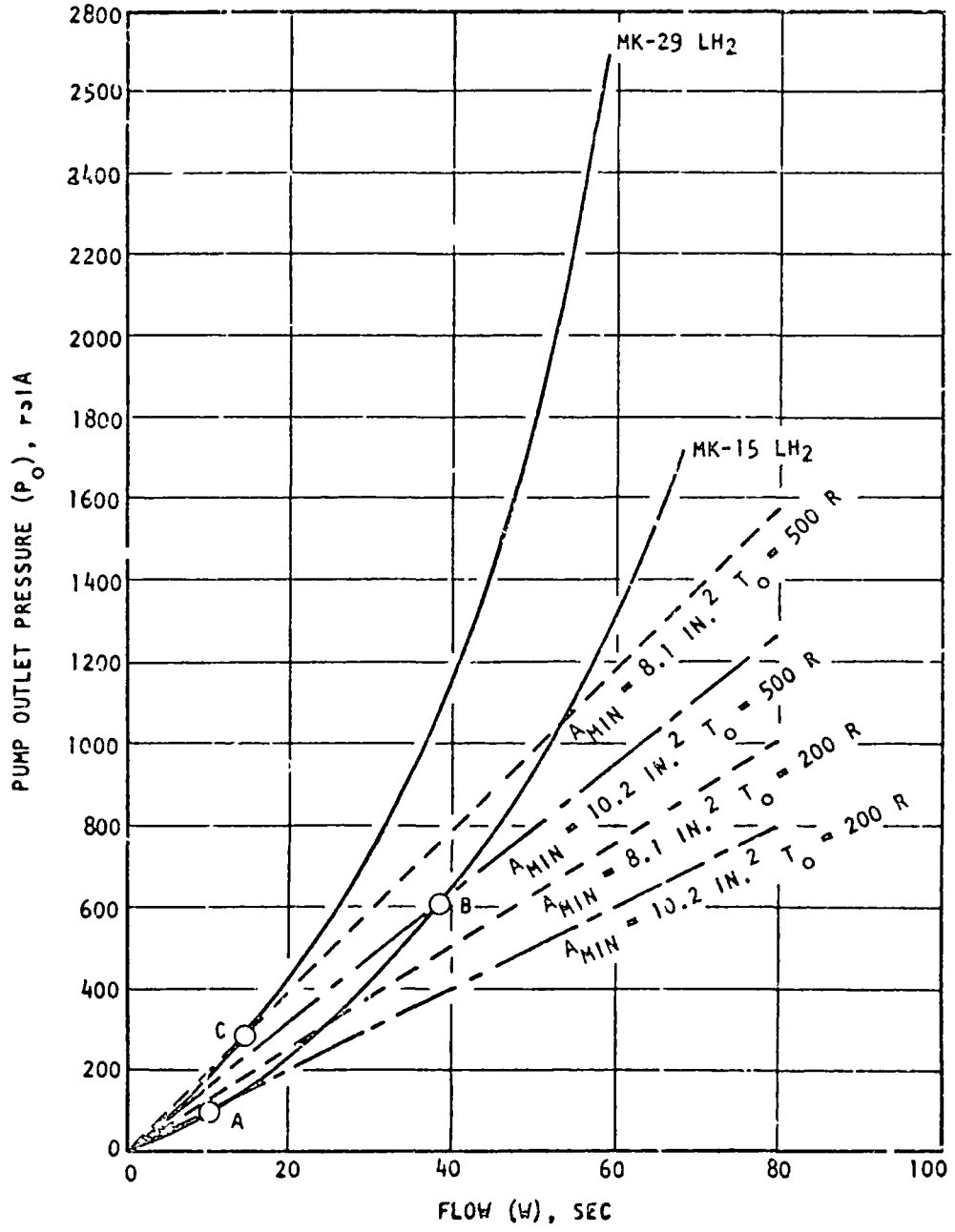

Figure 158. Stall Line and Operating Limit Line Interception Definition

Thrust Chamber Wall Material Influences

J-2S and J-2 engines are fabricated from 347 CRES tubing with throat region wall thicknesses of 0.009 and 0.012 inch, respectively. In keeping with a requirement for an increased throat coolant passage area to minimize thrust chamber stall and thermal conditioning problems, selection of alternate tube materials appears to offer possibility especially for advanced higher pressure regenerative designs. A comparison of typical material candidates with O_2-H_2 operating conditions for 1200 psia pressure (31 Btu/in.^{2}-sec) is shown below

Material	Conductivity (Btu/hr-ft-F)	Thickness, inch	Γ_{WG}, F	Γ_{WC}, F
347 CRES	11	0.009	1300	295
Nickel 200	36	0.015	1500	942
OFHC Copper	210	0.030	950	758
Be-Cu (10)	160	0.025	1000	791

It is shown that the effect of elevating the coolant side wall temperature as a result of a higher conductivity wall material will allow a larger coolant passage area, roughly in proportion to the difference between the coolant side wall to coolant fluid temperature. Consideration of the higher conductivity wall materials can be made for higher pressure O_2-H_2 and F_2-H_2 configurations.

J-2S and J-2X Stall Line Margins

Comparison of tests 115 (J-2X), 123 (J-2X), and 006 (J02S) are shown in Fig. 159 for idle-mode start conditions. The sum of the fuel bypass line area (6.7 in.^{2}) and thrust chamber throat coolant passage area (8.1 in.^{2}) totals 14.8 in.^{2}, which allows a substantial stall margin for the pump compared to the J-2S values shown for the 8.1-in.^{2} throat area condition for 200 and 500 R choked line flows in Fig. 158. In the case of the

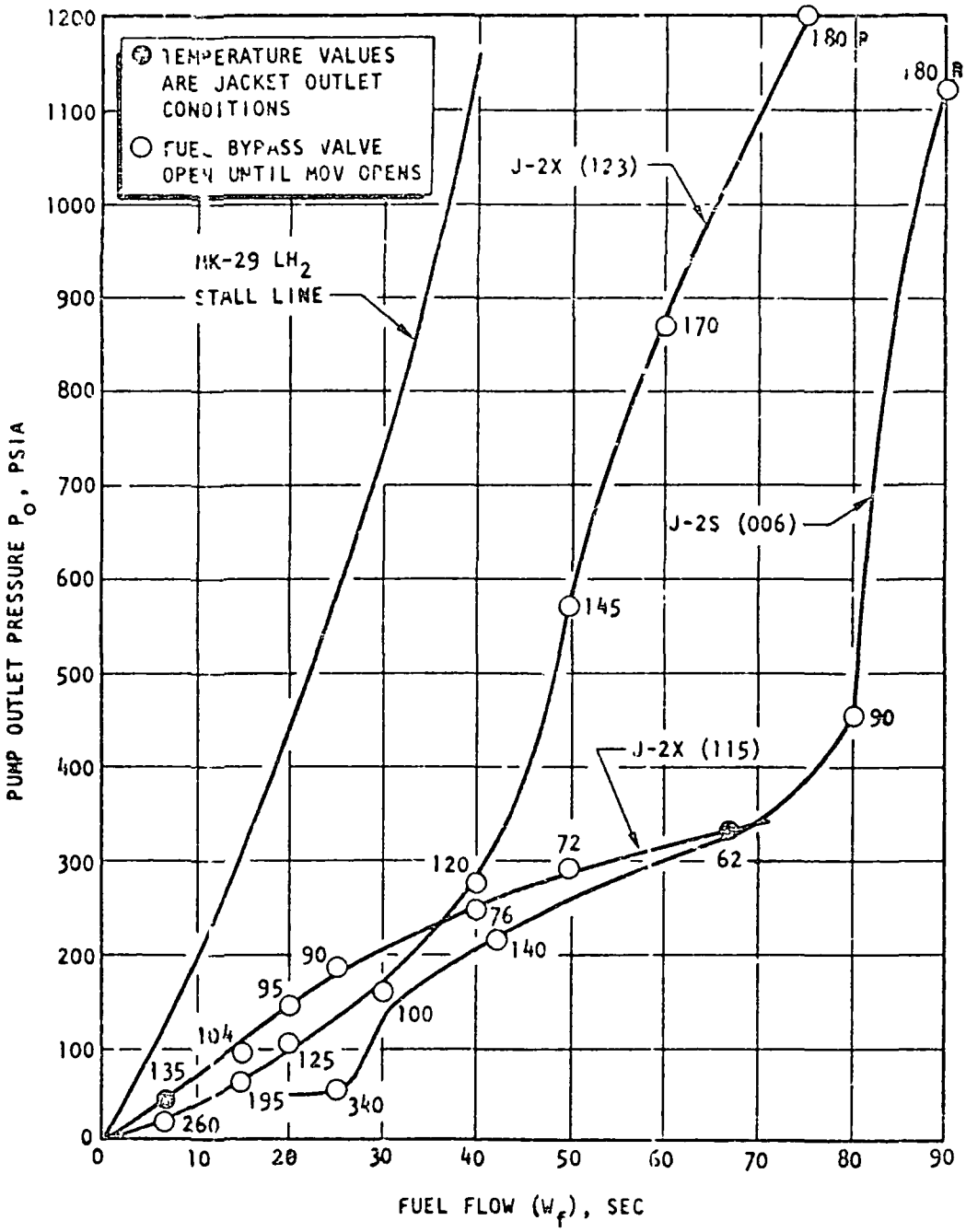

Figure 139. J-2S and J-2X Tests at Idle Mode Compared to Stall Line Conditions

bypass circuit testing, the equivalent flows must be established by a weighting of the areas through the bypass line and thrust chamber tubes. During the tests shown, no attempt was made to separate accurately the fuel flowrates through the bypass line and through the thrust chamber tubes during idle mode and transition. Tests with a reduction in the bypass line area from the present value coupled with a low mixture ratio idle-mode start would indicate the amount of thermal conditioning necessary for elimination of the bypass line during thrust chamber transient operation. The wide stall flow margin with respect to mainstage flowrate conditions for the Mark 29F fuel pump would appear (with possibly some thrust chamber coolant passage area enlargement) to allow a no stall start without bypass line and no thrust chamber chilldown.

The criteria of establishing a fuel pump chilled sufficiently to develop a favorable head flow line, coupled with a pump wide design stall margin, with as large a thrust chamber throat coolant passage area as feasible (with regard to operating tube life) appear to allow the possibility of engine start with little thrust chamber thermal conditioning.

Stall Line Considerations

The near parabolic behavior of the stall or surge line for the axial and centrifugal pumps, respectively, allows a definition of its behavior to be analytically prescribed approximately by the relation

$$P_s = K_s w_s^2 \qquad (79)$$

where K_s, P_s, and w_s are stall line constant, pressure, and flowrate, respectively. K_s values of the Mark 29F and the Mark 15F fuel pumps appear to be, respectively

$$K_s = 0.72 \quad (sec^2/in.^2\text{-}lb)$$

$$K_s = 0.37 \quad (sec^2/in.^2\text{-}lb)$$

Consideration of the thrust chamber and injector operating line for a compressible gas at a Mach number near one and a minimum throat coolant passage area A_{min} can be expressed by the relation:

$$\frac{\dot{w}}{A_{min}} \frac{\sqrt{T}}{P} = K(\gamma, M) \text{ (Compressible Gas)} \qquad (80)$$

The simultaneous solution of the above two relationships can be formulation. If it can be assumed that the thrust chamber flow and stagration pressure become

$$w = w_s$$

$$P = P_s$$

the solution becomes

$$P_s = T/k_q \left(K(\gamma, M)\right)^2 A_{min}^2 \qquad (81)$$

It can be shown as a result that the minimum area in the feed system downstream of the pump will strongly influence the stall pressure point with minimum areas resulting in a low-pressure stall point. A low fluid temperature, large area, or a large stall line constant k_q can be seen to result in either a lack of intersection of the stall line and the assumed compressible gas operating line or the occurrence of the stall condition at a low flow point where the condition can be overcome. Designs that allow a high stall constant k_q and wide flow stall margin at the design pressure point will inherently allow a greater system flexibility in regard to temperature conditioning and start ramp transients.

A sacrifice in the efficiency in the pump at the design operating point may appear to be necessary if a thermal conditioning problem is to be avoided under all circumstances since generally a reduced stall margin at the design point results in a higher pump efficiency.

The compressible gas equation combined with the assumed parabolic stall line at the design pressure results in the following relation in terms of the stall line flow w_s and chamber flow w_c.

$$\frac{\sqrt{T_c}}{K_s A_{min}} \quad \frac{w_c}{w_s^2} = k(\gamma, M) \tag{82}$$

Defining the stall flow margin at the design pressure point by Δw_s, as

$$\Delta w_s = F w_s \tag{83}$$

$$w_c = w_s + \Delta w_s = w_s (1 + F) \tag{84}$$

This becomes

$$\frac{1 + F}{w_s} = \frac{k(\gamma, M) k_s A_{min} P_c}{\sqrt{T_c}} \tag{85}$$

Combining with

$$(1 + F)^2 = \frac{k[(\gamma, M)]_D^2 k_s A_{min}^2 P_D}{T_D} \tag{86}$$

The above equation then represents the normal operating pressure point P_D. Substitution of Eq. 81 results in the stall pressure relative to the design pressure as:

$$\frac{P_s}{P_D} = \frac{1}{(1 + F)^2} \left(\frac{T_s}{T_D}\right) \frac{[k(\gamma, M)]_D^2}{[k(\gamma, M)]_s^2} \tag{87}$$

For the special case of near choking conditions and equal temperature values in the minimum area restriction, the allowable throttle ratio before stall becomes:

$$\frac{P_s}{P_D} = (T.R.) = \frac{1}{(1 + F)^2} \tag{88}$$

$$(T_s = T_D),\ K\ (\gamma,M)_D = K\ (\gamma,M)_s \qquad (89)$$

In actuality, during engine throttling, the resultant temperature in the cooling jacket will increase approximately to the 0.2 power of the pressure ratio. Consequently, this case will become for near equal Mach number conditons

$$\left(\frac{P_s}{P_D}\right) = \frac{1}{(1+F)^{5/3}} \qquad (90)$$

which shows a reduced capability for throttling. Figure 160 illustrates the latter two relationships. The chilldown case can be compared by the assumption of an engine start with a heat input from the thrust chamber liner and body. If the start is attempted on a partially chilled thrust chamber condition, the heat input to the thrust chamber is composed of the sum of the gas-side heat input Q'_c and warm metal structure inputs to the hydrogen coolant Q'_w (with Q' terms of Btu/lb)

$$\frac{(Q'_c + Q'_w)_s}{(Q'_c)_D} = \frac{(\Delta H_s)}{(\Delta H_D)} \approx \frac{(T_s)}{(T_D)} \qquad (91)$$

The above R.H.S. approximation holds only if the H_2 coolant temperature is significantly above the base temperature of 36 R (i.e., 200 to 500 R). With an assumption of a startup in a condition with heat input to the coolant from both the gas side and metal structure, Eq. 88 can be written as (for equal flow Mach numbers)

$$\left(\frac{P_s}{P_D}\right) \approx \frac{1}{(1+F)^2}\left[\frac{(Q'_c + Q'_w)_s}{(Q'_c)_D}\right] \qquad (92)$$

Reduction of the value of $(Q'_c + Q'_w)$ during the early powered portion of the turbopump spinup can be accomplished by:

1. Low mixture ratio (low Q'_c)
2. Low wall heat input (low Q'_w)

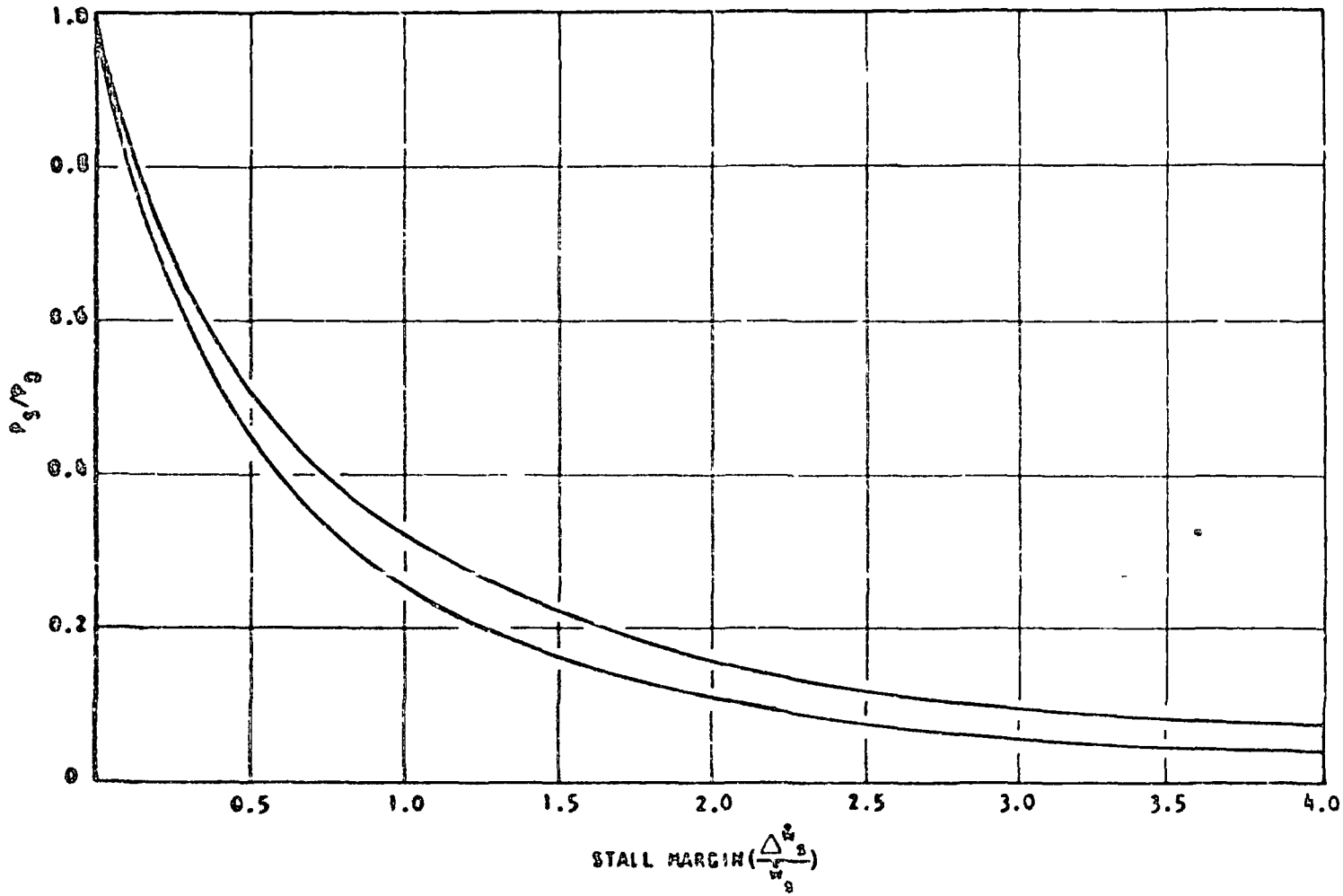

Figure 160. Stall to Design Pressure vs Stall Margin at Design Assumed Parabolic Stall Line ($P = h_s \sigma_s^2$)

The latter can be accomplished by a chilldown of the thrust chamber during idle-mode blowdown Minimization or elimination o' the stall problem on startup and the elimination of extensive idle mode or thrust chamber chilldown would appear to be best accomplished by the w dest possible stall margin (F) at the design point. This will allow the greatest engine system flexibility. Thrust chamber design changes which can contribute to a better design with possible elimination of thrust chamber bypass operation and restrictive start transients should be examined further during future study

J-2 and J-2X Thrust Chamber Test
Chilldown Characteristics

A review of AS-20x data with a J-2 engine configuration, and J-2X testing for test runs 113 and 123 were made to establish the thrust chamber chilldown characteristics with idle-mode starts with and w. hout heat input from combustion at low mixture ratio idle-mode conditions.

J-2 Flight AS-203 Data from this flight was reduced for the S-IVB stage with regard to the temperatures in the injector on the H_2 fuel side. For the 8 lb/sec chilldown flow, the bulk injector manifold temperature measurement (C200) is shown in Fig. 101 It is seen that at this flowrate the initial maximum coolant temperature is approximately 300 R At the end of a 6 5-second period, the coolant temperature has reduced to the pump discharge value of approximately 40 R For a 6 5-second cooldown period, approximately 5- pounds of LH_2 were utilized with a tank pressure of 24 psia providing an 8 lb/sec flow through an already prechilled pump.

Figure 102 illustrates the heat removal rate and integral of heat removal based on the thrust chamber nominal flow and temperature measurements. It is shown that the peak heat removal rate was 7500 Btu - and the total integrated heat rate was 31,000 Btu after a 6,5-second period. The heat rejection per pound of H_2 is shown in Fig. 103. A maximum of 910 Btu lb is shown to be input to the H_2 coolant

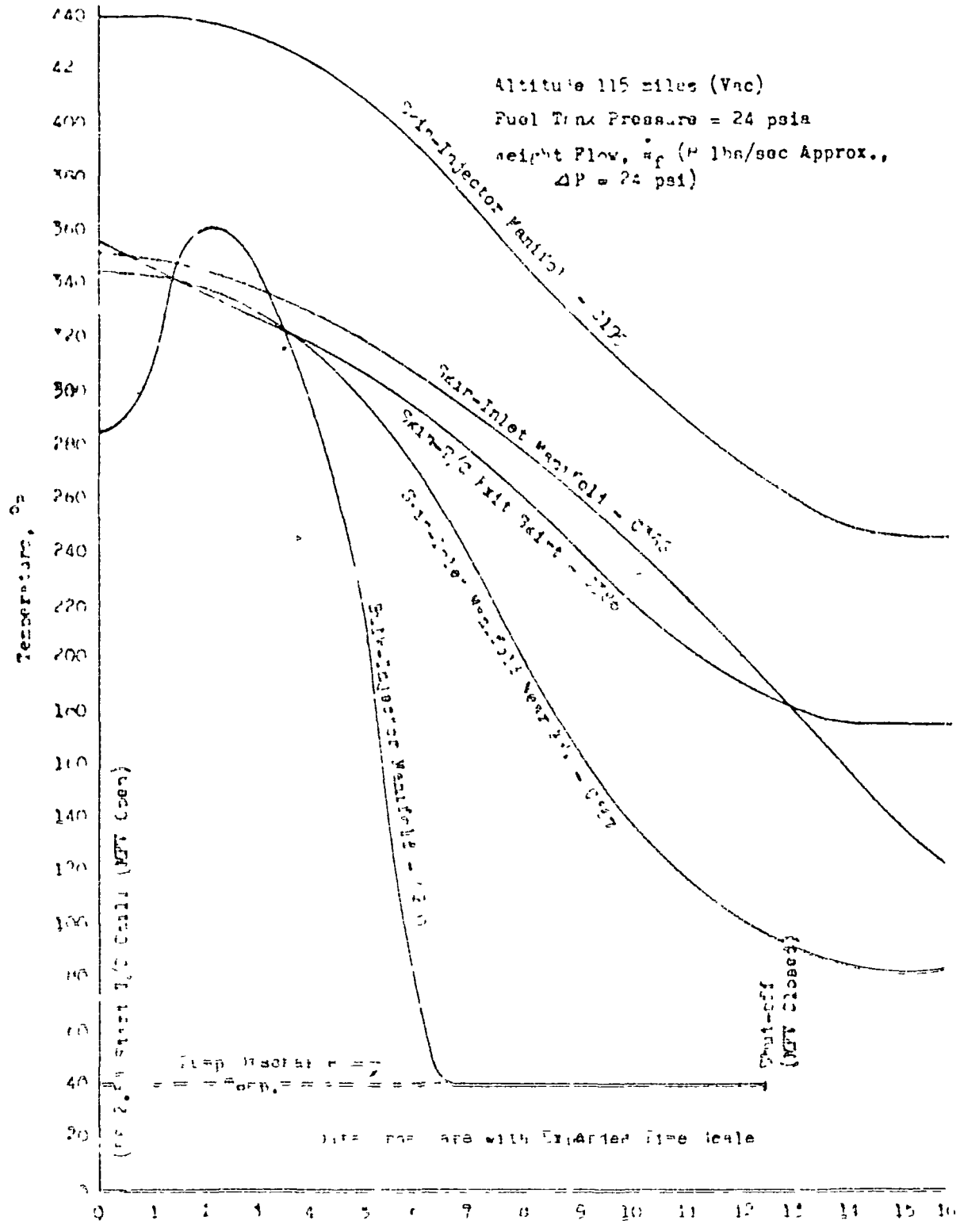

Figure 161 I-2119-A-20 Fuel Lead Experiment Peak Heat Shield (Run 1 No. 1 Ignition)

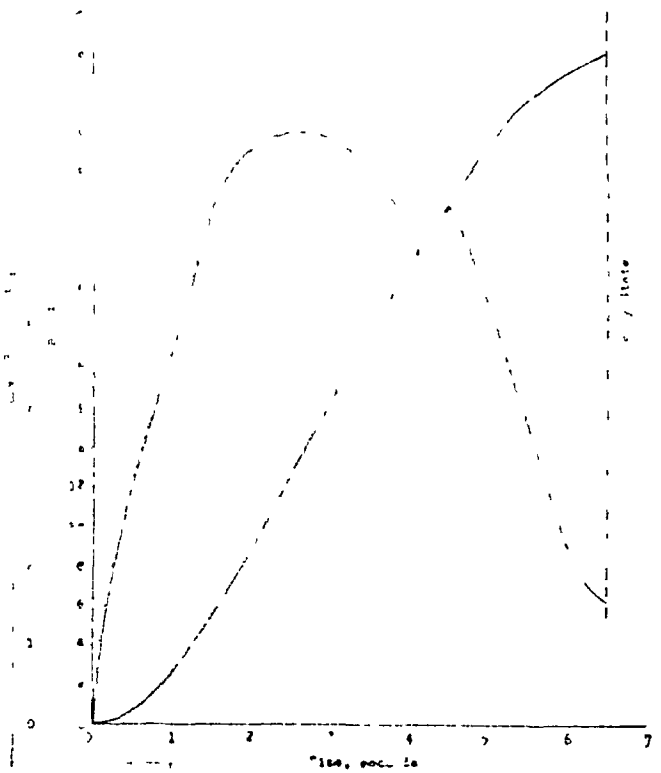

Figure 162 J-2019-AS203 Heat Rejection Rates vs Time

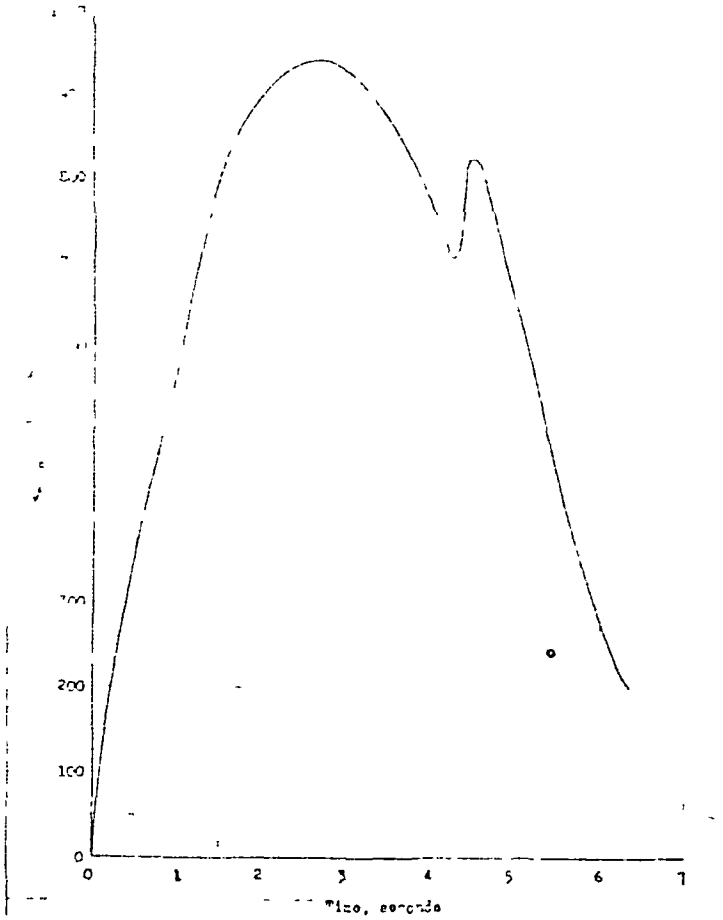

Figure 163 J-2019-AS203 Heat Rejection per Pound to Thrust Chamber Coolant

Higher tank pressures would result in a commensurately shorter chilldown period, but no data are available with flight engine system conditions A simultaneous chilling of the thrust chamber and pump with blowdown of 50 to 100 pounds of H_2 prior to start would appear to allow a substantial chill of the pump and thrust chamber H_2 wetted surfaces Pump chilldown tests indicated that a lower flow than 8 lb/sec would occur initially due to pump hydraulic resistance in the warm condition This would result in a lengthening out of the chilldown time period with perhaps a greater total LH_2 flow due to the extraction of a larger fraction of the pump and thrust chamber heat content.

J-2X Test 115 Idle-Mode Thrust Chamber Chilldown. Analysis of J-2X test 115 data was made to evaluate the chilldown of the thrust chamber during an idle-mode prestart For this test, the main fuel tank was pressurized to 40 psia. At time zero, both the J-2X bypass line and thrust chamber coolant jacket received a LH_2 coolant flow. Analysis of the heat rejection from the thrust chamber jacket was made assuming a flow split between the bypass line and the thrust chamber of 63 and 37 percent, respectively, proportioned according to the flow areas. Following pump chill, at the end of a 5-second period for test 115, the main oxidizer valve was opened 12 degrees to control mixture ratio and at 6 seconds pump start and chamber pressure buildup was initiated At 20 seconds, cutoff occurred with a chamber pressure of 234 psia. Figures 164 and 165 illustrate the data parameters for this test.

During the first 6 seconds of chilldown, a fuel flow of 6.2 lb/sec was obtained through the pump and thrust chamber system During this period, the main oxidizer valve was closed and a thrust chamber chilldown characteristic of the previously mentioned J-2 AS-203 flight was observed. The peak heat removal rate from the thrust chamber metal was 5000 Btu/sec with an integral heat pickup estimated at 18,000 Btu at the end of the 6-second initial period, as shown in Fig. 166 Figure 167 illustrates the heat rejection per pound of H_2. It is seen that the maximum structural heat input during the 0- to 5-second period overshadows the combined

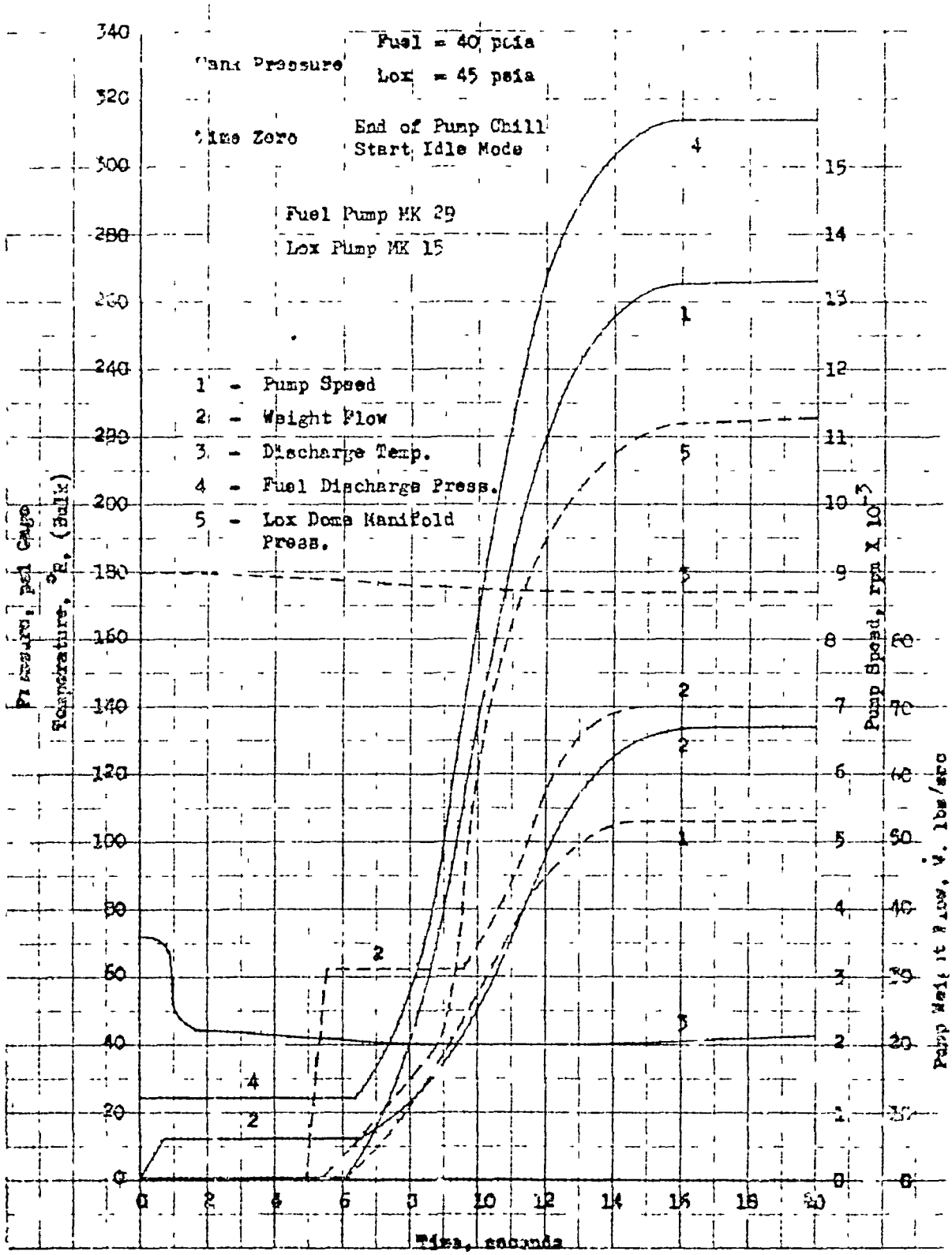

Figure 164. Test J-2X-115 Data Parameters Idle Mode and Tank Head Start

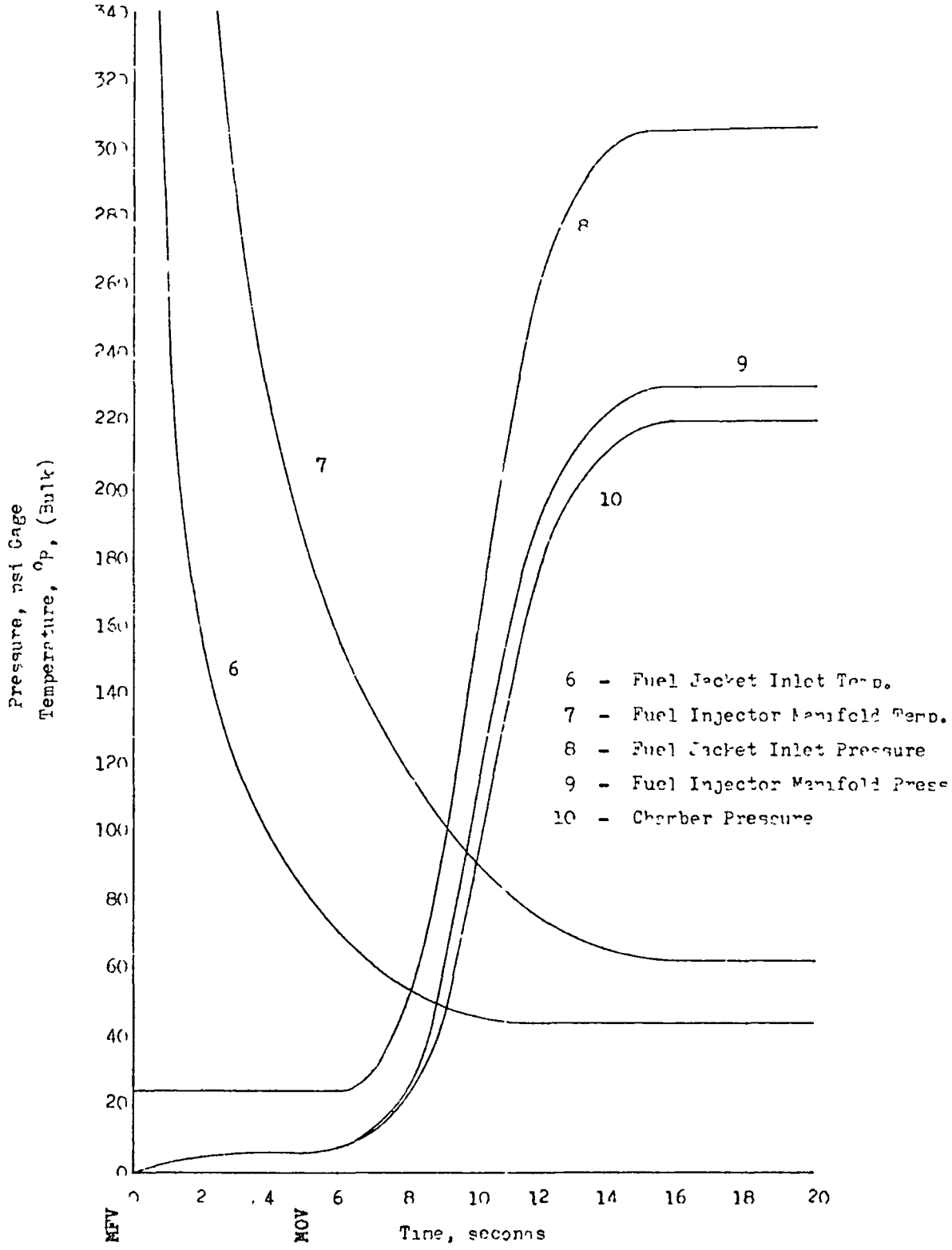

Figure 165. Test J-2X-115 Data Parameters (Engine Initial Temperature 480 F at Idle Mode Start

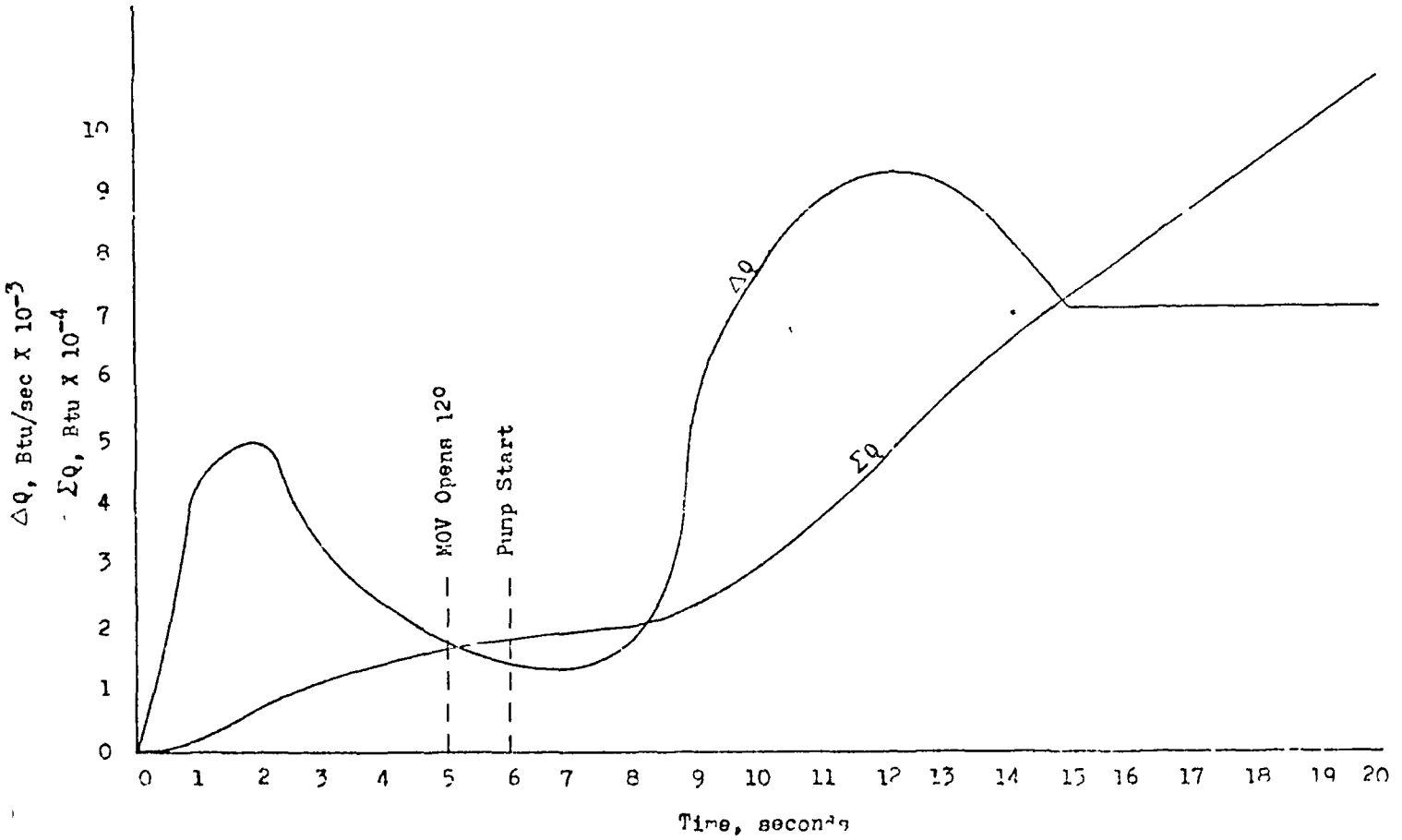

Figure 166. J-2X-115 Test Thrust Chamber Heat Rejection Rates vs Time

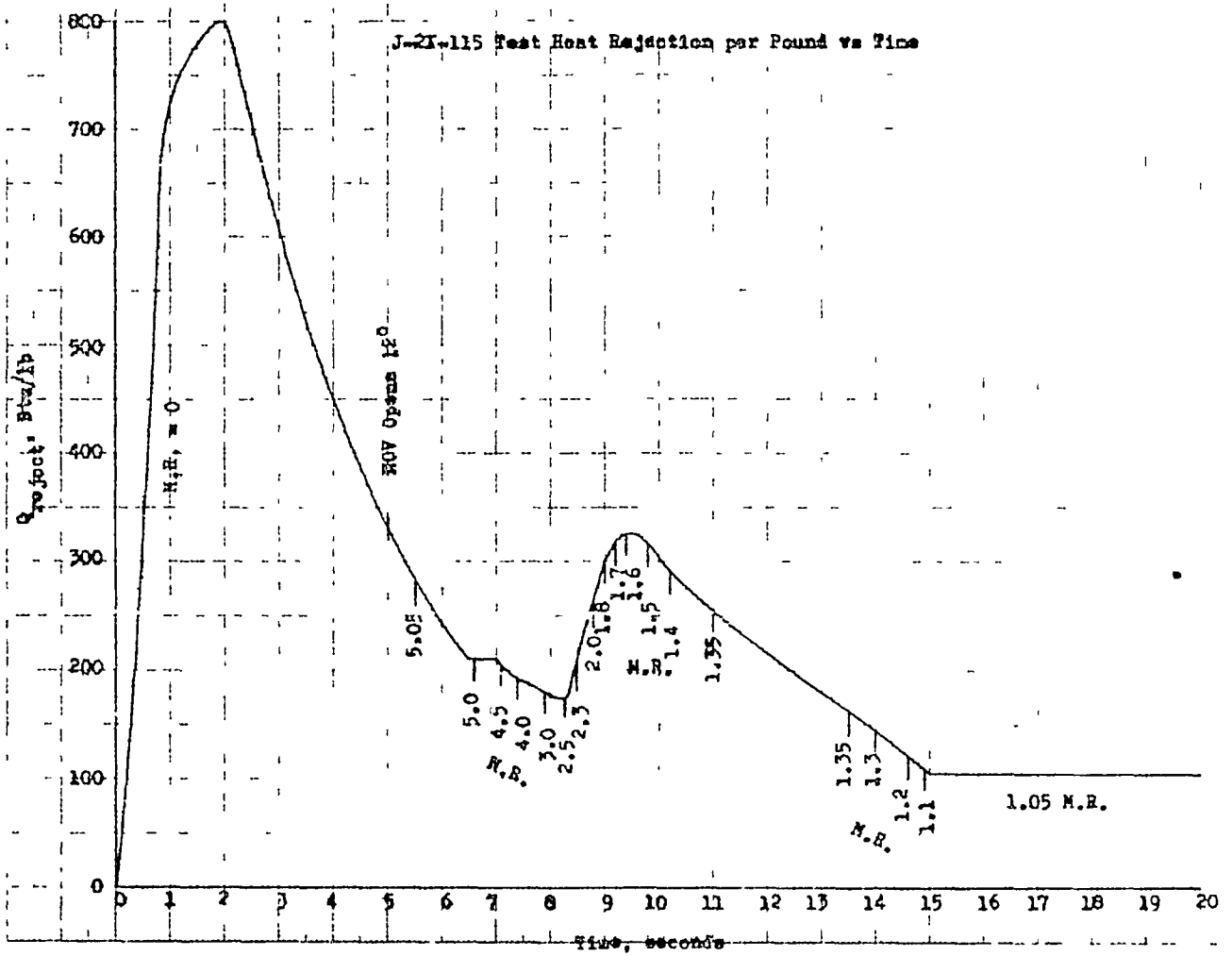

Figure 167. J-2X-115 Test Heat Rejection per Pound vs Time

combustion and residual structural heat input during the remainder of the test. The 800 Btu/lb maximum heat rejection rate compares favorably with that for the flight test AS-203.

J-2 Test 123 Idle-Mode Thrust Chamber Chilldown Figure 168 illustrates for test 123 similar behavior to test 115 except for an added combustion and a corresponding chamber pressure rise occurring at time zero. The main oxidizer valve is partly opened and the main fuel valve is opened with a 28-psia tank head at time zero At 6 seconds, as before, the pump ramp is initiated with a chamber pressure rise to 914 psia at the 20-second shutoff point. Figure 169 illustrates the heat input rate and accumulated heat input versus time from the combustion process and the main structure. The peak heating rate before pump start is 7600 Btu/sec, which is higher than for test 115 due to the combustion heat input during the first 6-second period. Hydrogen heat input per pound during the initial 6-second period reaches 1220 Btu/lb, which is substantially above the 800 Btu/lb value shown for test 115 (Fig. 170).

A comparison of the three tests in terms of heat input per pound of LH_2 is shown in Fig. 171. A higher heat input is shown for test 123 on the J-2X when compared with the Saturn flight data on the J-2 and also test 115 on the J-2X. An analysis of the component weights of the thrust chamber assembly was made on the J-2S engine and a calculation of the heat content in the thrust chamber above 40 R was made. At an 80 F test condition, a total heat content of 45,500 Btu is stored in the thrust chamber as shown in Fig. 172. Tests 115 and 123 of AS-203 at the end of a 6.5-second chill show accumulated heat inputs absorbed by the H_2 coolant to be 34,000 (J-2), 18,000, and 40,000 Btu, respectively. It would be expected that test 123 would show a higher heat input due to the combustion occurring during this initial period.

A comparison of the component chilldown testing results on the Mark 15 LH_2 turbopump showed an analytical heat content of 8950 Btu with accumulated heat contents removed the LH_2 chill during chilldown testing

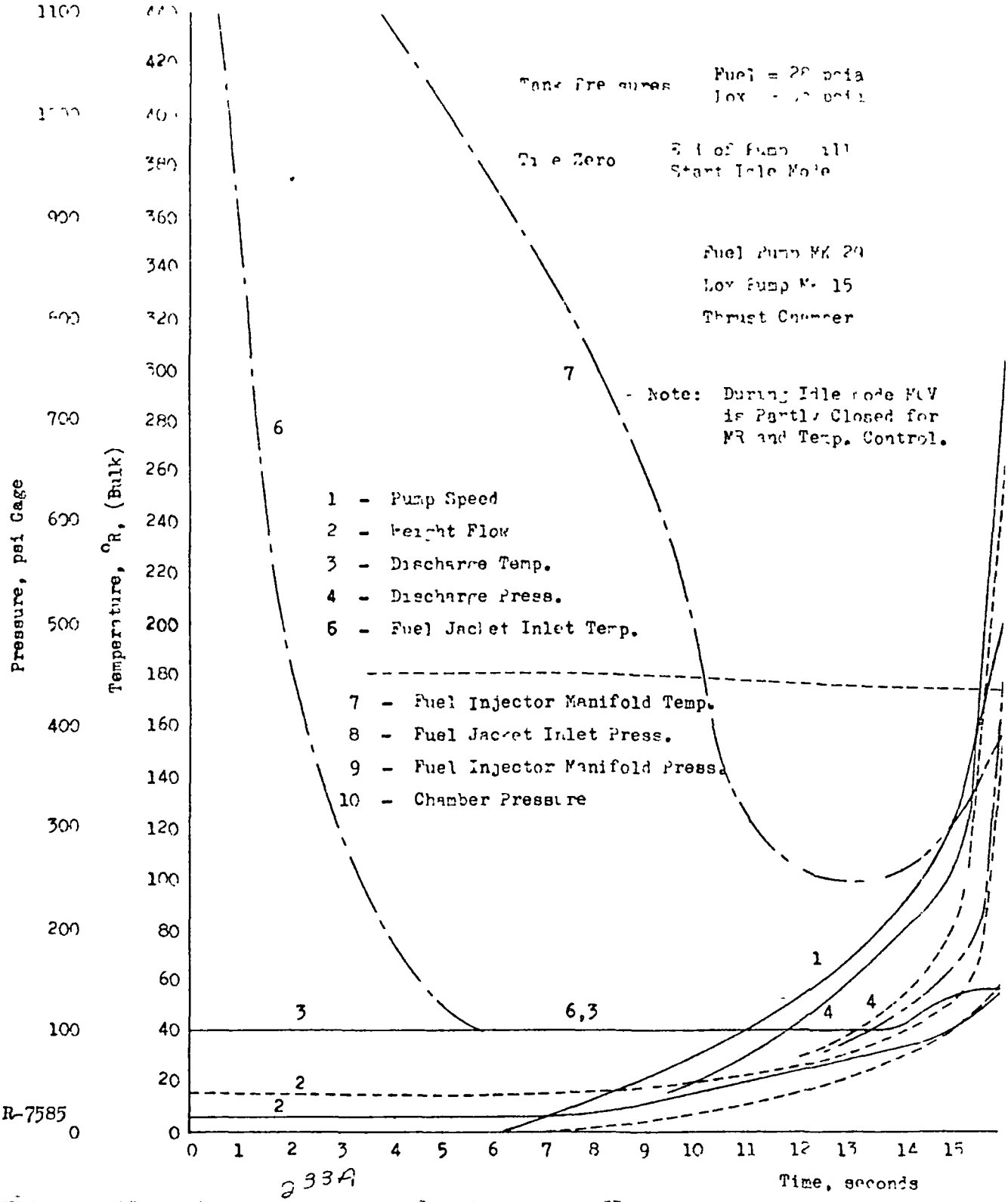
Tank Pressures
Time Zero
Fuel Pump MK 29
Lox Pump MK 15
Thrust Chamber
Note: During Idle mode MFV is Partly Closed for MR and Temp. Control.
1 - Pump Speed
2 - Weight Flow
3 - Discharge Temp.
4 - Discharge Press.
6 - Fuel Jacket Inlet Temp.
7 - Fuel Injector Manifold Temp.
8 - Fuel Jacket Inlet Press.
9 - Fuel Injector Manifold Press.
10 - Chamber Pressure
Pressure, psi Gage
Temperature, °R, (Bulk)
Time, seconds
R-7585
233A

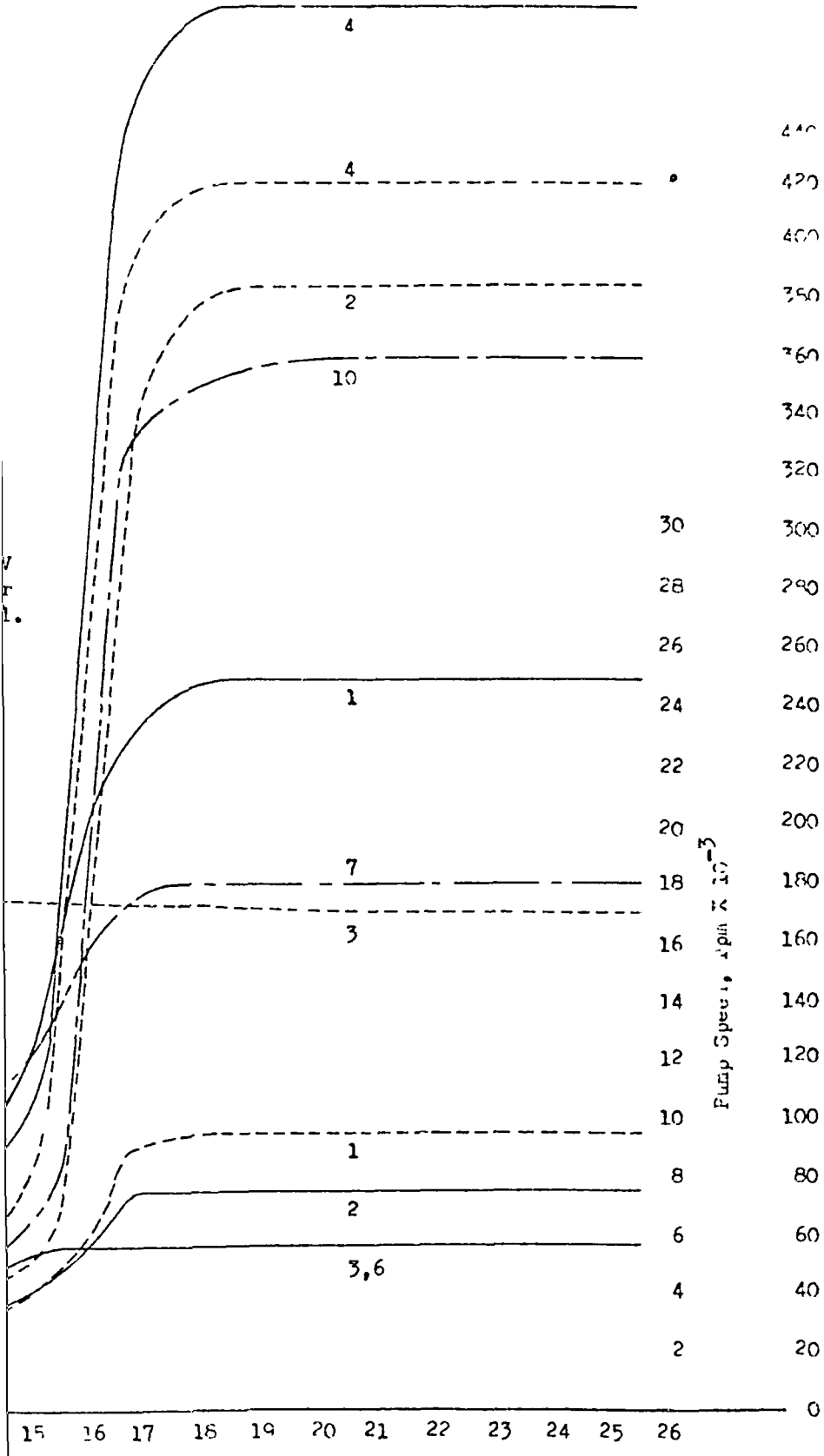

Figure 168. Test J-2X-123 Data Parameters

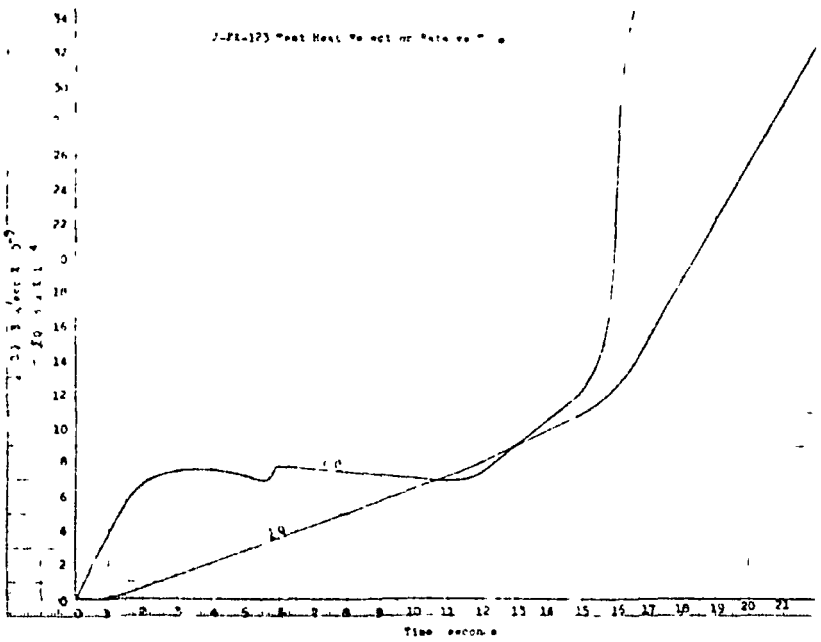

Figure 169 J-2X-123 Test Heat Rejection Rate vs Time

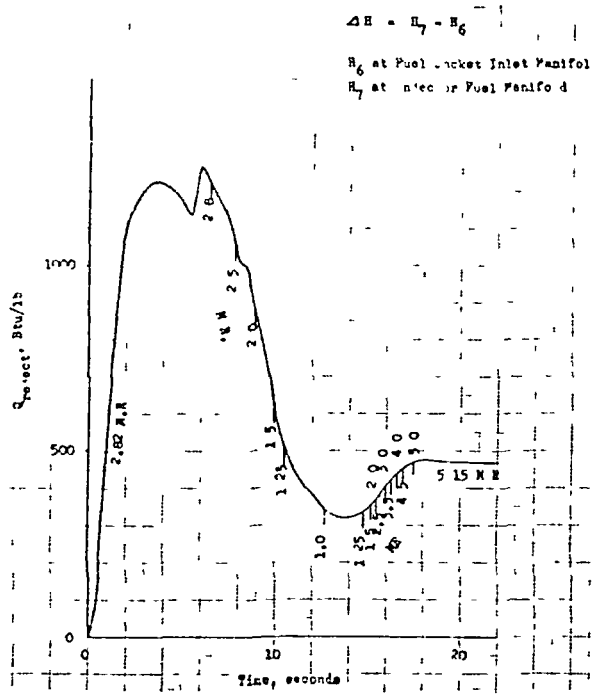

Figure 170. J-2X-123 Test Heat Rejection Rate vs Time

Figure 171 Comparison of Thrust Chamber Rejection Rates

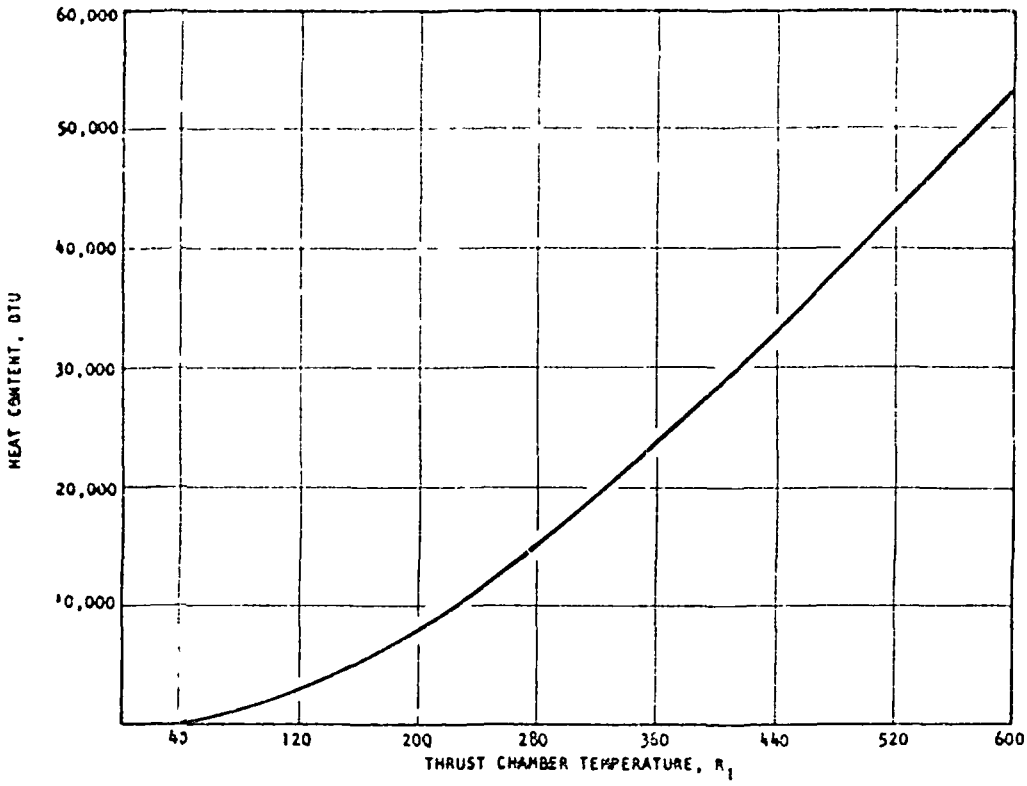

Figure 172 Thrust Chamber Heat Content Above 40 R (J-2S)

amount to 57 to 71 percent of the stored heat content. This percentage compares favorably with a 75-percent value for the thrust chamber on test 115 J-2X. It is seen that at the comparatively high flowrate for the thrust chamber (7 percent of mainstage fuel flow), the heat content in the interior parts of the metal walls and manifolds is unavailable to the cooled surface for a short chilldown period.

J-2 Flight AS-501. The available data from this flight were reduced and plotted on Fig. 173 and 174. Figure 173 shows the predicted and actual accumulated H_2 gaseous flow versus time during the coast period of the S-IVB Saturn V flight. The actual quantity of H_2, if passed through the pump and thrust chamber, is more than sufficient to chill the engine system for engine startup.

Figure 174 is a plot of temperature of various locations of the turbine versus time during the coast period. This figure shows how the warm turbine parts loose heat through conduction to the pump and through radiation to the atmosphere. The temperature nearly reach steady state after 5000 seconds of coast period. For example, it is seen that the crossover duct temperature drops from 600 F to 50 F in 5000 seconds and drops from 50 F to 0 F in another 5000 seconds.

HEAT SOAKBACK ANALYSIS

Theoretical Heat Soakback Analysis

The heat transfer analysis of the J-2X Mark 29, 1- /2 stage, LH_2 pump was made on the basis of the nodal point distribution shown for the pump in Fig. 175. For the heat soakback analysis made, the initial temperature distribution assumed, the relative component weight ratios used, and the inlet gas temperature assumed were all based on J-2 turbopump performance data. Figure 176 shows the nodal distribution and the initial temperature of each node within the pump. The different materials involved were kept isolated, when possible, and temperature-dependent physical property

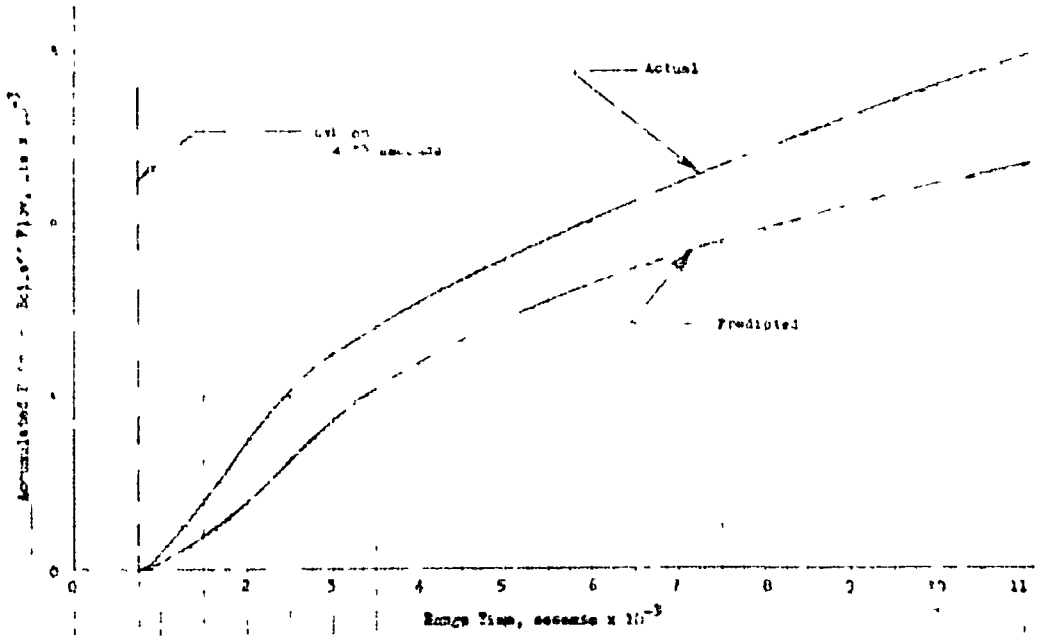

Figure 173. Accumulated Hydrogen Boiloff Flow vs Time During the Coast Period of the S-IVB-Saturn V Flight, AS-501

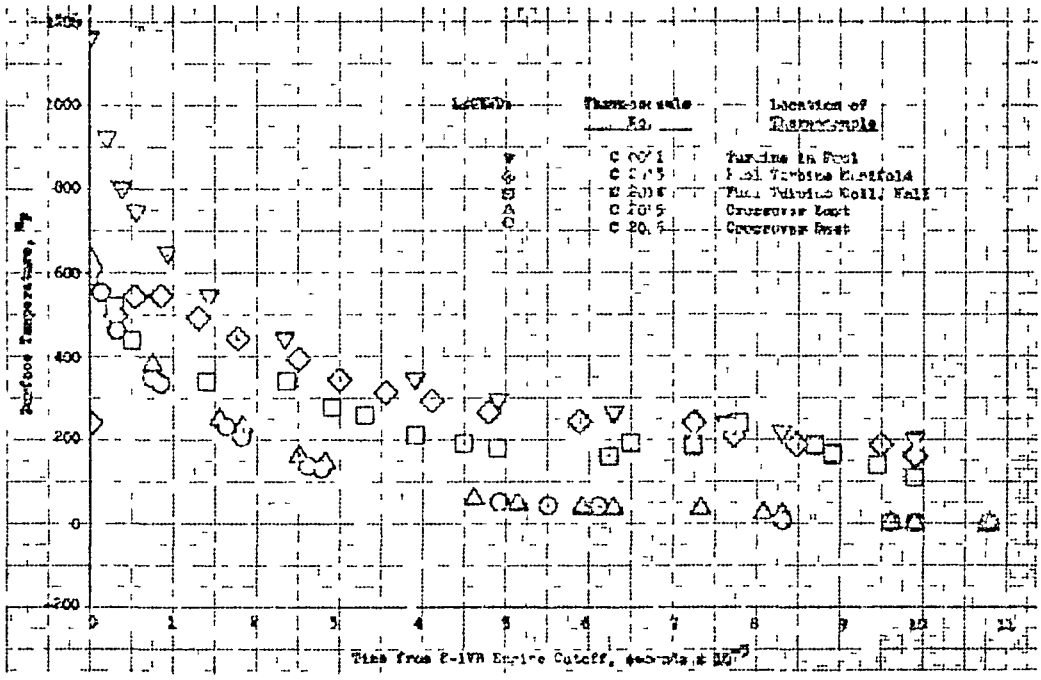

Figure 174. Surface Temperature vs Time From S-IVB Engine Cutoff for Various Parts of the Fuel Turbine and Manifolds, AS-501

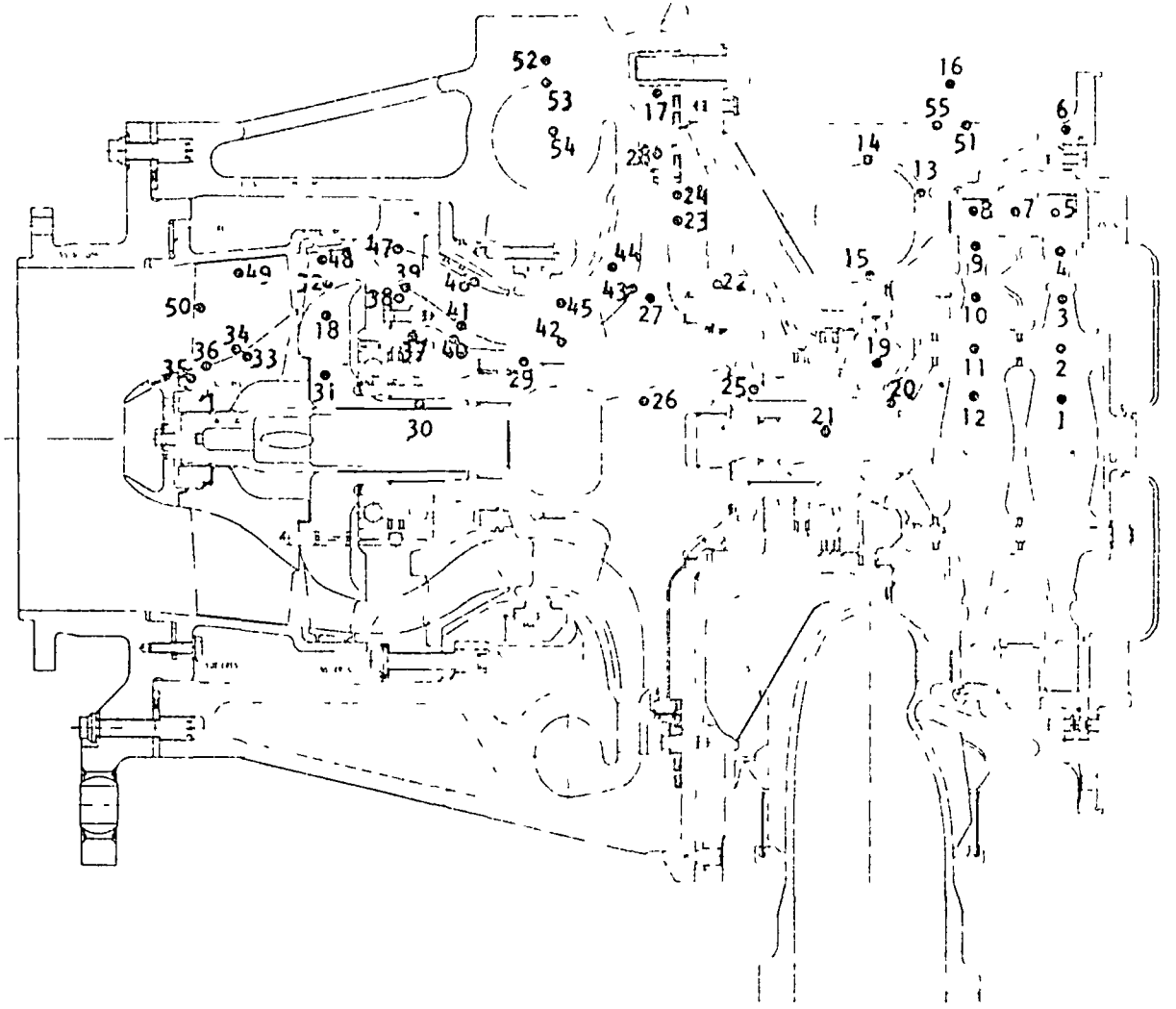

Figure 175. Mark 29 Single-Stage Liquid Hydrogen Turbopump Nodal Point Distribution

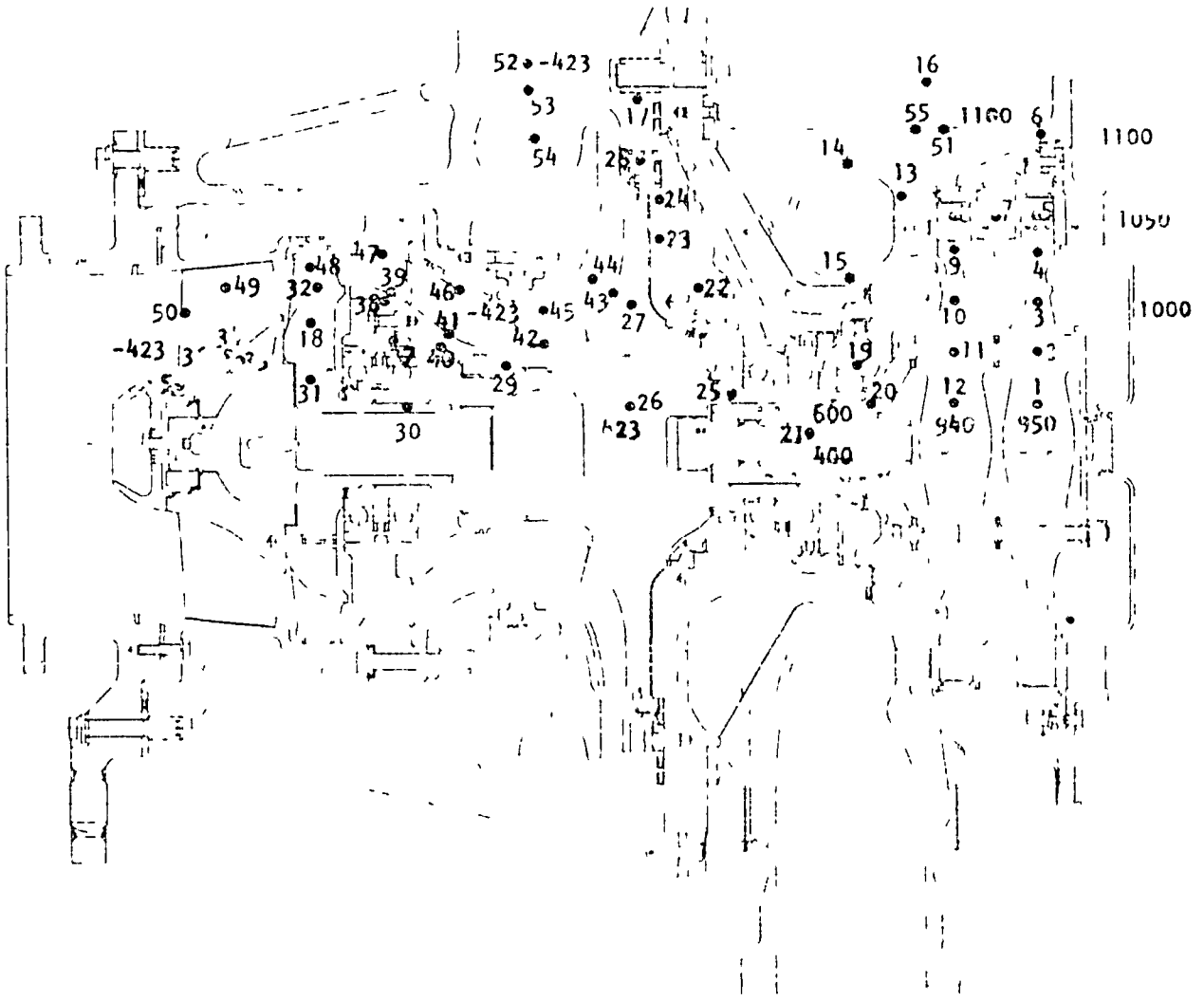

Figure 17. Mark 29 Single-Stage Liquid Hydrogen Turbopump Nodal Point Distribution and the Temperature of the Nodes Immediately After Engine Shutdown (Heat Soakback Time = 0)

tables for each material were used. Where the isolation of the materials appeared impractical due to creating very small volume (this increases the computer machine time) two or more materials were lumped into one node and their weighted average properties were used.

The thermal analyzer program described in Ref. 1 was utilized for the heat soakback analysis that was carried out for a duration of 12 hours (Fig. 177). Figure 177 indicates that after 12 hours some heat soakback is still in progress. If sufficient time is allowed between engine firings, the temperature throughout the turbopump will reach an equilibrium temperature estimated to be about 60 to 70 degrees.

Figure 178 shows the temperature distribution of the nodes after 3 hours of heat soakback. It is seen that the temperature of the turbine wheel and turbine housing is decreasing while the temperature of the impeller and inducer is increasing. Also, it was assumed that heat is lost from the turbine housing to its surroundings by means of radiation. Node 55 of Fig. 178 is the surface node and is radiating to the node 16, which was assumed to be a constant-temperature heat sink node.

Mark 29 LH_2 Turbopump Test Data

The thermocouple locations in the rear support of the Mark 29 LH_2 turbopump is shown on Fig. 179. These thermocouples were located in the rear support (turbine end) to measure the temperature distribution in this region to determine the associated thermal stresses involved. The temperature-time history of the rear support was the objective of these tests for the stress analyses. Therefore, the thermocouples were located in the rear support region of the turbopump (Fig. 179). The data pertain to a chilldown period, a test run period, and a heat soakback period. After the pump is chilled sufficiently, the flow resistance of the pump is determined for both locked and free rotor. The LH_2 flows through the pump because of the difference in the tank pressure and the pump downstream pressure. The pressure drop across the pump is measured during these

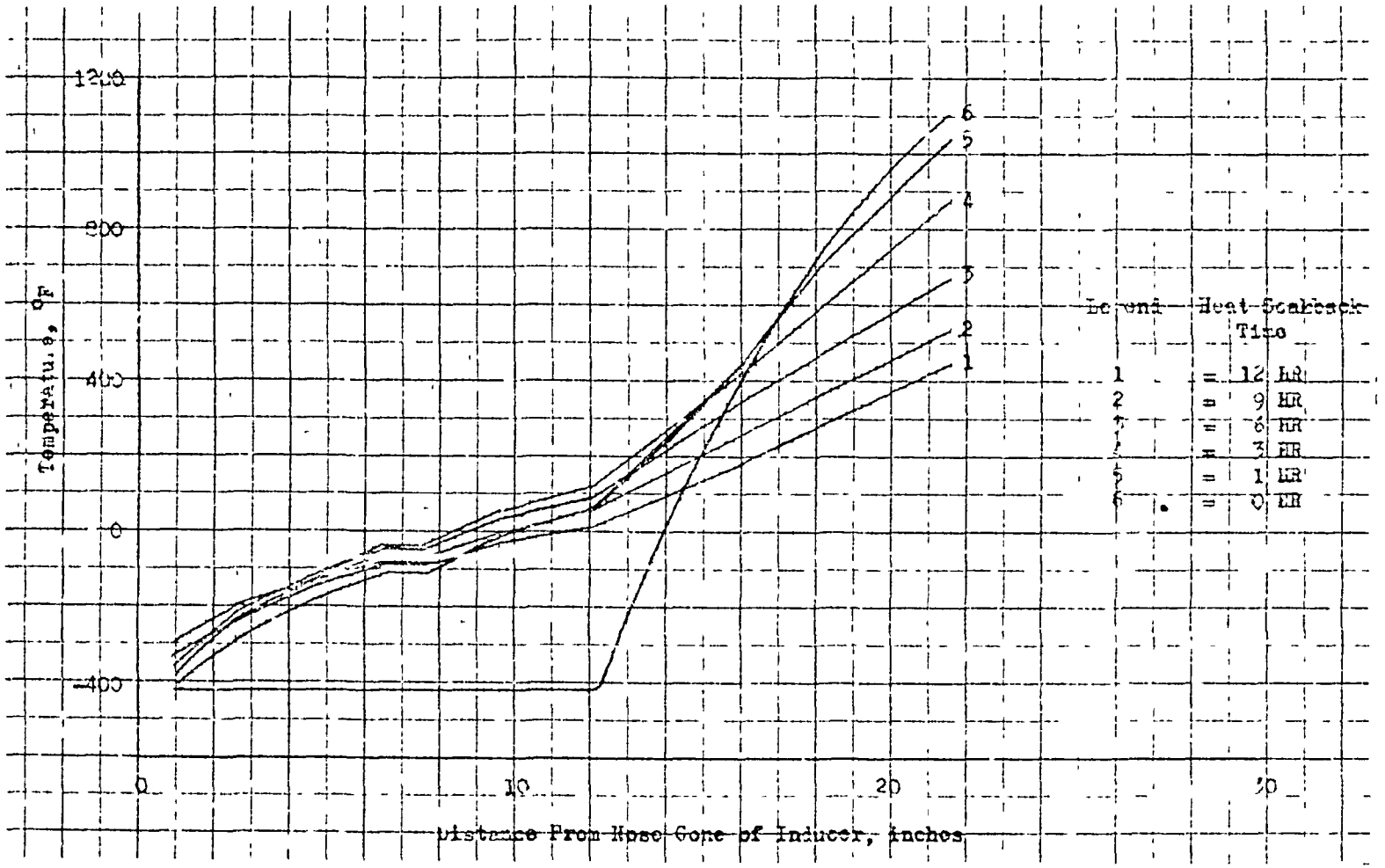

Figure 177 Mark 29 J-2 Hydrogen Turbopump Average Internal Temperature Distribution During Heat Soakback

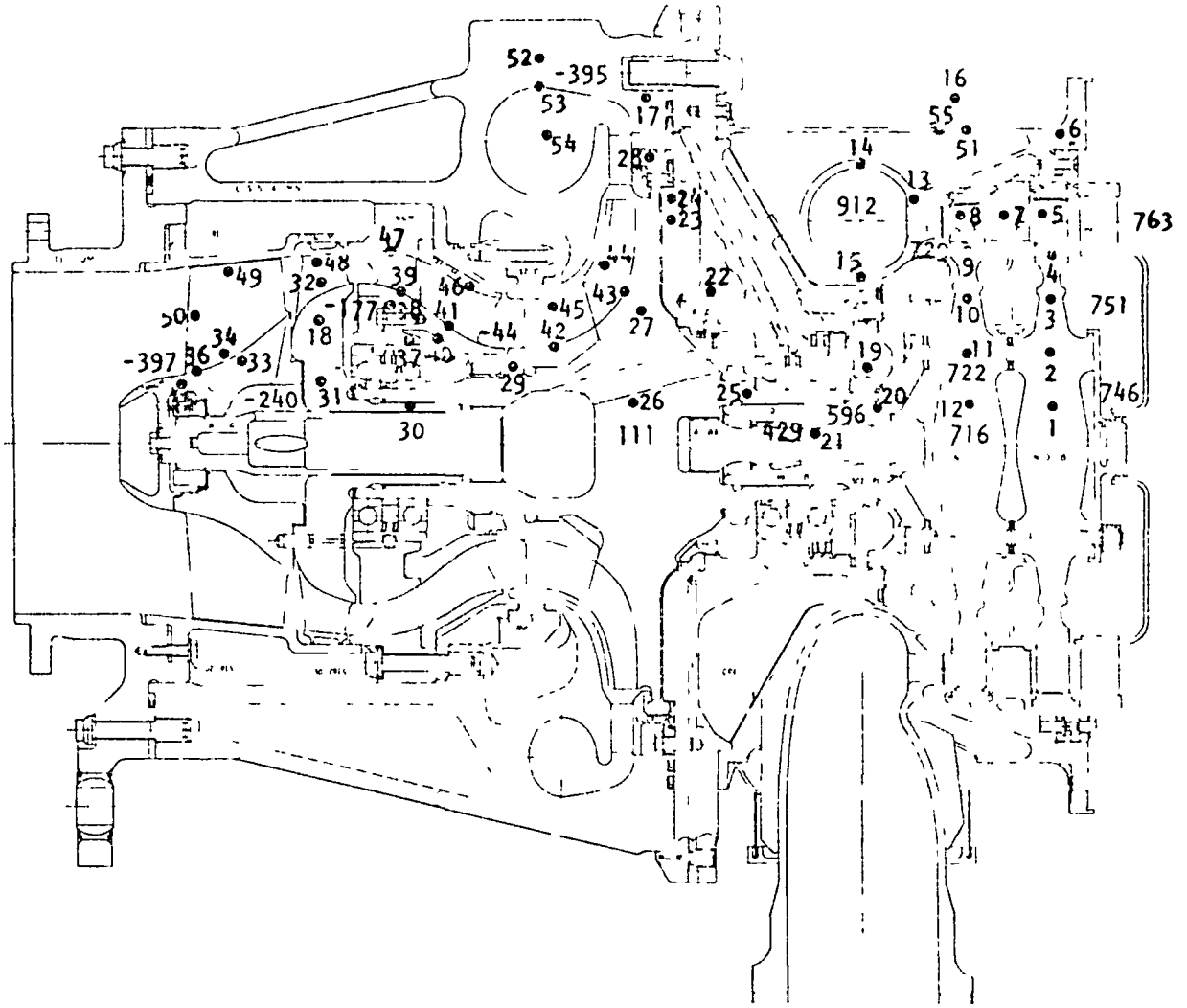

Figure 178 Mark 29 Single-Stage Liquid Hydrogen Turbopump Nodal Point Distribution and the Temperature of the Nodes After 3 Hours of Heat Soakback

SPECIAL THERMOCOUPLE MEASUREMENTS
ON MARK 29F TURBOPUMP P003-1

(6) Rear Support Skin No. 1 at 6.625 Inches in Radius
(7) Rear Support Skin No 2 at 5.875 Inches in Radius
(8) Rear Support Skin No. 3 at 4.125 Inches in Radius
(9) Rear Support Skin No 4 at 3.125 Inches in Radius
(10) Rear Support Skin No 5 at 3.50 Inches in Radius
(11) Seal Cavity Wall at 2.95 Inches in Radius
(12) Seal Cavity—Mid Cavity
(13) Turbine Manifold Shroud

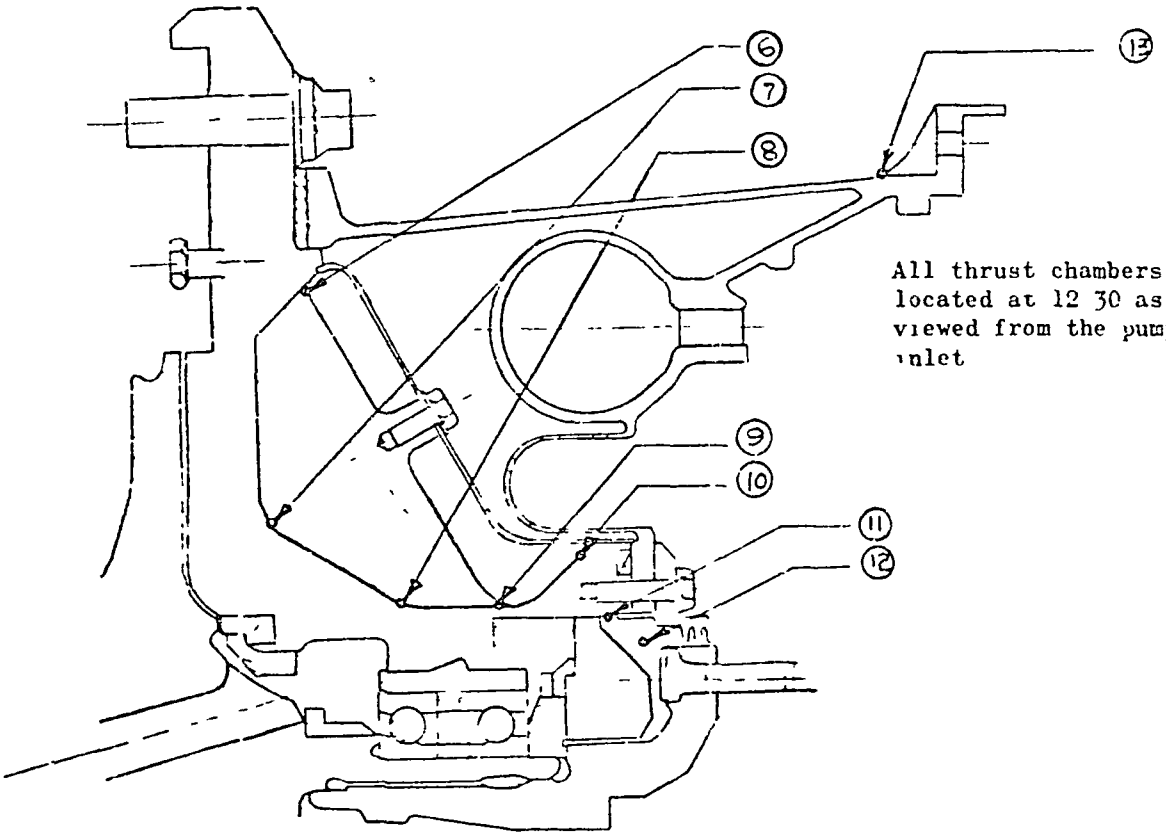

Figure 179. Position of the Thermocouples in the Rear Support of the Mark 29 Turbopump

tests. Figure 143 is a plot of LH_2 mass flowrate through the pump versus the pressure drop across the pump.

The flowrate through the pump is not measured during the chilldown process. The best estimate of the pressure drop across the pump during the chilldown period is about 4 psi. Therefore, the LH_2 flowrate can be predicted (from Fig. 143) to be about 2.2 lb/sec. This is about 2.4 percent of the total flow at full stage

Figure 180 depicts the variation of the temperature as a function of time as measured during the chilldown time. The theoretically predicted temperature of node 23 of Fig. 174 is also plotted on Fig. 180 for comparison purposes. Since the theoretical chilldown study was conducted for 0, 1.44, and 5 percent of total flow, the temperature of node 23 was interpolated between 1.44 and 5 percent to correspond with the 2.4 percent of the experimental value. The analytical chilldown study was carried out for a duration of 180 seconds, which is not sufficient for comparison with experimental results. However, at the end of 180 seconds, certain discrepancies exist between the two. The experimental results indicate a temperature drop of about 20 F whereas the analytical result shows a temperature drop of about 2 F. This difference could be attributed to:

1. Wrong LH_2 heat transfer coefficient prediction
2. Error in estimation of the LH_2 flow through the pump during experiment

In the analytical studies, however, it was assumed that no heat is transferred to the LH_2 trapped between the impeller and the rear support. This assumption may not be valid. In future theoretical analyses, attempts will be made to determine the nature of heat transfer in this region. Figure 181 shows the temperature variation with time as measured by the thermocouples during a hot test run. No analytical studies were carried out for this case.

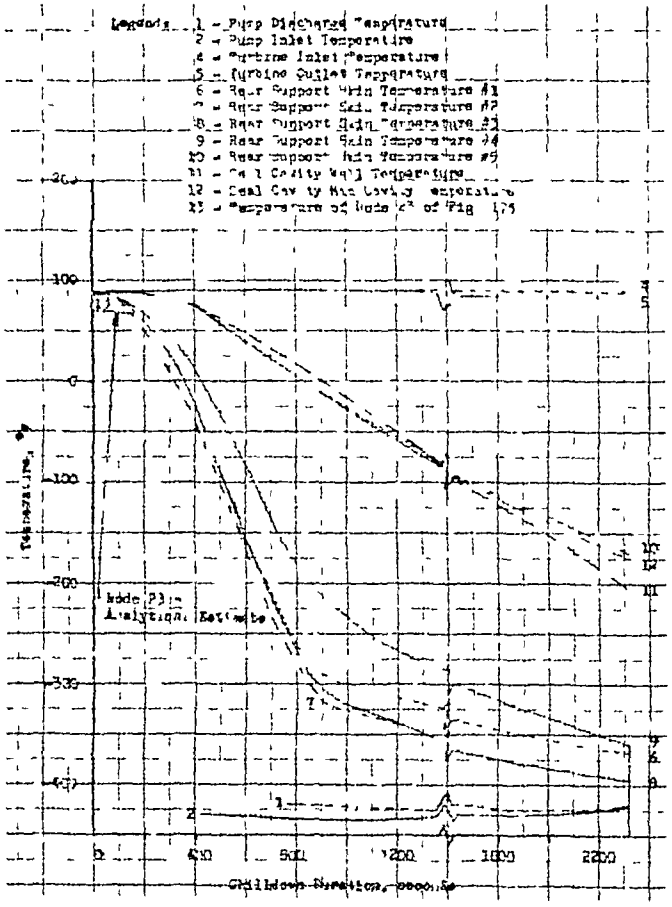

Figure 180. Temperature vs Chilldown Duration for Mark 29 LH_2 Turbopump Rear Support

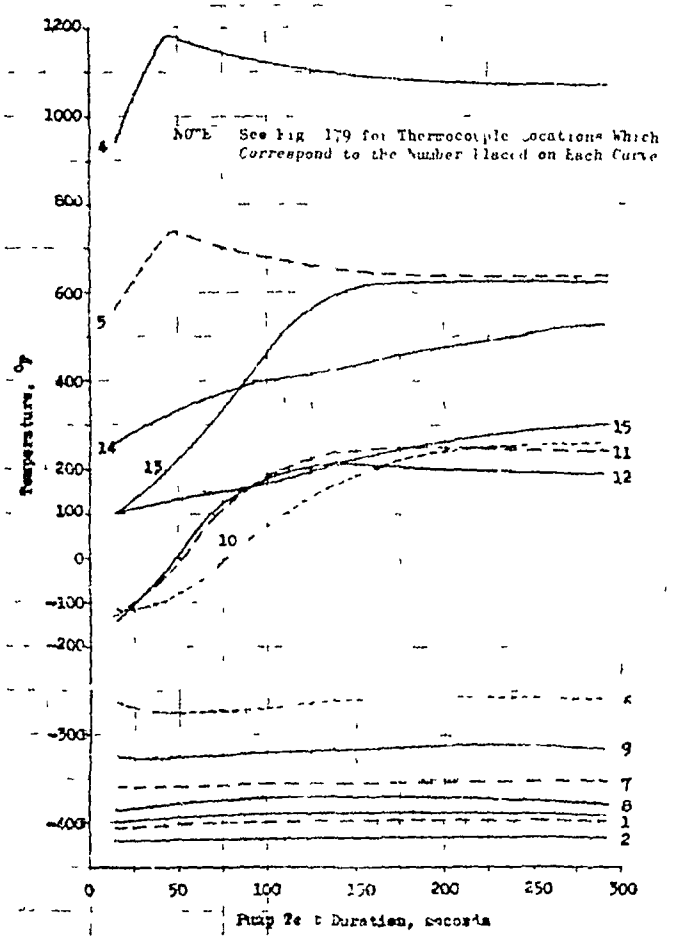

Figure 181. Temperature vs Pump Test Duration for Mark 29 LH_2 Turbopump Rear Support

Figure 181 shows the heat soakback temperature, as a function of time as recorded by the thermocouples located in the rear support region. Also, the temperature variation of node 23 (Fig. 175) is plotted in Fig. 182. It is seen that the temperature of node 23 (curve number 15) does not increase as rapidly as nodes 6 and 7 of (experimental data). This difference is due to difficulties involved in defining the exact heat flow path and the conductances for the analytical model. Additional thermocouples (Fig. 183) were installed in the pump end portion of a Mark 29 test turbopump (S/N 0003-2). A satellite test request to obtain heat transfer chilldown and soakback data was completed but this test program was cancelled, thereby preventing the acquisition of additional data for comparison with the completed analytical analysis.

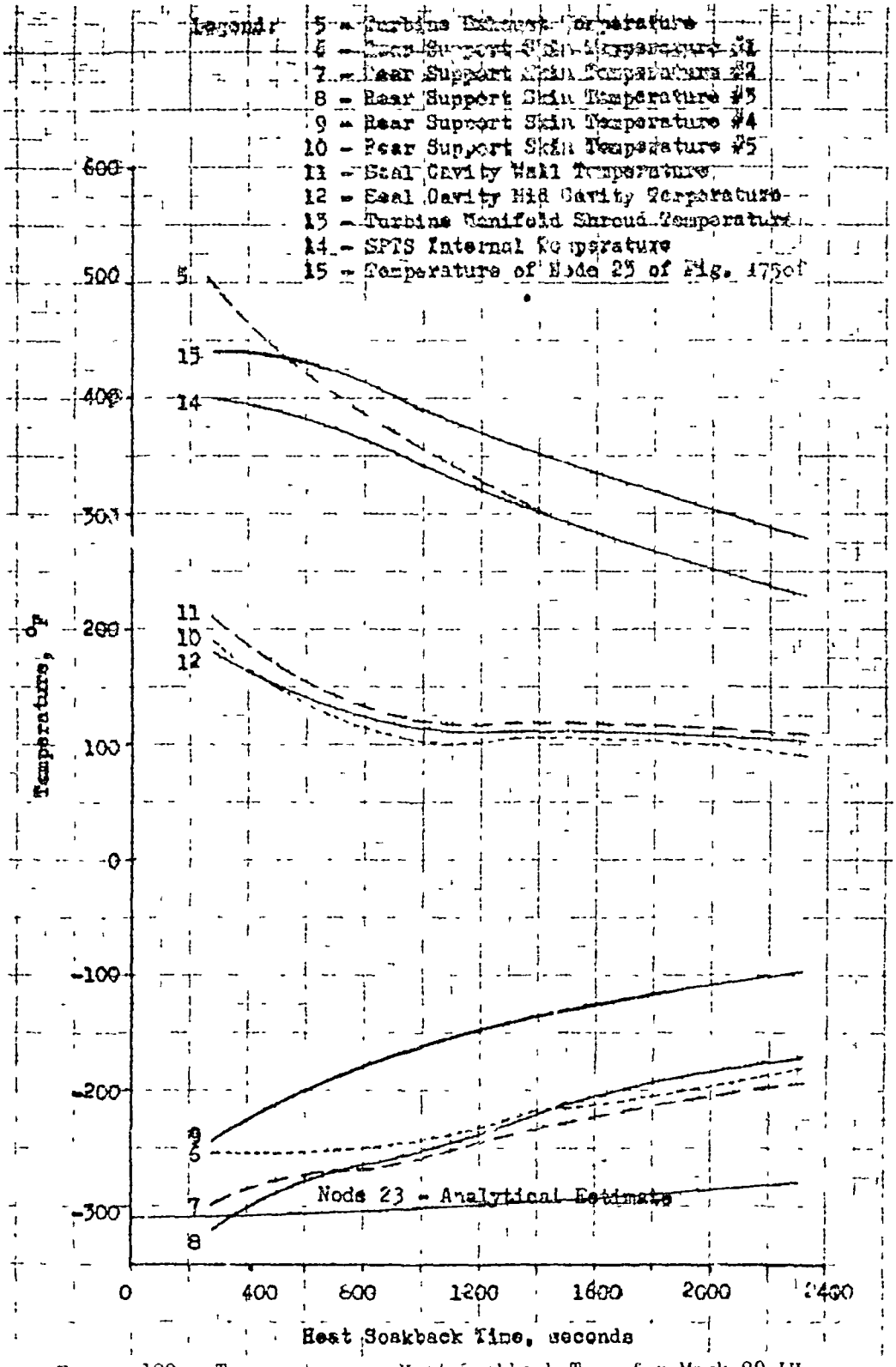

Figure 182 Temperature vs Heat Soakback Time for Mark 29 LH_2 Turbopump Rear Support

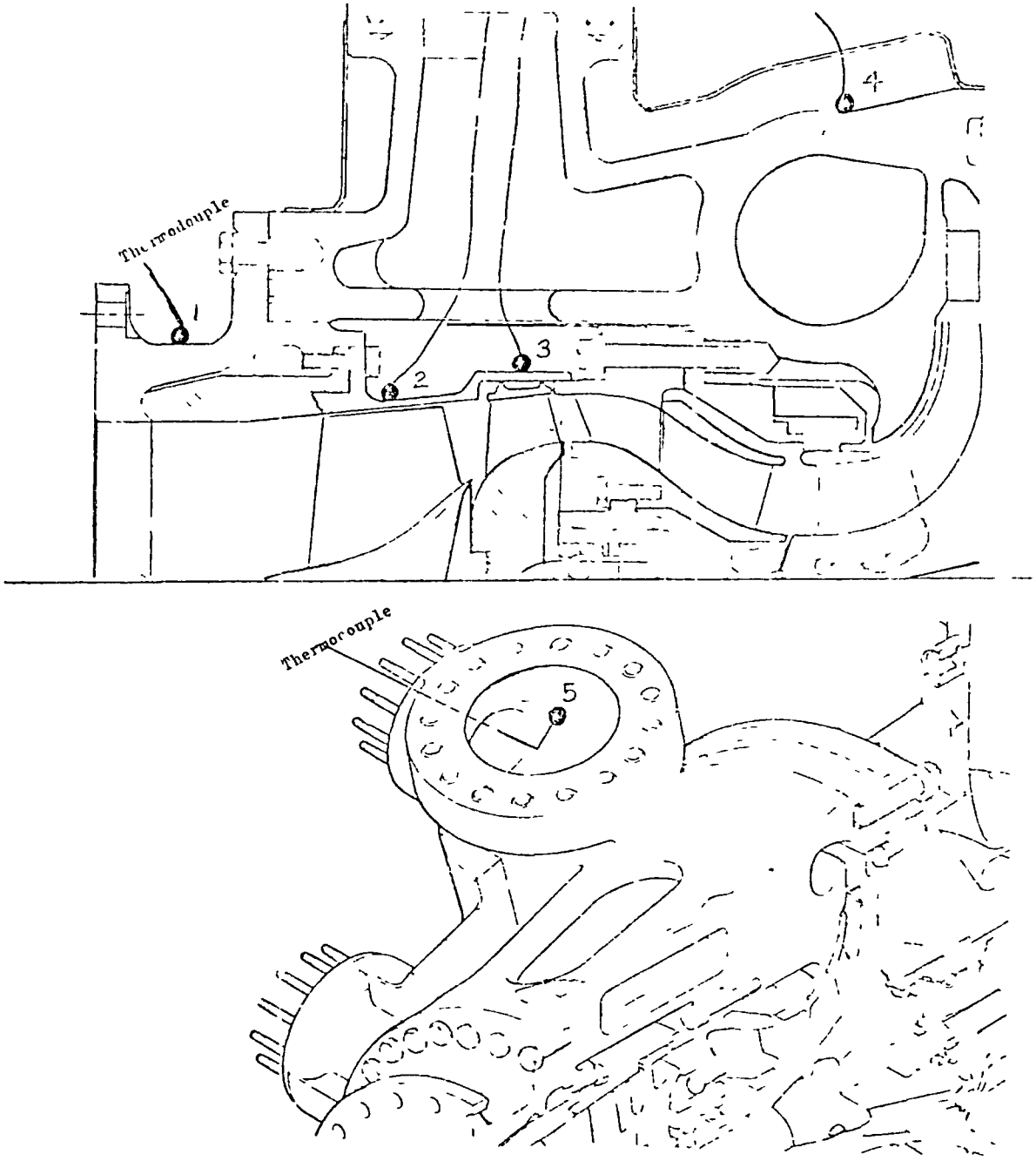

Figure 183 Thermocouple Locations on the Mark 29 Fuel Turbopump (S/N P00302)

ENGINE START ANALYSIS

CHILLDOWN AND FLOW TRANSIENTS FOR INLET LINES

Two-phase flow study and the evaluation of the LH_2 pump capability to develop the necessary head while pumping two-phase fluid was discussed under Section I. The purpose of the analytical work was to investigate the changes in the quality of the H_2 due to heat input from the inlet duct. To carry out this investigation, the Mark 29 inlet duct of the J-2S engine system was transformed into a simplified model (Fig. 184) for IBM 360 computer machine. The TAP-5 "Thermal Analyzer Program" was used in these studies and is very diversified and capable of accounting for fluid bulk temperature changes and the pressure drop variation with time and location. The determination of the heat transfer coefficient was based on the equation

$$h = 0.00065\ G^{0.5} \quad \text{Btu/in}^2\text{-sec-F}$$

During these studies the following assumptions were made

1. Initial duct temperature was 70 F.
2. H_2 was initially saturated liquid as it entered the inlet duct
3. Negligible pressure drop in the inlet duct.
4. H_2 temperature everywhere in the duct remains equal to the inlet temperature.

The computational procedures are as follows

$$h = 0.00065\ G^{0.5} \tag{93}$$

$$\frac{\partial Q}{\partial \theta} = (W\ C_p)_w \frac{dT}{d\theta} = hA\ (T_W - T_B) \tag{94}$$

Total Weight 81.2 Pounds

Inco 718

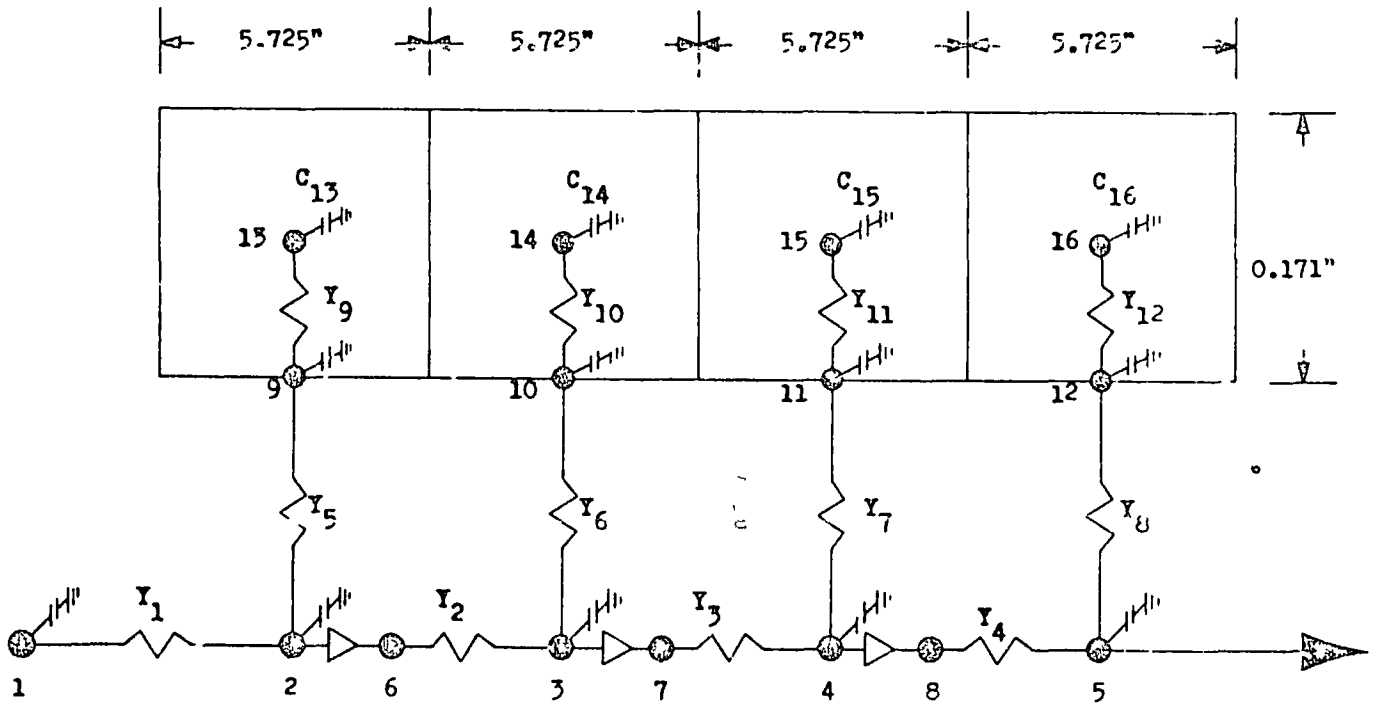

Figure 184. Mark 29 LH_2 Pump Inlet Duct Breakdown

$$V = \frac{dQ/d\theta}{H} \tag{95}$$

$$\text{Quality} = \frac{V}{\dot{W}}$$

The above equations were solved for each segment of the duct. The quality at the second segment was determined by adding the vapor from segment 1 to that of segment 2 and dividing this sum into $\dot{W}$. This process was continued throughout the length of the duct for each time increment. The flowrates assumed for these analyses are plotted in Fig. 185. The results of the study are shown in Fig. 186 and 187. Figure 185 shows that the maximum quality (percent by weight) takes place about 1 second after the H_2 starts flowing and is about 54 percent at the Mark 29 LH_2 pump inlet. This quality drops very rapidly, as the H_2 flowrate increases with time, and becomes equal to about 2 2 percent after 55 seconds of H_2 flow (275 pounds) in the duct On the other hand, the maximum quality shown in Fig. 187, which also occurs after 1 second of H_2 flow, is about 6.5 percent by weight. Again, the quality decreases with time as the heat input from the inlet duct tends to diminish. After 60 seconds of H_2 flow (450 pounds), the maximum quality at the pump entrance is approximately 1.1 percent. Therefore, it is apparent that a high H_2 flowrate is required if very low quality H_2 is to enter the pump. The following equations indicate this characteristic

$$Q \approx \dot{W}^{0.5} \tag{97}$$

$$V = \frac{Q}{H} \approx \frac{\dot{W}^{0.5}}{H} \tag{98}$$

$$\text{quality} = \frac{V}{\dot{W}} \approx \frac{\dot{W}^{0.5}}{H\dot{W}} = \frac{1}{H\dot{W}^{0.5}} \tag{99}$$

Equation 99 states that the quality is inversely proportional to flowrate to 0.5 power and, consequently, quality decreases as the flowrate is increased. It is seen that assumption 4 is valid, for as long as vaporization

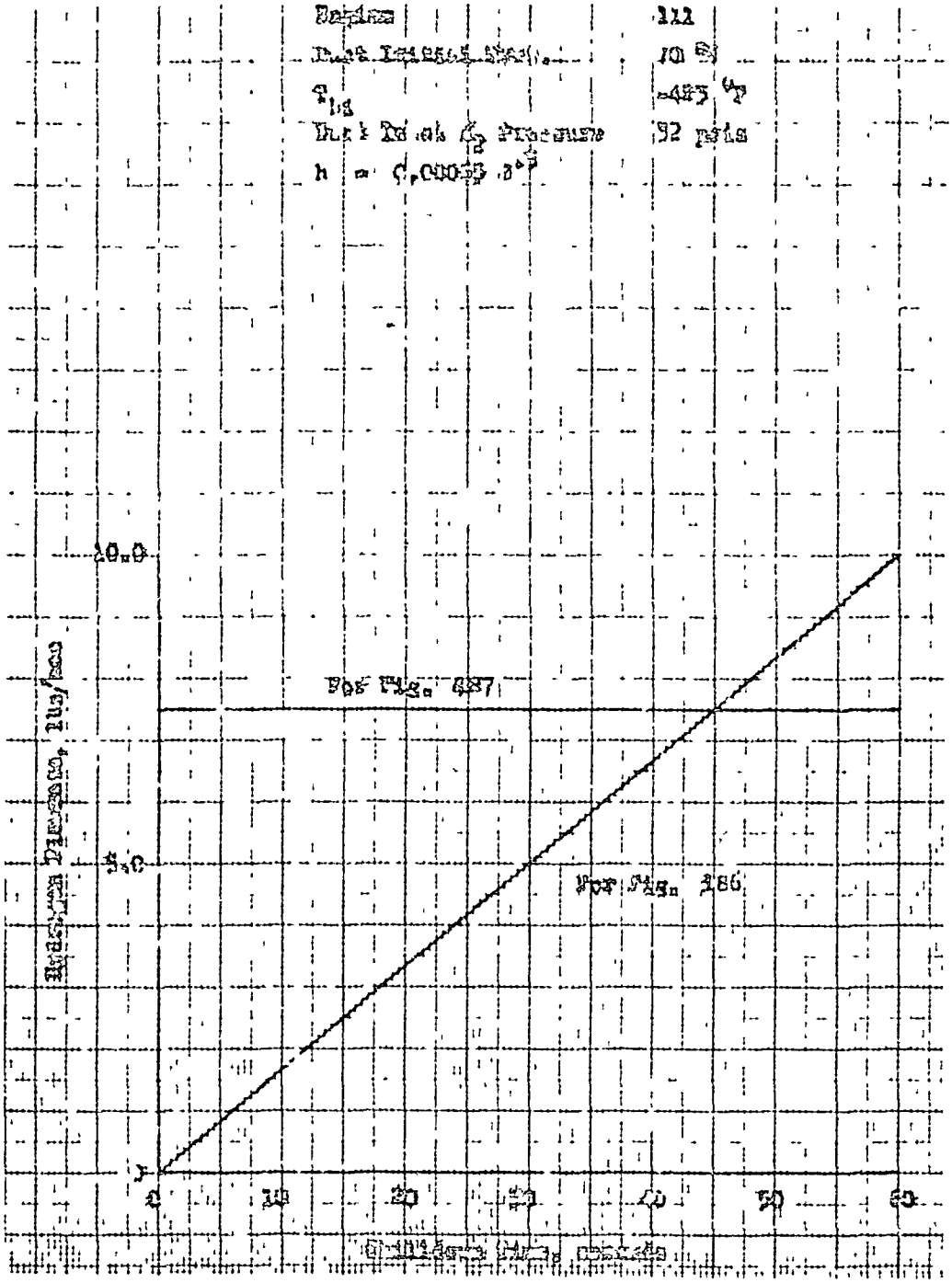

Figure 185. Hydrogen Flowrate vs Chilldown Time for the Mark 29 Inlet Duct

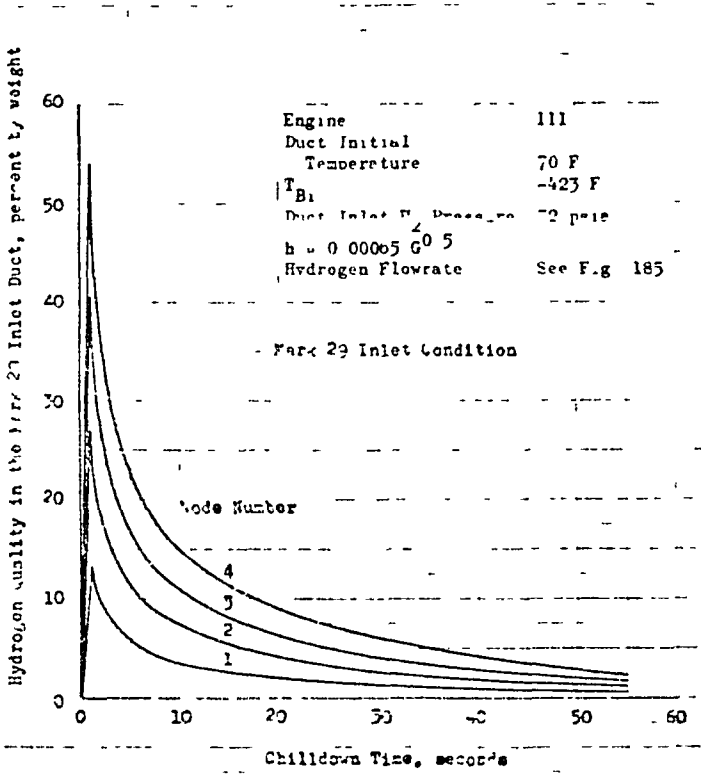

Figure 186 Hydrogen Quality vs Chilldown Time for the Mark 29 Inlet Duct

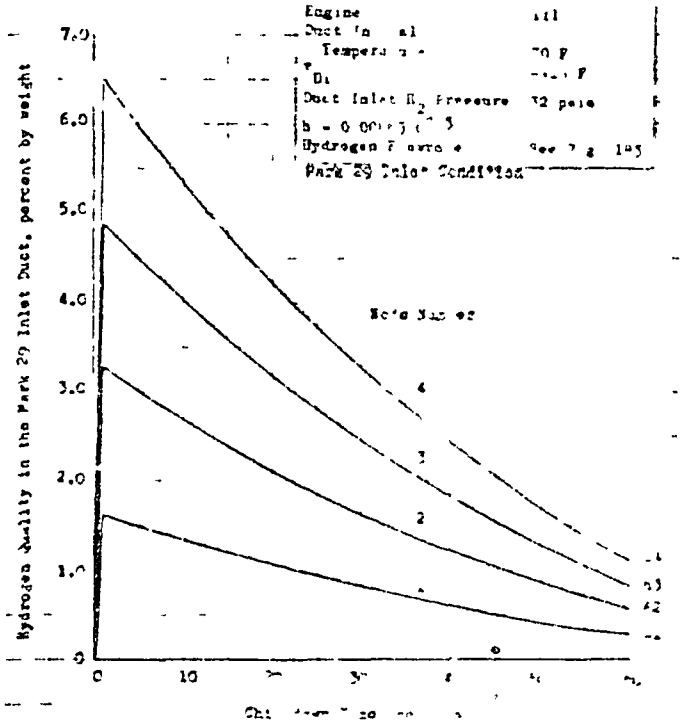

Figure 187 Hydrogen Quality at the Mark 29 Inlet vs Chilldown Time for the J-2S Engine System

of the H_2 takes place and the pressure remains constant (if pressure drop is nil in the inlet duct even for the metering flowrate), the bulk temperature of the H_2 will not vary in the inlet duct. It is recognized that the one simple correlation given for the estimation of the heat transfer coefficient may not be quite satisfactory in the entire range of ΔT. However, in nearly all cases, the heat transfer coefficient for H_2 is a function of flowrate raised to a power which is less than 1 (quality will always decrease with an increase in flowrate). If the qualities under the two sets of flowrates studied here are high for the pump, higher H_2 flowrates should be considered and investigated. However, the resistance downstream of the pump restricts the H_2 flowrate. Therefore, an increased flowrate will require increased fuel tank pressure.

PUMP PERFORMANCE MAPS

As shown in Fig. 23 of the Mark 15-F pump test data analysis, the assumption of a constant quality flow process through the pump will predict somewhat conservative pump discharge pressures but, for the Mark 15-F pump, will accurately predict the two-phase pumping limit. However, from the Mark 25 pump preliminary test data analysis, the two-phase pumping limit may be a two-phase flow coefficient of 135 to 140 percent of design rather than the two-phase flow coefficient at which the head coefficient goes to zero. As soon as the two-phase pumping limitation is understood, pump performance map predictions will be made, various pump geometries will be evaluated, and the analysis will be reported. However, a comparison of the two-phase pump test results with the inlet line chilldown transient study indicates that pump starts are possible within 2 minutes after flow begins. If the bearing coolant and the balance piston flow are not recirculated through the pump, this time lag can be reduced to about 1 minute. This is shown by both the Mark 15-F (Fig. 26) and the Mark 25 pump test data analysis in which pumping capability is indicated for up to 30-percent inlet vapor volume fraction if the recirculation flow is eliminated. At 32 psia, this is equal to 1.73 percent quality which, in turn, is roughly equal to the inlet line discharge qualities (Fig. 186 and 187) after 60 seconds.

ENGINE START MODEL

Propellant feed system conditioning problems are characteristic of engine systems operating with cryogenic propellants such as with the RL-10 and J-2 engines. To obtain satisfactory J-2 engine starts, propellants are circulated through the turbopumps and associated propellant ducting for a relatively long period prior to engine start to provide pure liquid flow at the pump inlet with resultant sufficient NPSH to the pumps. Various techniques for simplifying this system have been devised. In the J-2S program, for example, various improvement features were incorporated to eliminate the need for extensive preconditioning. To eliminate the need for chilling the thrust chamber, a duct and valve were provided to bypass fuel around the thrust chamber jacket directly to the injector until turbopump speed has been built up. The elimination of propellant recirculation through the pumps is made possible by a solid-propellant turbine starter (SPTS) which provides more energy than the existing J-2 H_2 start tank bottle, and by the thrust chamber bypass system which provides a low resistance flow path for the fuel while the tube bundle is being chilled. The SPTS duration is such that all of the fuel and most of the oxidizer in the ducts are pumped before SPTS burnout occurs. After the duct volume is evacuated, subcooled bulk liquid from the tank is available. The idle mode operation, which is included in the J-2S engine for propellant settling prior to restart on the S-IVB stage, moves enough propellant through the feed system for inlet ducting and pump chilldown so that recirculation systems are not required for restart.

A study was conducted to analytically develop well-defined trends in engine start characteristics with other variations in the operating environment to determine if areas exist where further simplifications and improvements can be made in future engine systems. To accomplish this, a simplified mathematical model of engine operation during the start transient was developed and used to study the effects of mixed-phase flow in the system under various conditions. The situations examined were start transients with. (1) only liquid (i.e., incompressible) flow

throughout the system, (2) two-phase flow in the fuel pump, (3) mixed-phase flow in the lines and tube bundle, and (4) a combination of these latter two conditions. To determine the relative importance of each of these effects, the mathematical model was formulated so as to enable separate study of each phenomenon. The model used for each condition is described below.

Liquid-Propellant Flow

To determine fundamental control requirements for a rapid and efficient engine start, the start model was formulated initially on the basis of pure liquid-propellant flow throughout the system. For the purposes of this analysis, the engine system is depicted as shown in Fig. 188. The flow through lines and valves is represented by an incompressible dynamic form of Bernoulli's equation as follows

$$P_t + \Delta P_p - P_c = \sum_i R_i \dot{W}_i^2 + \sum_i \frac{\ell_i}{g_c A_i} \frac{d\dot{W}_i}{dt}$$

or if represented in terms of nominal steady-state values, the normalized flowrate becomes

$$\bar{W} = \frac{\dot{W}}{\dot{W}_n} = \left(\frac{\Delta P^*}{\dot{W}_n}\right)\left(\frac{1}{\sum_i \frac{\ell_i}{A_i g_c}}\right)\int\left[\left(\frac{P_T}{\Delta P^*}\right)_n \bar{P}_t + \left(\frac{\Delta P_p}{\Delta P^*}\right)_n \Delta\bar{P}_p - \left(\frac{P_c}{\Delta P^*}\right)_n \bar{P}_c - \bar{W}^2 \sum_i \left(\frac{\Delta P_i}{\Delta P^*}\right)_n \bar{R}_i\right] dt \tag{100}$$

where

$$\Delta P^* = (P_T + \Delta P_p - P_c)_n$$

To account for initially unprimed feed lines, the line lengths and resistances are assumed to be variable with time until the lines become fully primed. Pump pressure rise is determined from polynominal approximations

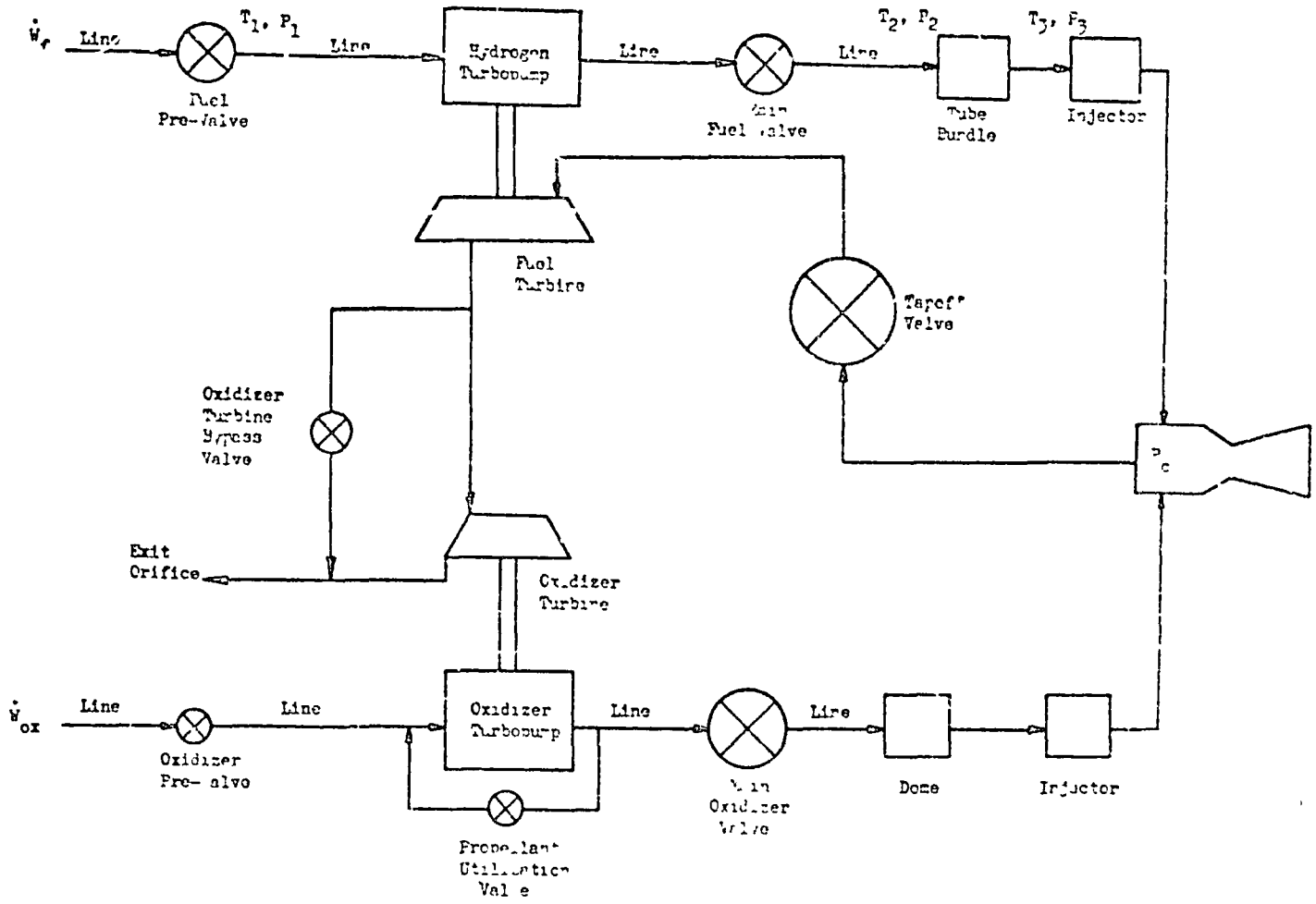

Figure 188. Flow Schematic for Start Transient Analysis

to appropriate head-flow curves for each pump. Operating parameters (e.g., turbomachinery performance characteristics, steady-state conditions, etc.) and chamber geometry were chosen to be representative of the J-2S engine. Chamber pressure which provides the driving force for the series turbines (tapoff cycle) is assumed to be dependent on mixture ratio and flowrate only, i.e., the engine operates in a vacuum so that the nozzle is choked at all times. Control of the engine operating parameters during start is provided by the position of the main propellant valves, oxidizer turbine bypass valve, and chamber tapoff valve during the start sequence. This model, which has been programmed for a high-speed digital computer, enables simultaneous computation of various operating parameters such as weight flow, chamber pressure, pump speed, mixture ratio, etc., as a function of time during the start transient.

Two-Phase Flow in the H_2 Pump

Of major concern in starting the engine without the benefit of hardware preconditioning is the ability of the fuel turbopump to pump mixed-phase flow and, therefore, relatively low-density propellant through the system. In this study, the effects of two-phase flow in the pump were initially examined independently from system chilldown or heat transfer effects. The analysis was initially conducted assuming that, while two-phase H_2 is present throughout the system, the flow through the system is still incompressible. It was further assumed that the heat input to the flow in the feed system up to the pump inlet is such that the vapor volume fraction (α) at the pump inlet varies linearly with time over specified time periods.

Under these assumptions, the mathematical formulation of the start model remained unchanged, except that the pump pressure rise curve in the portion of the model describing the fuel feed system has to be revised to reflect the influence of two-phase flow in the pump. Therefore, the predicted constant quality pump performance trends were simplified and

incorporated into the start model for this portion of the study. Engine operating controls used in this "cold" pump analysis are identical to those used with the basic model illustrated in Fig. 188.

Chilldown Effects

Heat input to the cold propellant from a warm feed system (no preconditioning) results in an increase in the bulk temperature of the fluid with an attendant decrease in fluid density, which is essentially equivalent to an increase in system resistance. A rigorous treatment of this situation would assume compressible mixed-phase flow throughout the feed system, and pressure drops and flows through various portions of the system would be computed on the basis of instantaneous fluid properties and heat inputs. However, this procedure is complicated, and therefore costly, and can be simplified significantly by recognizing that even though Eq. 100 characterizes incompressible flow, the gross effects of heat input to the fluid during the start transient can be simulated by adjusting the fluid resistance term in this equation according to a change in flow density corresponding to the variation in some representative fluid temperature during the chilldown period. While this "lumped parameter" technique will not yield rigorous results regarding actual engine operation, the predicted trends are sufficiently well defined to indicate chilldown effects on the control system requirements, and this approach was therefore adopted for use in the current study.

The temperature at which the fluid bulk density was evaluated was taken to be the temperature at the injector inlet. In determining this temperature, it was assumed that the fluid bulk temperature at the pump discharge (T_2 in Fig. 188) is variable with time and can be obtained from known chilldown data for various systems. The fluid temperature at the injector is then obtained from the known pump discharge temperature and heat input to the tube bundle as follows

$$T_3 = T_2 + \Delta T_{T.B.}$$

or in terms of normalized quantities

$$\bar{T}_3 = \left(\frac{T_2}{T_3}\right)_n \bar{T}_2 + \left(\frac{\Delta T_{T.B.}}{T_3}\right)_n \Delta \bar{T}_{T.B.}$$

where

$$\Delta T_{T.B.} = \frac{q_{T.B.}}{\dot{W} C_p} \approx \frac{k P_c^{0.8}}{\dot{W} C_p}$$

The fluid density corresponding to this instantaneous temperature and pressure (at the injector) can then be obtained from property data for H_2 and used to adjust the resistance term in Eq. 100 as follows.

$$\bar{\dot{W}} = \frac{\dot{W}}{\dot{W}} = \left(\frac{\Delta P^*}{\dot{W}_n}\right)\left(\frac{1}{\sum \frac{\ell_1}{A_1 g_c}}\right)\int\left[\left(\frac{P_t}{\Delta P^*}\right)_n \bar{P}_t + \left(\frac{\Delta P_p}{\Delta P^*}\right)_n \Delta \bar{P}_p - \left(\frac{P_c}{\Delta P^*}\right)_n \bar{P}_c - \bar{\dot{W}}^2 \sum_1 \left(\frac{\Delta P_1}{\Delta P^*}\right)_n \left(\frac{\bar{R}_1}{\bar{\rho}}\right)\right] dt \quad (101)$$

Both chilldown and tube bundle heat transfer gross effects are reflected by Eq. 101. This relation was originally developed for incompressible flow, and must be modified for the actual operating conditions (compressible). The combined effects of two-phase pump flow and system chilldown and heat transfer were analyzed simply by incorporating the revised pump curves for two-phase flow into the chilldown start model represented by Eq. 101.

ENGINE START TRANSIENTS

Start transients were generated with each of the representations discussed above for various assumed operating environments. Initial studies were directed toward establishing valve sequences which would provide a smooth efficient engine start for reference purposes, but no attempt was made to

determine an optimum valve sequence. Also, no attempt was made to avoid pump stall and mixture ratio overshoot. The additional control needed here would overly complicate the two-phase flow analysis without significantly altering the study results. Start transients reflecting the influence of heat transfer and two-phase flow were analyzed using the second and third models described above to determine the influence of these phenomena on the basic engine operation during start. The results of this study are presented below.

Liquid-Propellant Flow

It was first discovered that to obtain enough initial power to start the engine, the size of the chamber tapoff duct and valve had to be somewhat larger than nominal for the parameters used in this study. The tapoff valve was then gradually closed to its normal position during the latter portion of the start transient. Once a satisfactory tapoff valve area was determined, this value remained fixed throughout the remainder of the study. It was also assumed that the main propellant valves open instantaneously to their nominal positions at the beginning of the start sequence, and that the propellant lines are fully primed up to these valves. The position of remaining control element and the oxidizer turbine bypass valve were found to be rather sensitive to the engine operating conditions.

Chamber pressure versus time data representing typical start transients for purely liquid-propellant flow in the system are presented in Fig. 189. It is readily seen that the time at which the oxidizer turbine bypass valve is opened has a strong influence on the progress of the start transient. Opening this valve too soon results in a failure to start, and opening the valve too late causes a chamber pressure overshoot. According to the data in Fig. 189, an efficient start transient can be obtained by opening the turbine bypass valve approximately 0.8 second after the beginning of the start sequance. Mixture ratio, pump speed, and flowrate data corresponding to this latter valve time sequence are presented in Fig. 190 through 192. As indicated in Fig. 190, mixture ratio initially

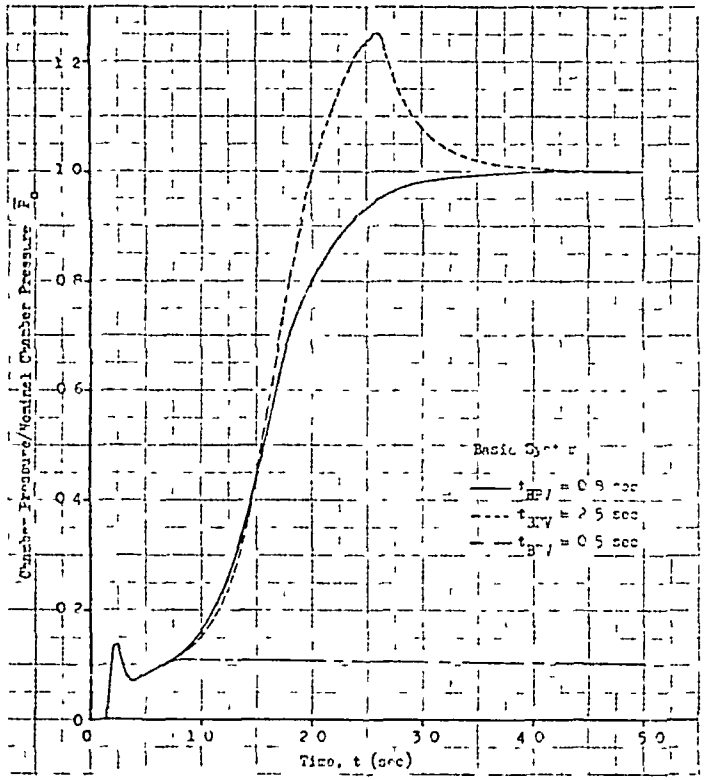

Figure 189 Effect of the Oxidizer Turbine Bypass Valve Opening Time on the Engine Start

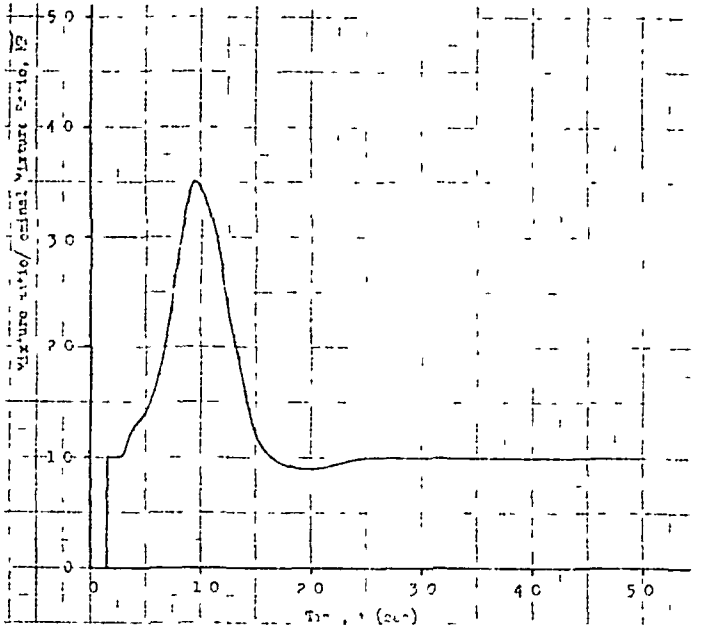

Figure 190 Normalized Mixture Ratio vs Time for the Basic System with t_{BPV} = 0.8 Second

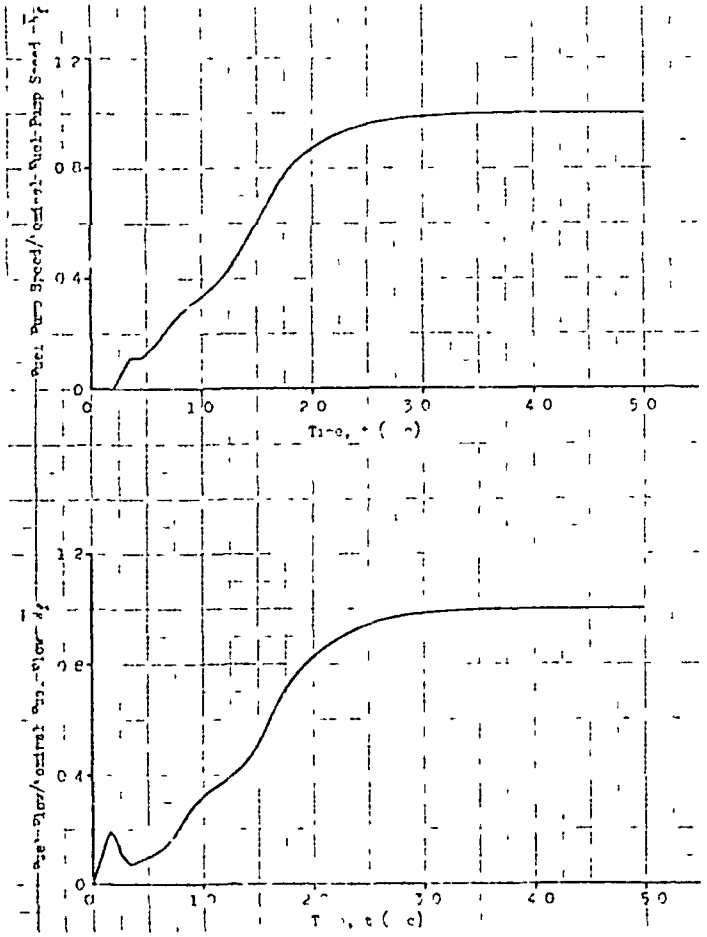

Figure 191. Normalized Fuel Pump Speed and Flow for the Basic System with t_{BPV} = 0 8 Second

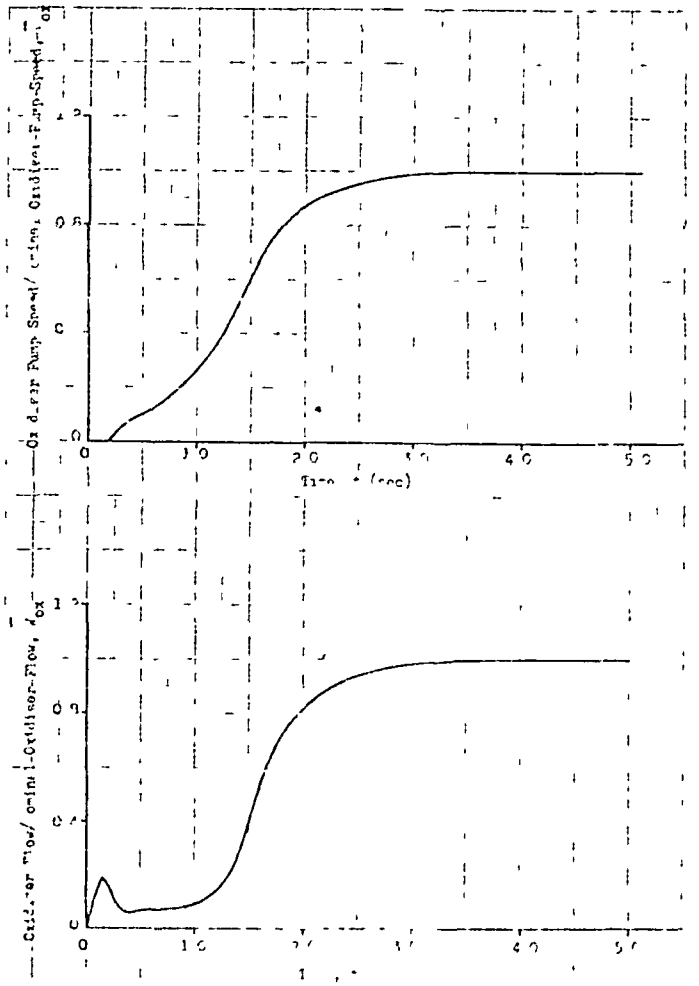

Figure 192 Normalized Oxidizer Pump Speed and Flow for the Basic System with t_{BPV} 0 8 Second

oscillates well above its nominal value, which is attained after about 2 seconds of operation. This overshoot may be accompanied by a distinct temperature rise, but can be eliminated by utilizing additional elements to provide mixture ratio control, such as the oxidizer pump bypass valve shown in Fig. 188, but this was not attempted in this study. The data in Fig. 189, 191, and 192 indicate that all operating parameters reach 90 percent of their nominal values within 2-1/2 seconds after the beginning of the start sequence.

Effect of Two-Phase Flow in the H_2 Pump

It was found that constant quality, two-phase flow in the pump has a significant effect on the engine start characteristics. Typical results are shown along with reference pure liquid data from Fig. 189 and 193 for pump inlet quality variations that are linear with time over time periods of 2 and 4 seconds. As indicated, if GH_2 remains in the flow for only a very short time, the effect is only a slight delay in the start. However, if the inlet flow remains of poor quality for longer periods, the result can be a failure of the engine to start. For the cases shown in Fig. 193, this is caused by the reduced pumping capability of the H_2 pump, which results in insufficient power to sustain engine operation after the oxidizer turbine bypass valve is opened. It was found that smooth start transients could be obtained for these cases simply by delaying the opening time of the oxidizer turbine bypass valve until 1-1/2 seconds after the main valves are opened, as shown in Fig. 194. This has the undesirable side effect of exaggerating the mixture ratio overshoot shown in Fig. 190, indicating a probable increased need for additional elements for mixture ratio control (the technique mentioned earlier) with two-phase flow in the pump.

The data in Fig. 193 represent chilldown times that are very short, such as might be obtained with partial preconditioning and/or high insulation coatings on the pump surfaces and feed lines. The effect of two-phase flow in the pump for more prolonged chilldown periods characteristic of

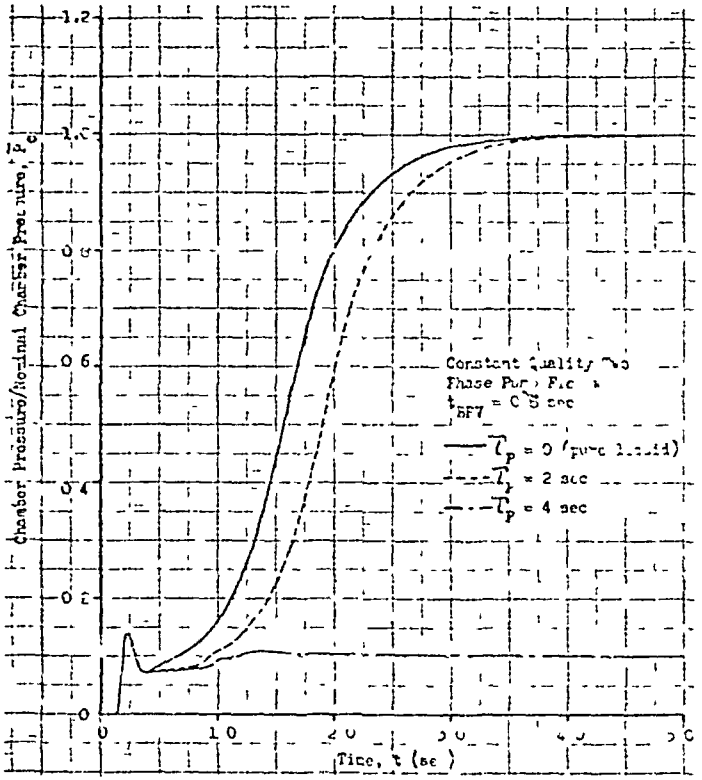

Figure 193. Effect of Reduced Pumping Capability Caused by Two-Phase Flow in the Pump on the Engine Start With t_{BFV} = 0.8 Second

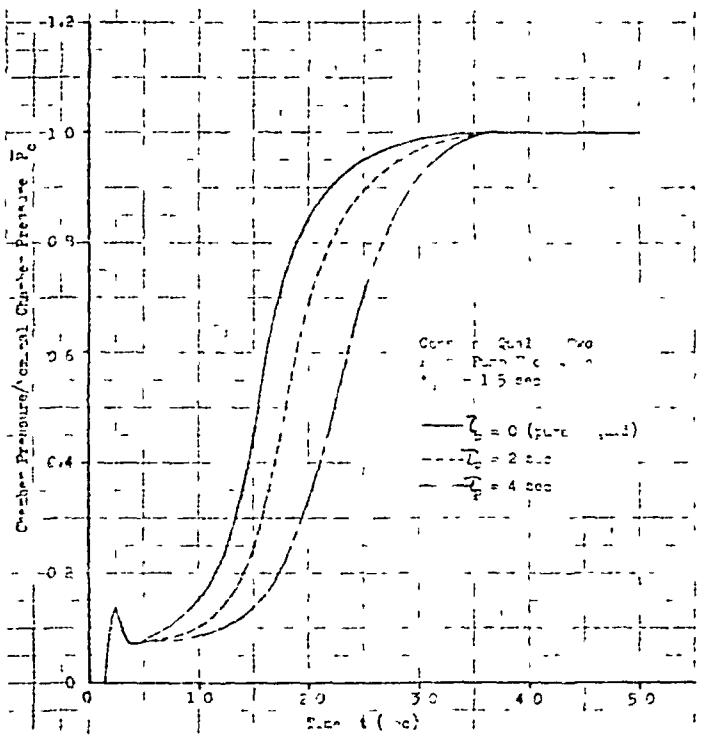

Figure 194 Effect of Reduced Pumping Capability Caused by Two-Phase Flow in the Pump on the Engine Start with t_{BFV} = 1.5 Seconds

present systems is illustrated in Fig. 195. As before, the opening time of the turbine bypass valve must be delayed to enable engine operation to approach near steady-state values. Also, a chamber pressure overshoot is encountered which cannot be eliminated simply by adjusting the turbine bypass valve. This was found to be the result of a fuel pump overspeed condition which is nearly independent of the sequencing of this control element and persists as long as two-phase flow remains in the pump, as illustrated in Fig. 195. Therefore, further control elements may be required to prevent the occurrence of this phenomenon. It is interesting to note that near steady-state values are reached nearly as fast as if the poor quality flow exists in the pump for only a short time, as shown by comparison with Fig. 194. This indicates that the reduced pumping capability may not hamper the prolonged start transient seriously. Thus, it appears that while the control requirements may become increasingly severe if the time that the pump is required to pump two-phase flow becomes excessive, the start time required to reach the 90-percent operating level may not be significantly delayed with precise valve sequencing

Chilldown Effects

Engine operating trends with representative rapid flow chilldown times and normal (liquid propellant) pump performance are illustrated in Fig. 197. The reference curve in Fig 197 (prechilled engine) is shifted slightly to the right from that shown in Fig. 189 because of the influence of nozzle tube bundle heat transfer. It can be seen that the effect of increased flow resistance is similar to, but slightly more severe than, reduced pump capability with two-phase flow (compare the sequence necessary for a smooth start here with the bypass valve opening and start times in Fig. 194). It should be noted that once an efficient valve sequence is determined, a smooth transient is apparently obtained for a wide variation in chilldown rate as long as the chilldown period if fairly short.

The bulk temperature of H_2 in a typical system decreases almost linearly from ambient (530 R) to about 45 R in approximately 36 seconds. An engine

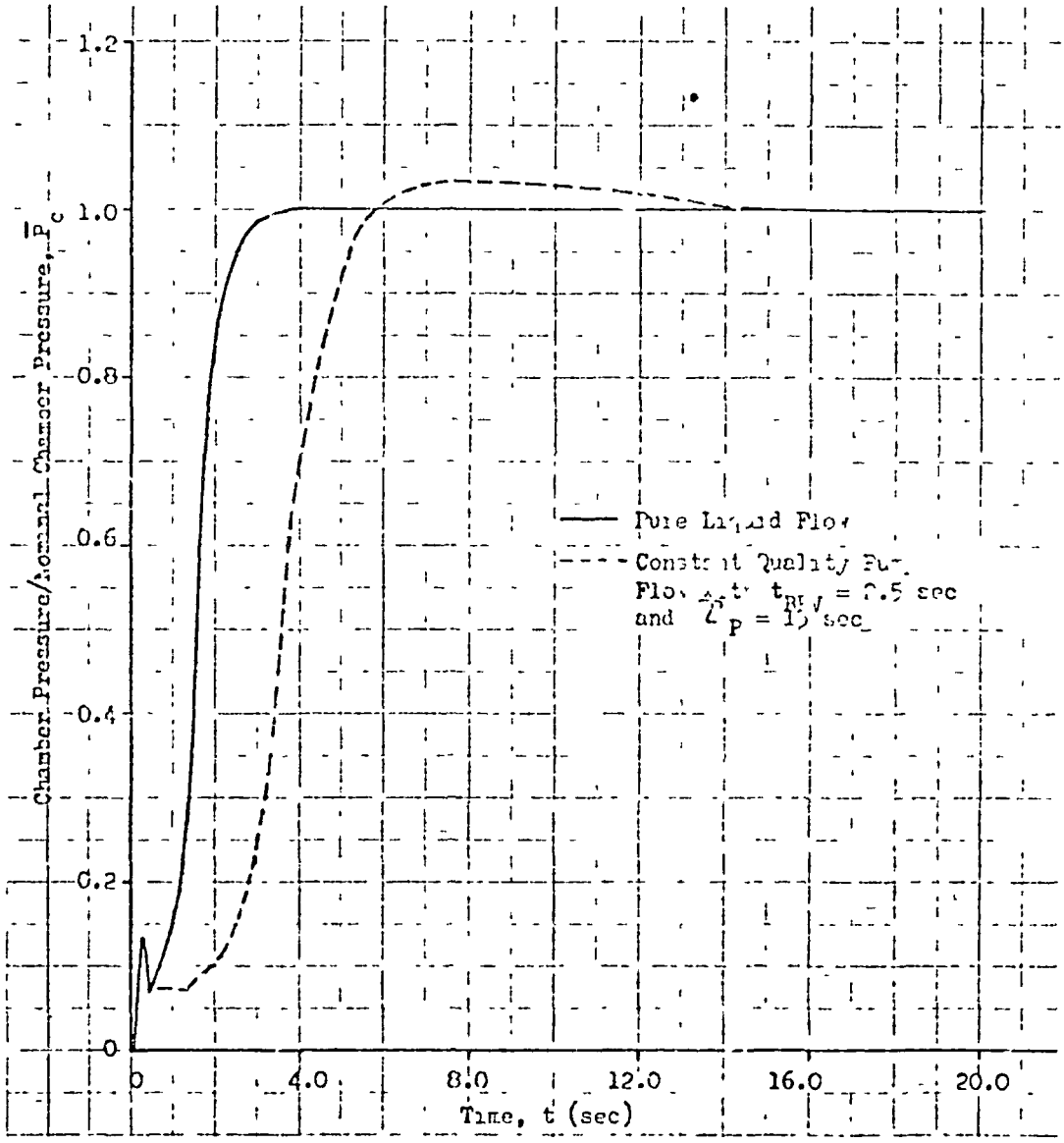

Figure 195. Effect of Reduced Pumping Capability Caused by Two-Phase Flow in the Pump on the Engine with τ_p = 15 Seconds and t_{BIV} = 2.5 Seconds

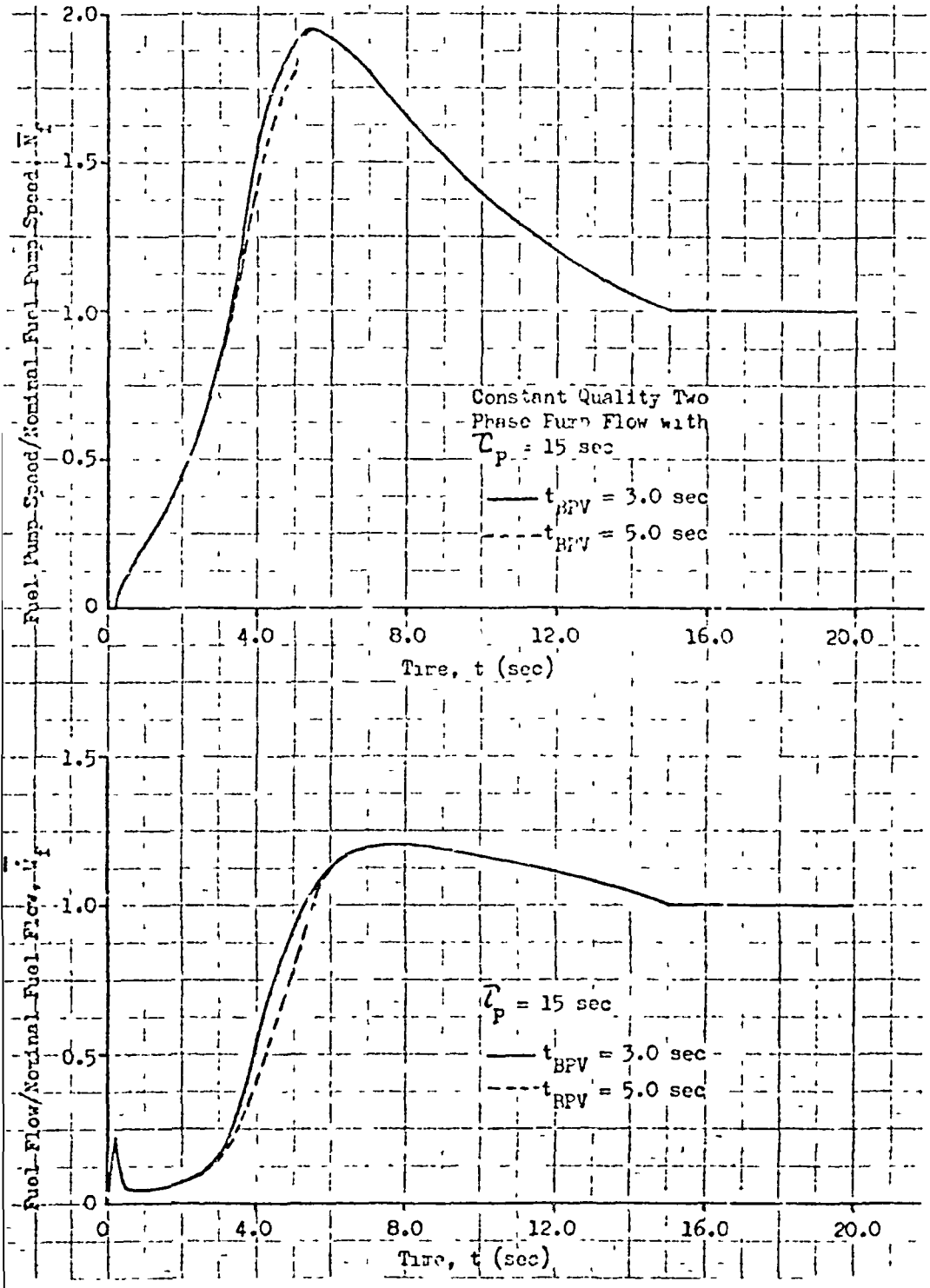

Figure 196. Effect of Two-Phase Flow in the Fuel Pump on Pump Speed and Flow

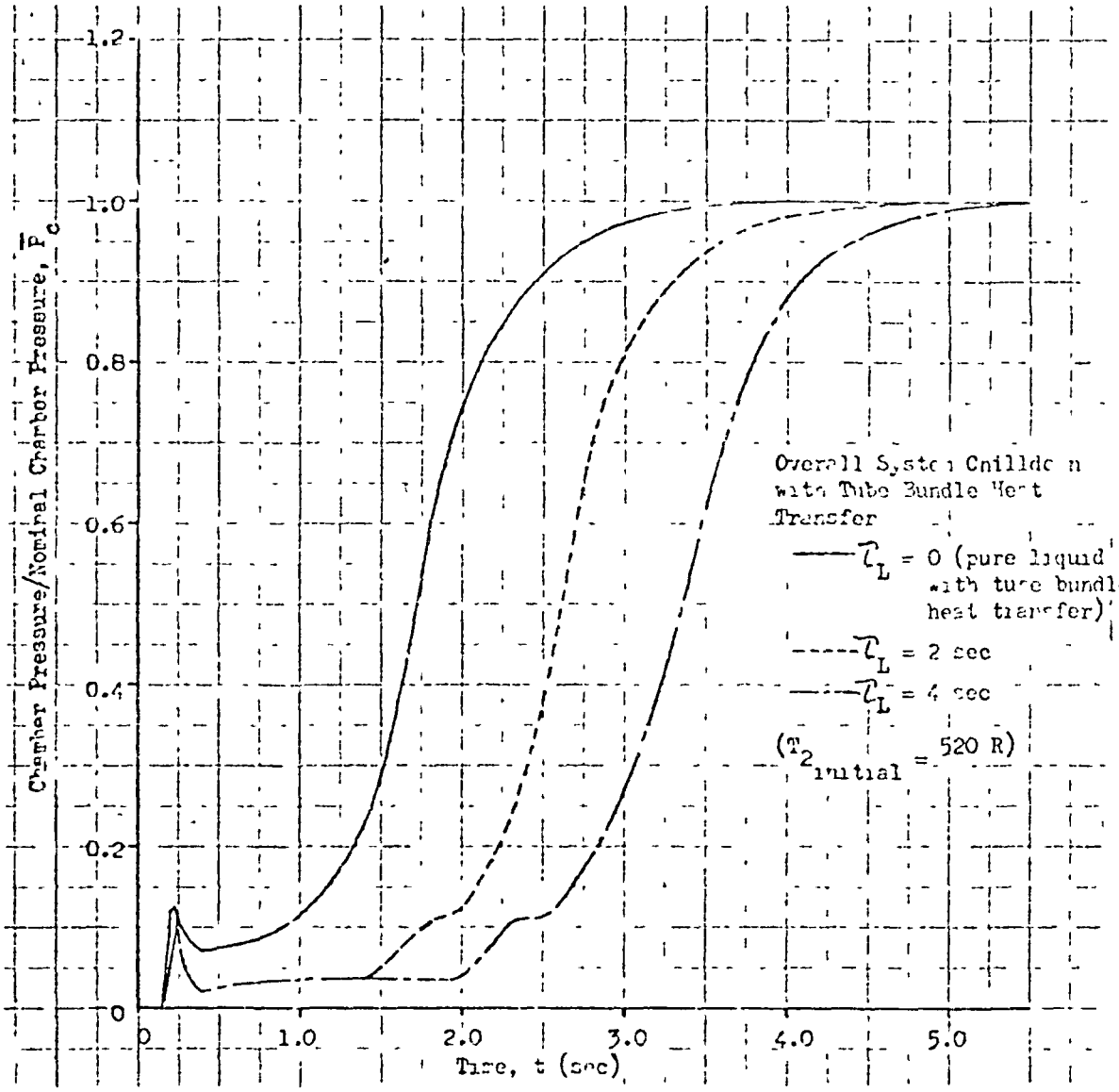

Figure 197 Effect of System Chilldown on the Engine Start With t_{BIV} 2 5 Seconds

start transient which begins in the final 15 seconds of this chilldown period is shown along with data from Fig. 197 and 198. As indicated, prolonging the chilldown time has an effect similar to maintaining two-phase flow in the pump for extended periods. Ninety-percent engine operation is reached rapidly (4 seconds), but steady-state chamber pressure is not reached until the chilldown is complete. The increased flow resistance over the longer duration results in a pump overspeed condition after about 3 seconds of operation, but as shown in Fig. 199, this condition is much less severe than that encountered previously with two-phase flow in the H_2 pump. Neither H_2 flow nor chamber pressure increase beyond their nominal values because of this phenomenon. The overspeed condition can probably be eliminated through proper scheduling of the chamber tapoff valve position as before.

Overall Chilldown Effects

To be completely consistent within the engine system, the quality at the pump inlet should correspond to some degree with the temperature and pressure at the pump exit in an analysis of the combined effects of reduced pumping capability caused by constant quality two-phase flow in the pump and increased system resistance due to heat transfer. However, initial study in this area was directed toward establishing the combined effects of the two cases with chilldown and two-phase flow effects occurring only over the first 4 seconds of engine operation, which were discussed separately above. The objective of this effort was to determine if the separate effects are directly additive.

The resulting start transients with mixed-phase flow throughout the system are shown in Fig. 200. As indicated, the oxidizer turbine bypass valve must remain closed for still longer times to obtain a smooth start. However, it can be seen from the comparison presented in Fig. 201 that the reduced pumping capability and increased system resistance do not superimpose directly. In fact, the start transient reflecting both effects is

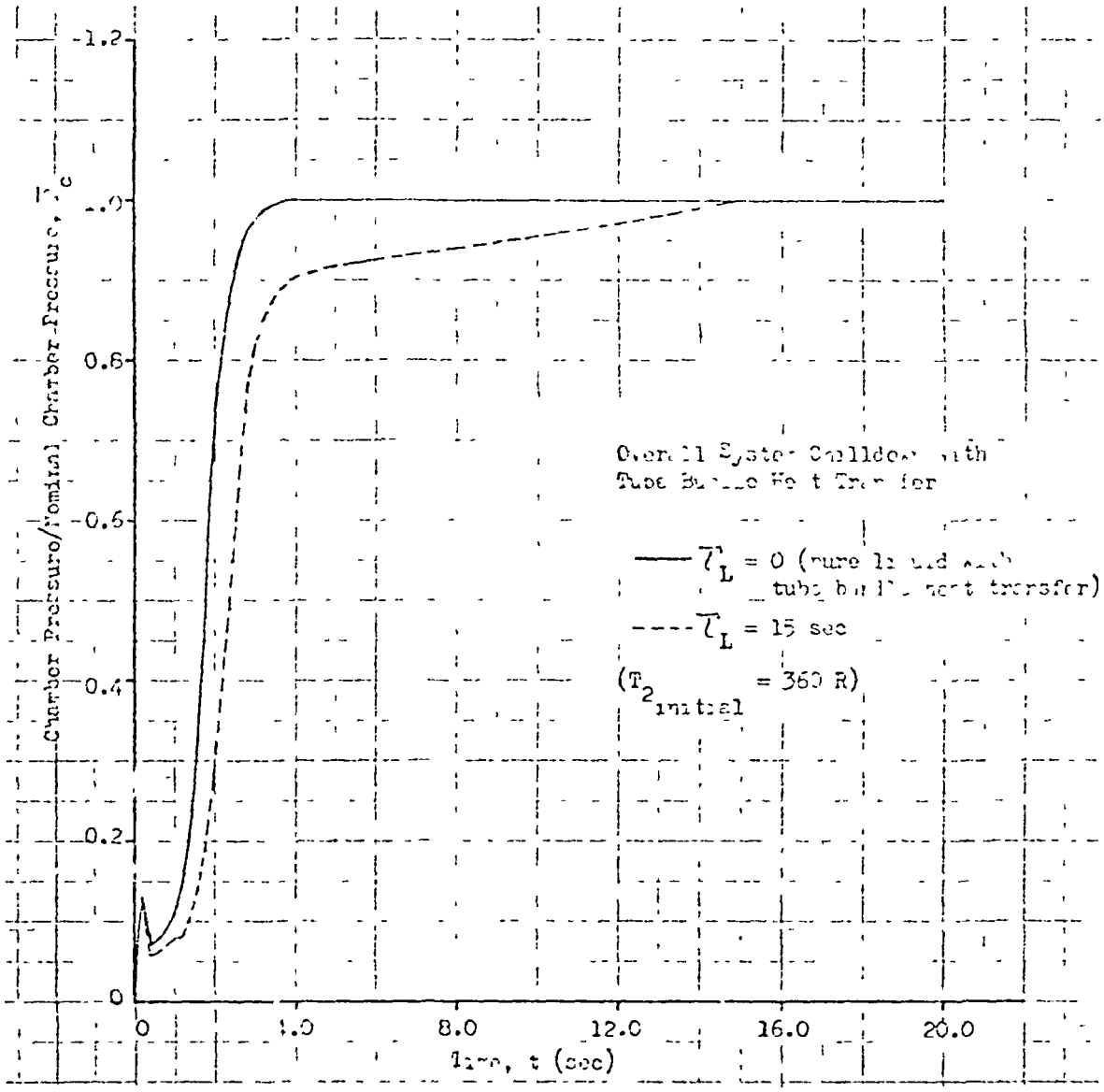

Figure 136 Effect of System Chilldown Over an Extended Time Period on the Engine Start with t_{BIV} = 1.5 Seconds

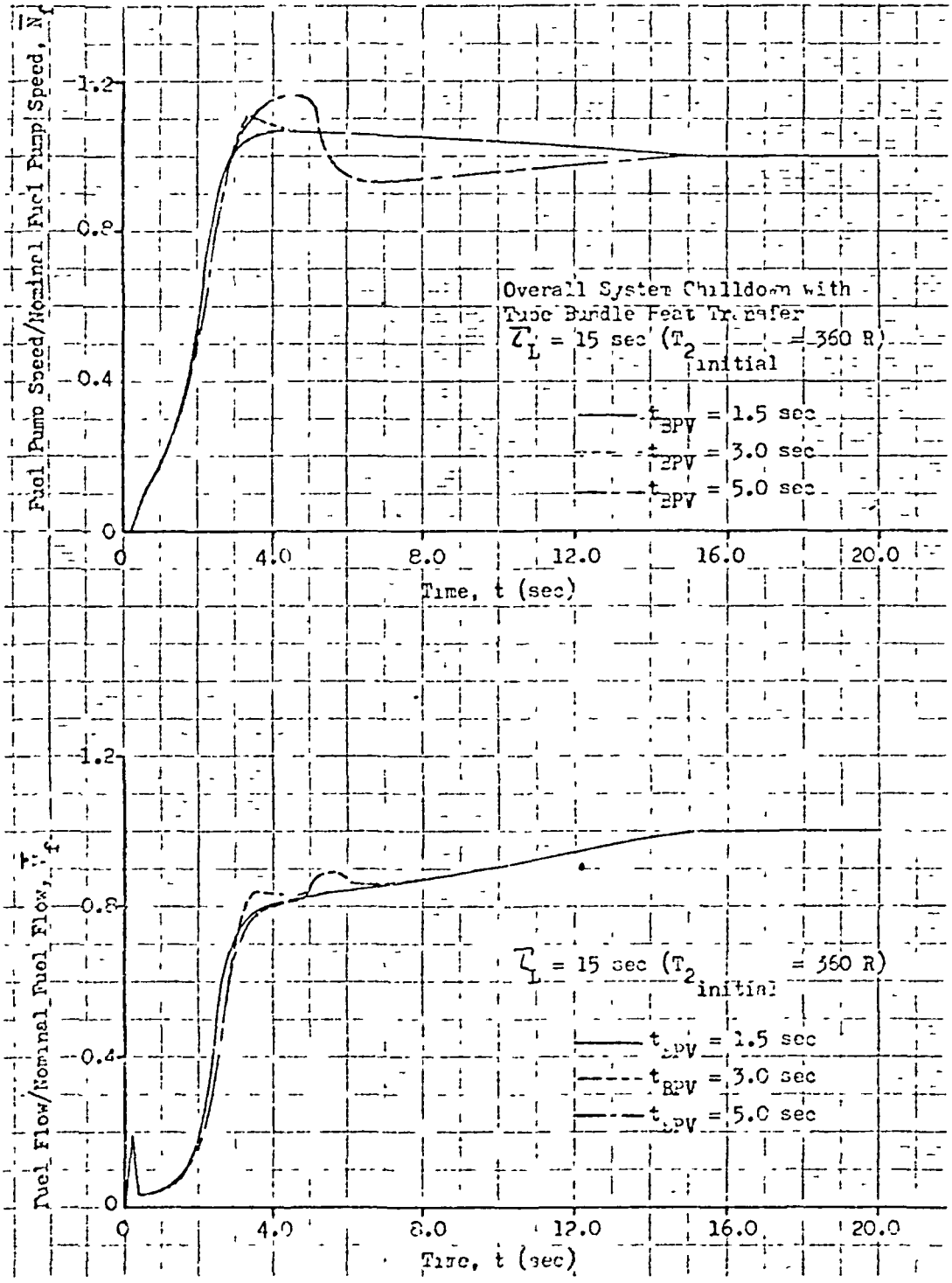

Figure 199. Effect of System Chilldown Over an Extended Time Period on Fuel Pump Speed and Flow

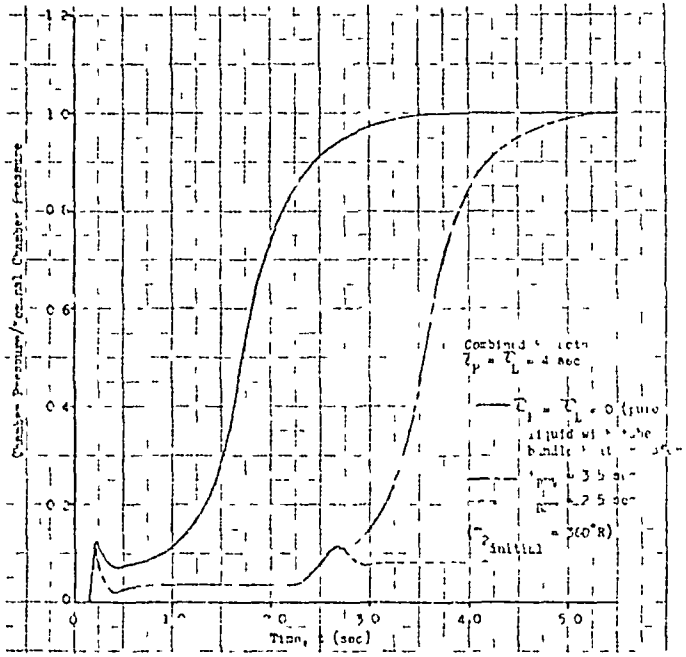

Figure 200 Combined Two-Phase Pump Flow and Chilldown Effects on the Engine Start With $\tau_p = \tau_L = 4$ Seconds

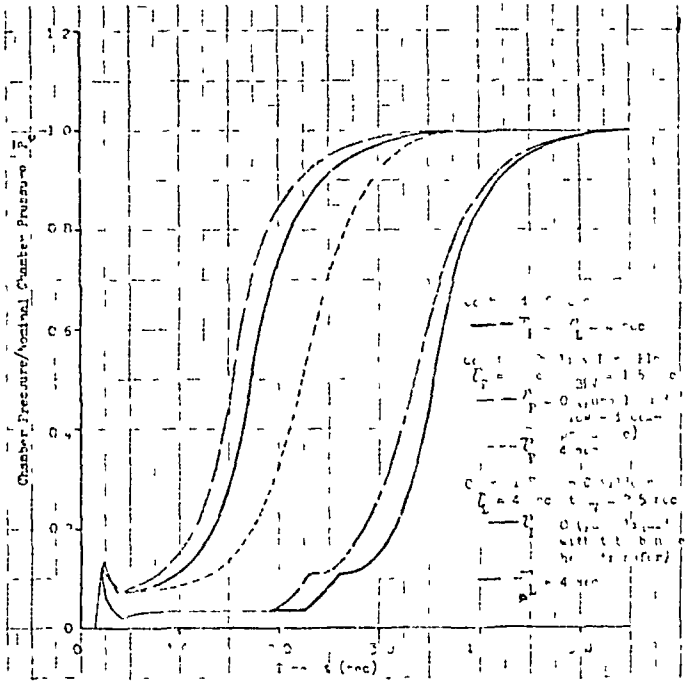

Figure 201 Comparison Between Various System Chilldown Effects for Engine Starts without Hardware Preconditioning

not much longer to the 90-percent level than the transients showing only the single effects of increased system resistance and two-phase flow in the pump. This indicates that both conditions must be improved simultaneously, as has been done with the current J-2S engine, to effect the largest change in the engine start characteristics. Analysis of other conditions in this area is continuing under the current phase of this program

NOMENCLATURE

A = area

A = area normal to impeller relative velocity vector

A = pump inlet line area

a = $\frac{\rho_p V_3 \dot{W}_V}{\pi D (X_3 - X_2)}$

Bi = Biot number

Bo = Boiling number

b = $D/4\, \ell_{V_3} C_{pV_3} + r\, \delta \rho_W C_{W_3}$

Cm = impeller meridian flow velocity

C_p = specific heat

c = acoustic velocity

c = specific heat

D = diameter

d = diameter

e = exponential (2.718)

F = stall line margin

f = friction factor, final

G = mass velocity

g, g_c = acceleration of gravity (32.2 ft/sec^2)

H = enthalpy

H = head

h = enthalpy

h = enthalpy, heat transfer coefficient

h_c = coolant side heat transfer coefficient

ID = inside diameter

J = conversion factor (778 ft lb/Btu)

K = thermal conductivity, specific heat ratio

L = length

ℓ = line length

M = Ratio $\frac{(W\ C_p)_P}{(W\ C_p)_F}$, Mach number

MR = mixture ratio

m = mass

N = rotational speed

N_{Nu} = Nusselt number

N_{Pr} = Prandtl number

N_{Re} = Reynolds number

N_{ST} = Stanton number

NPSH = net positive suction head

OD = outside diameter

P = pressure

ΔP = pressure drop (psia)

Q = heat transfer rate

Q = volume flowrate

Q/A = heat flux

R = gas constant

R = liquid-to-vapor density ratio

R = warm pumping capability parameter

R = resistance, $R = 1/A^2\ (2\ g_c \rho)$

r = radius

r = warm pumping capability parameter

S = blade solidity

s = entropy

T = temperature

t = time

U = impeller tangential velocity

V = velocity

V = volume

W = mass, function

W = impeller relative flow velocity

$\dot{W}$ = weight flowrate

X = inducer geometrical factor

X = quality, depth

$$X_{tt} = \left(\frac{1-X}{X}\right)^{0.9} \left(\frac{\mu_\ell}{\mu_F}\right)^{0.1} \left(\frac{\rho_F}{\rho_\ell}\right)^{0.5}$$

x = vapor fraction by weight (quality)

Z = length

α = vapor fraction by volume

β = impeller flow angle relative to tangent

γ = gas specific heat ratio

δ = wall thickness

ϵ = surface roughness

η' = inducer efficiency based on static pressure

θ = time

λ = heat of vaporization

λ = hub-to-tip diameter ratio

μ = viscosity

ν = kinematic viscosity

ν_{T_B} = kinematic viscosity at coolant bulk temperature

$\nu_{T_{WL}}$ = kinematic viscosity at coolant side wall temperature

ρ = density

τ = period of time two-phase flow exists in the pump or feed lines

ϕ = flow coefficient (C_m/U)

2 = two phase

ψ = function

ψ = head coefficient

SUBSCRIPTS

0 = total flow condition, tank

1 = inducer inlet, inlet line, station number

2 = impeller discharge, station number

3 = inducer inlet, station number

a = ambient

Ah = adiabatic wall

av = average

B = bulk temperature

BPV = oxidizer turbine bypass valve

c = coolant

c = main chamber conditions

calc = calculated

cm	=	combined
cs	=	constant quality flow process
D	=	design
d	=	design
LQ		equilibrium flow process
exp	=	experimental
F	=	fluid
f	=	film, fluid
fb	=	film boiling
fc		forced convection
fm	=	film mean
g	=	gas, combustion gas
i	=	inside, initial
i	=	ideal, or summation index
In	=	in
inlet	=	inducer inlet
L,l,liq	=	liquid
m	=	mixture
max	=	maximum
min	=	minimum
n	=	nominal (steady state) quantity
0	=	outlet, outside
P	=	pipe
P	=	pump
R	=	rotor
RMS	=	root mean square

r = Hub

s = isentropic flow process

T = tip

TB = tube bundle

T.P. = two phase

t = tip

t = tank

tp = two phase

v = vapor

vapor = vapor

wall = flow passage surface

WC = wall coolant side

WG = wall gas side

W = wall

wo = outside wall

ws = inside wall

SUPERSCRIPTS

* = throat region

* = total system pressure drop

- = average

- = quantity normalized with respect to nominal steady-state value

REFERENCES

1. R-7138, Thermodynamic Improvements in Liquid Hydrogen Turbopumps, Interim Report, Contract No. NAS8-20324, Rocketdyne, a Division of North American Aviation, Inc., Canoga Park, California, July 1967.

2. Tangren, R. F., C. H. Dodge, and H. S. Seifert "Compressibility Effects in Two-Phase Flow," Journal of Applied Physics, Volume 20, No. 7, pp 637-645, July 1949.

3. Smith, R. V., "Some Idealized Solutions for Choking, Two-Phase Flow of Hydrogen, Nitrogen, and Oxygen," Advances in Cryogenic Engineering, Vol. 8, pp 563-573, Plenum Press, New York, 1963.

4. Smith, R. V. Choking Two-Phase Flow Literature Summary and Idealized Solutions for Hydrogen, Nitrogen, Oxygen, and Refrigerants 12 and 11, Technical Note No. 179, Cryogenic Engineering Laboratory, National Bureau of Standards, Boulder, Colorado, 3 August 1963.

5. Gouse, S. W., and G. A. Brown A Survey of the Velocity of Sound in Two-Phase Mixtures, ASME Paper No. 64-WA/FE, Winter Annual Meeting, New York, 29 November - 4 December 1964.

6. Brennan, J. A., D. H. Edmonds, and R. V. Smith Two-Phase (Liquid-Vapor), Mass-Limiting Flow with Hydrogen and Nitrogen, Technical Note No. 399, Cryogenic Division, Institute for Materials Research, National Bureau of Standards, Boulder, Colorado, 30 January 1968.

7. Moses, R. A. Physical and Thermodynamic Properties for Heat Transfer Analysis, Pub. 575-4-5, Lecture 2 of Advanced Heat Transfer Seminar, Rocketdyne, a Division of North American Aviation, Inc., Canoga Park, California.

8. Eddington, R. B. Investigation of Shock Phenomena in a Supersonic Two-Phase Tunnel, AIAA Paper No. 66-87, Third Aerospace Sciences Meeting, New York, 24-26 January 1966.

9. Connelly, R. E., and P. R. Meng Inducer Performance with Hydrogen Liquid-Vapor Mixtures, 9th Liquid Propulsion Symposium, Vol. 2, presented 25-27 October 1967 at St. Louis, Missouri, Chemical Propulsion Information Agency

10 Warren, I. Modern Developments in Heat Transfer, Academic Press, pages 85-138, 1963

11 Straight, D. M "Heat Transfer and Flow Data with Cryogenic Hydrogen for Nuclear Rocket System Design," N64-26019, August 1963.

12 Lewis, J. W., J. A. Clark, and H. Merte, Jr "Boiling of Liquid Nitrogen in Reduced Gravity Fields With Subcooling," 07461-20-T, NASA-20028, May 1967.

13. Wright, C. C., and H. H. Walters "Single Tube Heat Transfer Tests, Gaseous and Liquid Hydrogen," IR59-423, WADC, August 1959

14. R-5598, Boiling Heat Transfer for Cryogenics, NAS8-5337, Final Report, Rocketdyne, a Division of North American Aviation, Inc., Canoga Park, California, 11 May 1965

15. Cooling, K. J., J. A. Clark, H. Merte, Jr., and E. R. Grady "Incipient Boiling of Cryogenic Liquids," 07461-28-T, NASA 20228, December 1967.

16. R-68-4, Study of Cooldown of Metals, Flow Stability, and Heat Transfer in Two-Phase Flow Hydrogen, L. Munson and W. S. Miller, Rocketdyne, a Division of North American Rockwell Corporation, Canoga Park, California, 1968

17. R-6529, Investigation of Cooling Problems at High Chamber Pressures, Final Report, Rocketdyne, a Division of North American Aviation, Inc., Canoga Park, California, 15 September 1966.

18. Hsu, Y. Y., G. R. Corgill, and R. C. Hendricks "Mist-Flow Heat Transfer Using Single-Phase Variable-Property Approach," NASA TND-4149, December 1967.

19. Cowley, W. C., J. W. Tenson, and A. J. Sawdye "A Method for Improving Heat Transfer to a Cryogenic Fluid," Advances in Cryogenic Engineering, Vol. 7, Proceeding of the 1961 Cryogenic Engineering Conference, University of Michigan, Ann Arbor, Michigan, 15-17 August 1961, Plenum Press, N. Y., 1962.

20. Schapiro, A. H. The Dynamics and Thermodynamics of Compressible Fluid Flow, Vol. II, Chapter 24, Ronald Press Co., New York.

21. Steward, W G., T. T Nagamoto, J. H Wilson, and R. B. Jacobs Research on Cooldown of Cryogenic Transfer Lines, Final Report, Contract No (33-616), U S Department of Commerce, National Bureau of Standards, Cryogenic Engineering Laboratory, Boulder, Colorado, 1960

22 Jakob, M Heat Transfer, Vol 1, pp 275, John Wiley and Sons, Inc., New York

23. Schmidt, E , L Lehert, and V. Grigull "Jahrbuch der Deutchen Luftfahrtforschung," Vol 2, pp 53, 1939

24. Goldman, K "Proc of the 1961 Int Heat Transfer Conference," pp 561, 1961.

25. Goldman, K Chem. Progr Symposium Ser Nuclear Engr., Vol 50, No 11, 1954

26. Firstenberg, H , NDA-2131-12, June 1960

27. Holman, J. P and J. H. Boggs Journal of Heat Transfer, Vol. 83, pp 176, 1961.

28. Hines, W S., and H Wolf, ARS Journal, Vol 32, pp. 361, 1962

29 Zuber, N An Analysis of Thermally Induced Flow Oscillations in the Near-Critical and Super-Critical Thermodynamic Region, Final Report, NAS8-11422, 25 May 1966.

30 Thompson, R S LAMS-3070, TID-4500, 1964.

31. Shitzman M E. "Teplofizika Vysokih Temperature," Vol. 1, pp 267, 1963.

32. Shitzman, M E. paper No. 1-59, "Second All-Union Conference on Heat on Mass Transfer," Minsk, 1964.

33. Flynn, T. M "Liquid Hydrogen Engineering Instrumentation," Cryogenics Division, NBS Institute for Material Research, September 1963.

34. Lapple, C. E "Fluid and Particle Mechanics," Chapter 6, University of Delaware, Newark, Delaware, March 1956.

35. McAdams, W. H Heat Transmission, Third Edition, McGraw-Hill Book Co., Inc., New York, 1954.

END

DATE

FILMED

JUN 10 1969